UILU-ENG-79-2001

CIVIL ENGINEERING STUDIES
STRUCTURAL RESEARCH SERIES NO. 459
Illinois Cooperative Highway and Transportation Research
Program Series No. 177

# LABORATORY TESTS OF TWO-SPAN PRESTRESSED REINFORCED CONCRETE BRIDGE GIRDERS CONSTRUCTED FROM THREE LONG SEGMENTS



by
W. L. GAMBLE
R. G. DREW

Issued as the Final Report on an
Investigation of Field-Made Joints in
Prestressed Reinforced Concrete
Highway Bridge Girders
Project IHR-303
Illinois Cooperative Highway and Transportation Research Program

Conducted by
THE STRUCTURAL RESEARCH LABORATORY
DEPARTMENT OF CIVIL ENGINEERING
ENGINEERING EXPERIMENT STATION
UNIVERSITY OF ILLINOIS AT URBANA-CHAMPAIGN
in cooperation with the
STATE OF ILLINOIS
DEPARTMENT OF TRANSPORTATION
and the
U.S. DEPARTMENT OF TRANSPORTATION
FEDERAL HIGHWAY ADMINISTRATION

UNIVERSITY OF ILLINOIS
AT URBANA-CHAMPAIGN
URBANA, ILLINOIS
FEBRUARY 1979

TECHNICAL REPORT STANDARD TITLE PAGE

| 1. Report No. | 2. Government Accession No. | 3. Recipient's Catalog No. |
|---|---|---|
| FHWA-IL-UI-177 | | |

| 4. Title and Subtitle | 5. Report Date |
|---|---|
| Laboratory Tests of Two-Span Prestressed Reinforced Concrete Girders Constructed from Three Long Segments | February 1979 |
| | 6. Performing Organization Code |
| 7. Author(s) | 8. Performing Organization Report No. |
| W. L. Gamble and R. G. Drew | UILU-ENG-79-2001 |
| 9. Performing Organization Name and Address | 10. Work Unit No. |
| Department of Civil Engineering<br>University of Illinois at Urbana-Champaign<br>Urbana, IL 61801 | 11. Contract or Grant No.<br>IHR-303 |
| | 13. Type of Report and Period Covered |
| 12. Sponsoring Agency Name and Address<br>Illinois Department of Transportation<br>Bureau of Materials and Physical Research<br>126 East Ash Street<br>Springfield, IL 62706 | Final: April 1972 - December 1977 |
| | 14. Sponsoring Agency Code |

15. Supplementary Notes

Prepared in Cooperation with the U. S. Department of Transportation, Federal Highway Administration. Project Title "Field Made Joints in Prestressed Reinforced Concrete Highway Bridge Girders"

16. Abstract

Tests of two prestressed concrete composite bridge girders which were continuous over two spans are reported. Both were I-section girders with cast-in-place decks, and had spans of about 37 ft (11 m), and were approximately 1/3 scale models of structures spanning 125 ft (38 m). Each girder was constructed from three segments which were joined end-to-end by cast-in-place concrete splices.

Model 1 was post-tensioned after erection of the girders and casting of the deck and splice concrete. The two end segments, each supported on the final abutments and on temporary supports located about 1/3 of the span from the central pier, were pretensioned for their dead loads plus the deck concrete. The central segment, which was supported on the central pier of the structure plus the two temporary supports was precast reinforced concrete, plus a small amount of pretensioned reinforcement. Model 2 was externally similar, but was not post-tensioned. The segments were pretensioned for the final moments, and were joined by splicing reinforcing bars which extended into the splice region.

Both structures were subjected to a series of loadings to the service load, design ultimate, and high over-load levels. Both had capacities which were significantly higher than the design ultimate values. The capacities were generally predictable on the basis of flexural strength calculations, and shear did not cause major problems. Joint details in Model 1 lead to difficulties in two tests, and this aspect of the design is discussed in detail.

| 17. Key Words | 18. Distribution Statement |
|---|---|
| Prestressed concrete, Post-tensioned concrete, Highway bridges, Analysis, Structural Testing, Cracking, Deflections, Reactions, Precast Concrete | No restrictions. This document is available to the public through the National Technical Information Service, Springfield, VA 22161 |

| 19. Security Classif. (of this report) | 20. Security Classif. (of this page) | 21. No. of Pages | 22. Price |
|---|---|---|---|
| Unclassified | Unclassified | 264 | |

Form DOT F 1700.7 (8-69)

TABLE OF CONTENTS

LIST OF TABLES

# LIST OF FIGURES

Figure | Page

# 1. INTRODUCTION

## 1.1 Background Information

This report is the second and last describing research work done in order to find and confirm solutions to structural engineering problems created when highway safety standards relating to grade separation were changed. In the past, the normal overpass structure was a four-span structure such as shown in Fig. 1.1. However, as a result of changes in the minimum standards for horizontal clearances on divided, limited access highways, the shoulder pier had to be eliminated, and the resulting structure became that shown in Fig. 1.2.

The largest spans in the four span structures were usually 70 to 80 ft (21 to 24 m), and the bridges were often constructed using precast, pretensioned I-section girders with cast-in-place composite decks that also provided continuity for live load forces.

However, the two span structure required spans of at least 105 ft (32 m) and in some instances 125 ft (38 m), and these spans were not feasible using the same techniques with pretensioned concrete girders, for at least two reasons. First, the sections available in Illinois were not large enough to resist the additional moments required by the longer spans, and second, if they were available, they were so heavy that transportation and construction problems often prohibited their use.

Elimination of prestressed concrete from this market had the undesirable effect of reducing the competition (with structural steel) which had tended to minimize cost increases.

This study had the objective of developing at least one method to enable prestressed concrete girders, preferably with as many precast components as possible, to be used for the longer spans. To this end, a two-span girder having spans of 125 ft (38 m) was designed, using three long precast segments placed end-to-end and then post-tensioned to form a continuous girder.

A full-scale girder, with composite deck and two spans of 124 ft (37.8 m), was built and tested; that phase of the project has been described in an earlier report, Ref. 1.

After the successful completion of the tests on the prototpye girder, two similar bridge structures were built by the Illinois Department of Transportation. These bridges were completed in 1976 and are in service. A photograph of the first is shown in Fig. 1.3. This structure has two spans of 106.5 ft (32.46 m) and crosses Interstate Route 72 just west of Monticello, Piatt Co., Illinois. Standard 48 in. (1220 mm) girders were used. The second structure had spans of about 112 ft (34.1 m) and 103 ft (31.4 m) and had 54 in. (1370 mm) deep girders modified from the standard sections by adding 1 in. (25 mm) to the width to accommodate the post-tensioning ducts.

This report is concerned with the tests of two model girders, each at approximately 1/3 scale, that were designed and built using the same general configurations as in the full-scale test girder and in the two bridge structures. Two different concepts were used in the models, and these will be described in the following section, in general terms, and in detail in Chapter 2 of this report. These two models were subjected to live load tests to several load levels, and the description and analysis of their behavior forms the major part of this report.

## 1.2 Brief Descriptions of Construction Procedures

The concepts of the two models may be best understood by referring to two series of drawings showing the construction steps. The first series is appropriate to the full-scale girder which was tested, to the first two bridges constructed in Illinois, and to Model 1 described in this report.

Figure 1.4 shows a two-span girder divided into three components. There are two similar end segments, which are supported on the end abutments of the bridge and on two temporary supports. The central segment, or pier module, is supported as a two-span beam on the central pier of the bridge and the two temporary supports. The three components were precast concrete, and each contained ducts for the later insertion of post-tensioning tendons. The end segments were pretensioned so that they could support their own weights plus the weight of a cast-in-place composite deck without cracking. The central segment was precast, reinforced concrete in the full-size structures, but Model 1 had a small

amount of pretensioning in addition to the reinforcing bars in order to limit tensile stresses which occurred during post-tensioning.

After the three segments were placed on the piers, the post-tensioning ducts were jointed, the composite deck was cast, and the joints were concreted, as shown in Fig. 1.5.

Post-tensioning strands were then placed in the ducts and stressed. This had the effect of completing the structure by establishing continuity between the three segments.

Immediately after the post-tensioning was completed, the temporary supports were removed, and the structure was then complete and appeared as in Fig. 1.6. The post-tensioning forces tend to lift the structure free of the temporary supports, and in the test girder the temporary supports were completely unloaded. In the first field structure and in the laboratory model, the supports were not completely unloaded, and the structures were lifted slightly with jacks to remove the shimming so that the temporary piers could be removed.

The joints in all of the structures contained some reinforcing bars, and a number of different details were used in the different structures. This steel has some influence on the final behavior of the structures, and is discussed later.

Model 2 appeared quite similar to Model 1, but the concept of the structure was different. Model 2 was constructed without post-tensioning. The three segments were placed on temporary and permanent piers in exactly the same way as was described earlier. However, in this case the segments were heavily pretensioned to resist all of the final design forces, with the assistance of the deck reinforcement in the areas to be subjected to negative moments.

The joints were reinforced with Grade 60 ($f_y$ = 414 N/mm$^2$) reinforcing bars which were anchored in the segments and extended into the joint areas. These bars were then joined end-to-end by Cadweld* Splices, and these spliced bars then provided all of the positive moment capacity existing at the joints. The segments with the spliced bars are shown in Fig. 1.7.

---

* Trademark of ERICO, Inc., Cleveland Ohio.

After the splices were completed, the deck and joint concretes were cast, and the bridge appeared as in Fig. 1.8; the structure was hardly distinguishable from the post-tensioned version.

After the deck and splice concretes were adequately cured, the temporary supports were removed. In this case the structure had to be lifted free of the shimming, and in the laboratory this was done using a hydraulic jack. The temporary piers were then removed, and the structure was then a two-span bridge such as is shown in Fig. 1.9.

In this structure, there is total dependence on the splices made in the reinforcing bars in the joints. The characteristics of the Cadweld Splices used are discussed in Sec. 6.4 of this report.

## 1.3 Acknowledgements

This work was conducted as part of the Illinois Cooperative Highway and Transportation Research Program, Project IHR-3-3, "Field-Made Joints in Prestressed Reinforced Concrete Highway Bridge Girders," by the Department of Civil Engineering, in the Envineering Experiment Station, University of Illinois at Urbana-Champaign, in cooperation with the Illinois Department of Transportation and the U. S. Department of Transportation, Federal Highway Administration.

The contents of this report reflect the views of the authors who are responsible for the facts and the accuracy of the data presented herein. The contents do not necessarily reflect the official views of or policies of the Illinois Department of Transportation or of the Federal Highway Administration. This report does not constitute a standard, specification or regulation.

# 2. DESIGN AND CONSTRUCTION OF MODELS

## 2.1 General Description of Models

### 2.1.1 Model 1

Model 1 was an approximately 1/3-scale model of a prototype. A single girder and contributory deck compose the two-span model bridge. Three precast girder segments were spliced together to form one continuous girder. The continuous two-span bridge was supported on rollers near each end and rested on a hinge support at the center pier. Figure 2.1 gives the overall dimensions of Model 1, and a more detailed view of the supports is given in Fig. 2.2. Cross sections and elevations of the girder and deck are shown in Figs. 2.3 to 2.8. Additional details are given in Figs. 2.9 to 2.12.

Each girder was pretensioned and cast separately. Upon completion of a seven day curing period, the forms were stripped and the pretensioned cables cut. The two end girders were then each placed so that one end rested on a permanent roller support, and the other end rested on a temporary support. Finally, the center girder rested on these temporary supports and on the hinged support at the central pier.

Establishing continuity of the three girders was the next objective. Two continuous post-tensioning tendons provided the primary means of continuity. Seven 3/8 in. (9.5 mm) diam strands ran the entire length of the model in each of two ducts. Post-tensioning was done after the splices and deck were cast and cured; seven days later the ducts were grouted.

### 2.1.2 Model 2

Except for minor variations in length, the overall dimensions of Model 2 are the same as Model 1, as are the support conditions. Girder and splice lengths, as well as cross-sections of the girder and deck are given in Figs. 2.13 to 2.19. Additional details are given in Figs. 2.20 and 2.21.

The major difference was that Model 2 contained no post-tensioned reinforcement. Each segment was heavily pretensioned, and the splices were reinforced by six #7 (22.2 mm diam) deformed Grade 60 (414 $N/mm^2$) reinforcing bars, located in the bottom flange of each girder and extending into the splice area, as shown in Figs. 2.15 and 2.21. The bars extended to within 3/16 in. (5 mm) of each other and were connected together by the process of Cadwelding. Some details of the splices are shown in Figs. 2.22 and 2.23. Their behavior is discussed in Sec. 6.4. Finally, the splice area was filled with concrete at the same time as the deck was cast.

## 2.2 Design of Model Structures

### 2.2.1 General Remarks

If the models had been direct geometric scale models of a particular prototype, there would have been little design work involved. All linear dimensions would have been reduced by the same scale factor, and all area dimensions by the scale factor squared. Some work leading to reasonable compromises between the required steel area and the area obtainable using available strand and reinforcing bar sizes would have been necessary.

In addition, some analysis would have been required to find an optimum system of dead load compensation, since the dead load moments scale at different rates than areas and section modulus values.

The two models were conceptual scale models rather than direct scale models. That is, they were designed and built in the same way as a prototype structure but they were not accurate models of any particular prototype.

Several different criteria were used to obtain model structures which would be expected to behave approximately the same as the prototypes when subjected to loads and overloads. The materials in both were assumed to be of the same quality. The basic design provisions were that the average

prestress, $F_{se}/A$, and the precompression stress at the tension face under dead load (including the dead load compensation) should be about the same in both model and prototype at various critical sections. Considerably less attention was paid to trying to match compressive stresses in sections subjected to compression from live load, and a close agreement would have been impossible in any event since the model and prototype sections were not geometrically similar.

Once the precompression was determined for the maximum positive moment section, the allowable moment, when $f_t = 6\sqrt{f'_c}$ tension, was calculated. Both $f_t$ and $f'_c$ have units of lb/in.$^2$. (In S. I. units, $f_t = 0.5\sqrt{f'_c}$, where both stresses are in N/mm$^2$.) Using this moment, a "design vehicle" loading was found. This three-axle vehicle, as shown in Fig. 3.1, was then moved along the structure and moment and shear envelopes were constructed so that proportioning of the rest of the sections could be done.

This vehicle, which effectively includes the impact force, was used with the appropriate load factors from the 1969 and 1973 AASHTO Specifications (2, 3)* in checking the required ultimate moment capacities.

Concretes with compressive strengths of $f'_c$ = 6,000 and 3,500 lb/in.$^2$ (41 and 24 N/mm$^2$) were assumed for the girders and decks, respectively. The pretensioning and post-tensioning were done using Grade 270 7-wire strand, 3/8 in. (9.5 mm) in diam, which has a minimum breaking stress of 270 k/in.$^2$ (1860 N/mm$^2$). All reinforcing bars were ASTM A-615, Grade 60, which has a minimum specified yield stress of 60 k/in.$^2$ (414 N/mm$^2$). All material strengths exceeded the specified minimum values, and the measured values are given in Sec. 2.3.

### 2.2.2 Model 1 Design

The design process basically followed the same sequence as was used for construction, and followed the requirements of the 1969 AASHO Specification (2). Each segment was first designed to support its dead

---

* Numbers in parentheses refer to entries in the list of references.

load, the supplementary dead load from the large concrete weights, and the deck, assuming that the precast girder section carried all moments and shears while supported on the temporary and final supports, as shown in Fig. 2.1. The bending moment diagram for half the structure, for conditions immediately after deck placement and including the supplementary dead load, is shown in Fig. 6.1.

The end segments were pretensioned so that the full dead load (with temporary supports in place) produced approximately zero stress at the bottom at midspan of the segment. Only a relatively small amount of pretensioned steel was required, and all strands were straight. It appears from experience with this model and the prototype (1), and a similar structure built in Piatt County, Illinois, that this steel will be about 1/3 of the total prestressed steel area required in the completed structure.

The central segments were designed as precast reinforced concrete beams for two loading conditions. First, considering only the weights of the girder, they were designed so that they could be lifted or supported either by the ends or by the center alone. This was done in the prototype structure so that the members could be handled and transported in any way convenient to the contractor, but it was also recognized that the temporary supports might not all be at the correct elevations. This could lead to moment distributions significantly different than normally computed for a two-span beam

The moments resulting from the deck weight and the supplementary dead load were then found, assuming the beam to be an ideally supported two-span member for this increment of load. Reinforcement for these moments was added to that found previously.

The reinforcement in the bottom of the central segment eventually acts as compression steel at the section over the central pier. Its area is taken into account later when evaluating the ultimate moment capacity of the section, and it may then be found desirable or necessary to increase its area to control the neutral axis position, and hence the strains in the tension steel, at flexural failure.

The reactions from all dead loads on the two temporary supports were then computed. The bending moments due to the removal of the temporary supports were then computed, assuming these reactions to be applied to the completed two-span structure. Live load moments were added to the moments resulting from support removal, and the stress ranges due to these moments were computed at various sections, and at the top and bottom of the girder and deck. These stresses were added to those existing while the structure was still on the temporary supports, giving a fictitious set of stresses which would exist if the material were able to resist them.

The next step was to find a post-tensioning force and profile such that all of the concrete tensile stresses would be reduced to values within the allowables, without at the same time exceeding the allowable compressive stresses. The post-tensioning force can be thought of as producing three separate stress effects (two primary and one secondary) at any given section, and the designer has some control over their relative values through the selection of the cable profile.

One primary effect of the post-tensioning is the introduction of a uniform axial compression in the member, with the value of $F_{se}/A_{comp.}$, where $F_{se}$ = Post-tensioning force at section considered, and $A_{comp.}$ = Transformed area of composite section. (For the normal bridge situation, the deck and girder concretes have different values of $E_c$, and the deck concrete is replaced by some equivalent area of material having the same $E_c$ as the girder before $A_{comp.}$ is found.) The second primary effect is the introduction of a bending moment related to the eccentricity of the tendon from the center of gravity of the transformed section. The moment may be expressed as $F_{se}(e)$, where e is the eccentricity at the section considered.

The third effect is that due to secondary moments induced in the structure by the post-tensioning forces. Although these forces are called secondary moments, they may be either small or large, and they depend on the cable profile along the entire length of the structure. The secondary moments may be calculated using methods and aids presented by Khachaturian

and Gurfinkel (4) if it can reasonably be assumed that the tendon force is constant along the length of the member, or by more basic methods such as were presented by Fadl (5) if the friction between tendons and ducts must be taken into account.

In terms of stresses in the concrete, these three components may be combined into the following equation:

$$f_{c_{post\text{-}tens}} = -\frac{F_{se}}{A_{comp.}} \pm \frac{F_{se}(e)y}{I_{comp.}} \pm \frac{M_{secondary}(y)}{I_{comp.}}$$

where $I_{comp.}$ = Moment of inertia of transformed section,

$y$ = Distance from center of gravity of transformed section to fiber considered; and

$M_{secondary}$ = Secondary moment at section considered.

Compression has been taken negative and tension positive.

The designer's task was then to find a tendon force and profile that would result in stresses within the allowables both when the structure was subjected to dead load plus service live load and when subjected only to dead load. Initially the critical sections at the central pier, at the splices, and at the region of maximum positive moment were considered, and other sections were checked later.

In this structure, tensions due to positive moments in the span were serious problems, and the tendons were intentionally placed with large downward eccentricities through much of the span, and then raised very high in the section near the central pier. This resulted in large positive secondary moments, which added to the precompression in the deck over the central pier, but somewhat reduced the precompression at the bottom of the girder in the positive moment regions. The secondary moment at the central pier was so large that tensions were induced in the lower flange at that section under dead load alone, and the four 3/8 in. (9.5 mm) diam strands shown in Fig. 2.8, Sec. 4-4, were added as pretensioned steel in the pier module in order to control this stress. Without this steel, stresses as high as 500 lb/in.$^2$ (3.5 N/mm$^2$) tension would have existed at sections 7 ft from the

central pier immediately after post-tensioning. This was a quirk of the model girder, which had a lower flange which is relatively undersized when compared with the prototype described in Ref. 1.

The strengths of the sections were then checked against the required ultimate moments. All sections were adequate with the reinforcement used for the stress design proportioning. The negative moment capacity was computed taking into account all of the bonded reinforcing bars existing in the deck and the top of the girder as well as the post-tensioned reinforcement, and the steel in the bottom of the girder was considered as compression steel. The post-tensioning ducts were grouted after stressing, and it was assumed that the tendons had adequate bond. If the negative moment capacity had not been adequate, additional reinforcement would have been placed in the deck in the region over the central pier.

### 2.2.3 Model 2 Design

The design of Model 2 proceeded somewhat differently than that of the first model since there was no post-tensioning force and hence no secondary moment. The absence of the secondary moment allowed the design to be done more directly. The design met the requirements of the 1973 AASHTO Specifications (3) in so far as they applied to the structure.

Using the same design vehicle as for the first model, live load moment and shear envelopes were constructed. An equivalent to the AASHTO lane loading was not considered although it should have been. Consequently the negative moment section was proportioned for a live load moment somewhat less than it should have been, and this oversight had some influence on the behavior of the structure under load.

The dead load moment diagram for the structure was computed in the same way as for the first model, considering first the structure supported on both final and temporary supports and then adding the moments caused by removal of the temporary supports.

Once the dead and live load moments were known, only the proportioning of the reinforcement at the various sections for these moments

remained. Because of the complex nature of the structure, the design criteria deserve special comment.

The maximum positive moment regions, near the middle of the end segments, are relatively simple pretensioned sections. The design process was basically to find a pretensioning force so that the allowable tensile stress at the bottom of the section would not be exceeded under dead plus live loads. The entire pretensioning force had to be resisted by the precast girder, and the girder section had to support those dead load moments existing after the dead load compensating blocks were hung on the beam and after the deck was cast, but while the temporary supports were still in place. The moments due to the removal of the temporary supports and due to the live loads were resisted by the full composite section.

In the model, the pretensioning required for the final moments induced unacceptably high tension at the top of the end segment girders since the dead load of the girder alone was relatively small. In order to control these tensions, the end segments were post-tensioned externally near the top of the section while the girders were still on the prestressing bed, before the straight strands were cut. After the segments were in place on the piers and part of the dead load compensating blocks were hung in place, the external post-tensioning was removed.

In a prototype, the dead load of the end segment girders would probably be large enough to eliminate the tension at the top of the section, but that is an aspect of the design that would have to be checked for each particular structure.

The splice section contains no prestressed reinforcement, and consequently was designed as a reinforced concrete section. The design was done by using ultimate strength principles, and the AASHTO load factors were applied to the live and dead load moments to obtain the design moment. The bars in the splices were all joined by Cadweld splices. The area of reinforcement at the splice was selected assuming that the spliced bars were fully effective.

The #7 bars (22.2 mm diam) in the splice were continuous through the length of the center segment of the structure. They extended into the end segments by about the development length of the strands, considering recommendations similar to those of Ref. 6, and the six bars were terminated in pairs rather than all at one section to minimize stress concentrations at the cut-off points.

The negative moment section over the central pier was the subject of considerable study, as there are no design criteria which are particularly suited to a composite section in which the cast-in-place concrete is on the tension rather than compression face of a precast, pretensioned member. In the end, the section was proportioned in two steps. The pretensioning in the girder was selected so that the computed tensile stress at the top of the girder was about 6 $\sqrt{f'_c}$ (0.5 $\sqrt{f'_c}$ N/mm$^2$) when the structure was subjected to service dead and live loads. The full composite section of girder plus deck was considered for this computation.

The use of this section was an error in judgement, as it later turned out, since the deck stresses were much higher than the tensile strength of the concrete and the deck concrete was consequently cracked and useless for resisting tension when the service load was reached. A more reasonable section would have been a transformed section comprised of the girder plus the deck reinforcement, suitably transformed into equivalent concrete. This section would have required somewhat more pretensioned reinforcement, but a redesign has not been pursued to determine how great the difference would have been.

The section was then proportioned for the ultimate moment computed considering the AASHTO load factors. The pretensioned steel in the girder was considered, and some reinforcement was added to that already supplied in the deck to make the negative moment capacity adequate. The bonded reinforcement in the bottom of the girder was taken into account as compression reinforcement.

### 2.2.4 Design for Shear

The proportioning of the shear reinforcement was done after the flexural design had been completed, for both structures. The ultimate shear

envelopes were constructed considering the load factors in the 1973 AASHTO Bridge Specifications, and the shear resistance of the structure was evaluated using the methods and equations from the 1963 ACI Code (7). The almost-similar 1971 ACI Code (8) was not used because of the omission of a d/2 term in the flexure-shear equation (Eq. 11-11) that reduced the generality of the expression, and increased the amount of shear reinforcement that would be required.

Two different concepts of shear failure were considered. A flexure-shear failure is a shear failure in which the critical shear crack is an extension of or is triggered by a flexure crack, and consequently the shear force at failure of an unreinforced web is closely related to flexural cracking at the section considered. Web-shear cracking is cracking which is initiated when the principal tensile stress in the beam web, in a region remote from flexural cracks, reaches the tensile strength of the concrete. The shear capacity of the concrete was taken as the lower of the flexure-shear or web-shear cracking loads.

Once the shear capacity of the concrete had been determined, web reinforcement in the form of stirrups was proportioned to carry all of the shear force in excess of that resisted by the concrete. Since the web of the beam, at 4 in. (100 mm) thick, was relatively heavy compared to that of the prototype, the shear capacity of the concrete was relatively high and the maximum stirrup spacing requirements governed most of the length of the beams.

Extra stirrups were provided arbitrarily at the ends of each segment to help insure that the splices would not be the controlling sections if the structures were subjected to realistic moving loads. Extra stirrups were also added at the outer ends of the structure to provide resistance against anchorage zone cracking.

The equations used in evaluating the shear resistance of the concrete sections are given in detail in the report on the prototype structure (1). The background of the provisions in the ACI Codes is presented in Ref. 9.

## 2.3 Materials

### 2.3.1 Concrete - Models 1 and 2

The concrete used in the beams and splices was made in the laboratory at the Civil Engineering Building. The deck concrete was ordered from a ready-mix plant. Design strengths for the beams and splices were 5000 lb/in.$^2$ (34 N/mm$^2$) at seven days and 6000 lb/in.$^2$ (41 N/mm$^2$) at twenty-eight days. A twenty-eight day strength of 3500 lb/in.$^2$ (24 N/mm$^2$) was needed for the deck concrete.

Type III cement, high-early strength, was used in the beam and splice concretes. Type I cement was used in the decks. The aggregates in the concrete made in the lab consisted of Wabash River Valley sand, and crushed limestone with a maximum size of 3/4 in. (19 mm), while the maximum aggregate in the ready-mix concrete was 1-1/2 in. (38 mm). The effective water-cement ratio was actually somewhat less than the 0.59 value indicated in Tables 2.1 and 2.2 since dried aggregates used in the lab mixed concrete absorbed some of the mix water. The effective water-cement ratio was about 0.50. Tables 2.1 and 2.2 contain the concrete mix data and strength data for Models 1 and 2, respectively. The difference in slump between the beam and splice concrete in both models was unexpected, because the mix was supposed to be the same.

Problems were encountered in both models with the deck concrete setting too quickly. The Model 1 deck was poured continuously from one end of the bridge to the other. By the time the workers got to the middle of the bridge, a period lasting approximately fifty minutes, the mix had undergone initial set. It was necessary to vibrate the concrete just to get it out of the drop bucket, therefore, water was added to facilitate the process.

For Model 2, the process was changed slightly. Casting began at each end and worked toward the middle. Again, by the time the central portion of the bridge was reached, the mix had undergone initial set. This time water was not added and finishing was carried out as well as could be expected. In this model, the regions where compression in the deck was

critical had well consolidated and finished concrete. In both cases, the deck concrete cylinder strengths may not accurately represent the actual deck strength.

Each beam required three batches of concrete, and six cylinders, each 6 in. by 12 in. long (150 x 300 mm) were made for each batch. Twelve test cylinders were made from both the splice and deck mixes. The cylinder concrete was consolidated with an internal vibrator. The rough end of each cylinder was capped with a sulfur-based capping compound. Compression tests, using a Riehle 300,000 lb (1330 kN) machine,were performed on cylinders from each beam, splices, and deck, at the following times: a) seven days after casting, b) about the time of starting testing, and c) upon completion of testing. Only the failure load was recorded for the 7-day strength. Strains as well as stresses were recorded for the last two tests. During the strength tests, the cylinders were loaded at a rate of about 100 kips (450 kN) per minute. A slightly slower speed was required when reading strains. Typical stress-strain curves for Model 1 beam and Model 2 deck concretes are shown in Fig. 2.24.

### 2.3.2 Prestressing and Post-tensioning Strands

The strand used in all prestressing and post-tensioning for both models was 3/8 in. (9.5 mm) diam, ASTM A-416, seven wire prestressing strand, stress relieved, grade 270. Two specimens from the single reel of strand were tested and reached ultimate stresses of 274 and 277 k/in.$^2$, (1890 and 1910 N/mm$^2$), respectively. See Fig. 2.25 for the stress-strain curves. Strains were measured on a 24 in. (610 mm) gage length. Neither sample failed within the 24 in. (610 mm) gage line, and reliable ultimate elongation readings were not obtained. Young's modulus for the strand was 28 x $10^6$ lb/in.$^2$ (193 kN/mm$^2$).

### 2.3.3 Post-tensioning Ducts in Model 1

The two ducts, except for the last 18 in. (450 mm) at each end, were made of 1 1/2 in. (38 mm) O.D. galvanized steel electrical conduit

with a wall thickness of 1/16 in. (1.6 mm). The conduit was bent in the lab to coincide with the fourth degree curves that comprised the shape of the post-tensioning cables (See Figs. 2.10 and 2.11). Each conduit contained seven 3/8 in. (9.5 mm) diam strand.

Figure 2.11 shows details of the end sections of the duct. A 1 1/2 in. (38 mm) conduit would not leave enough room to post-tension and anchor seven cables. For that reason an 18 in. (450 mm) long cone, spreading from 1 1/2 in. (38 mm) diam at the conduit end to 4 1/2 in. (114 mm) at the beam end, had to be installed. Flush with the beam end, two 9 in. (230 mm) square bearing plates were cast into the beam. The cone fit into a 4 1/2 in. (114 mm) diam hole in the bearing plates, and was then welded to the bearing plates and duct. A #4 (13 mm diam) rebar spiral surrounded the connection between duct and cone in order to prevent the conduit from bursting under the cable forces. Finally, each cable passed through a 7/16 in. (11.1 mm) diam hole drilled at a 1.9 in. (48.3 mm) radius in the anchor plate, where they were anchored with strand grips normally used to anchor pretensioned strands. With this spacing it was possible to fit the post-tensioning equipment around the cables.

### 2.3.4 Grout

Grout was used to fill the post-tensioning ducts in Model 1. The initial mix, Batch I (see Table 2.1), had a water-cement-sand ratio of 1:2:2, by weight. As outlined later in Sec. 2.4.9, problems were encountered with sand plugging up the bulkhead cone and pump hose. Batch I was used only for the west half of the upper duct.

Another mix, Batch 2, was made. This mix contained no sand. It was intended to flow easier and not plug the hoses. Batch 2 was used for the east half of the upper duct and the entire lower duct.

The aluminum powder in both mixes was intended to prevent shrinkage of the grout, and provide a small expansion.

Strength tests were run on cylinders made from the grout (see Table 2.1). The discrepancies between the 7-day and 28-day strengths for both Batch 1 and Batch 2b were unexpected and remain unexplained.

## 2.4 Construction Process

### 2.4.1 (a) Pretensioning the Girders - Model 1

Each girder was pretensioned individually. The prestressing bed consisted of wood forms, steel bulkheads, and massive concrete abutment blocks aligned as shown in Fig. 2.26. The prestressing strands were strung through a jacking chair, the stressing bulkhead, beam end-forms and on through the girder to the other end. Holes drilled in the bulkheads positioned the prestressing strands properly. Since all strands were straight in Model I, no mechanical hold-downs or hold-ups were needed.

As soon as all strands were strung, they were secured at each end by strand grips. Jacking was done from one end and calibrated aluminum load cells on each strand were read at the other end. The load cells consisted of aluminum tubes with a four-arm bridge of resistance strain gages.

First, the strands were hand-tensioned to remove the slack, and the strand grips were locked in place. Next, zero readings were taken on the load cells just prior to stressing the strands.

Prestressing was accomplished using an incremental loading pattern. First one strand was stressed to a fraction of its design value (189 k/in.$^2$ [1300 N/mm$^2$] or 16.1 kips/strand [71.6 kN/strand]), and then another strand was stressed to the same value, and so on, until all strands were stressed approximately the same. The order of stressing used kept eccentricity of loading to a minimum. This process was continued several times until all strands were at or very near their design values, see Table 2.3. This incremental process was used because the stressing bulkheads were so flexible that stressing one strand had a significant effect on the force in the previously stressed strands.

Dates of casting and grouting and dates and ages at failure tests are shown in Table 2.5.

### 2.4.1 (b) Model 2 Pretensioning

Other than the variation in number and position of strands, as is shown in Figs. 2.16 to 2.19, the only difference from Model 1 was that some

strands were draped. To facilitate the change in slope, mechanical hold-downs and hold-ups were placed in the stressing bed to run the strands through. The hold-downs were anchored through the floor. Hold-ups were connected by a rod to a double-channel beam above the girder. The channel beam rested on concrete blocks which also provided lateral stability to the formwork. The hold-up equipment is shown in Fig. 2.27. The final values of the prestressing forces are given in Table 2.4. Dates and ages at key events are shown in Table 2.6.

### 2.4.2 Nonprestressed Reinforcement in the Girders

All longitudinal reinforcement in Model 1 was straight. The #7 (22.2 mm diam) bars in the bottom flange of the center beam and the #3 bars in the top flange (Fig. 2.6) ran the entire length. In the end beams, the top reinforcement consisted of two continuous #5 bars (15.9 mm), while the bottom reinforcement, five - #7 bars (22.2 mm diam), was cut-off 6 ft-3 in. from the splice end of the girder. The #7 bars (22.2 mm diam) from both the end beams and center beam extended 13 in. (330 mm) into the 15 in. (380 mm) splice, as did the top reinforcement.

Stirrups were bent from #3 (9.5 mm diam) reinforcing bars and intentionally left sticking two to three inches above the beams in order to serve as shear connectors with the cast-in-place deck. A typical stirrup is shown in Fig. 2.8.

All longitudinal rebar reinforcement in Model 2 was also straight. Cross-section and side views are given in Figs. 2.15 and 2.17 to 2.20. The cut-off points for the #7 bars (22.2 mm diam) were staggered. This was to reduce stress concentrations at the cut-off points and discourage a failure at these sections. Also, the #7 bars (22.2 mm diam) were extended alternately 6 in. (150 mm) or 14 in. (355 mm) into the splice, as can be seen in Figs. 2.21 and 2.22. By staggering these bars, the process of Cadwelding could be done easier, and the splices were not all at exactly the same section.

A typical stirrup and the spacings are shown in Figs. 2.19 and 2.20, respectively. Fig. 2.18 shows six pieces of auxiliary reinforcement spaced at 6 in. (150 mm) near the ends of each beam. This reinforcement was required by the AASHTO Specification (3).

Deck Steel - All reinforcement used in the decks of both models was #3 bar (9.5 mm diam). The slab cross-section for Model 1, with steel included, is shown in Figs. 2.4 and 2.5. The deck steel arrangement for Model 2 is given in Fig. 2.14. The only difference between the two models as far as deck steel is concerned is that Model 2 required extra negative moment steel that extended 10 ft (3.05 m) either side of the central pier. Model 1 had the post-tensioned steel, which combined with the deck steel to provide an adequate ultimate moment capacity.

The steel in both the beams and deck was tied with #14 (2.0 mm diam) gage black annealed wire. The deck steel had to be lapped no less than 15 in. (380 mm). The laps were tied with wire.

### 2.4.3 Casting of the Beams

The formwork consisted of oiled plywood framed with 2 in. by 4 in. (50 by 100 mm nominal) boards. Before the beams were cast, slump tests were performed and test cylinders made of the concrete, which was mixed in the lab. Each beam was formed and cast individually, as only one set of forms was available. Casting and curing took place in the air conditioned laboratory. Three identical batches were needed for each beam plus test cylinders.

The concrete was poured from a bucket and consolidated by two electrical internal vibrators. A rough finish was left on the top face of each beam to insure better bond between beam and deck. Wet burlap and plastic were placed around the beams several hours after casting. The beams were allowed to cure until test specimens showed a compressive strength of 5000 (35 $N/mm^2$) psi, at about seven days. At this time the forms were removed and the prestressing force released.

### 2.4.4 Release of Prestress

In Model 1, the prestressing cables were cut by use of an acetylene torch. An effort was made to cause a gentle failure of each strand by gently heating it over a length of several inches before causing fracture. The strands were cut in an established order so as to minimize eccentric loading. Each strand was cut on the opposing ends of the beam. Next, the matching strand on the other side of the cross-section centerline was cut. Using this method, no more than a small unbalanced force occurred at a time.

In Model 2, the strands were also cut with an acetylene torch. Even with the precautions mentioned above, a few wires were broken in the grips of certain cables when entirely different cables were cut.

The general procedure for cutting the cables in Model 2 was as follows:

1) The draped strands were cut first. The procedure described in Model 1 was used.
2) For the end segments only, external prestressing was applied by a pair of threaded rods with end bars which were fitted near the top of the beam. The nuts were tightened until a prestressing force of approximately 30 kips was reached. This external prestressing was applied to prevent tensile cracking of the top flange after the bottom straight strands were cut and before the external dead load weights could be hung. No external prestressing was applied to the center beam; the stresses along the bottom flange were at a safe level.
3) The draping point hold-downs and hold-ups were released.
4) The straight strands were cut in a similar manner to that in Model 1.

Overall, this gentle release manner was successful. A few short, very narrow, horizontal anchorage-zone cracks occurred in the webs near the ends of some Model 2 segments, and these did not cause any problems.

2.4.5 Additional Dead Load - Models 1 and 2

After each beam was placed on its temporary supports, weights of approximately 3,400 pounds (1540 kg) each were hung from the top of the girder. The weights consisted of 48 by 30 by 28 in. (1220 by 760 by 710 mm) concrete blocks. Due to their size and the position of the central pier and two temporary supports, the spacing was not quite uniform. Between supports the blocks were spaced at three feet. Each end beam held seven weights and the center beam supported six weights, for a total of twenty. The spacings are shown in Fig. 2.28.

The purpose of the concrete blocks was to simulate additional dead load stresses of the girders, and they were necessary since the dead load moments in the model are reduced by different factors than are the cross-sectional properties such as the section modulus.

In a model in which all dimensions are reduced by the same scale factor $\lambda$ ($\lambda \approx 1/3$ in this model), the cross-sectional area and consequently the dead load per unit length are reduced by $\lambda^2$, assuming the material densities are the same in the prototype and model. The span also is reduced by $\lambda$, and since the dead load moment is proportional to the span squared, the dead load moment in the model is reduced by $\lambda^4$ from that of the prototype.

However, the section modulus, I/c, relating moment to stress through the definition of stress in flexure, $\sigma = \frac{Mc}{I}$, is reduced only by a factor of $\lambda^3$ in the model. Hence the dead load stress in the model is $\lambda$ times that in the prototype, and the dead load moment of the model must be increased by a factor of $1/\lambda$ if the stresses are to be the same as in the prototype. The series of concrete weights provided the additional dead load moment.

It can be shown that the stresses due to prestressing are the same in the model as in the prototype. It can also be shown that, in order to produce the same stresses in a model, a prototype concentrated load must be reduced by $\lambda^2$ before application to the model, a uniformly distributed line load (lb/ft) by $\lambda$, and a uniformly distributed area load ($lb/ft^2$) remains the same on model and prototype.

Reduction of all dimensions by the scale factor results in reducing cross-sectional areas of both concrete and reinforcement by $\lambda^2$, so that the reinforcement ratios, $\rho$, are the same in model and prototype.

2.4.6 Cadwelding Process - Model 2

To provide continuity in Model 2, the #7 (22.2 mm diam) reinforcing bars had to be joined in the splice area. The process used to splice the bars is called Cadweld Rebar Splicing.*

The three girders were placed on their temporary and permanent supports so that a 3/16 in. (5 mm) gap occurred between the protruding #7 bars. These bars were alternatively extended 6 in. (150 mm) and 14 in. (355 mm) from the ends of the girder. A confined working area made this staggering of splice points necessary, and the stagger is also helpful in limiting crack sizes (10).

The ends of the rebars must be free of rust, loose mill scale, dirt, or any other foreign matter. Cleaning must be continued back from the bar end 2 in. (50 mm) beyond where the end of the bar sleeve will be located. A wire brush serves this purpose well, and sand blasting is an excellent method.

The rebar ends must be flame dried with an oxy-acetylene torch to remove all moisture and/or burn away any other foreign matter. The flame should be soot free and not leave any residue or deposits on the bar ends.

The process used for horizontal splicing of rebars is outlined in detail in Appendix A. For #7 bars (22.2 mm diam), a 5 in. (127 mm) long hollow splice sleeve with an inside diameter of 1 1/8 in. (28.6 mm) and an outside diameter of 1 5/8 in. (41.3 mm) is placed so that a 1/2 in. (12.7 mm) diameter tap hole in the side of the sleeve is aligned directly with the 3/16 in. (5 mm) gap. The sleeve is composed of AISI-C1026 steel The sleeve is shown in Figs. 2.22 and 2.23.

---

* A process developed by Erico Products, Inc., Cleveland, Ohio.

When the apparatus described in Appendix A is set up, the powder is ignited. The powder contains iron oxide, finely ground aluminum powder, and fluxing agents. Upon ignition, the powder produces a molten metal which flows through the tap hole in the splice sleeve into the gap between the bar ends and into the space between rebars and splice sleeve, as shown in Fig. 2.22. The filler metal is basically a low carbon iron, with the carbon being introduced from the graphite crucible shown in the pictures in Appendix A.

The Cadweld splice is a mechanical splice rather than a weld, in spite of the name. The force from one bar is transmitted by mechanical bond or interlock to the filler metal, and then to the sleeve. The deformations on the bar and the grooves machined on the inside of the sleeve provide the necessary roughness. There is no welding involved, except possibly some accidental welding in the gap between the bar ends, but this is of no real consequence because the filler metal is relatively weak in tension.

Cadweld splices are supplied for a number of different design applications. The sleeves used in the construction of Model 2 were full-tension splices. That is, they were designed to develop the full strength of the bar, or a minimum stress in the bar of 90 k/in.$^2$ A slightly different splice might be supplied if the design value were 125 percent of the yield stress, and a considerably different splice can be supplied if the bar is subjected only to compression. This splice allows effective bearing splices even with shear-cut bars.

A spliced bar may fail in tension by one of three modes. The bar may fail at a section away from the splice sleeve. The bar may pull out of the sleeve, or the sleeve may break at the reduced section at the middle where the fill-hole is located. A full-tension splice for a Grade 60 bar is designed to develop a minimum of 90 k/in.$^2$ The failure that occurs in a test will depend on the actual strength of the bar and on the exact details of the deformations on the bars, though the length of the sleeve has been selected to insure that the desired stress can be developed

without a bar-pullout even with the least favorable deformation pattern produced, and with deformations missing as may occur at a mill-mark.

Some information of the stress-deformation characteristics of bars with Cadweld splices has been published (10), and information on the statistical distribution of strengths of tension specimens is presented in Ref. 11. The stress-strain characteristics of the splices used in the model are discussed in Sec. 6.4.

### 2.4.7 Casting of the Deck and Splices

Casting of the deck and splices for Model 1 occurred before post-tensioning and grouting. Casting for Model 2 occurred after the rebars were spliced. Deck forms consisted of oiled plywood forms fitted against the girders and braced with 2 by 4 in. (50 by 100 mm) wood, metal rods, and steel brackets. The splices were formed on the bottom and sides by fitted plywood pieces connected by form ties. A hole, 1 1/2 in. (38 mm) in diameter, was cast into the deck at every position directly above the holes in the lab floor. This was to allow loading rods, used in the testing phase, to pass through the floor and deck.

Concrete, mixed in the lab for a 7-day design strength of 5000 psi (35 $N/mm^2$) was placed in the splice area first. A hand held electric vibrator consolidated the concrete into place. Several minutes later the ready-mix concrete, with a 28-day design strength to 3500 psi (24 $N/mm^2$), was placed. As mentioned in the "Materials" section, the deck was cast from one end to the other in Model 1, as opposed to Model 2, where the deck was cast from the two ends toward the middle. The problems encountered with the concrete setting up too quickly were spelled out in "Materials". The deck above the central pier was not as structurally sound as that near the end of the model. Wooden screeds were used to strike off the top surface of the deck after the concrete had been consolidated.

The slab and forms were covered with wet burlap and plastic the same day and allowed to cure for one week. At this time the test cylinders

were broken to insure adequate strength, followed by removal of coverings and forms. Nine days later, jacks were used to lift Model 2 so that the temporary supports could be removed.

2.4.8 Post-tensioning - Model 1

Two continuous post-tensioning ducts, containing seven 3/8 in. (9.5 mm) strands each, ran the entire length of the bridge (see Fig. 2.1). Fig. 2.11 shows the combined center of gravity of the ducts relative to the bottom fiber of the beams. The ducts rested on small two-arm stands spaced throughout the beam and were also tied to the stirrups.

The seven strands were threaded through each conduit as a unit. Then a load cell and strand chuck was placed on one end of each strand. On the other end was a strand chuck, a U-shaped loading frame, jack, and a second strand chuck.

The prestress losses of concern were mainly the "short-term" losses, at this stage. These included friction losses, elastic shortening losses, and anchor-set losses.

The strands were pulled from one end and the load was measured at the opposite end. Due to curvature of the cables, friction occurred between the sliding cables and the surrounding ducts. The loading frame and jack had to be switched to the other end and the cables were pulled again so that the stresses in each cable were symmetric about the center line of the bridge. That is, all strands were post-tensioned from both ends.

The equation used in finding the friction losses was (6-5), pg. 175, Ref. 4. The assumed values of the wobble coefficient, K, and the coefficient of friction, $\mu$, were 0.0005 per ft and 0.15, respectively. The actual forces in the cables, at the non-jacking end, averaged 12.7 k (56.5 kN) per strand as compared to the calculated value of 13.7 k (60.9 kN) per strand. Allowing the assumed value of the wobble coefficient to remain the same, the coefficient of friction was then calculated to be 0.225.

As the tensioning of the cables proceeded, one-by-one, the cables that were initially tensioned suffered a loss in prestress due to the elastic

shortening of the beam. These losses can be computed by using equation (6-8), page 177, Ref. 4. For example, for a design force of 16.1 kips (71.6 kN) at the jacking end of the first cable, a pulling force of 16.4 kips (72.9 kN) was required.

When the jack is released, the pulling force of the cable is transmitted to the anchorage device. Before the force is taken up by the anchorage device, some amount of slip occurs, causing a loss of prestress. Problems were encountered as the forces were released from the jack and transferred to the bulkhead by means of strand grips. The forces were dropping from 16.1 kips (71.6 kN) to 12 or 13 kips (53 to 58 kN). As a result, four cables, two from each duct, were repulled to forces of 18.3 kips (81.4 kN). The average force before release was 16.7 kips (74.3 kN); after release the average was 14.4 kips (64.1 kN) (jacking end). Therefore, on the average, 2.3 kips (10.2 kN) of force were lost per cable due to slippage in the strand grips.

After all cables had been tensioned, the bridge had lifted 0.073 in. (1.85 mm) and 0.041 in. (1.04 mm) at the west and east temporary supports, respectively. This was not enough to free the shims on the temporary supports. Four jacks were used to lift the bridge slightly so that the temporary supports could be removed.

### 2.4.9 Grouting - Model 1

An initial mix (Batch I) was pumped into the west end of the upper conduit with a hand pump. Initially water was forced into the conduit to wet the inside. Problems arose due to air leaks and water leaks near the pump due to gaps in the grips, between the plates, and between the strands. Water coming out of the grout flowed back through the grips, and the system jammed on the third charge of the pump. Sand was found firmly backed in the bulkhead cone and the pump hose.

To remedy the situation, the leaks were plugged with sealant and an air hole was drilled through the deck and into the top conduit. A vacuum was placed in this hole while grout (batch 2) was pumped into the

east end of the upper duct. The pump-vacuum combination was able to pull the grout the entire distance (38 ft [11.6 m] from the end to the center line).

For the lower conduit, a pump was set at the east end and a vacuum at the west end, so as to pump the grout the entire length of the conduit. This set-up was inadequate. Seventy-five ft (23 m) was too long a distance to pump this grout mix through a 1 1/2 in. (28 mm) conduit containing seven 3/8 in. (9.5 mm) strands. The pump was switched to the opposite end and grout was pumped in as much as possible to seal off the west end. Figure 2.29 shows the extent of grouting in each conduit, as determined during demolition of the structure after testing was completed.

# 3. INSTRUMENTATION AND TEST PROCEDURE

## 3.1 General Remarks

The instrumentation was generally similar in the two test structures. Strains were measured at many locations using a 10 in. (254 mm) gage length mechanical strain gage. Reinforcement strains were measured at some locations using electrical resistance strain gages attached to the bars before the concrete was cast. Deflections were measured at a few points. Reactions at the two ends of the structure and the applied loads were measured with load cells. The details of the instrumentation are given in the following sections.

## 3.2 Concrete Strain Gages

After the forms were removed, each beam was prepared for application of gage points. The beam was first allowed to become surface dry as the positions for gage points were marked. The contact area was made smooth with a carborundum block, then scrubbed with acetone to remove any dust or other substances.

Micro-Measurement 200 catalyst was applied to the gage points while M-bond 200 was applied to the concrete. Through the use of a spacing bar the gage points were placed 10 in. apart. Pressure was applied against the spacing bar for one minute to assure a good bond.

The gage points were 1/2 in. (13 mm) square by 3/16 in. (5 mm) thick pieces of stainless steel having a 1/8 in. (3 mm) deep tapered hole, drilled with a #1 center drill, in the middle of the square face. The spacer bar had points that fit into the gage point holes, and served to maintain the initial distance between points very close to 10 in. (254 mm) apart.

A 10 in. (254 mm) gage length Whittemore strain gage, which read the change in length in units of 0.0001 in. (0.00254 mm) was used to measure strain. Therefore, the strain ($\Delta\ell/\ell$) was measured to 0.000,01, or $10^{-5}$. The tips of the gage which fit into the tapered holes in the gage points were spherical, and were about 0.09 in. (2.3 mm) diam.

The locations and designation of gage lines are given in Fig. 2.28. The patterns were nearly identical on the two models. Model 1 had three sets of gage lines at the central pier while Model 2 had only two. The layout was symmetrical about the center line of the bridge. The gage lines on the deck and splices were applied several days after casting.

Temperature compensation was provided by comparison of the strain readings with readings on a steel "standard" bar. The relatively heavy steel bar, about 2 in. (50 mm) square, was used so that it would respond to temperature changes slowly and in addition would be so stiff that perfectly uniform bearing conditions would not have to be provided under the bar before repeatable readings could be obtained. Since all of the readings have been taken in the laboratory, temperature fluctuations were small.

The Whittemore strain gage was checked against the "standard" before and after each set of readings. A set of gage readings were taken after each load increment. Readings were always taken at zero load before and after each separate test.

## 3.3 Strain Gages on Reinforcement

Micro-Measurement 1/2 in. (12.7 mm) gage length metal foil strain gages, type EA-06-500 BH-120, were applied to each #7 bar (22.2 mm diam) in both splices in Model 2, for a total of 12 gages. In order to obtain a smooth surface, the deformations in the #7 bars (22.2 mm diam) were filled away, taking precautions not to reduce the cross-section any more than necessary. AE 10/15 adhesive was used to secure gages to steel. To prevent damage during casting, a semi-cured rubber water-proofing compound was wrapped around each gage. All gages survived casting of the concrete.

Four similar strain gages were placed on the deck reinforcement in Model 1. These gages were directly above the central pier, and were distributed across the width of the slab.

## 3.4 Axle Loads and Reactions

A calibrated aluminum load cell was placed above each hydraulic jack to measure the applied loads. The load cells used to measure the reactions consisted of calibrated axially-loaded steel tubes.

The end reactions were measured. Two load cells acted in parallel at the west support and one load cell was used at the east support. Four-arm bridge resistance strain gage circuits facilitated the measurements in both load and reaction cells.

The cells used for load measurements were 6 in. (152 mm) long aluminum tubes which were 2 in. (51 mm) O.D. and 1-1/8 in. (28.6 mm) I.D. Their nominal capacity was 60 kips, (267 KN) and the sensitivities were about 80 to 85 $lb/10^{-5}$ strain (0.36 to 0.38 $KN/10^{-5}$). Four-arm bridge gage circuits were also used on these cells.

The reaction cells had measuring sections which were 3.50 in. (88.9 mm) I.D. and wall thicknesses of 0.10 (2.5 mm) or 0.20 (5.0 mm) in. The sensitivities were about 130 or 270 $lb/10^{-5}$ strain (0.58 or 1.20 $KN/10^{-5}$) respectively. They were also 6 in. (152 mm) long, and were located as shown in Fig. 2.2 (b).

All electrically determined strains (reinforcing bars, load cells, and reactions) were measured by Baldwin Strain Indicators.

## 3.5 Deflection Measurements

Deflections were measured along the center-line of the girders. Locations of the gages are shown in Fig. 2.28. Dial gages with a minimum reading of 0.001 in. (0.025 mm) were used to measure the deflections. During the latter states of testing a steel rule was used to measure deflections relative to the floor.

In addition, elevation measurements were made using a Wild N-3 precise level. The readings were direct to 0.001 ft, (0.305 mm) and were estimated to 0.0001 ft (0.03 mm). The level readings provided the bulk of the deflection data for Model 1. They provided supplementary data for Model 2.

## 3.6 Loading Equipment and Procedures

Each test involved the application of a load representing a three-axle vehicle which was positioned to produce maximum shear or moment at a splice or maximum positive moment in one span. The three axles had relative forces of 4-4-1, as in the AASHTO standard design vehicles. The axle spacing was 3 ft (914 mm) and was determined by the spacing of loading points on the test floor rather than by direct scaling considerations.

Each model was subjected to a series of tests at service load, design ultimate load, and higher overloads, as will be described in the next chapters. The vehicle positions used in the tests are shown in Fig. 3.1 and 3.2 for Models 1 and 2,respectively. The loading positions were used in both spans, but not all loadings were used at all load levels.

Each axle load was applied by two 30-ton (267 KN) center-hole hydraulic rams acting on a spreader beam, as is shown in Fig. 3.3. Different depths of spreader beams were used in different tests, depending on the maximum load level. A section through the test specimen and the laboratory floor is shown in Fig. 3.4, to give an overall view of the scheme. The laboratory floor is actually the top flange of a large box girder, and the test structures were oriented parallel to the box girder webs.

The loads were applied in several increments during each test, with strain and deflection measurements, plus searches for new cracks, after each increment. The four jacks loading the two heavy axles were connected to a common manifold and one hydraulic pump. The two jacks loading the light axle were connected to a second pump. All six jacks were loaded at the same time, and the loads were kept as close as possible to the correct ratios during loading, especially at the higher loads. Both electric and hand pumps were used, depending on load levels and expected deflections.

The magnitudes of the loads used during the design ultimate load tests deserve comment, as their determination was not completely straight forward. In addition, different criteria were used for the two models because the first was designed to meet the 1969 AASHTO Specification, and the second to meet the 1973 version.

The 1969 AASHTO Specification uses load factors as follows:

$$\text{Load Factor} = 1.5\,D + 2.5\,(L + I)$$

where D = Dead load effect,

L = Live load effect, and

I = Impact effect.

The 1973 AASHTO Specification uses lower load factors, as follows:

$$\text{Load Factor (Group I)} = \frac{1.30}{\Phi}\left[D + \frac{5}{3}\,(L + I)\right]$$

where $\Phi$ = Section strength factor, which is

= 1.0 for Flexure in precast prestressed concrete,
= 0.95 for Flexure in cast-in-place post-tensioned concrete,
= 0.90 for Shear in prestressed concrete,
= 0.90 for Flexure in cast-in-place reinforced concrete, and
= 0.85 for Shear in reinforced concrete.

The section strength factor, $\phi$, is intended to account for unexpected deficiencies in the nominal cross-sectional capacities which may occur as a result of material deficiencies or small accidental deviations from the planned dimensions. This factor has been taken as 1.0 in so far as it influences the selection of overloads to be applied to the structure.

It was not reasonably possible to increase the dead load of the test specimen, including the dead load compensation blocks, by 50 or 30 percent, as would be required to meet the AASHTO requirements exactly, so the vehicle loading was increased to partially offset the dead load factor. In order to do this, some particular criterion had to be selected. Shear strength at the splice was considered to be the greatest unknown in both test specimens. Consequently, the applied shear was selected as the controlling parameter, and the vehicle load was selected that would produce the same shear at the splice as would have resulted if the additional dead load had been applied uniformly distributed along the structure, plus the live load factor of $1.30 \times \frac{5}{3}$ $(L + I) = 2.17\ (L + I)$, or $2.5\ (L + I)$.

The service live plus impact load was about 24 kips (107 KN), distributed to the three axles. The design ultimate load, computed as described above, was about 69 kips, (307 KN) for Model 1, and about 55 kips (245 KN) for Model 2, and they are different primarily because of the differences in the load factors between the 1969 and 1973 AASHTO Specifications. There were also small differences in the dead load shears and service live loads.

# 4. RESULTS OF TESTS OF MODEL 1

## 4.1 General Remarks

The results of the tests on the two model structures are presented in this and the next chapter. Descriptions, drawings, photographs, and graphs are used to describe the observed response of the structures to the applied loads. This information is presented with only a minimum amount of interpretation in this chapter. The bulk of the interpretations and comparisons with expected results is delayed until Chapter 6.

Model 1 was subjected to a series of 12 tests, at service, design ultimate, and high overload levels. The load positions and maximum loads are listed for each test in Table 4.1. At the end of testing, the east splice had been largely destroyed and the positive moment capacity had been reached in the west span, with some crushing of deck concrete at the maximum moment section.

## 4.2 Service Load Tests on Model 1

### 4.2.1 Condition of Structure at Beginning of Tests

The structure was examined for cracks before testing began, and no cracks were found.

### 4.2.2 Service Load Tests on Model 1

Tests 1 to 4 reached the service load level only. Each test was conducted with a series of five approximately equal load increments until a final combined load of about 24 kips (107 kN) was reached on the three axles. Tests 1 and 3 applied maximum shear to the east and west splices, respectively, while tests 2 and 4 applied maximum moment at the east and west splices.

No cracks were found during the working stress tests. The structure remained elastic, as is evidenced by strain data taken on the

bridge itself. The maximum tensile strain in any of the working stress tests occurred at gage line E-53 for the maximum load in test 1. The same test produced the maximum strain in a splice. These values at the two sections were 0.00019 and 0.00014, respectively, and both are well below the elastic limit and indeed less than the precompression strain.

The maximum deflections at service loads at gage line 50 and the splice were 0.185 in. (4.7 mm) and 0.155 in. (3.9 mm), respectively, both in test 1. The theoretical elastic deflection at gage line 50 was 0.183 in. (4.6 mm), computed with $E_c$ = 5,200 kip/in.$^2$ (35.9 kN/mm$^2$). Very small residual deflections were measured with 0.01 in. (0.25 mm) being the maximum. Load-deflection curves for the four service load tests are shown in Figs. 4.1 to 4.4.

The reactions measured at the two end supports agreed quite closely with elastic theory. Figure 4.5 shows load-reaction curves for tests 1 and 2.

The behavior of the bridge under the two types of service load tests was quite satisfactory.

## 4.3 Design Ultimate Tests on Model 1

Tests 5 through 10 involved loads up to the design ultimate load, 71.2 kips (317 kN). The maximum loads and load locations are shown in Table 4.1.

Test 5 was for the design ultimate loading causing maximum shear in the west splice. The first cracks began to appear at step 53 at a total load of 34.5 kips (153 kN). This was the first step past the previous working load level. These cracks were inclined about 30 degrees above horizontal, starting about 2 in. (50 mm) up in the web above the lower flange, and extended for a length of several inches. As the load increased, these cracks extended and entirely new cracks developed. At load 54 (45.4 kips) (202 kN) a flexure crack developed in the deck directly above the center support. After load 55 (56.8 kips) (253 kN) several long shear cracks were inclined at 45° just west of the west splice, with one crack crossing full the height of the web but not penetrating the flanges. Several 4 in. (100 mm)

long flexure cracks formed in the bottom flange near the middle axle. Application of the final increment of test 5 (68.4 kips)(304 kN) caused audible cracking noises, and a number of flexure cracks developed between the rear axles, near the splice. More shear cracking also developed, and new flexure cracks developed in the deck on both sides of the center support.

The slope of the load-deflection diagrams changed noticeably after increment 53 (34.5 kips) (153 kN), as can be seen in Fig. 4.6. At maximum load (68.4 kips) (304 kN), the deflections at west gage line 50 and the west splice were -0.80 in. (20.3 mm) and -0.65 in. (16.5 mm), respectively, compared to the theoretical elastic values of -0.55 in. (14.0 mm) and -0.41 in. (10.4 mm), respectively. It is clear the bridge had departed from elastic behavior during this test. As far as the data is concerned, this departure started after increment 53 (34.5 kips) (153 kN), which was the first step past working load level. Residual deflections of 0.08 in. (2.0 mm) and 0.05 in. (1.3 mm) remained in the loaded span upon removal of all load.

The reaction at the west support increased by 20.4 kips (90.7 kN) while the east reaction decreased 6.6 kips (29.4 kN) in test 5. The reactions remained very close to the theoretical elastic values in all six design ultimate tests, except for some deviations in tests 9 and 10.

Tensile strains underwent dramatic changes during the design ultimate tests, especially when a crack occurred. At gage line W53, which was located on the bottom flange, the strain after load 55 (56.8 kips) (253 kN) was only 0.00067, but after a 20 percent increase in load to 68.4 kips (304 kN) the strain jumped to 0.00103. The jump, of course, was due to development of a flexure crack which ran through the gage line. Strains for a number of gage lines are plotted versus applied load in Fig. 4.7, and are the average of values on the two sides of the beam. Before cracking the strains on the two sides of the beam were always about the same. After cracking, there were often large differences.

The neutral axis appears to have moved up higher than even gage line W41 elevation (1 3/4 in. [44 mm] below the deck-girder connection)

late in test 5. A small tensile strain was read at this location for both steps 55 and 56. On the other hand, both gage lines 31 and 51 read compressive strains. This appears to be a local variation in the level of the neutral axis, corresponding to a position directly below the rear axles of the truck loading. This high neutral axis position was most likely caused by propagation of a shear crack into the gage line area.

Many new cracks developed in the vicinity of the west splice during test 6. This test caused maximum moment in the west splice for design ultimate load. However, most of the cracks that developed were inclined shear cracks either in the splice or very close to it, and the crack pattern was similar to that in the previous test. This is not surprising since the loading apparatus was shifted only 3 ft (914 mm) closer to the center support. A number of flexure cracks also developed. A series of short flexure cracks, 2 to 3 in. (50 to 75 mm) in length, appeared in the inclined portion of the bottom flange just east of the west splice. One flexure crack directly above the center support was caused by this loading. The deck experienced very little cracking. One of the inclined cracks in the web of the west splice opened wide enough so that the conduit of the post-tensioning steel was visible.

Deflections for test 6 were slightly smaller than for test 5. The downward deflections at gage line W50 and the west splice were 0.61 in. (15.5 mm) and 0.59 in. (15.0 mm), respectively. The east splice experienced an upward deflection of 0.27 in. (6.9 mm). The deflections are plotted against load in Fig. 4.8.

Except for gage lines 20-23 and 30-33, which were located under the two rear axles, the measured strains were slightly smaller than those measured during test 5. The maximum tensile strain was 0.00105 at W 43. The maximum compressive strain of 0.00029 occurred in the bottom flange directly above the center support. The residual strains were smaller for test 6 than for test 5.

Tests 7 and 8 were the same loading conditions as tests 6 and 5, respectively, except the east splice area was loaded. Load-deflection curves for these tests are plotted in Figs. 4.9 and 4.11, respectively.

Test 7 caused maximum moment in the east splice under design ultimate load. Small horizontal cracks appeared in the east splice after step 73 (34.7 kips) (154 kN). Two long diagonal shear cracks developed in the east splice and just east of the splice during loads 74 (45.6 kips) (203 kN) and 75 (47.5 kips) (226 kN). These cracks extended from top to bottom of the web. Several flexure cracks developed in the bottom flange of the east splice area. Flexure cracks that extended down to about mid-depth of the deck appeared over the center support and a few feet east of the west splice.

Sharp cracking sounds, as if someone was tapping a pencil on a piece of metal, were audible. Subsequent investigation failed to locate any cracks in the vicinity of the noises. It was assumed the post-tensioning strands were slipping within the conduit.

The completion of test 7 (68.6 kips) (305 kN) brought about cracks that were mostly continuations of shear cracks in the east splice. More flexure cracks appeared in the deck over the central support.

The measured deflections of symmetrical points for tests 6 and 7 were very close to the same values, as they should be since both tests caused maximum moment at a splice for design ultimate loading. The same was true for tests 5 and 8.

The maximum measured compressive strain was 0.00030 at the bottom fiber of the center support, compared to 0.00029 at the top fiber of the mid line of the east splice. The gage line E-S 43 experienced the maximum tensile strain of 0.00093. A few load-strain curves are given in Fig. 4.10.

Test 8, the design ultimate load giving maximum shear in the east splice, proceeded much the same as the three previous design ultimate loadings. The first new crack did not appear until the fourth increment of loading (46.0 kips) (205 kN), and then it was only a 2 in. (50 mm) extension of a flexure crack about 10 in. (250 mm) east of the east splice. The rest of the cracking occurred after increments 85 and 86. Most of the cracks were short vertical flexure cracks extending from the splice or

beam bottom and long diagonal shear cracks through the web or splice. For the first time a number of inclined shear cracks developed in the center beam just east of the center support. These cracks, which traveled about 12 to 15 in. (300 to 375 mm), started at about the lower 1/4 point of the web and traveled at a 30 degree angle above the horizontal and away from the support. At the end of load 86, the cracks reached into the inclined portion of the upper flange. The concrete strains were about the same as or slightly smaller than those measured in test 7.

Test 9 was the design ultimate loading causing maximum positive moment in the east span. The truck model faced east with the center axle of the truck 22.5 ft (6.86 m) from the central pier. Strain gauge lines E 50-53 were located between the rear axles of the truck. Load 92, which was the service load level, did not cause any new cracks. Load 93 also failed to produce any new cracks, but the previous cracks in the deck near the center support were approximately 0.004 in. (0.10 mm) in width.

A large amount of cracking occurred after loads 94, 95, and 96. Load 96 was the design ultimate load. Load 94 brought a series of small intermittent shear cracks at the web-lower-flange intersection near the rear of the truck. A good deal of cracking noise followed load 95 (58.4 kips) (260 kN). The deflection increment was 40 percent larger than in the previous load step, and the deflections are shown in Fig. 4.12. A series of fairly evenly spaced flexure cracks appeared in the loading area. These cracks extended a few inches into the web. A few small extensions of shear cracks in the loaded span and two new negative moment cracks near the west splice were caused by this loading.

The design ultimate load, load 96, (68.8 kips) (306 kN) caused several new flexure cracks near the front of the truck and extensions of old cracks. The new and old flexure cracks now extended from the bottom of the beam to the web-top-flange intersection, as did the shear cracks between the rear of the truck and the splice. A negative moment crack in the deck over the central pier increased from 0.004 in. (0.10 mm) at step 93 to 0.007 in. (0.18 mm). The flexure crack most nearly under the

central axle was 0.012 in. (0.30 mm) in width at a location 1/2 in. (13 mm) above the bottom of the beam.

The deflections at the east splice, east gage line 50, and east gage line 60 were 0.73, 1.09, and 0.72 in. (18.5, 27.7, and 18.3 mm), respectively. The deflection at the east splice according to elastic theory should have been 0.58 in. (14.7 mm). The upward deflection at the west splice was 0.29 in. (7.4 mm).

At this stage of loading, the beam did not appear to be very badly deformed, especially considering the applied load level.

The maximum strains occurred at the center support and gage lines E 50-53. The tensile strain at deck top over the central support was 0.00063, while the compressive strain at mid-height of the bottom flange was 0.00034. Due to arrangement of the loading apparatus, the most likely maximum compressive strain at gage line E50 could not be read. From step 95 to step 96 the tensile strain at gage line EN53 jumped from 0.00088 to 0.00093, but on the other side (ES53) the jump was from 0.00070 to 0.00170, probably due to cracking in or near the south gage line. Load-strain curves for a few gage lines are plotted in Fig. 4.13.

Upon removal of the load, the residual deflection at the splice was 0.03 in. (0.8 mm) and the negative moment crack closed to 0.002 in. (0.05 mm) in width.

Test 10 was a combination of design ultimate and overload tests that caused maximum positive moments in the west span. The test was first to the design ultimate load, and then was continued to higher load levels. Only the behavior up to design ultimate load is described here. The remainder of the test is described on the next section.

Several cracks were monitored for width. A shear crack in the west splice stayed about the same width throughout the test. This occurred in the east splice for test 9 also. A negative moment crack over the central pier increased in width from 0.004 in. (0.10 mm) at step 102 (22.9 kips) (102 kN) to 0.0007 in. (0.18 mm) at design ultimate, step 106 (69.8 kips) (310 kN). A shear crack approximately 3 ft (1 m) west

of the west splice opened to 0.014 in. (0.36 mm) and a positive moment crack one ft (300 mm) west of the central axle load was 0.008 in. (0.20 mm) at the design ultimate load.

Loads 104-106 caused many new cracks to develop. These cracks radiated outward from a point directly underneath the center axle load. Not all these cracks reached to the bottom of the beam, but were strongly influenced by shear and remained largely in the web.

The west span deformations at load 106 were larger than the east span deformations at load 96 even though the loads were about the same and were applied in symmetrical positions. The deflections were about 10 percent larger, as can be seen by comparing the load deflection curves in Fig. 4.14 with those in Fig. 4.12.

Load-strain curves are shown in Figs. 4.15 and 4.16. The concrete strains at loads up to 69.8 kips (310 kN) were generally comparable in the two spans except at gage line W53. The strain at E53 was 0.00132 at load 96, while that at W53 was 0.00233 at load 106. The difference is very large, and appears to be related to cracking. At load 96, one crack passed through gage line E53 and another just outside the line, missing a gage point by about 1/2 in. (13 mm). At load 106, three cracks went through gage line W53. There were considerably more cracks in the west span than the east at design ultimate loads, and while the cause of such a difference in cracking has not been determined, the difference in cracking can explain the differences in deformations.

The following is a short summary of the results of the design ultimate loading tests.

Tests 5 to 8, which caused either maximum moment or shear on the splices, were quite similar in results. This was to be anticipated as the loading configurations were shifted only 3 ft (914 mm) between moment and shear tests.

Most of the cracking was in the splice area. Short flexure cracks in the lower flange and longer shear cracks that traversed the entire web were the most dominant. A few negative moment cracks in the deck, mostly over the central pier, appeared during these tests. Also, the first shear cracks in the web near the central pier were caused by test 8.

Test 9 and 10 caused cracking of a different nature. Flexure and flexure-shear cracks dominated a region that radiated outward from a point beneath the center axle load. Directly beneath this point, the cracks were vertical flexure cracks, starting at the bottom of the beam and reaching upward. As one moves away from this point, the cracks again started as flexure cracks, but at a point near the web-flange intersection they bent and ran diagonally through the web pointing toward the center axle load. The spacing of these cracks was fairly uniform, about 1 ft (300 mm) apart, and they were symmetrical about the center axle. As distance from the center axle increased, the cracks become more "shear" in nature and the angle of inclination from vertical increased. The crack patterns in the two spans after completion of the six design ultimate load tests are shown in Figs. 4.17 and 4.18. The cracks which occurred in the later parts of test 10 are also included in these drawings. West span positive moment cracks reached the bottom of the deck only late in test 10, and negative moment cracks penetrated to mid-depth of the beam web over the central pier late in the same test.

The greatest measured deflection was 1.19 in. (30.2 mm) at gage line 50 for load 106. Very little residual deflection remained after removal of the load, even though a load of 92.2 kips (410 kN) was applied before unloading.

The compressive strains reached were much smaller than ultimate and the maximum tensile strain was 0.0023. The neutral axis in the positive moment regions did not reach as high as the bottom of the deck.

All in all, the structure appeared to be in sound shape upon completion of the design ultimate tests. The residual strains and deflections were small, and the crack widths were small where the cracks were even visible.

## 4.4 Overload Tests on Model 1

The first overload test was a continuation of Test 10, the design ultimate test that caused maximum moment in the west span. The load was increased to 75.0 kips (334 kN) for the first increment (107) and

increased three more times until a total load of 92.2 kips (410 kN) was reached for load 1010.

Major increases in flexural crack widths occurred beneath the model truck load. One positive moment crack jumped from 0.011 in. (0.28 mm) in width to approximately 0.03 in. (0.76 mm). Shear cracks in and near the west splice did not open appreciably. Negative moment cracks opened slightly, e.g., from 0.009 in. to 0.011 in. (0.23 to 0.28 mm) for a crack in the deck over the central support.

These overloads caused extensions of the flexure cracks under the loads so that several cracks reached to within an inch (25 mm) of the deck. Quite a few short flexure cracks developed in the bottom flange between the longer, previously existing cracks. These loads also caused major extensions of shear cracks and development of entirely new ones, especially in the regions extending about 6 ft (1.8 m) on either side of the center axle of test loading.

The deck in the negative moment region became fairly evenly marked with negative moment cracks that were caused by loads 108 thru 1010. The closer to the center pier, the further these cracks traveled down into the beam. A vertical crack located directly over the center support started at the top of the deck during load 108 and traveled to the midpoint of the upper inclined flange. After load 1010 the same vertical crack had extended to midheight of the web. Another crack a foot (300 mm) to the west started in the same manner, but bent sharply toward the center support when it reached the inclined portion of the flange. It travelled downward at about a 45° angle to the horizontal and stopped slightly beneath midheight of the web.

An interesting occurrence took place after load 107. A flexure crack located about 2 in. (50 mm) east of the central load point began dripping water as if it were weeping. The water most likely was coming from the post-tensioning duct, which may have indicated that a joint in the conduit was open. (A joint was found in the conduit at this location when the bridge was demolished).

The deflections at the end of test 10 were -2.59 in. (65.8 mm), -1.59 in. (40.4 mm), and +0.67 in. (17.0 mm) at W-50, the west splice, and the east splice respectively. The computed elastic deflection at W-50 was -0.78 in. (19.8 mm).

Major changes in the load-deflection diagram took place, as can be seen in Fig. 4.14. The change in slope was most pronounced after load 105, 58 kips (258 kN). The deflection increased by 0.43 in. (10.9 mm) for this step alone at gage line W-50. It is evident from the shape of the load-deflection curves that the structure was behaving more and more inelastically with each load step.

As the load increased toward the maximum in the test, the stiffness of the structure obviously was dropping continuously. In addition to the absolute changes in stiffness, there were also relative changes in stiffness, and the structure was tending to form a hinge under the loads. The changes in relative stiffness along the length of the girder caused changes in the rate of increase of the reactions, and measured end reactions are plotted versus load in Fig. 4.19. Reactions computed using elastic theory are also plotted to give a basis for comparison.

The measurements are not entirely consistent, since the east reaction follows the theoretical curve exactly for loads up to about 55 kips (245 kN), while the west reaction is always smaller than the theoretical value. This difference may be due to errors in force measurements or due to moments induced by friction at the central pier as the bearing device rotated, or both. However, the measurements are consistent in that both indicate reasonable changes in slope at higher loads, and in terms of the bending moment diagram, both measurements indicate that the negative moment at the central pier was increasing at a significantly greater rate than expected from elastic theory.

Load-strain curves are shown for a number of points in the west span in Figs. 4.15 and 4.16. Extremely large strains were recorded at line W53, which was located between the two large applied loads and hence was in the immediate vicinity of the maximum positive moment section. The strain at the end of the test was 0.0041 tension. The prestrain in both

the pretensioned and post-tensioned steel was about 0.006, and it appears that the total strain in the prestressed reinforcement was about 0.01, which corresponds to a stress of about 260 k/in.$^2$ (1790 N/mm$^2$) considering the stress-strain curves for the strand which are shown in Fig. 2.25.

The strain at line 00, on the top of the deck over the central pier, was 0.00155, which is about 3/4 of the nominal yield strain for the reinforcing bars in the deck. However, the deck reinforcement was in compression at the beginning of the test, and in addition was considerably stronger than the minimum 60 k/in.$^2$ (414 N/mm$^2$) yield stress so this steel was actually even further from its yield stress than the first interpretation of the strain would indicate.

The maximum compression strain was 0.00059, at line 03, on the bottom flange of the girder over the central pier, which is only 20 percent of the expected compression failure strain, neglecting the influence of the precompression existing at the beginning of the test.

The specimen was unloaded at this point. Most of the deflection was recovered. A residual deflection of only 0.2 in. (5.1 mm) was left at gage-line W-50 and 1/8 in. (3 mm) at the west splice. These residuals decreased further in a few hours after unloading.

Test 10 was stopped at this stage so that an east span loading could be conducted while the structure was still relatively undamaged. The west span was certainly extensively cracked due to positive moments, but since the cracks closed up reasonably well and the span was to be subjected to negative moments in the following test, the damage from test 10 was not too significant. The decision about when to stop was of course quite arbitrary, but was based primarily on the trends being exhibited by the load-deflection curve.

The loads applied during test 11 caused maximum shear in the east splice. This position also produced nearly the maximum moment in the splice.

Two cracks were monitored throughout the test. One was a shear crack in the east splice, which was checked for width at mid-depth of the web. The other was a negative moment crack in the south edge of the

deck over the central pier. The splice shear crack originally opened during load 75, which was an increment of the design ultimate moment test for the splice. The negative moment crack originally opened during load 54, an increment of the design ultimate shear test in the west splice. The shear and moment cracks were both 0.003 in. (0.08 mm) in width at load 112. The positive moment cracks in the vicinity of the loads seemed to be tightly closed at this time.

Behavior was quite good for the first seven load increments (111-117). Not much major cracking occurred, with mostly extensions of old cracks and only a few new cracks, both flexure and shear, occurring. At the end of load 117, the splice and negative moment cracks were 0.006 in. (0.15 mm) and 0.007 in. (0.18 mm) wide respectively.

However, as the next load (118) was being brought to the right value the east splice essentially failed. The failure involved shear and bond forces, and produced splitting of the lower flange. The beam deflected an additional 0.2 in. (5.1 mm) at the splice, and the load dropped from about 83.8 kips (372 kN) to about 70 kips (311 kN). A crack opened up, at the lower edge of the beam, which was 1/4 to 3/8 in. (6 to 9 mm) wide. After the break, the load on the front axle increased substantially while load on the rear two axles decreased significantly. The front axle picked up 5 kips (22 kN) since the last load, while the two rear axles dropped a total of 12 kips (53 kN). The load changes were partially due to the fact that loads were applied with hydraulic rams. When the structure deflected, and changed shape as well, the absolute and relative values of the loads change unless the oil pressure to the rams is maintained constant and equal. In this case, the oil systems were nearly sealed, and no maintenance of pressure was done.

The failure crack originated on the under side of the beam in the east splice, at the point where the center beam and splice came together. The crack, which crossed the entire width of the beam at the beam-splice interface, started at the bottom fiber, ran vertically upward approximately 2 in. (50 mm) and then began to turn towards the center of the splice.

When the crack reached the inclined portion of the flange it had become almost horizontal. From this point, the crack ran parallel to the horizontal and branched into two cracks. These cracks reached into the east beam. A photograph of the east splice is shown in Fig. 4.20.

Due to the initial path traversed by the crack, it was clear, after some examination of the beam and the reinforcement details, that a bond failure between lapped bars extending into the splice from the two beams segments was the cause. The crack was horizontal because of splitting parallel to the bars.

Next, an attempt was made to reload the bridge back to the level of load 117. However, the jacking resulted in a loss of load on the rear two axles rather than an increase, so the attempt was abandoned.

The structure was then unloaded and, surprisingly enough, recovered most of the deflection that had been imposed. Load-deflection curves are shown on Fig. 4.21. The failure crack was still quite wide and visible.

The reactions are plotted versus load in Fig. 4.22. The west reaction was nearly the same as the elastic theory reaction until the peak load was reached, and then increased significantly beyond the elastic value. This reaction is a direct measure of the negative moment at the central pier, and the reaction indicates a significant increase at that moment when the east span splice failed. The east span reaction was always smaller than the theoretical value, and the difference increased after the east splice failed. The fact that the east reaction was always smaller than the theoretical value probably is a result of an unbalanced moment at the central pier as a result of friction in the bearing device, but may also include measurement errors.

Five days later loads were again applied in the same position that caused the failure in a test 11A. The deflection after five increments of loading (58.7 kips) (261 kN) was 24 percent larger than the deflection produced in test 11 at the same load. Deflections at the east splice are plotted against load in Fig. 4.23 for test 11 and 11A.

The structure was then unloaded and there was an additional residual deflection of about 0.14 in. (3.6 mm) at the east splice. There was a reasonable amount of cracking and popping noise from the beam during the loading and during the period the maximum load was sustained. There was not any marked drop off in the load during the intervals between load readings, but these loads were not maintained for very long periods of time, either.

The test was ended so that the east span would not be completely destroyed, and thus would be at least partially effective in resisting negative moments when the west span was again loaded on test 12.

The load applied during test 12 was an overload causing maximum positive moment in the west span. This was the same loading position used for test 10, in which a maximum load of 92.2 kips (410 kips) was reached. Test 12 included fourteen steps, starting at zero load and continuing until the load was in the range of 90-100 kips (400-445 kN), with the last few steps being controlled by deflection rather than load, as little change in load occurred. Load-deflection curves are shown on Fig. 4.24.

As in tests 10 and 11, a few crack widths were monitored. These cracks were a negative moment crack in the deck over the center support, a positive moment crack in the beam directly beneath the central load, and a shear crack about 2 ft west of the west splice. The negative moment and shear cracks were monitored in test 10; the positive moment crack was a different one because the positive moment crack monitored in test 10 was damaged by chipped edges and was not suitable for width measurements.

At load 124 (46.8 kips) (208 kN) the positive moment crack was 0.007 in. (0.18 mm) in width, the negative moment crack was 0.004 in. (0.10 mm), and the shear crack was 0.008 in. (0.20 mm) wide.

The deflections for test 12 were generally higher than the deflections for test 10. For example, the deflections at the west splice ranged from 16 to 41 percent greater during test 12 as compared to test 10 at comparable load levels.

Seven or eight minutes after load 125 (58.5 kips) (260 kN) was applied there was a minor compression failure in the pier module at the

east splice. Concrete on the north side of the beam and on the bottom of the beam was spalled off to a depth of 1/4 to 3/8 of an in. (6 to 10 mm). This was in many respects a problem of not being able to close up old cracks, since there was a very large, nearly horizontal, crack in the splice. This crack did not close very well and simply could not carry the additional compression that was now being imposed by the negative moment being induced at the splice. The bottom part of the cross section was badly disrupted during test 11. This loading merely extended the damage.

After load 126 the spalling and crushing of concrete on the bottom of the east splice extended across the whole width of the beam. Crack widths were: positive moment - approximately 0.02 in. (0.5 mm), shear crack - 0.012 in. (0.30 mm), and negative moment crack - 0.006 in. (0.15 mm).

In addition to spalling of concrete off the bottom of the pier module, there was crushing in the splice concrete itself in the tapered part of the lower flange. This again was a case where a wide crack could not close properly and the mis-fit caused large local stresses. Two other areas about 1 foot and 1-1/2 ft (300 and 450 mm) east of the splice experienced minor spalling. The compressive strain at gage line EN42, which was at mid-height of the web just east of the splice, experienced a significant increase from 0.00018 to 0.00067.

Loads 127 thru 129 did not cause major damage. Most of the new cracking was in extension of old cracks. The load deflection diagram remained nearly parallel to that obtained in test 10 and the stiffness deterioration from these 3 loads is no more than that caused by the first several increments. Not much additional spalling occurred in the east splice area.

Load 1210 caused additional cracking and spalling of the east splice area. A large triangular piece of concrete about 2-1/2 ft (760 mm) long by 8 in. (200 mm) high appeared to be trying to fall out of the beam, but it was restrained by the reinforcement. Load 1210 also caused a number of new cracks between the loads and west support of the beam.

These cracks were nearly horizontal and extended for about 2 ft (600 mm), and were located near the junction of the lower flange and web.

Figure 4.25 shows the development of major cracking and spalling in the vicinity of the east splice, and the major crack from test 11 is also marked. This is a simplified view of the north side of the beam. The other side differed in many small details, but the general pattern was the same. Many other, smaller, cracks have been omitted. Photographs of the south side of the beam in the same vicinity are shown in Figs. 4.26 and 4.27.

Directly under the load, 3 or 4 flexure cracks extended as high as the bottom of the deck, but none could be traced into the deck at load 1210.

The next load, 1211 to 97.4 kips (433 kN), extended these cracks about 1-1/2 in. (381 mm) up into the slab. The crack directly under the central load dripped water as it did in test 10.

The twelfth increment, load 1212, produced 1/2 in. (13 mm) of downward deflection at W-50 but the load dropped from 97.4 kips (433 kN) to 95.0 kips (423 kN). At least a scoop-shovel full of concrete had fallen out of the east splice by this time. Eight or ten minutes after this load was applied the beam was still emitting occasional cracking noises from the east splice vicinity.

A small increase in load to 98.2 kips (437 kN) (load 1213) caused an additional 0.74 in. (18.83 mm) of deflection under the axles. The tearing off of the bottom flange of the east splice had all the appearances of a dowel splitting failure from shear although the shear forces would not have been a major influence in this particular loading. Cracks at the lower face of the beam directly underneath the loading opened up considerably during the last two increments. Some of the cracks were approximately 1/8 in. (3 mm) wide at the lower edge of the beam.

Load 1214 produced another 1 in. (25 mm) of deflection under the axles even though the load dropped 0.6 kips (3 kN) to 97.6 kips (434 kN). The deflection at W-50 was 6.3 in. (160 mm). The appearance of the structure late in the test is shown in Fig. 4.28.

The general impression was that a hinge developed at the east splice, and an abrupt angle change was visible. The means of resistance of the east splice to the prestressing force was not obvious. There were open cracks more or less through the whole thickness of the deck, the web was crushed up to the level of the top flange, and there are shear cracks across the top flange.

The load was removed because the structure had obviously been loaded beyond ultimate. Further loading would have required retracting all jacks because several were at their stroke limit. It did not appear that this could be done safely while the structure was loaded, and unloading to gain additional stroke would not have been very effective since the rebound on unloading was over 4 in. The residual deflection at the west splice was 1.13 in. (27.7 mm) as compared to a maximum deflection of 3.87 in. (98.3 mm), and the residual at W50 was 1.79 in. (45.5 mm).

A small amount of crushing of deck concrete was found near the central load point after the model was unloaded. This is a further indication that the structure was very close to total collapse when the test ended.

The end reactions are plotted against applied load in Fig. 4.29. The west reaction was smaller than the elastic theory reaction throughout the test, and the east reaction was larger than the elastic theory reaction from a load of about 50 kips (222 kN) until the last three load increments were reached. The reactions indicate that the negative moment at the central pier was larger than the elastic moment through much of the range of loading, in spite of the fact that the east splice, in the unloaded span, was already severely damaged and was being subjected to relatively large negative moment increments. This apparently occurred because the great decreases in stiffness that were occurring in the west span as it became more extensively cracked were more important than the east span changes. The complete failure of the east splice as the maximum load was approached caused a decrease in negative moment at the central pier as the splice moment capacity decreased.

After completion of the last test, the cracks were recorded, and Figs. 4.30 and 4.31 show the cracks observed on the south side of the specimen. The two figures represent the composite results of several tests with loads in different positions in both spans, and there consequently are many more cracks than could be produced by a single loading to failure. The crack patterns near the splices are of special interest, and it is apparent that the presence of the splices caused no basic changes in the cracking patterns. There are local deviations in the paths of individual cracks, but the basic patterns are not disturbed.

During demolition of the structure for removal from the laboratory, prestressing ducts were cut open at several points to determine the effectiveness of the grouting operation. Figure 2.29 is a diagram showing the areas that were grouted, partially grouted, or not grouted at all.

# 5. RESULTS OF TESTS OF MODEL 2

## 5.1 General Notes

Model 2 was subjected to 15 tests, and the load positions and magnitudes are listed in Table 5.1. At the end of testing, the positive moment capacity had been exceeded in the east span, where the three draped pretensioned strands were broken, and the west splice was destroyed, resulting in the total collapse of the west end segment of the bridge.

## 5.2 Condition of Structure at Beginning of Testing

The structure was examined for cracks after the temporary supports were removed and again before the first loads were applied. Cracks were found at both splices, near the bottom of the beam. Cracks were found in the deck near the central pier, and over the east splice, and are shown in Figs. 5.1 and 5.2.

The cracks in the lower part of the splices were expected, as the girder is of reinforced concrete without prestressing at those sections. The cracks in the deck over the central pier were due to tension from both dead load negative moments and from restrained shrinkage of the deck concrete, and were in an area of generally poorly consolidated concrete as well. The deck cracks over the east splice were probably a result of lifting the bridge too high at that point when it was jacked up to remove the temporary support.

The sloping cracks in the splices were not expected and were 0.006 to 0.008 in. (0.15 to 0.20 mm) wide when testing started, in spite of the presence of stirrups which should have limited the widths to smaller values.

One horizontal crack resulting from anchorage zone stresses was found at the east end of the east segment, at about midheight of the beam web. This crack was adequately restrained by the stirrup reinforcement and was both quite narrow and extended only a few inches.

Strains were measured during the process of removing the temporary supports. The west support was removed first, and its removal caused an average tensile strain 0.00038 in the reinforcing bars in the west splice, as measured with the electrical resistance gages. The strains in individual bars varied widely, from 0.00023 to 0.00056. Compressive strains averaging 0.00001 were measured in the east splice.

Removal of the east temporary support caused tension in the east splice bars, and the average tensile strain at the east splice was 0.00022, with considerably less scatter than at the west splice. Removal of the east support caused additional strain changes at the west splice, with a final average of 0.00043 tension. Some of the increase may have been due to time-dependent cracking during the short time between readings, as there was considerable growth in cracking during the first week after the temporary supports were removed.

The mechanically measured strains were different because of differences in gage lengths, because of cracks, and because the mechanical gage lines effectively spanned across the Cadweld splice sleeves. After both supports were removed, the west splice tensile strain was 0.00021, while the strain at the east splice was 0.00009. These strains are for the gage lines with 33 designations, and are the average of the measurements on the two sides of the beam.

Tensile strains in the lower flange adjacent to the splices varied widely, with individual values ranging from 0.00004 to 0.00029, depending primarily on whether a crack crossed the gage line. Tensile strains of about 0.00008 were measured in the deck directly over the central support. Compressive strains in the deck were about 0.00007 over the splices, and all other strains were considerably smaller.

## 5.3 Service Load Tests on Model 2

Six tests were conducted to the full service load of 22 to 24 kips (98 to 107 kN), which was applied in five approximately equal increments. The loadings were placed to produce maximum moment or shear at a

splice or maximum positive moment in a span, and were placed in both spans, as listed in Table 5.1.

Load-deflection curves for four different points for each of the three service load tests on the east span are shown in Figs. 5.3 to 5.5. The curves for the west span loadings were very similar and are not given here. The curves are more nearly of the shape expected for reinforced concrete rather than prestressed concrete. The curves generally show greater changes in stiffness with increased load than in the case of fully prestressed members such as in Model 1, and the residual deflections are relatively larger. The residual deflections from the second and third loading are smaller than those from the first loading, and this too is to be expected in reinforced concrete. Even so, the maximum deflections were about span/2000, which is very small.

The first test, with the load positioned to produce maximum positive moment in the east span, caused one new crack near the splice, and minor extensions of other cracks in the same area. It also caused several new cracks in the deck, with the last crack 7.5 ft (2.3 m) west of the central pier. These cracks remained small. One of the larger deck cracks was 0.003 in. (0.08 mm), while an inclined crack at the center of the splice was 0.010 in. (0.25 mm). The inclined cracks in the splices were 0.006 to 0.008 in. (0.15 to 0.20 mm) wide under dead load alone.

Test 2 produced maximum shear at the east splice, and also produced larger negative moments at the central pier. Two additional cracks formed in the central beam near the east splice and in the splice. The inclined crack in the splice was 0.011 in. (0.28 mm), and a flexure crack at the bottom of the splice was 0.007 in. (0.18 mm). Deck cracks near the central pier were 0.003 to 0.004 in. (0.08 to 0.10 mm) wide.

Test 3 produced maximum positive moment in the east splice, and higher shear at the central support than had occurred in the previous tests. There was very little change in the cracking at the splice, with only small extensions of old cracks. Three web-shear cracks were found in the beam web near the central support.

Tests 4, 5, and 6 were loadings in the west span which simply repeated Tests 1, 2, and 3, respectively. The behavior of the two spans was nearly identical in terms of load-deflection response and cracking. Cracking in the east and west spans at the end of the service load tests is shown in Figs. 5.6 and 5.7, respectively.

End reactions are plotted versus load for tests 1, 2, and 3 in Fig. 5.8. Reactions as determined by elastic theory are also shown for purposes of comparison. In test 1, the measured and theoretical reactions were very close to the same throughout the test. In test 2, the changes in both end reactions were smaller than the theoretical values, which probably indicates measurement problems rather than unusual moment distributions, since the west reaction indicates that the negative moment at the central pier was smaller than expected, while the east reaction indicates the same moment was larger than anticipated. The test 3 reactions were reasonably close to the theoretical values except at the second load step, and the differences were consistent, in that both indicate that negative moment at the central pier was smaller than the elastic value.

These deviations of measured reaction from expected values, or at least from consistent values, do not appear large when just the reactions are considered. Unfortunately, however, the deviations are large enough to make the computation of a moment at some section well away from the end of the structure rather uncertain because of the long lever arms associated with the moment computations. For example, the east reaction was 303 in. (7.696 m) from the section near the center of the splice which has been used for comparisons. An error in the reaction measurement of 0.5 kip (2.22 kN) at service load thus corresponds to an error of 151 kip-in. (17.1 kN-m). The maximum moment to be expected at the section is about 1400 kip-in. (158 kN-m), when computed using an elastic analysis with the load at the most critical location, and consequently the uncertainty is high. The situation is worse for the loading giving maximum positive moment in the span since the moment at the splice is much smaller, but the potential uncertainty remains about the same. It must be concluded that

the reaction measurements must be used cautiously, and that they should be used more for indicators of trends than for reliable numerical values.

The average strain in the splice bars in the east splice was 0.00043 at the end of test 1. A residual of 0.00011 remained when the structure was unloaded. Tests 2 and 3 produced considerably larger moments at the splice, and the maximum strains in the two tests were 0.00061 and 0.00064, respectively, and both strains include residuals from previous tests. Tests 2 and 3 each resulted in additional residual strains of about 0.00003, for a total of about 0.00017.

The same three tests produced compression strains of about 0.00015 in the spliced bars in the west splice, and the residuals were extremely small.

The west span loadings caused comparable tensile strains in the bars in the west splice.

Several load-strain curves for tests 1, 2, and 3 are presented in Figs. 5.9 to 5.11. In each figure, the first curve is the average of the strains measured in the six reinforcing bars in the splice, and the measurements were made with electrical resistance gages attached to the bars. The other curves are from mechanical strain gage measurements made on the surface of the concrete. Gage line E33 was on the lower flange of the beam, and was centered on the splice length. Line E43 was on the precast end segment adjacent to the splice, and E23 was on the precast central segment near the splice. The mechanical gage readings were averaged from the two sides of the beam, and consequently E33 represents the average of NE33 and SE33, for example.

There is never perfect agreement between the two measurements of strain in the splice, but the agreement is good enough to support the consistency of the measurements. The surface measurements are strongly affected by cracking, and this shows up very plainly in the change in slope in the curve for E33 in test 1, Fig. 5.9, at a load of about 9 kips (40 kN). The transition from partially to fully cracked is much less pronounced in the measurements on the bars, but once the cracking developed the slopes of the two curves remained about the same to the

end of the test. The strains measured by the two different means were about the same during much of tests 2 and 3.

Figure 5.11 also includes a load-strain curve for gage W10, which was on the deck adjacent to the central pier. The curve indicates that a crack formed at about 10 kips (44 kN) load, and the maximum live-load strain of 0.00020 is typical of the deck strains at service load levels.

## 5.4 Design Ultimate Load Tests on Model 2

Four tests were conducted to the design ultimate load level. Loads were positioned to produce the maximum positive moment in the span and the maximum shear at the splice, and were repeated for each span. The loadings producing maximum positive moment at the splice were not done since the moments produced were only slightly larger than those occurring in the splice shear loadings. The maximum loads in each test were 54 to 55 kips (240 to 245 kN), and were reached in eight increments. The maximum load corresponded to the AASHTO ultimate load, of 1.3 $(D + \frac{5}{3}[L + I])$, with the applied load selected on the basis of shear at the splice, as in the case of Model 1. The fourth load increment in each test was to an "operational overload" with a live load of $\frac{5}{3}[L + I]$, which was about 39 kips (173 kN).

Test 7 produced maximum live load shear at the west splice, and load-deflection curves are shown in Fig. 5.12. The upward deflections in the unloaded span were nearly linear with load, and exhibited little residual deformation on unloading. The loaded span deflections were linear with load until the service load was exceeded, and then exhibited decreasing stiffness, or increasing rates of deflection, with increasing load. Figure 5.13 shows the deflections at the west splice for test 7, and also for the three previous live load tests in the same span. The cumulative deflections since the beginning of the live load testing are shown, including the residuals from each test, except that the small upward camber at the end of test 3 on the east span is not shown.

Each successive increment of load brought new cracks and extensions of old cracks. At load 74, crack widths ranged from 0.003 to

0.008 in. (0.08 to 0.20 mm) in the deck. Flexure cracks in the precast elements were 0.003 to 0.006 in. (0.08 to 0.15 mm) wide, and shear cracks were often wider. A shear crack near the central support was 0.010 in. (0.25 mm), and one at the center of the west splice was 0.013 in. (0.33 mm). At load 78, design ultimate load, flexure cracks reached down to mid-depth of the precast section over the central pier, and the widths were 0.005 and 0.011 in. (0.13 and 0.28 mm) near the top of the precast section. The shear crack closest to the pier in the loaded span was 0.013 in. (0.33 mm) wide, at mid-depth of the girder. A flexure crack near the center of the splice was 0.02 in. (0.51 mm), when measured near the bottom of the section. A shear crack in the splice was estimated between 0.025 and 0.03 in. (0.6 and 0.8 mm), as its width was greater than the range of the optical comparator being used. Positive moment cracks in the precast members were generally smaller, in the range of 0.003 to 0.007 in. (0.08 to 0.18 mm) wide.

The last positive moment crack was about 23 ft (7 m) west of the central pier, or about 4.5 ft (1.4 m) in front of the vehicle loading. Negative moment cracking in the deck in the east span was randomly distributed from the central pier to about 13 ft (5.3 m) east, near the east edge of the east splice. No new negative moment cracks occurred in the west span. Two shear cracks near the splice extended to within 2 in. (50 mm) of the top of the girder.

Test 8 was a loading to produce the maximum positive moment in the west span, and the initial stages of the test were plagued with minor problems with load cells and hydraulic oil leaks. These problems were repaired, and the test was finished without further incident.

No new cracks were found until load 85, 43.7 kips (194 kN), had been reached. Six new flexural cracks were then found directly below the loaded area, and the following three increments of load caused nine additional cracks in the same region, with the last crack 27.5 ft (8.48 m) from the central pier, or about 2 ft (0.6 m) in front of the load. Two new negative moment cracks were found in the east span, both within two ft (0.6 m) of the central pier. The positive moment crack widths at load 88

were in the range of 0.004 to 0.008 in. (0.10 to 0.20 mm), when measured on the lower flange. The widest crack in the vicinity of the loads was a slightly inclined crack which was 0.009 in. (0.23 mm) wide at mid-depth of the beam web.

It was noted after the structure was unloaded that the positive moment flexural cracks away from the splice region were no longer visible, even though they had been marked and consequently one knew where to look. The shear cracks remained visible.

Load-deflection curves for test 8 are shown in Fig. 5.14. The nature of the curves is about the same as for test 7, although the greatest deflections were measured under the load rather than at the splice, as is reasonable. Test 7 produced considerably larger residual deflections than test 8, but this is typical of the response of a reinforced concrete (as opposed to fully prestressed) structure, since the first loading to a new level produces most of the new cracking, and the inability of the cracks to close completely is responsible for at least a large portion of the residual deflection.

Tests 9 and 10 produced maximum shear at the east splice and maximum positive moment in the east span, respectively. The response of the structure to those two tests was very similar to the response to the west span loadings, and the development of cracking was quite similar.

Load-deflection curves for tests 9 and 10 on the east span are shown in Figs. 5.15 and 5.16, respectively. The pattern of smaller residuals in the second loading is again noted.

After completion of the design ultimate load tests, both spans of the structure were extensively cracked. The cracks are shown in Figs. 5.17 and 5.18, respectively, for the east and west spans. It is seen that the positive moment tension cracks were fairly uniformly distributed along the length of the beam through the region of the splice without major interruptions of the pattern. The same is also true of the shear cracks, although the east splice cracking is not quite like that in the adjacent beams. The negative moment cracking is quite random, although there is an obvious concentration near the central support.

Several load-strain curves for test 7 are shown in Figs. 5.19 and 5.20. The load was positioned to give maximum shear at the west splice, and the accompanying positive moment at the west splice was nearly the maximum as well. The east span was subjected to negative live load moments, and the strains in the east splice bars consequently were compressive. The graph indicates some increase in stiffness in the east splice, due to closing of cracks at the lower face of the girder in the early stages of the test.

The strains in the west splice bars and in gage line W33 were similar at applied loads up to about 29 kips (129 kN). Beyond that load, the strains in W33 increased considerably faster than in the bars. This is at least partially due to the differences in the measurement methods, but is also due to the fact that the concrete surface strain includes the extra elongation due to slip that was occurring in the Cadweld splices in this loading range. This question will be more fully explored in Sec. 6.4 of this report. Strains in lines W23 and W43 were considerably smaller than in the splice, as is to be expected since there are no splices in the reinforcing bars within these gage lines, and in addition the pretensioned reinforcement must have been having some effect.

Gage line E10, on the top of the deck, indicated a maximum strain of 0.00145 during test 7. There was a great reduction in stiffness at a load of 22 kips (98 kN), and the load-strain slope then remained constant to the end of the test.

Gage line W53 indicates a great reduction in stiffness at loads above 45 kips (200 kN), and minor, gradual, losses in stiffness at loads above 30 kips (133 kN). The first crack crossing the gage line was found when the load was 51 kips (227 kN), although the load-strain curve indicates that it may have occurred as low as 46 kips (205 kN).

The curves for lines W30 and W50 are typical of those in compression regions. The response was nearly linear throughout the load range, and the residuals were small.

A few load-strain curves for test 8 are shown in Fig. 5.21, and all are for points in the west span. The strains in the splice bars and in W33 are nearly identical, and both are linear. This loading produced maximum positive moment in the west span, and the moment at the splice was considerably smaller than in test 7. The splice was consequently being reloaded to moments lower than previously reached, and little new cracking or slip in the Cadweld splices would be expected, and the linear response thus is as would be predicted. Sections at W53 and W63 were subjected to larger strains than in previous tests. Section W63 was about 18 in. (460 mm) beyond the last positive moment crack, and consequently responded approximately linearly with load. W53 was already cracked, from test 7, but since the moments were larger the strains were considerably larger. The load-strain curve clearly indicates that the cracks at W53 reopened when the load exceeded 21 kips (93 kN), and that some additional damage occurred when the load exceeded 52 kips (231 kN).

Measured reactions are plotted against applied load in Figs. 5.22 and 5.23 for tests 7 to 10. Theoretical elastic reactions are also plotted, to provide a basis for comparisons. The measured values are generally close to the theoretical values, and are generally consistent. Both reactions in test 7 indicate that the negative moment at the central support was slightly lower than expected from the elastic analysis. In test 8, and to a lesser extent in tests 9 and 10, the measurements indicate that the negative moments were somewhat larger than the elastic values, especially late in the tests. This is particularly marked in test 8, where there is a distinct change in the slope of the reaction curves when the applied load exceeds 35 kips. This change in behavior is consistent with the observed crack development in the structure. In test 8, large numbers of new positive moment cracks developed, while there was comparatively little growth in the negative moment cracking. This would lead to greater reductions in stiffness in the positive moment regions than in the negative moment regions, and consequently to some changes in the moment distributions.

## 5.5 Failure Load Tests on Model 2

Five tests were conducted in which maximum loads greater than the design ultimate load were reached. Tests 11 and 13 had the load positioned to produce maximum positive moment in the east span, and the capacity of that section was reached at a high overload. Tests 14, 16, and 18 had the load positioned to produce maximum shear at the west splice, and ended with the total collapse of the west end segment of the girder, at an extremely high overload. The tests were not numbered consecutively because several had more than 10 increments.

Eleven increments of load were applied in test 11. Once the previous maximum load of 54 kips (240 kN) had been exceeded, new cracks appeared with each successive load increment, and the old cracks in the vicinity of the loads got longer. At load 114, 59.3 kips (264 kN), cracks reached the top of the precast section directly under the central axle load. Load 115, to 62.5 kips (278 kN), produced audible cracking noises, with new flexure and shear cracks being found.

Load 116 produced one sharp noise from the beam just as the 67.0 kip (298 kN) load was reached. New negative moment cracks were found in the west span, near the splice, and positive moment cracking occurred as far as 4.5 ft (1.4 m) east of the east load in that span. The load-deflection curve shown in Fig. 5.24 shows that the stiffness of the structure was much less than the original stiffness by the time this load was reached. The curve for test 10 is also plotted in the same graph. It was noted that the load dropped off considerably more during the interval required to read strain and deflection gages than it had dropped during previous increments, which is another indication of damage.

Load 117 was to about 72 kips (320 kN) applied load. The load was reached, but as the relative values of the front and rear axle loads were being given their final adjustment, there was a very sharp noise from the beam, and the load dropped to 58.3 kips (259 kN) with no significant change in deflection.

The structure was examined without finding any clear indication of the source of the noise, but it was found that several cracks located between the two rear axle loads had opened considerably. There were five wide cracks on the north side of the beam, with widths ranging from 0.04 in. (1 mm) to 0.11 in. (2.8 mm), and four on the south side of the beam. Most of the deformation on the south side was concentrated on two cracks of 0.14 in. (3.5 mm) each, with the measurements being made on the lower flange of the beam. Two cracks reached 2 in. (50 mm) into the deck, indicating a neutral axis depth of only 2 in. (50 mm).

Several negative moment cracks in the east span near the central pier had penetrated into the girder, and connected up with shear cracks in the beam web.

It was later found that the noise and loss of capacity occurred when the three draped strands broke in the strand deflector which was located between the two rear axle loads.

An attempt was then made to reload the structure. The maximum load reached was 62.7 kips (279 kN), after an additional deflection of 1.2 in. (30.5 mm). This reached the limit of extension of the hydraulic jacks, and the structure was then unloaded, with a recovery of about 2.2 in. (55.9 mm).

The structure was reloaded with the same load positions in test 13. Additional deformations were imposed, to a maximum deflection of about 4.8 in. (122 mm), including residuals from tests 10 and 11, without exceeding 65 kips (289 kN) load, and the test was ended. The load-deflection curve for this test is also plotted in Fig. 5.24, and it can be seen that the response was nearly linear until the load at the end of test 11 was reached. After that load level had been reached, the deflection curve was clearly an extension of the curve from test 11.

Comparisons of the three curves in Fig. 5.24 shows that considerable damage was done in test 11. The initial slopes of the curves for tests 10 and 11 are nearly identical, with the first 20 kips (89 kN) load producing about 0.24 in. (6.4 mm) deflection in each case. The first 20 kips (89 kN) load in test 13 caused slightly more than 0.5 in. (13 mm) deflection.

Load-deflection curves for two points in each span are shown in Figs. 5.25 and 5.26 for tests 11 and 13, respectively. Although the visible damage was predominantly in the loaded east span, large residuals occured in both spans.

Load-reaction curves for tests 11 and 13 are shown in Fig. 5.27. The reaction forces were close to the elastic theory values in the earlier stages of both tests, and the changes in both tests indicate that the negative moment at the central support became larger than the elastic theory value as the loads increased above about 60 kips (267 kN) in test 11 and above 50 kips (222 kN) in test 13. The failure of the three strands in test 11 of course caused large changes in the reaction which are consistent with a loss of positive moment capacity and stiffness, and caused an accompanying increase in negative moment.

After the final tests on the east span, the west span was still relatively intact, and the east span appeared to be capable of resisting negative moments. Consequently, three tests were conducted on the west span with the loads located to produce maximum shear in the west splice. The loading also produced large bending moments in the splice. The tests could be viewed as three parts of the same test, as the breaks were determined by time restrictions and by reaching the limit of extension of the hydraulic jacks. The tests were numbered 14, 16, and 18.

Load-deflection curves for the three tests for a point near the center of the west span are shown in Fig. 5.28, where the continuity of the three tests can be seen. The deflections at the west splice were larger, especially late in the test series, but the deflection data from that point were not of consistently good quality and are not used for this comparison. The west splice deflections were largely determined with a steel tape rather than a dial gage, because of the obviously high probability of smashing the gage when the beam failed.

Load-deflection curves for four points in the structure for each of the last three tests are plotted in Figs. 5.29 to 5.31.

The average strain in the six reinforcing bars in the west splice is plotted against applied load in test 14 in Fig. 5.32. The trace ends

well before the test, as every strain gage exceeded the range of the measuring device before the end of the test. Early in the test, the six readings were not greatly different. However, for loads in excess of 67 kips (298 kN) large differences developed. Since these strains were greater than the yield strain, and also since the bars were probably being subjected to bending as well as to tension, these differences may not be significant. At a load of 78 kips (347 kN), the two remaining gages indicated strains of nearly 0.01 during test 14 alone, not including residuals from earlier tests or strains due to dead load moments.

The early part of test 14 produced only minor new cracking or extensions of cracks. Load 146, to 67.3 kips (299 kN), caused one new shear crack in the west splice, plus the spalling of a small piece of concrete from the upper flange of the precast girder adjacent to the west splice. A few additional deck cracks were found, with one 16.5 ft (5.0 m) east of the central pier.

Load 147, to 71.0 kips (316 kN), caused the very large increase in strain in the splice bars which was noted earlier. Cracks in the west splice were as wide as 0.03 to 0.04 in. (0.75 to 1.0 mm). In the east span, five of the negative moment cracks in the deck penetrated into the precast girder.

The larger loads brought wider cracks in the west span, but few new cracks. Additional negative moment cracks formed in the east span.

Load 149, to 78.4 kips (349 kN), brought a major change in the development of the crack pattern. The strain in the steel in the splice was considerably in excess of the yield strain, and a crack at the west edge of the west splice (at the splice-girder interface) had opened to the top of the girder section. Since the joint interface was relatively smooth, all of the shear force was being resisted by the deck, without significant aid from the girder. At this load, there was a large increase in the width of shear cracks in the splice, plus the beginning of a separation of the west precast girder segment from the deck.

This resulted in downward sliding of the west precast segment relative to the splice concrete. By the end of the test at increment 152, 85.2 kips (379 kN), there was about 1/2 in. (13 mm) relative displacement

between the splice and girder at the top of the section. There was no relative displacement at the bottom of the section, apparently because of dowel forces developed in the splice bars. The difference between movements at the top and bottom of the sections was taken up in opening of inclined cracks in the splice. Fig. 5.33 is a sketch which shows the major cracks, with the crack inside the deck being drawn on the basis of the failure section seen after the structure collapsed in a later test.

Test 16 was a continuation of test 14, and the distortion in the west splice region continued to develop as the structure was reloaded. At load 163, to the design ultimate load at 54.7 kips (243 kN), the separation between the deck and girder had increased to 3/4 in. (19 mm). At load 168, to 75.1 kips (334 kN), new cracks were found in the deck near the center axle load, which was about 3.5 ft (1.1 m) west of the splice. This cracking was associated with the deck separation problem, as the cracks did not join cracks in the girder.

At load 171, 86.0 kips (383 kN), a positive moment flexure-shear crack opened to 3/16 in. (5 mm) at a point 18 in. (460 mm) in front of the front axle load. The lower end of this crack was at the point where the last two reinforcing bars from the splice terminated.

At load 172, 87.8 kips (391 kN), the deck separation was about 7/8 in. (22 mm). The crack 18 in. (460 mm) beyond the loading position was 3/8 in. (10 mm) wide at the lower edge of the girder, and was 1/8 in. (3 mm) wide at mid-depth of the girder. This crack sloped upward toward the east, toward the section of maximum moment, and penetrated about 2 in. (50 mm) into the deck. The lower part of the crack crossed gage line W53.

A maximum load of 89.9 kips (400 kN) was reached. The general impression of the structure was that no explanation could be found for the fact that it was still standing and resisting the maximum load. The structure was then unloaded because of lack of time of additional loading, and because the jacks were again approaching the limit of their travel. It might be noted that equipment was available to allow jacks to be retracted under load, but that this generally required people to work on top of the structure, and this did not appear to be safe.

Test 18 was conducted two days later, again with the same loading positions. The test can be characterized by the simple statement that the cracks kept getting bigger. The same patterns of damage continued. At load 189, 78.2 kips (348 kN), the separation between deck and girder was 15/16 in. (24 mm). Pieces of concrete started falling off the lower flange of the girder at the major crack at gage line W53, where two of the #7 bars (22.2 mm diam.) stopped.

Load 193 was planned to be approximately 94 kips (418 kN), and the intended load was reached on at least two of the jacks. However, at that time there were several loud noises from the west splice region. There was a decrease in the load on the front axle and increases in at least some of the rear axle loads, as the structure changed shape and deflected. Within a minute of the first noises, the west girder segment completely collapsed, falling on the blocking which was positioned a few inches below it. The splice concrete was destroyed, and the deck failed completely. Some loads remained on the rear axles, but they were resisted by the pier segment which was then acting as a cantilever.

A number of photographs are presented in order to help describe the damage which occurred late in the test of Model 2. Figure 5.34 shows the structure at load 173, 89.9 kips (400 kN), which is the largest load sustained long enough for the load cells to be read. The deflection of the west span is quite visible, and the east span still has a small downward deflection remaining from the earlier tests.

Figure 5.35 shows the south side of the west splice at load 173. The cracks were not marked on the south side of the beam, but several large cracks are quite visible without marking. Figure 5.36 is from about the same point immediately after failure, and Fig. 5.37 shows the area just west of the splice so that the separation of deck from girder is readily visible.

Figures 5.38 and 5.39 show the cracks which had occurred in the structure by the end of all testing.

Load-reaction curves are plotted for all three of the tests in the west span in Fig. 5.40. The reactions are quite consistent throughout

the full load range of all three tests. In each test, the reactions indicate that the negative moment at the central pier is initially lower than the theoretical value from an elastic analysis.

At higher load levels, and especially above 70 kips (311 kN) applied load, the trend of the reactions changed somewhat, and indicates that the negative moments were increasing at a slightly greater rate than the positive moments. It is interesting to note that the reactions were close to the theoretical values throughout the final test, in spite of the fact that the splice in the west span was very badly damaged.

# 6. DISCUSSION OF BEHAVIOR OF TEST SPECIMENS

## 6.1 General Remarks

The behavior of the two test specimens will be discussed in this chapter, with the emphasis being placed on comparisons between observed and expected loads at cracking and at failure, considering primarily flexural modes of failure. Some attention will also be given to the redistribution of moments which occurred at high loads.

Model 1 will be discussed in Sec. 6.2, and Model 2 in Sec. 6.3. The behavior of the Cadweld splices on the reinforcing bars in the joints was very important to the behavior of Model 2 and Sec. 6.4 will be devoted to an examination of the stress-strain and other characteristics of these splices.

## 6.2 Discussion of Results of Tests of Model 1

A series of moment diagrams are presented in Figs. 6.1 to 6.3, to illustrate the changes that occurred in the process of building the structure. Each separate construction step also corresponded to a specific step in the analysis and design process.

Fig. 6.1 shows the dead load moment diagram for the structure while it was still on the temporary supports. The dead loads of the girder, deck, and auxiliary dead load blocks were present. Fig. 6.2 shows the moments induced by removal of the temporary supports, and also includes the secondary moments due to post-tensioning. This was computed including the effects of friction along the length of the ducts, using the method presented in Ref. 5.

The dead load moment diagram immediately after post-tensioning and removal of the temporary support is shown in Fig. 6.3. There is a small positive moment at the central pier rather than a negative moment of $w\ell^2/8$ normally associated with a two span continuous beam because of the construction sequence and the importance of the secondary moments induced by the post-tensioning forces. The final dead load moment diagram is very similar to that in the prototype girder described in Ref. 1, where a small positive moment occurred at the central support.

The concrete was assumed to weigh 150 lb/ft$^3$(2400 Kg/m$^3$). The dead loads from the large concrete blocks was assumed to be uniformly distributed along the length of the beam even though there was a block ommitted at each splice. The computed uniformly distributed load was 1.44 kip/ft(20.9 kN/m), which leads to the correct total weight even though the actual distribution was not quite correct. The errors in moments are entirely in the dead load moments and amount to no more than about 3% of the maximum positive moment due to dead load.

The distribution of the compressive stresses along the top of the deck and the bottom of the girder are shown in Fig. 6.4. The stresses were computed considering the construction sequence. Prestress losses of 35 k/in.$^2$ (241 N/mm$^2$) from the pretensioned strands and 25 k/in.$^2$ (172 N/mm$^2$) from the post-tensioned strands were included, and it was assumed that the loss from the post-tensioned strands affected stress in the full composite section. There are large discontinuities in stresses at the bottom of the girder at the edges of the splice because the end segments had a substantial amount of pretensioned steel in addition to the post-tensioned steel, the central segment had some pretensioned steel at a large eccentricity, and the splice had only post-tensioned steel. The transitions were not as abrupt as they are drawn because of bond slip in the pretensioned strands, but the transfer distances are expected to be only 18 to 24 in. (450 to 600 mm) for the 3/8-in. (9.5 mm) strand. These discontinuities do not affect deck stresses, where the irregularities are primarily due to the local variations of the support removal moments.

Using the stress distribution data developed for Fig. 6.4, expected cracking moments were computed and are plotted in Figs. 6.5 and 6.6 for positive and negative moments, respectively.

The gross cracking moments are plotted for the positive moments. These were calculated by adding the estimated modulus of rupture of $6\sqrt{f'_c}$ or $7.5\sqrt{f'_c}$ ($0.5\sqrt{f'_c}$ or $0.62\sqrt{f'_c}$ N/mm$^2$) to the precompression acting when the dead load was present (as shown in Fig. 6.4) and then multiplying this total stress by the section modulus to obtain the live load cracking moment. The dead load moment was then added to the live load moment to obtain the gross or total positive cracking moment, which is plotted in Fig. 6.5.

The negative live load moment at cracking was calculated in the same way, and is plotted in Fig. 6.6, but without the dead load moment component.

The observed positive cracking moments for both spans are also shown in Fig. 6.5. Since the loading steps were relatively large, the cracking moments could not be determined exactly, but instead a range was established. For example, a crack was found at load step 95 at a section 23 ft (7m) east of the central pier, and it is known that the crack had not occurred at load 94. The vertical line plotted at this location gives the moments at loads 94 and 95, and thus establishes the possible range of moments in which this crack occurred. The lines plotted in this figure represent initiation of only a few of the cracks, and other cracks occurred at higher moments. Most of the cracks selected for inclusion were the first cracks in a particular region of the beam, and were generally 1.5 to 2 ft (0.45 to 0.6 m) from the nearest earlier crack so that they were not greatly influenced by the adjacent cracks.

It is apparent that the cracking moments in the two spans were quite similar, and also that the observed moments were substantially greater than the computed moments except at sections adjacent to the splices.

There may be a number of reasons for this difference. There may be some error in evaluating the actual moments. The moments which are plotted were the computed elastic live load moment plus the dead load moment as shown in Fig. 6.3. There may have been minor deviations from the elastic moments in some tests, although the reaction measurements do not show any significant differences. The dead load moment distribution probably changes somewhat with time due to various creep and shrinkage effects (Ref.5). A change in the dead load moment distribution would not change the comparisons directly since the same dead load component exists in both the theoretical and observed cracking moments. However, a change in the dead load moment distribution would change the stresses in the sections, and hence change the stress range available to resist live load moments before cracking. An increase in the negative moment at the central pier would increase the compression in the bottom fiber, and consequently would increase the positive live load cracking moment.

The principal source of the difference between the expected and observed cracking moments probably lies in the evaluation of the prestressing force. The precompression was computed using prestress forces after all losses, but only part of these losses may have occurred by the time of the tests. The losses assumed for the pretensioned steel had probably occurred, as the model took a long time to build, the members were relatively thin so the creep and shrinkage rates were high, and the laboratory air was generally dry, especially in the period after the deck had been cast. However, the girders were quite old at post-tensioning, and this would have resulted in relatively smaller losses in the post-tensioned strands since the creep of old concrete is much smaller than that of young concrete.

The theoretical cracking moment curves were drawn with sharp discontinuities at the edges of the splices, while there is in reality a transition zone in the area where the stress in the pretensioned strands is being developed by bond. Cracks at the center of the splice developed at moments considerably higher than the expected values. Cracks at the edges and up to about 1 ft (300 mm) or more from the joint were at about the expected values, while cracks 2 ft (600 mm) or more from the joint were at moments higher than the theoretical values. This implies that the transfer length for the small pretensioned strands was no more than 2 ft (600mm).

Theoretical negative cracking moments are plotted in Fig. 6.6. However, negative moment cracking occurred at moments much lower than the computed moments. The first crack occurred at the central pier at load 54, at a live load moment of about 1,900 kip-in. (215 kN-m), while the expected moment was about 4,800 kip-in. (542 kN-MO). The moment was substantially above the moment caused by single service vehicle in one span, but was only slightly higher than the service load moment due to a lane loading. Other cracks also formed at much lower moments than had been anticipated.

Since this model was built and tested, analyses of the creep and shrinkage effects on stresses in many continuous, composite, post-tensioned structures have been completed (5). The results of these analyses can help in understanding some reasons for the observed cracking moments to be so much lower than the expected values. While the computer analysis developed cannot exactly model this structure as it was built, with some pretensioned and some precast reinforced elements, it is clear that differential creep and shrinkage strains between the beam and deck concretes have an enormous influence on the time-dependent behavior. It does not appear unreasonable

to expect that two-thirds of the compression existing in the deck over the central pier immediately after the structure was post-tensioned was lost within a few months.

The main reason for this large reduction in deck precompression is the large difference in age between the deck and girder concretes. The girder concrete would have exhausted most of its shrinkage potential by the time the deck was cast. This is especially true since the girder was relatively thin, which speeds the drying shrinkage, and since it was always dry rather than being outdoors all of the time. The girder concrete would consequently restrain the shrinkage of the newer deck concrete, developing tension in the deck and compression in the top part of the girder. The creep potentials of the girder and deck concretes were also very different because of the difference in age, and there was a strong tendency to transfer force from the deck to the girder as a result of the different rates of creep.

Finally, the deck concrete in the region of the central pier was not consolidated as well as the remainder of the deck. This would have had some influence, but it cannot readily be assessed. The tensile strength component accounted for about 35 percent of the nominal cracking moment at the central pier, so the complete absence of tensile strength alone could not have accounted for cracking at load 54.

This loss of precompression from the deck in the negative moment region appears to be unavoidable with this particular kind of precast, composite, post-tensioned construction. The loss can be reduced by the use of a deck concrete with low creep and shrinkage potentials, and by casting the deck when the girders are as young as possible. Unfortunately, however, the losses can probably be only slightly reduced with any reasonable degree of control, and negative moment cracking under service live loads must eventually occur in a prototype structure.

It must be noted that the situation is not worse than with current deck construction. Some precompression will remain, so the cracks should close when the structure is unloaded. The normal deck reinforcement is adequate to control the widths of the cracks, and the load-deflection curves showed that there was no sudden or significant change in stiffness of the structures accompanying cracking of the deck.

The structure was loaded to very high overloads three times at the end of the test series. Large inelastic deformations occurred in all three tests, and the last two tests caused serious damage, with the splice in the east span being nearly destroyed.

There were significant changes in the distribution of bending moments during these three tests, and the changes can be related, at least in general terms, to the damage that was occurring. These distributions are shown in Figs. 6.7 to 6.9, which are graphs of the negative moment coefficient at the central support, - M/PL, versus the applied load,P. In these graphs, P has been taken as the total of the three loads applied in the span, M is the moment computed from the measured reaction as is explained below, and L is the span, center-to-center of bearings.

The measured reactions for Tests 10, 11, and 12 on Model 1 are plotted versus load in Figs. 4.19, 4.22, and 4.29, respectively. As was noted in Chapter 4, the measurements are not entirely consistent. Both reactions generally indicate that the negative moment at the central pier was greater than the elastic moment, but the two reactions do not lead to the same moment on the two sides of the central support.

The actual moments may not be the same on the two sides of the central pier because of friction in the bearing. However, the differences should not be large, and the friction is assumed to be zero in the following discussion.

The negative moments plotted in Figs. 6.7 to 6.9 were determined using idealizations of the measured reactions. If the reaction measurements were perfect, the deviations from the theoretical elastic reactions would have been equal at the two ends of the structure. Since the measured deviations were not equal, the deviations were averaged, and the average values then were used in computing the moments. In some cases the deviations were different to a significant degree, and negative moment coefficients computed using either of the individual reactions would have been significantly different than those plotted. However, in all cases, the general trends would have been the same except at the lowest load levels.

A 20 percent increase in the negative moment coefficient occurred in Test 10, the first overloading for positive moment in the west span. There was little change during the first four load increments, and there was little new cracking in the structure. The next load increments brought a large number of new positive moment flexural cracks, especially in the region under the loads at increments 5 and 6. The last four increments caused fewer new positive moment cracks, but instead primarily caused extension of cracks. Load steps 8 to 10 also caused many new negative moment cracks near the central pier, primarily in the east span.

The changes in the moment coefficients consequently can be explained in terms of three stages of behavior. Initially, there were few new cracks and the relative stiffnesses of the sections did not change, and consequently the negative moment coefficient did not change. Later, there was a large amount of positive moment cracking which greatly reduced the stiffness of much of the west span. This caused the substantial increase in the negative moment, where the section stiffness was not reduced. Then, in the last three increments of the test there was a great deal of cracking in the negative as well as the positive moment region. During this interval, the stiffness of all sections was apparently degrading at about the same rate, and there consequently were no additional changes in the relative moment distribution.

The initial parts of the graph of -M/PL versus load for test 11, Fig. 6.8, were similar to the results from test 10. The loading produced maximum shear and a high moment in the east splice. The first several load steps produced only minor deviations in the graph, and loads 6 and 7 caused some increase in the moment coefficient, probably because of the occurrence of many new positive moment cracks. The eighth increment caused a major increase in the negative moment coefficient, and this occurred when the bond failure occurred in the lower part of the east splice. This failure greatly reduced the positive moment at the east splice, and caused the major increase in the negative moment coefficient. The structure tried, with some success, to transform itself from a two-span continuous beam to a two-span beam with a hinge at the location of the east splice, and the moment diagram changed to reflect this transition. There was actually a small increase in the negative moment at the central pier, but the major drop in load makes this appear as a major increase in the moment coefficient.

Test 12 was another loading for maximum positive moment in the west span, with the loads in the same positions as in test 10. The initial negative moment coefficient was higher than in earlier tests, presumably as a result of the accumulation of damage in those tests.

There was minor but erratic increase in the negative moment coefficient in much of the test. Some spalling of concrete from the bottom of the east splice occurred after load 5 had been in place for a few minutes and there was a small drop in the negative moment coefficient at that load. The next several load steps brought additional erratic increases in the moment coefficient. Load 11 caused a drop in the moment coefficient which was within the scatter band of the data, but the reduction was actually a warning of later events. Major new cracking was starting in the bottom of the east splice at this load, and the following two load steps did great damage to the splice. As the splice was damaged, its moment capacity dropped, and consequently the negative moment at the central pier was reduced, in both relative and absolute terms. Further attempts at increasing the load caused only minor changes in the load but caused major changes in the distribution of the moments as the splice was destroyed. As an illustration of the change in the absolute reaction due to live load, the east reaction due to the applied load was 9.95 kips (44.3 kN) downward at load 11, and it dropped to 7.65 kips (34.0 kN) at load 12, even though the load decreased by only 2.5 percent. The last two load increments brought very small increases in the reaction, and small changes in the negative moment coefficient as the splice was further damaged and lost additional capacity. The change in moment coefficient was accompanied by a 19 percent decrease in the actual negative moment from load 11 to load 14, although the load was essentially the same.

The changes in the negative moment coefficient which occurred in Test 10 were similar to those that occurred in the prototype test (Ref. 1, Fig. 7.11) in many respects. The negative moment in the prototype was less than the elastic value early in the tests, but there was a marked increase in the negative moment coefficient as the load was increased, until late in the test. The last few load increments then caused little change in the negative moment coefficient, and apparently for about the same reasons that there was little change in the model. Large amounts of negative moment cracking occurred in both model and prototype. Test 10 and the final test

on the prototype appeared to have caused comparable levels of damage in most respects, except that there was more shear distress in the prototype, in the region immediately adjacent to the splice in the loaded span.

Several moment diagrams are shown in Figs. 6.10 to 6.12, and these also help one to understand the behavior of the structure at the end of the tests. Fig. 6.10 shows three diagrams for loadings for maximum positive moment in the west span. Test 10 ended at load increment 10 without causing major damage to the structure, and the moment diagram for this case is shown. The applied moment is well within the envelope of moment capacity as it varies along the span, although the moment at 22.5 ft (6.9 m) was about 96 percent of the capacity.

Test 11 caused a positive moment failure in the east splice just as load increment 8 was reached. No readings of loads or reactions were made, and consequently a moment diagram cannot be constructed with too much confidence. The moment diagram for load increment 7 is shown in Fig. 6.11, and is based on the measured reactions, averaged as described earlier. The moment diagram shown for load 7a is an approximation for the peak load reached in the test, about 83.8 kips (373 kN), and has been drawn assuming the same distribution of live load moments that was found for load 7, even though there was probably some increase in the negative moment coefficient during that interval.

The variation in the moment capacity along the span is also shown. There is a reasonable amount of uncertainity about the actual value of $M_u$ near the splice, as it was reinforced by the post-tensioned strands and by a group of #7 (22.2 mm diam) reinforcing bars which were joined by an inadequate lap splice.

The minimum strength of the splice section is that corresponding to the post-tensioned steel only and that moment capacity is indicated by the solid horizontal part of the graph through the splice length. The capacity added by the five #7 bars (22.2 mm diam) is quite uncertain. The basic development length for these bars is 21 in. (533 mm) according to the 1974 AASHTO Interim Specification for Bridges (12). A lap splice of all bars would require 1.7 times this basic length, or about 36 in. (915 mm), while the bars were lapped only 14 in. (356 mm). It consequently might be assumed that the spliced bars could develop only

14/36 = 0.39 of the yield stress, or about 24 k/in.$^2$ (165 N/mm$^2$). A moment corresponding to the capacities contributed by the post-tensioned reinforcement plus the low stress in the lapped reinforcing bars is plotted as a broken horizontal line in the graph. This probably represents an upper limit on the actual moment capacity, as the two components of this moment may not be summable. The 24 k/in.$^2$ (165 N/mm$^2$) stress in the reinforcing bars will be reached at a relatively small curvature in the section, while the limiting stress in the post-tensioned steel is associated with a much larger curvature.

Consequently, it is not surprising that the east splice failed as load 11-8 was applied, but it is likewise clear that the exact failure load was not predictable.

The lapped bars, in hindsight, were clearly a detailing mistake. They were not required in the section, as the moment capacity given by the post-tensioned reinforcement was adequate to meet the design requirements. The five #7 bars in the central segment were required near the central pier, both as tension reinforcement for handling of the segment and for compression reinforcement to control the neutral axis position as ultimate was approached. However, the bars could all have been cut off by the time the end of the segment was reached.

Instead, the bars were left to continue into the splice, and bars were added to the end segments, in order to give some reinforcement for crack control, as the post-tensioned strands were in ducts and were not near the lower surface of the splice concrete.

It appears now, without tests to confirm the behavior, that at most the two outside bars should have continued from the central segment into the splice. Then, two smaller bars should have been added to the end segments, to extend into the splice and lap with the bars from the central segment. Two #3 or #4 bars (9.5 or 12.7 mm diam) would have been adequate, they would have developed their yield stress without bond failure, and if they had failed in bond, they would not have disrupted the cross-section so greatly.

There has been recent work in the area of bond strength with closely spaced bars, [13,14] which suggests that even the low reinforcement stresses implied by the AASHTO Code may be considerably too

large, but this is an area in which much additional information would be needed in order to fully define the problem.

The reinforcement in the splices in the prototype structure described in Ref. 1 was quite different than in Model 1. The four #9 (28.7 mm diam) bars in the south splice of the prototype, in the span subjected to the large overloads in the final test, were lapped by 38 in. (965 mm). The basic development length for the Grade 40 steel (276 $N/mm^2$) was about 21 in. (525 mm) for concrete with a compressive strength of 6,000 $lb/in.^2$ (41.4 $N/mm^2$), and this was treated as a Class C splice requiring a lap of 1.7 times the basic development length. There were no difficulties with this splice, and the moment at the splice was about 95 percent of the calculated capacity at the end of the test. The calculations were made assuming that the full yield stress could be developed.

The comparatively small amount of reinforcing bar steel in the splice plus the long lap length combined to produce an adequate joint detail.

The bars in the north splice in the same test structure were jointed with Cadweld splices, and there were no problems. The moments applied to this splice were much smaller than those applied to the south splice.

The first in-service structure, shown in Fig. 1.3, had a different joint detail. Four #9 (28.7 mm diam) from the central segment and two #6 (19.1 mm diam) from the end segment extended into the splice area. The splice had a keyed shape, and was 12 in. (300 mm) long at the lower flange. All bars were hooked. Since only the force of the two smaller bars had to be developed in the splice, the detail also appears adequate. No tests of the particular connection detail have been performed.

After the test on the east span was ended, an additional test was run on the west span. Test 12 was a loading for maximum positive moment, and the loads were in the same locations as for test 10. The initial parts of test 12 were much like test 10, except that the negative moments at the central pier were generally higher.

A peak load was reached at increment 11, to 97.4 kips (433 kN), at which time the east splice started undergoing very serious distress due to the imposed negative moments. The moment diagram for the loaded

span is shown in Fig. 6.10, along with the moment diagram for the last step in test 10 and the moment capacity diagram. It can be seen that the positive moment at the central load, 22.5 ft (6.86 m) from the central pier, was equal to the computed ultimate moment.

After considerable additional deformation, the test was ended at increment 14, with 97.6 kips (434 kN) as the final load. By this time the negative moment capacity of the east splice had been reduced considerably and the negative moment at the central pier had fallen from about 4880 to 3960 k-in. (551 to 447 kN-m). This caused an accompanying increase in the positive moment throughout the span, and the positive moment at the central load was about 5 percent greater than the calculated ultimate moment. This section was in fact very close to failure, as the first signs of a crushing failure were found in the top of the deck under the central loading beam when it was removed after the test. This crushing occurred only in the top-most layer of the concrete, to a depth of perhaps 1/8 in. (3 mm), but it extended across the full width of the deck.

The moment diagram for the unloaded span is shown in Fig. 6.12, for load increment 12-11, which produced the maximum negative moment measured at the central pier. The nominal capacity is also plotted along the span, and it can be seen that the applied moment was always considerably less than the nominal capacity. The negative moment failure which occurred in the east splice during the final test was obviously initiated by the disruption of the compression zone which had occurred when the bond failure occurred in the splice.

The structure apparently would have been able to support more load if the east splice had not failed. However, it is also relatively clear, considering that the positive moment was very close to the ultimate value, that any additional load would have been accompanied by very large additional deflections.

The shear strength of the structure was not evaluated after the testing was completed. There was no evidence of impending shear failure, and the additional information that might be gained appears minimal. The original design for shear had been done quite conservatively, and after it was done some direct substitutions of #3 bars (9.5 mm diam) for #2 bars (6.4 mm) were made so that #3 bars could be used throughout.

## 6.3 Discussion of Results of Tests of Model 2

The results of the tests of Model 2 are discussed in this section, and the information will be presented and developed in about the same way as done for Model 1 in the previous section.

Three moment diagrams are shown in Figs. 6.13 and 6.14, to help understand the behavior of the structure. First is the moment diagram existing when the structure was still on its temporary supports. At this stage, the full dead load is present, including the blocks used for dead load compensation, but the moments at the splices are still zero. Fig. 6.13 also shows the moments caused by the removal of the temporary supports. The total final moment diagram, which is the summation of the moments while the structure was supported on the final and temporary supports plus the moments due to removal of the extra supports is in Fig. 6.14. The final negative moment at the central support was about 76 percent of the moment of $wl^2/8$ normally associated with a uniformly distributed load on a two span beam. The moment is lower because of the construction sequence.

The actual negative moment may have been slightly smaller than the value plotted in Fig. 6.14. The moments plotted are the results of a series of elastic analyses. The change in end reaction due to the removal of the temporary supports was measured, and was found to be 3.9 kips (17.3 kN) while the computed value was 3.64 kips (16.2 kN). The agreement is relatively good, but the difference indicates that the negative moment at the central pier may have been smaller than the expected value.

The stress distributions along the top and bottom of the member due to the combined effects of the final dead load moments and the prestressing forces are plotted in Fig. 6.15. The calculations were made based on uncracked section properties, even though some cracks were found immediately after completion of the structure and removal of the temporary supports.

The indicated stresses at the splice and near the central pier were in excess of 500 lb/in.$^2$ (3.5 N/mm$^2$), and consequently the observed cracking was generally as expected. The stress gradients near the ends of the precast members were naturally not as sharp as are shown. Because of

the transfer length of the strand, there are really transition zones extending from the edges of the splice into the precast elements by as much as 1 ft or more (600 mm). The reality of this is apparent in the crack patterns shown in Figs. 5.1 and 5.2, which show the cracks which occurred due to dead load alone. There were cracks in each splice, and also in each precast element on each side of both splices. These cracks occur at distances up to about 12 in. (300 mm) from the splice face.

After the stress distributions shown in Fig. 6.15 were determined, cracking moments were computed. The precompression existing at dead load was added to the modulus of rupture of the concrete, and the sum was multiplied by the appropriate section modulus to obtain a net cracking moment in excess of the dead load moment.

For the case of the positive moment, the dead load moment was then added to obtain the total or gross cracking moment, and the variation of this quantity along the span is plotted in Fig. 6.16. Two different values of the expected cracking moments are shown. The tensile stresses considered were $6\sqrt{f'_c}$ and $7.5\sqrt{f'_c}$, where both the tensile stress and $f'_c$ have units of $lb/in.^2$ If $f'_c$ is expressed in $N/mm^2$, the numerical constants are 0.5 and 0.62, and the tensile stress is in $N/mm^2$.

In the case of the negative moment at cracking, the net moments in excess of the dead load moment are plotted versus position in the span in Fig. 6.17.

The observed positive moments at cracking are also plotted in Fig. 6.16. Since the loads were applied in finite steps, there is some uncertainity about the precise moments precipitating cracking at a particular point, so a range of moments was evaluated. As an example, load 93 caused a crack 17 ft (5.2 m) east of the central pier, and the moment is plotted as a triangle in the figure. It was known that this crack had not occurred at load 92, and the moment caused by load 92 is plotted directly below that for 93, and the two points are connected by a short vertical line.

The moments were computed assuming that the moments were elastically distributed for tests 1 through 10, and the deviations from the elastic distributions were taken into account for the later tests. The reaction measurements presented in Chapter 5 indicated some deviations

from the elastic values during the initial tests, but the deviations were generally small, and usually not consistent with each other.

Considering sections more than 15 ft (4.6 mm) from the central pier, the east span cracking moments were generally smaller than the expected values. The west span values were slightly higher than in the east span, and sometimes exceeded the expected values. The differences between the two end segments were not large, but they were consistent. There were no significant differences in concrete quality in the two segments, and the workmanship appeared to be the same. There may be some differences in the actual moment distributions, but these cannot be reliably assessed. The west span was loaded to the cracking level before the east span, and the response to the later tests may have been slightly different.

The reality of the finite development length of the pretensioned strands is again readily apparent. The observed cracking moments in the regions 2 to 3 ft (600 to 900 mm) each side of the splice are much lower than the moments computed assuming that the strands were fully developed at the ends of the segments. However, it is also apparent that the stresses were being developed, as the cracking moments 1.5 ft (450 mm) from the splice were appreciably larger than at the splice. The development of precompression in this region is complicated by the presence of the #7 (22.2 mm) splice bars which were also carrying significant stresses in this region.

Some information about the negative moment cracking is given in Fig. 6.17. The net cracking moments for the two different values of the modulus of rupture are plotted, along with the live load negative moment diagrams for several different loads. On each moment diagram is also plotted a circle or triangle that corresponds to the crack which occurred farthest from the central support at that particular load. Thus, load 64 caused a crack about 3.5 ft (1.1 m) east of the support, and load 117 caused a negative moment crack 14.5 ft (4.4 m) west of the support.

The agreement between the predicted and observed extent of negative moment cracking is relatively poor, and the predicted values are nearly always too high. For example, load 92 caused cracks as far as 13 ft (4 m) from the central support, while the prediction would have

been that the last crack would have been about 5.5 ft. (1.7 m) from the support. In addition to the lack of agreement about the location of the crack, it occurred at a live load moment of about 850 kip in (96 kN-m), while the predicted value was nearly 3,000 kip-in. (340 kN-m).

The generally low cracking moments for negative moments must be largely due to differential shrinkage between the cast-in-place slab and the precast beam. The concretes were of comparable qualities, but of quite different ages. The deck was cast much later than the beams, and it would have undergone considerable shrinkage during a time interval when the girders were not shrinking appreciably. This shrinkage would have been restrained by the girder concrete, and this would have induced tension in the region near the central support, and cracking resulted at dead load alone. Farther from the central support, the removal of the temporary supports induced compression in the deck, but this compression would have been reduced with time by the shrinkage forces, and this would have led to the low negative moments at cracking.

The compression that originally had been resisted by the deck would have been partially transfered to the girder, and there would have been some large redistributions of stress across cross sections with time.

These redistributions are extremely hard to measure, but they have been predicted by the analyses presented in Refs. 5 and 15.

The premature cracking of the deck did not have any major influence on the later behavior of this structure. The cracks remained small, as the deck reinforcement was both adequate in area and well distributed, and was quite capable of limiting the crack widths to relatively small values.

The final five tests, numbered 11 through 18, were to high overloads, and all caused significant damage to the structure. Test 18 ended with the total collapse of the west segment of the structure because of destruction of the west splice.

Test 11 was a loading for maximum positive moment in the east span. Before the end of this test three pretensioned strands were broken at one of the draping devices, and this caused a large change in the distribution of the bending moments in the structure. The negative

moment coefficient, - M/PL, for the section at the central pier is plotted versus applied load in Fig. 6.18, and it illustrates the changes which occurred. Initially the moment coefficient was considerably less than the elastic value, but it increased gradually with increasing load until a load of 67 kips (298 KN) was reached. This gradual increase probably continued until 72 kips (320 KN) had been applied, which was the load when the strands broke, but no readings of loads and reactions were obtained.

The low initial moment coefficient was probably due to the state of the structure at the end of the previous tests. The positive moment regions had been cracked, but because of the pretensioning forces the cracks were tightly closed under the dead load forces. The negative moment regions were also cracked, but the cracks in the deck were generally not tightly closed under dead load forces. Consequently, for the initial part of the loading, the structure responded as a non-prismatic member with larger values of EI in the positive moment regions than in the negative moment regions.

As the load increased, the positive moment cracks reopened as the precompression was overcome, and the negative moment coefficient increased gradually as the section rigidities approached the same values.

Then, when the three strands broke in the east span, there was a large change in the moment distribution as the structure relieved itself of some of the positive moment, and in doing so greatly increased the negative moment both as a moment and a moment coefficient at the central piers.

Further attempts at loading the structure, which eventually brought the load back to about 62 kips (276 KN), caused further increases in the negative moment coefficient and also caused large increases in deflections.

Test 13 was a second loading to produce maximum positive moment in the east span, with the loads in the same position as in Test 11. The interpretation of the reaction data to give negative moment coefficients is somewhat complicated in this test by the presence of significant residual forces in the structure at the end of test 11.

The exterior reactions were 2.0 kips (8.9 KN) smaller at the end of test 11 than they had been at the beginning of the test. This indicates that the negative moment under dead loads only at the central pier was considerably larger after the test than it had been at the beginning of the test. Consequently it is possible to interpret the results of test 13 either including or ignoring the locked-in forces resulting from the damage caused by test 11.

Fig. 6.18 includes two curves of negative moment coefficient versus applied load for test 13. The one marked "no residuals" is the moment coefficient obtained using only the reactions measured during test 13. This graph indicates a gradual increase in the moment coefficient with increasing load until a load of about 60 kips (267 KN) was reached, and then a major increase in the coefficient accompanied further increases in load. In the other curve for test 13, the 2 kips (8.9 kN) residual reaction from test 11 was included in the evaluation of the negative moment coefficient.

Both curves for test 13 indicate a great change in behavior when the load of 60 kips (267 KN) was exceeded. Inclusion of the residual reaction force leads to a moment coefficient at the end of test 13 which was comparable to that at the end of test 11, which is a quite reasonable agreement. These data can be interpreted to mean that the structure reacted more or less as a prismatic beam to the applied load as long as that load was low enough. Once the load exceeded 60 kips (267 kN), the positive moment capacity had been approximately reached, and the additional loads were resisted largely by negative moments rather than by increases in both positive and negative moments.

At the end of test 13, the residual reaction forces had increased slightly, so that the end reactions were 2.35 kips (10.5 kN) less than at the beginning of test 11.

Fig. 6.18 also includes two graphs of negative moment coefficient versus applied load for test 14, which was a loading for maximum shear at the west splice. One line includes the residual moment effects and the other does not. The curve which does not include the residuals is probably the best indicator of the behavior of the structure during the test. Initially the negative moment coefficient did not vary

appreciably with applied load. This is probably reasonable, as the structure had not been severely damaged as far as this particular loading position was concerned. The east span had been damaged by excessive positive moments, but this loading was producing negative moments in that span, and the damage was not so severe that the compression zone at the bottom of the beam was disabled.

The behavior of the structure changed when the applied load exceeded 67 kips (298 kN), and the negative moment coefficient increased steadily throughout the remainder of the test. The cause for this change in behavior was yielding of the reinforcing bars which provided the positive moment resistance in the splice. This can be seen very clearly in Fig. 5.32, which is a graph of reinforcement strain versus applied load. In that graph, the great reduction in slope of the curve also occurred at a load of 67 kips (298 kN). The load-deflection curves for the same test, Fig. 5.29, do not show such marked changes in slope but instead indicate a gradual increase in the rate of deflection with applied load until substantially higher loads were reached. This is not inconsistent, however, as the structure was able to support the additional loads because of increases in the negative moment since yielding had not occurred at the section.

In terms of the changes in the negative moment coefficients, the final tests on the structure were quite similar to test 14. That data will not be presented here, but was utilized in the construction of bending moment diagrams at various load stages, as are discussed next.

A series of moment diagrams are given in Figs. 6.19 to 6.21 to illustrate the behavior of the structure as the failure loads were approached.

Moment diagrams for three load steps in tests 11 and 13 are shown in Fig. 6.19. These loadings produced maximum positive moment in the east span, and the highest load reached was about 72 kips, immediately before the fracture of three strands. The moment diagram for this load has been plotted, along with the diagram showing the variation of the moment capacity along the span. No readings of load or reaction were recorded at this peak load, but the negative moment coefficient was assumed to be 0.083, on the basis of an extrapolation of the lower part of the curve for test 11 in Fig. 6.28 to a load of

72 kips (320 kN). The graph indicates that the applied moment was about 105 percent of the computed ultimate moment over a short length of the beam at about 22.5 ft (6.9 m) from the central support. The three strands fractured in the draping device located 1 ft (300 mm) from the point of maximum moment. At the same load, the negative moment was substantially less than the computed capacity.

The variation of moment capacity along the beam is complex. The central segment has a number of draped pretensioned strands, and in addition 6-#7 (22.2 mm diam) reinforcing bars. The moment capacity variation in this part of the beam is due to the variation in the effective depth of the strand. The splice itself contains only the 6-#7 (22.2 mm diam) bars. The end segment contains the 6-#7 bars, and draped and straight pretensioned strands. The last pair of the #7 bars ended just 6 in. (150 mm) short of the drape point. As a result of the termination of the bars and of the presence of the draping device in the same part of the beam, it might be argued that there was a stress concentration present which contributed to a premature failure of the three draped strands. However, the fact that the applied moment was apparently 5 percent greater than the computed capacity indicates that the failure was not particularly premature. A greater separation of the last bar cut-off point and the drape point would have been desirable, but this cannot be considered to be a significant detailing error. The draping device itself introduces a stress concentration because of the relatively abrupt change in the direction of the strand, and the failure of the strands at that point at the high moment sustained should not be surprising. Similar failures have been observed in other test specimens (16).

The strand deflector was made in the laboratory especially for the beam. The strands were spaced vertically at 1.5 in. (38 mm), and were deflected by passing over pulleys having diameters of about 1 in. (25 mm). This is comparable to the situation in prototype construction, in terms of the relative diameters of the strands and pulleys.

Fig. 6.19 also contains moment diagrams for two other loads. The diagram for 58.3 kips (259 kN) load is that existing immediately after

the failure of the three strands. The decrease in positive moment and small increase in the negative moment can be seen.

The moment diagram for test 13, at 64.8 kips (288 kN) is that existing at the maximum load reached after the failure of the three strands. There was a small increase in positive moment over that immediately after the failure, but most of the additional load was resisted by increased negative moments. This moment diagram was drawn including the residual forces remaining in the structure at the end of test 11.

Fig 6.20 contains three moment diagrams for loadings which produced maximum shear at the west splice. The moment diagram for load 146, to 67.34 kips (300 kN) was at the load step immediately before the strain gages indicated major yielding of the splice reinforcement. Load 152 was at the last step in test 14, and was to a total load of 85.22 kips (379 kN). The indicated moments are slightly less than the computed capacities at the central support and at the west edge of the splice.

The moment diagram for load 173, 89.87 kips (400 kN), indicates that the moment at the central pier was very slightly larger than the computed capacity, and that the capacity at the west edge of the splice had also been reached. This would indicate that the structure should have formed a flexural mechanism, and that is approximately the situation. This load was the last step in test 16, and was the maximum load applied to the structure. It also produced the largest negative moment found in any test. An additional test was conducted, but the structure collapsed before this load level was reached again.

These three moment diagrams were constructed including the accumulated residual reaction forces resulting from the damage caused in earlier tests. The end reactions at the beginning of test 14 were about 2.35 kips (10.5 kN) less than at the beginning of the overload testing, and they were about 2.63 kips (11.7 kN) less at the beginning of test 16. These values were obtained by summing the successive residuals of the earlier tests, and are the best available estimates. However, they may be too large as there was probably a tendency for the structure to "relax" during the periods between tests, with the

reactions tending back toward their earlier values. This cannot be evaluated, but if it happened the tendency would be for the negative moments to be smaller than those plotted, and the positive moments to be correspondingly larger.

There is at least some evidence that the positive moments were in fact larger than indicated in the moment diagrams. The measured steel strains in the splice, together with the information from the tests of the splices which is discussed in the following section, indicate that the steel stress at failure of the structure was significantly higher than the yield stress. Consequently, the moment at the splice should have been larger than the nominal computed capacity, and the negative moment smaller than indicated.

At the end of the test, the splice section was completely destroyed because of shear distress that followed large flexural deformations. However, the negative moment region was still relatively intact and did not appear to be close to a flexural failure condition. Neither compression nor tension strains at the central pier were approaching limiting values. It thus appears reasonable to assume that the final moment diagram is only an approximation to the real diagram, and that the negative moment shown in the diagram for load 173 is probably a little larger than the actual value. However, the error is probably not large, and the maximum load of 89.87 kips (440 kN) was in good agreement with the expected flexural failure load.

The moment diagram for the unloaded span at load 173 is shown in Fig. 6.21. The applied moment exceeded the computed capacity at the central pier by a very small margin and was considerably less than the capacity at all other sections. The normal reinforcement in the deck was adequate as reinforcement of the splice for negative moment. The damage that occurred in the east span in test 11 was not serious enough to interfer with the negative moment capacity required in test 14 and later.

The shear capacity will not be discussed. The failure mode was adequately described in Chapter 5, and the mode of failure is not one that lends itself to analysis, since it was due to sliding of sections on the two sides of a smooth flexural crack that opened after the flexural reinforcement had yielded.

## 6.4 Performance of Cadweld Splices

The Cadweld splices in the joints in model 2 were an extremely important part of the system, and consequently their behavior and general characteristics must be examined. The process for making the splices is described in Sec. 2.4.6 and in Appendix A.

The Cadweld splice is a mechanical splice, and its strength does not depend on welding of the bars. Instead, it depends on developing shear stresses in the filler metal, and stresses comparable to bond stresses between the spliced bars and the filler metal, and between the splice sleeve and the filler metal.

There is some slip between the bar and sleeve as the shear stresses develop, and consequently the stress-strain curve for a length of bar containing a splice is different than that for a continuous bar. A number of stress-strain curves are shown in Figs. 6.22 to 6.25 to illustrate this, and the first of the series is the curve for an unspliced bar, which serves as a basis for comparison.

Fig. 6.23 shows three curves for tests of new splices, that is, splices that had not been previously loaded. The strains were measured over a 10-in. (254 mm) gage length which was centered across the splice. Consequently, the strain is an average of the elongation in the exposed 5 in. (127 mm) of bar and in the 5-in. (127 mm) sleeve length. The curves differ in details but not in overall characteristics. The loss in load at first slip is partially dependent on the testing machine characteristics, and is prominent here because the machine used is very stiff. The drop in load after first slip was recorded only because the extensometer had an electronic elongation sensing device (LVDT), and this drop normally is not seen if a dial gage extensometer is used since a continuous record cannot be made.

The first major slip is believed to be the failure of whatever accidental welding that may have occurred between the bars and filler metal in the small gap between the bar ends. The filler metal is hot enough at this point in the splice to make some welding possible, but the characteristics of both filler metal and bars prevent any reliable welding, and the loads at first slip are normally quite erratic.

The splices were designed to develop 90 k/in.$^2$ (621 N/mm$^2$) tension in the bar, which is the specified minimum ultimate stress for the grade 60 (414 N/mm$^2$) steel. The failure can come as a result of breaking the bar at a section away from the splice, as a result of pulling the bar out of the splice sleeve, or as a result of breaking the sleeve at the fill-hole, which is the minimum cross-sectional area. The actual failure mode depends on the strength of the bars, and to some extent on the deformation pattern. The length of sleeve is selected (by Cadweld) so that the 90 k/in.$^2$ (621 N/mm$^2$) stress can be developed with the worst deformation pattern meeting the ASTM A-615 specification, even when transverse deformations are missing, as may occur at a mill or grade mark with some brands of bars.

After the failure of the structure, the splice bars were all cut from the structure and most were tested to failure in tension. All six bars from the east splice were tested. All bars in the west splice had reverse-curve bends in the bars as a result of the total failure of the splice section. Four of these bars were straightened and tested. The other two had bends so close to the end of the splice sleeves that it appeared likely that the straightening operation would cause further damage to the splice and mask the effects of the loading, so they were not tested.

The results of all the tests on #7 (22.2 mm diam) bars are shown in Table 6.1. In this series of tests, most tests ended with the failure of the splice sleeve, generally at very high stresses. This occurred because the breaking stress of the bars was about 109 k/in.$^2$, (752 N/mm$^2$) minimum stress. The bars were made by Inland-Ryerson Steel Co., and had large, closely spaced, deformations which prevented pull-out failures.

Some of the failure stresses shown in Table 6.1 deserve comment. Specimen Test-1 was not preheated, and it is not known whether this made any difference. In this case the bars and sleeves were certainly dry, which is one of the objects of preheating to about 200° F., (93° C.) so this should not have been too important. Test-2 would have been rejected on visual inspection as there was slag rather than filler metal in the tap hole, and excess metal was lost out of the ends of the sleeve

when it was filled. The splice was tested anyway, to see how it would perform. Even though the bar was slightly too weak, its strain at 60 k/in.$^2$ was the same as that in Test-3 and less than in Test-1 at the same stress.

The east splices were made first, and there was some difficulty with the first splices because of a needed adjustment in the pouring basin. Considerable filler metal was lost on three splices, resulting in inadequately filled splices. In the north bottom outside splice, the bar gap was too small and should have been trimmed with an acetylene torch, but this was not done. There were large voids between the bar and sleeve, and the sleeve was replaced.

The replacement of a sleeve is less of a challenge than it might first appear. The sleeve was removed by cutting it twice with a cutting torch. Each cut was off to one side of the sleeve, so that the flame did not impinge on the bar. Fig. 6.26 shows the locations of the two cuts. Two cuts were required, and the sleeve was then removed in four pieces, with a hammer and chisel, and the filler metal was knocked off the bar. Since the bars being spliced were attached to heavy concrete members, one bar had to be sprung to the side to get a new sleeve on the bars. This was done after heating one of the bars in the region 6 to 9 in. from the end, and then hot bending the bar. The new sleeve was slipped onto the other bar and the bar was bent back into alignment while it was still hot. The longer of the two bars was chosen to bend, so that the heated area would be farther from the concrete. In this case, the gap between the bar ends was enlarged before the new splice was completed.

Two other splices in the east joint also had excessive voids. The south bottom outside and south top splices had voids at the top of the sleeve at one end which were larger than would normally be allowed. They were not replaced primarily because of a judgement (in consultation with a Cadweld representative) that there would be no real problem because of the very favorable deformation pattern being used. The two voids appeared very similar visually and when probed with a thin wire. One developed 85.4 (589 N/mm$^2$) and the other 99.4 k/in.$^2$ (685 N/mm$^2$) in the failure tests, with no sign of excessive slip, and both failed by breaking the sleeve.

Stress-strain curves for three Cadweld splices cut from the east splice area are shown in Fig. 6.24. The curve from the south bottom inside bar had the lowest initial slope of any bar tested, and had the highest failure load of the group. This splice was properly filled, and the reason for the low initial stiffness is not known. The south top bar, which was not adequately filled by the visual inspection criterion, had the highest initial slope, and the north bottom inside bar had an intermediate slope. These curves are markedly different from the curves for first loading, as all of the slips had occurred during the loadings on the structure rather than during the splice test. However, the existence of the yield plateau indicated that the bars had not been stressed beyond yield in the bridge test.

Stress-strain curves for two splices cut from the west splice area are shown in Fig. 6.25. In these cases, the spikes resulting from slip on initial loading are all missing, and in addition the yield plateau is no longer seen. Comparison of the curves with those for the new splices shows that the curves are similar for stress values above about 80 k/in.$^2$ (552 N/mm$^2$). This provides a clue about the stress level in the bars during the final test, with an indication of about 80 k/in.$^2$ (552 N/mm$^2$) at a strain of about 0.015 across the splice sleeve, or nearly 0.02 in the adjacent bar. This is reasonably consistent with the incomplete strain measurements made during the final tests, in which strains of 0.01 were exceeded long before the structure collapsed.

The bridge designer needs information on fatigue resistance, but unfortunately very little data is available on fatigue tests of Cadweld spliced bars. Only three fatigue tests are known to have been performed (17), on #8 (25.4 mm diam) bars, with the following results:

| Specimen | Tensile Stress, k/in.$^2$* | | No. of Cycles to Failure |
|---|---|---|---|
| | Min. | Max. | |
| 1 | 5.0 | 25.0 | 409,450 |
| 2 | 5.0 | 25.0 | 530,250 |
| 3 | 12.5 | 25.0 | 1,999,450 |

* 1 k/in.$^2$ = 6.895 N/mm$^2$

All failures occurred at the bar-splice intersections, but in the bar.

The differences in fatigue life between specimens 1 and 2 may be due to some eccentricity in the loading. The first bar was apparently not quite straight, as indicated by a slight lateral movement with each load cycle. The lateral movement would be restrained if the bar were embedded in concrete, but it is not known whether this would change the fatigue life.

In the #8 (25.4 mm diam) bar splices, the 25 k/in.$^2$ (172 N/mm$^2$) peak stress was not high enough to cause the initial slip to occur, and it is not known what the effect of slip would be. Larger bars, such as #11 (35.8 mm diam) and #14 (43.0 mm diam), would normally experience their first slip at below service load levels, so reqults of small-bar tests must be extrapolated to larger bars with great caution, if at all.

Only one other relevant fatigue test is known (18). Two large beams reinforced with single #18 (57.3 mm diam) bars top and bottom were subjected to 400 cycles of fully reversed loading, with a single midspan load acting downward until the bottom bar yielded, and then acting upward until the top bar yielded. One beam had full length bars, and in the other both bars were Cadwelded at midspan. The stiffness of both beams decayed at comparable rates during the tests, and both survived the full 400 cycles. Both were then tested to failure under downward acting loads, with failures at comparable loads and deflections.

Two other articles which are related to Cadweld splice performance can be cited. Ref. 10 is a report of tests of a series of beams reinforced with #14 (43.0 mm diam) and #18 (57.3 mm diam) reinforcing bars. Most of the beams had all bars spliced with Cadweld splices, and as long as the splices were staggered so that not all were spliced at the same section, the behavior could not be distinguished from that of companion beams without splices. If all bars were spliced at the same section, a larger than normal crack occurred at each end of the splice sleeves and the deflections were slightly larger than in the companion beam without splices. The strength in flexure was not reduced, even in the beams with all bars spliced at one section.

Ref. 11 presents data on the strength of large reinforcing bars. Most of the bars tested were spliced with Cadweld splices designed to develop the full tensile strength of the bars, and in most of the cases the bars failed at sections away from the splice. The distributions and average stresses for bar failures and splice failures were similar for a group of 113-#18 (57.3 mm diam) bars which had an average breaking stress of 96.7 k/in.$^2$ (667 N/mm$^2$).

## 6.5 Comparisons of Behavior of Model 1 and of Prototype Test Girder

Model 1 and the prototype structure which is described in Ref. 1 were similar in many respects, and several direct comparisons of the observed behavior under high overloads can be made.

Both structures were post-tensioned, and both were designed to satisfy the same set of allowable tensile stresses in the concrete. Both were constructed following the same sequence, and both combined precast, pre-tensioned concrete with post-tensioning.

Figures 4.30 and 4.31 show the cracks which occurred in model 1 as a result of all of the tests. Figure 6.27 shows the cracks which occurred in the south span of the prototype test structure. This span was subjected to the greatest overload, with a maximum load of about 328 kips (1.46 MN) being reached. This load was positioned to produce maximum shear in the splice, and did not cause failure. The cracking in the north span of the prototype structure was much less extensive, as the maximum loads reached were less than 200 kips (900 kN). The cracks are not shown here, though they are reported in Ref. 1.

The east span of model 1 failed under a load positioned to produce maximum shear in the splice, so test 11 is directly comparable to the final test in the prototype. However, the model failed prematurely because of a poorly detailed splice, and the cracking in the east span, as shown in Fig. 4.31, was considerably less extensive than in the prototype.

The west span of model 1 reached its flexural capacity, and the cracks shown in Fig. 4.30 are similar in many respects to those in the south span of the prototype structure. The prototype had not reached its flexural capacity at the end of the test, but the applied moments were approaching the capacity at the critical section for positive moment.

The prototype had many more short, narrow shear cracks at the junction of the web and upper flange of the beam than did model 1, in the region between the splice and the central support. Both exhibited the same general form of cracking, but fewer cracks occurred in the model because its web was relatively much thicker than in the prototype. The prototype web was 7 in. (178 mm), while the model web was 4 in. (102 mm). The model web would have

been less than 3 in. (75 mm) if it had been geometrically scaled, but it would have been so thin that it would have been very difficult to place either the post-tensioning ducts or the concrete in the beam.

In both structures, the crack patterns are only locally disrupted by the presence of the splices.

Figure 6.28 shows a load-deflection curve for the prototype structure in the final test on the south span. Deflection was measured at a point 70 ft (21.3 m) south of the central pier, and the location is comparable to the E50 and W50 locations used with model 1. This curve clearly indicates that the structure had not been loaded to its ultimate capacity, as the curve still has a significant slope at the end of the test, and most of the nearly 11 in. (275 mm) deflection was recovered upon unloading.

Test 11 on model 1 was the comparable loading. However, the east splice of model 1 failed prematurely and with no ductility because the reinforcement details, and consequently the load-deflection curves shown in Fig. 4.21 do not include a region in which small changes in load caused relatively large changes in deflection.

In terms of flexural damage, the west span loadings on model 1 were more directly comparable to the prototype final test loading. The load-deflection curves shown in Fig. 4.24 exhibit a region in which very small changes in load lead to very large increases in the deflection. The flexural capacity of the section had been reached in the positive moments region of the west span at the end of tests 12, and in addition the east splice had been destroyed, and the two span girder had been reduced to a mechanism with two hinges.

The greater amount of flexural damage in model 1 also shows up in the residual deflection upon unloading. More than 1/4 of the maximum deflection remained after unloading, while less than 1/10 of the peak deflection in the prototype remained when it was unloaded.

Moment diagrams for model 1 are shown in Figs. 6.10 and 6.11, for the final tests. The comparable information for the prototype structure is shown in Fig. 6.29. The final test on the prototype was the loading for maximum shear in the south span. The moment diagrams shown in Fig. 6.11 are for the maximum shear loading on the east span of model 1.

It is clear that the moment in the prototype was only slightly less than the section capacity at the section 40 ft (12.2 m) south of the central support, or at the south edge of the splice. Figure 6.11 shows that the moment capacity of the splice had been reached by the end of test 11 on model 1. The variations in the value of the moment capacities along the length of the span were generally similar, but not identical because of differences in the details of the reinforcement, and particularly in the treatment of the non-prestressed reinforcement.

The negative moments at the central pier in both the prototype and model 1 were considerably smaller than the section capacity under the loading producing the maximum negative moments in the tests. In both cases the most critical section for negative moment was located in the unloaded span, in the pier segment near the splice. This occurred because of the profile of the post-tensioned tendons, but the maximum applied moments were still much smaller than the nominal capacities. In a structure in which an asphalt topping is applied to the deck, the critical section for negative moment will always be at the central support because of the extra dead load. It will also be at the central support for those loadings which produce the maximum negative moments used for the design of the structure.

The predicted and observed positive cracking moments are compared in Fig. 6.5 for model 1. Similar comparisons are made in Figs. 6.30 and 6.31 for the prototype structure. The agreement for the prototype structure was in general better than in the model. The predictions for the model were generally lower than the observed values, and the differences are small enough that they are within the potential uncertainties resulting from the effects of creep and shrinkage on the prestressing force. The tensile stress in the concrete at initiation of cracking was clearly in excess of $6\sqrt{f'_c}$ lb/in.$^2$ ($0.5\sqrt{f'_c}$ N/mm$^2$), and generally in excess of $7.5\sqrt{f'_c}$ ($0.62\sqrt{f'_c}$ N/mm$^2$), except at the interface between the precast segment concrete and the cast-in-place joint concrete.

The fact that the east splice of model 1 failed prematurely complicates the comparisons between the model and prototype, since the final loading on the prototype produced maximum shear in a splice while the final loadings on model 1 produced maximum positive moment.

However, the final tests on both structures produces somewhat comparable levels of flexural damage which resulted in appreciable redistribution of moments with increasing load. The most directly comparable tests are test 10 on model 1 and the final tests on the prototype. Figure 6.7 is a graph showing the change in the negative moment coefficient at the central pier as a function of the applied load, for model 1, test 10. Figure 6.32 contains similar information for the prototype structure in the final test, although the coefficient is in a slightly different form.

Both curves clearly show a marked increase in the negative moment coefficient during the tests, but both also show that this increase was not unlimited but rather that the moment coefficient stabilized at a value considerably higher than the elastic moment. The changes in both cases can be related to the progression of cracking in the structure, with significant growth of positive moment cracking occurring while the moment coefficient was increasing, and with large amounts of negative moment cracking also occurring during the later stages of the tests when the moment coefficients were relatively constant.

Both structures experienced considerably more negative moment cracking than was originally expected. At a load of 261 kips (1.16 MN) there were negative moment cracks in the unloaded span of the prototype girder in the entire region from the central pier to about 74 ft (23 m) north of the pier. The theory indicated that there should not have been any cracks. By the end of the test, cracks were observed 95 ft (29 m) into the unloaded span.

The first crack occurred in the deck of model 1, directly over the central pier, when the live load moment was about 1,900 in. (215 kM-m), while the predicted moment was about 4,800 k-in. (542 kN-n). The maximum negative moment ever reached at the central pier was 5,000 k-in. (565 kN-m), at the end of test 10, and this produced cracking to 15 ft (4.6 m) from the central pier, while it theoretically should have caused cracking only very near the central pier and near the splice.

The reasons for the large differences between the prediced and observed cracking behavior in the negative moment regions were discussed in Sec. 6.2, and they apply equally to the prototype and model structures.

With the exception of the detailing problems with the east splice in model 1, the behavior of the prototype and mode structures was quite similar. The similarities extend to the patterns of cracks, the general load-deflection characteristics, and the redistributions of moments that occurred under very high overloads. The work should establish considerable confidence in the usefulness of moderate size models as a tool for studying problems in full scale structures.

# 7. SUMMARY AND RECOMMENDATIONS

The results of tests of two prestressed reinforced concrete model bridge structures are described. Both models were designed as part of a study of new methods for building prestressed concrete bridges with spans up to about 125 ft (38 m) using girder segments no longer than about 90 ft (27 m).

Two methods for constructing such bridges have been investigated. In the first, which has also been used for the construction of a full sized girder which was tested to high overloads and for the construction of two in-services overpass structures in Illinois, utilized three precast girders which were post-tensioned together end-to-end to form the full-length two-span beam. The two end segments were precast, pretensioned concrete and the central segment was precast reinforced concrete in the prototype structures, but also contained a small amount of pretensioned reinforcement in the model.

The second method utilized three heavily pretensioned girders which were joined together without post-tensioning. In this system, reinforcing bars extending into the splice region were joined by Cadweld splices before concrete was cast to complete the splice and add the composite deck.

The construction of the two models is described in detail in Chapter 2 of this report. The behavior of model 1, which was post-tensioned, is described in Chapter 4, and that of model 2, which had the Cadweld splices on the joint bars, is described in Chapter 5.

The observed behavior of the two models is compared with the expected behavior in Chapter 6. Comparisons are made between predicted and observed cracking moments, and between the applied moments at failure and the computed nominal moment capacities. Changes in moment distributions which occurred during the tests are also discussed.

It can be concluded that either of the two systems can be used to construct satisfactory structures. In both cases, careful attention must be given to the joint details to insure that satisfactory performance will be obtained under high overloads.

The post-tensioned system can be expected to remain relatively free of cracks at dead and service load levels, although some negative moment cracking will probably eventually occur at service live load levels as a result of long-term changes in the distribution of internal forces at sections near interior supports. Any cracks which do occur should be closed under dead load alone.

The pretensioned system with spliced reinforcing bars can be designed to give satisfactory service, but it must be recognized that it will be cracked at the splices and probably near the interior support under dead load alone.

On the basis of the tests, the post-tensioned structure would have a smaller permanent set following the passage of a large overload, but both kinds of structures can be designed to have adequate capacity and neither would suffer permanent or serious distress from the operational overloads of 5/3(L + I) implied by the AASHTO Specifications.

The economics of the two systems have not been assessed. Both require about the same amount of reinforcement and of concrete, and the same erection procedure. The post-tensioning operation adds some cost, but so does the Cadwelding process and the preparations necessary to insure that the splice bars are properly aligned where they emerge from the ends of the segments. It does not appear that the costs would be appreciably different.

The results of the tests of the models and of the prototype girder, together with the experience gained during the design and construction of two in-service structures, adequately demonstrate that these systems are suitable for relatively widespread use when transportation and construction limitations prohibit the use of span-length girders.

# REFERENCES


1. Fadl, A. I., W. L. Gamble, and B. Mohraz, "Tests of a Precast Post-Tensioned Composite Bridge Girder Having Two Spans of 124 Ft," Civil Engineering Studies, Structural Research Series No. 439, University of Illinois, Urbana, April 1977, 170 p.

2. "Standard Specifications for Highway Bridges," American Association of State Highway Officials, Washington, D. C., Tenth Edition, 1969, 384 p.

3. "Standard Specifications for Highway Bridges," American Association of State Highway Officials, Washington, D. C., Eleventh Edition, 1973, 468 p.

4. Khachaturian, N. and G. Gurfinkel, "Prestressed Concrete," McGraw-Hill, 1969. 460 p.

5. Fadl, A. I. and W. L. Gamble, "Time-Dependent Behavior of Noncomposite and Composite Post-Tensioned Concrete Bridge Girders," Civil Engineering Studies, Structural Research Series No. 430, University of Illinois, Urbana, January 1977, 168 p.

6. Martin, L. D. and N. L. Scott, "Development of Prestressing Strand in Pretensioned Members," Journal ACI, Proc. Vol. 73, No. 8, Aug. 1976, pp. 453-456.

7. "Building Code Requirements for Reinforced Concrete," ACI Standard 318-63, American Concrete Institute, Detroit, June 1963, 144 p.

8. "Building Code Requirements for Reinforced Concrete," ACI Standard 318-71, American Concrete Institute, Detroit, 1971, 78 p.

9. Olesen, S. Ø., M. A. Sozen, and C. P. Siess, "Investigation of Prestressed Reinforced Concrete for Highway Bridges, Part IV: Strength in Shear of Beams with Web Reinforcement," University of Illinois, Engineering Experiment Station Bulletin No. 483, Urbana, 1967, 46 p. plus Tables and Figures.

10. Sozen, M. A. and W. L. Gamble, "Strength and Cracking Characteristics of Beams with No. 14 and No. 18 Bars Spliced with Mechanical Splices," Journal ACI, Proc. Vol. 66, No. 12, Dec. 1969, pp. 949-956.

11. Gamble, W. L., "Some Observations on the Strengths of Large Reinforcing Bars," Journal ACI, Proc. Vol. 70, No. 1, Jan. 1973, pp. 31-35.

12. "Interim Specifications, Bridges, 1974," American Association of State Highway and Transportation Officials, Washington, D. C., 1974, 133 p.

13. Ferguson, Phil M., "Small Bar Spacing or Cover--A Bond Problem for the Designer," Journal ACI, Proc. Vol. 74, No. 9, Sept. 1977, pp. 435-439.

14. Orangun, C. O., J. O. Jirsa, and J. E. Breen, "Re-evaluation of Test Data on Development Length and Splices," Journal ACI, Proc. Vol. 74, No. 3, Mar. 1977, pp. 114-122.

15. Mossiossian, V. and W. L. Gamble, "Time-Dependent Behavior of Noncomposite and Composite Prestressed Concrete Structures under Field and Laboratory Conditions," Civil Engineering Studies, Structural Research Series No. 385, University of Illinois, Urbana, May 1972, 517 p.

16. Hawkins, N. M., M. A. Sozen, and C. P. Siess, "Strength and Behavior of Two-Span Continuous Prestressed Concrete Beams," Civil Engineering Studies, Structural Research Series No. 225, University of Illinois Urbana, Sept. 1961.

17. Sozen, M. A., A Report to ERICO Products Inc., Cleveland, Ohio, 1976.

18. Sozen, M. A., and W. L. Gamble, A Report to ERICO Products, Inc., Cleveland, Ohio, Sept. 1967, 13 p.

Table 2.1 Concrete Data, Model 1

Concrete Mix Data - Model 1

| SPECIMEN | W/C Ratio (by Weight) | Cement:Sand:Gravel (by Weight) | Max. Agg. (in.) | Slump (in.) |
|---|---|---|---|---|
| Beams | 0.59* | 1:1.71:2.55 | 3/4 | 8 |
| Splices | 0.59* | 1:1.71:2.55 | 3/4 | 5 |
| Deck | 0.40** | 1:1.85:2.58 | 1 1/2 | 4 |

* Added water only, dryed aggregate used
** Added water only, wet aggregates used, Ready-mix concrete.

Concrete Strength Data, $f'_c$ (psi)

Average of 3 or more cylinders

| | | West | East | | |
|---|---|---|---|---|---|
| | Center beam C | End beam A | End beam B | Splices | Deck |
| Casting date | 10/23/73 | 12/6/73 | 1/10/74 | 2/26/74 | 4/8/74 |
| 7-day strength | *7080 | 6800 | 6930 | 7970 | 6430 |
| 28-day strength | **8180 | 9020 | 8300 | 9107 | 7670 |
| Post-tensioning (5-23-74) | 8710 | 9180 | 8420 | 9480 | 7000 |

* 10-day strength
** 46-day strength

All splice strengths and all post-tensioning strengths are based on one cylinder only.

Grout Mix Data

| | WATER (lb) | CEMENT (lb) | SAND (lb) | ALUMINUM POWDER (grams) |
|---|---|---|---|---|
| Batch 1 | 50 | 100 | 100 | 6 |
| Batch 2 | 78 | 188 | 0 | 14 |

Grout Strength Data

| | Batch 1 | Batch 2a | Batch 2b |
|---|---|---|---|
| Casting date | 5/29/74 | 5/31/74 | 5/31/74 |
| 7-day strength | 7100 psi | 7450 psi | 7860 psi |
| 28-day strength | 5060 psi | 9103 psi | 6684 psi |

---

1 in. = 25.4 mm
1000 lb/in.$^2$ = 6.89 N/mm$^2$
1 lb = 0.454 kg

Table 2.2 Concrete Data, Model 2

Concrete Mix Data - Model 2

| SPECIMEN | W/C Ratio* (by Weight) | Cement:Sand:Gravel (by Weight) | Max. Agg. (in.) | Slump (in.) |
|---|---|---|---|---|
| Beams | 0.59 | 1:1.71:2.55 | 3/4 | 7 |
| Splices | 0.59 | 1:1.71:2.55 | 3/4 | 3 1/2 |
| Deck | ready mix - 5 1/2 sacks cement per cubic yard | | 1 1/2 | 2 3/4 |

* Added water only. Dryed aggregate used.

Concrete Strength Data, $f'_c$

Average of 3 or more cylinders

| | West End Beam A | East End Beam B | Center Beam C | Splice | Deck |
|---|---|---|---|---|---|
| Casting date | 4/22/75 | 5/13/75 | 7/16/75 | 10/14/75 | 10/14/75 |
| 7-day strength | 6690 psi | 6220* | 6300 | 5065$^{\Delta}$ | 5330$^{\Delta}$ |
| 11/19/75 | 7070 psi | 7300 | 6450 | 7740$^{\Delta}$ | 7073 |
| 1/29/76 | 7990 psi | 7120 | 7380 | 8380 | 7880 |

* 6-day strength

$\Delta$ based on 2 cylinders only

7 day strength corresponds to release of prestressing force and removal of forms.

---

1 in. = 25.4 mm

1000 lb/in.$^2$ = 6.89 N/mm$^2$

1 lb = 0.454 kg

5 1/2 sacks of cement/cubic yard = 306 kg/m$^3$

a) Prestressing Forces

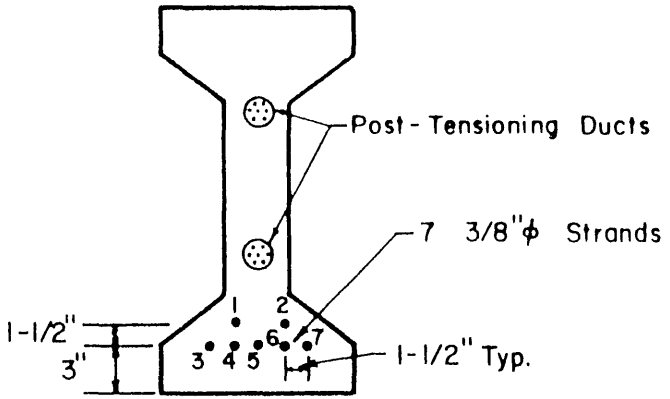


Beam A

| CABLE | $F_1$(KIPS) | $F_2$ (KIPS) |
|---|---|---|
| 1 | 16.5 | 16.7 |
| 2 | 16.5 | 16.6 |
| 3 | 15.4 | 15.5 |
| 4 | 16.2 | 16.4 |
| 5 | 15.9 | 16.0 |
| 6 | 15.4 | 15.6 |
| 7 | 15.6 | 15.7 |

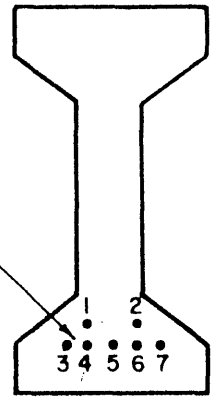


Beam B

| CABLE | $F_1$(KIPS) | $F_2$(KIPS) |
|---|---|---|
| 1 | 14.8 | 14.8 |
| 2 | 16.1 | 16.1 |
| 3 | 15.6 | 15.6 |
| 4 | 16.8 | 16.8 |
| 5 | 16.2 | 16.2 |
| 6 | 17.1 | 17.1 |
| 7 | 15.9 | 15.9 |

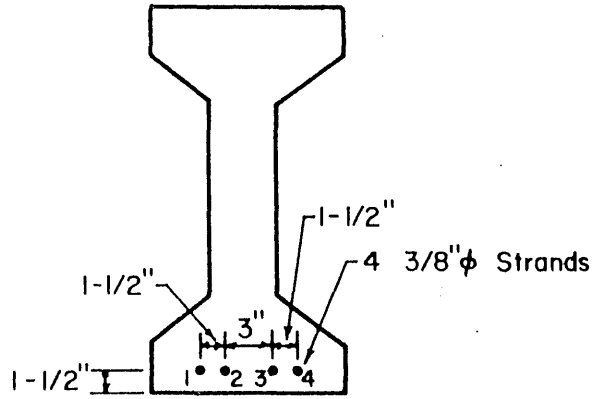


Beam C

| CABLE | $F_1$(KIPS) | $F_2$(KIPS) |
|---|---|---|
| 1 | 15.8 | 16.0 |
| 22 | 16.2 | 16.4 |
| 33 | 16.4 | 16.4 |
| 4 | 15.4 | 15.8 |

KEY: $F_1$-prestressing force prior to concrete casting

$F_2$-prestressing force at release (7 days later)

b) Post-tensioning Forces (see Fig. for Beam A)

At jacking end:

| Before Release | After Anchoring |
|---|---|
| high 18.3k | high 16.2k |
| low 16.1k | low 12.4k |
| ave. 16.7k | ave. 14.4k |

Table 2.3 Pretensioning and Post-tensioning Forces, Model 1

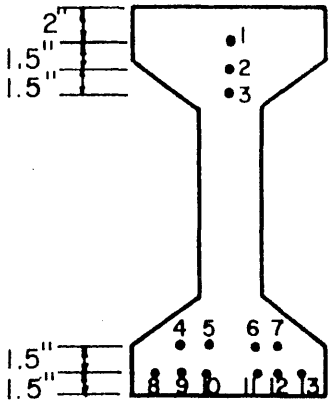


Beam A (Pier End)

| CABLE | $F_1$(KIPS) | $F_2$(KIPS) |
|---|---|---|
| 1 | 17.1 | 17.3 |
| 2 | 14.9 | 15.3 |
| 3 | 16.0 | 16.3 |
| 4 | 17.0 | 17.3 |
| 5 | 15.8 | 16.2 |
| 6 | 16.5 | 16.8 |
| 7 | 16.6 | 16.8 |
| 8 | 15.0 | 15.0 |
| 9 | 16.5 | 16.8* |
| 10 | 15.9 | 16.0 |
| 11 | 15.8 | 16.2 |
| 12 | 16.6 | 17.0 |
| 13 | 15.7 | 15.9 |

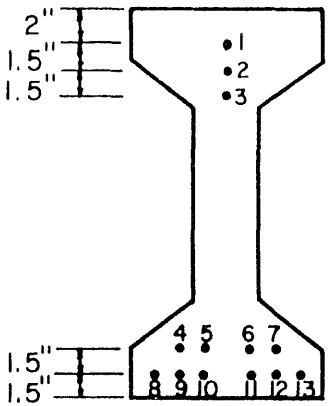


Beam B

| CABLE | $F_1$(KIPS) | $F_2$(KIPS) |
|---|---|---|
| 1 | 15.7 | 16.2 |
| 2 | 16.4 | 16.8 |
| 3 | 16.2 | 16.4 |
| 4 | 16.6 | 17.1 |
| 5 | 15.4 | 15.8 |
| 6 | 15.2 | 15.5 |
| 7 | 16.3 | 16.7 |
| 8 | 16.2 | 16.6 |
| 9 | 16.0 | 16.2 |
| 10 | 15.1 | 15.4 |
| 11 | 17.2 | 17.4 |
| 12 | 16.4 | 16.7 |
| 13 | 16.4 | 16.6 |

All Strands 3/8" $\phi$

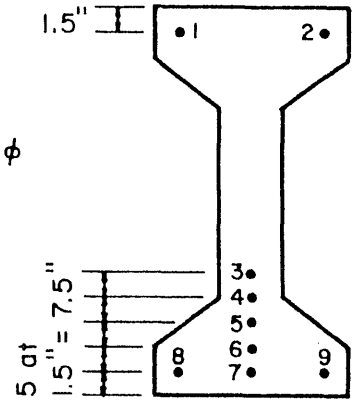


Beam C

| | $F_1$(KIPS) | $F_2$(KIPS) |
|---|---|---|
| high | 18.7 | 19.0 |
| ave. | 16.3 | 16.65 |
| low | 15.0 | 15.4 |

KEY: $F_1$ - prestress force prior to casting

$F_2$ - force prior to release (7 days later)

*approximate value

Table 2.4 Pretensioning Forces, Model 2

Table 2.5 RECORD OF EVENTS - MODEL 1

| Item Name | Date Cast | Prestress Release or Form Remvoal | | Postensioning 5-23-74 | Grouting | | Test to Failure | |
|---|---|---|---|---|---|---|---|---|
| | | Date | Age (days) | Age (days) | Date | Age (days) | Date | Age (days) |
| Beam C | 10-23-73 | 11-2-73 | 10 | 207 | 5-29-74<br>5-31-74 | 213<br>215 | | |
| Beam A | 12-6-73 | 12-13-73 | 7 | 169 | 5-29-74<br>5-31-74 | 175<br>177 | 10-10-74 | 308 |
| Beam B | 1-10-74 | 1-17-74 | 7 | 134 | 5-29-74<br>5-31-74 | 140<br>142 | | |
| Splices | 2-26-74 | 3-5-74 | 7 | 87 | 5-29-74<br>5-31-74 | 93<br>95 | 9-26-74<br>(East Splice) | 212 |
| Deck | 4-8-74 | 4-15-74 | 7 | 45 | 5-29-74<br>5-31-74 | 51<br>53 | | |

Table 2.6 RECORD OR EVENTS - MODEL 2

| Item Name | Date Cast | Prestress Release or Form Removal | | 1st Service Load Test | | Failure Load Test | |
|---|---|---|---|---|---|---|---|
| | | Date | Age (days) | Date | Age (days) | Date | Age (days) |
| Beam A | 4-22-75 | 4-29-75 | 7 | 12-2-75 | 224 | | |
| Beam B | 5-13-75 | 5-19-75 | 6 | 11-18-75 | 189 | 1-13-76 | 245 |
| Beam C | 7-16-75 | 7-23-75 | 7 | 11-18-75 | 125 | | |
| West Splice | 10-14-75 | 10-21-75 | 7 | 12-2-75 | 49 | 1-29-76 | 107 |
| East Splice | 10-14-75 | 10-21-75 | 7 | 11-25-75 | 42 | | |
| Deck | 10-14-75 | 10-21-75 | 7 | 11-18-75 | 35 | | |

Table 4.1 Loading Sequence for Model 1

| Test | Load Position | Increment Nos. | Total Load, Kips |
|---|---|---|---|
| (a) | Service Loads | | |
| 1 | E. Splice, Shear | 11 | 4.39 |
| | | 12 | 9.62 |
| | | 13 | 14.17 |
| | | 14 | 19.14 |
| | | 15 | 23.53 |
| 2 | E. Splice, Moment | 21 | 4.72 |
| | | 22 | 9.71 |
| | | 23 | 14.54 |
| | | 24 | 19.46 |
| | | 25 | 24.20 |
| 3 | W. Splice, Shear | 31 | 4.73 |
| | | 32 | 10.01 |
| | | 33 | 14.47 |
| | | 34 | 18.93 |
| | | 35 | 23.30 |
| 4 | W. Splice, Moment | 41 | 4.61 |
| | | 42 | 9.99 |
| | | 43 | 14.30 |
| | | 44 | 19.17 |
| | | 45 | 23.70 |
| (b) | Design Ultimate | | |
| 5 | W. Splice, Shear | 51 | 11.29 |
| | | 52 | 22.70 |
| | | 53 | 34.55 |
| | | 54 | 45.43 |
| | | 55 | 56.75 |
| | | 56 | 68.42 |
| 6 | W. Splice, Moment | 61 | 11.98 |
| | | 62 | 22.97 |
| | | 63 | 34.80 |
| | | 64 | 46.24 |
| | | 65 | 58.00 |
| | | 66 | 69.93 |
| 7 | E. Splice, Moment | 71 | 11.86 |
| | | 72 | 22.77 |
| | | 73 | 34.68 |
| | | 74 | 45.63 |
| | | 75 | 57.50 |
| | | 76 | 68.63 |
| 8 | E. Splice, Shear | 81 | 11.45 |
| | | 82 | 22.68 |
| | | 83 | 34.86 |
| | | 84 | 46.01 |
| | | 85 | 57.80 |
| | | 86 | 67.37 |

| Test | Load Position | Increment Nos. | Total Load, Kips |
|---|---|---|---|
| 9 | E. Span, Max. + Mom. | 91 | 12.02 |
| | | 92 | 23.49 |
| | | 93 | 35.67 |
| | | 94 | 46.95 |
| | | 95 | 58.41 |
| | | 96 | 68.84 |
| 10 | W. Span, Max. + Mom. (to high Overload) | 101 | 11.24 |
| | | 102 | 22.91 |
| | | 103 | 35.15 |
| | | 104 | 46.30 |
| | | 105 | 57.98 |
| | | 106 | 69.85 |
| | | 107 | 75.03 |
| | | 108 | 81.76 |
| | | 109 | 86.49 |
| | | 1010 | 92.23 |
| (c) | Ultimate Load Test | | |
| 11 | E. Span, Splice Shear | 111 | 12.24 |
| | | 112 | 23.90 |
| | | 113 | 36.17 |
| | | 114 | 47.65 |
| | | 115 | 58.70 |
| | | 116 | 70.92 |
| | | 117 | 77.34 |
| | | 118 | 70.34 |
| | | 119 | 69.48 |
| 12 | W. Span, Max. + Mom. | 121 | - |
| | | 122 | 23.00 |
| | | 123 | 36.00 |
| | | 124 | 46.81 |
| | | 125 | 58.46 |
| | | 126 | 69.99 |
| | | 127 | 76.21 |
| | | 128 | 82.02 |
| | | 129 | 87.71 |
| | | 1210 | 92.9 |
| | | 1211 | 97.4 |
| | | 1212 | 95.0 |
| | | 1213 | 98.2 |
| | | 1214 | 97.6 |

NOTE: 1 Kip force = 4.448 KN

Table 5.1 Loading Sequence for Model 2

(a) Service Loads

| Test | Load Position | Increment No. | Total Load, Kips |
|---|---|---|---|
| 1 | E. Span, Max. + M | 11 | 4.6 |
| | | 12 | 8.9 |
| | | 13 | 13.3 |
| | | 14 | 17.7 |
| | | 15 | 22.4 |
| 2 | E. Splice, Shear | 21 | 5.4 |
| | | 22 | 10.4 |
| | | 23 | 14.7 |
| | | 24 | 19.1 |
| | | 25 | 24.2 |
| 3 | E. Splice, Moment | 31 | 5.3 |
| | | 32 | 10.0 |
| | | 33 | 14.2 |
| | | 34 | 18.6 |
| | | 35 | 22.9 |
| 4 | W. Span, Max. + M | 41 | 4.8 |
| | | 42 | 9.9 |
| | | 43 | 14.4 |
| | | 44 | 19.4 |
| | | 45 | 23.6 |
| 5 | W. Splice, Shear | 51 | 4.8 |
| | | 52 | 9.4 |
| | | 53 | 13.9 |
| | | 54 | 18.4 |
| | | 55 | 23.1 |
| 6 | W. Splice, Moment | 61 | 5.3 |
| | | 62 | 10.9 |
| | | 63 | 13.6 |
| | | 64 | 18.5 |
| | | 65 | 23.2 |
| (b) | Design Ultimate Loads | | |
| 7 | West Splice, Shear | 71 | 22.2 |
| | | 72 | 28.3 |
| | | 73 | 33.3 |
| | | 74 | 37.7 |
| | | 75 | 42.0 |
| | | 76 | 46.3 |
| | | 77 | 51.0 |
| | | 78 | 53.8 |
| 8 | West Span, Max. + M | 81 | 21.3 |
| | | 82 | 28.6 |
| | | 83 | 34.8 |
| | | 84 | 39.3 |
| | | 85 | 43.7 |
| | | 86 | 47.6 |
| | | 87 | 51.8 |
| | | 88 | 55.3 |

| Test | Load Position | Increment No. | Total Load, Kips |
|---|---|---|---|
| 9 | East Splice, Shear | 91 | 23.4 |
| | | 92 | 30.0 |
| | | 93 | 35.3 |
| | | 94 | 39.7 |
| | | 95 | 43.8 |
| | | 96 | 48.0 |
| | | 97 | 51.0 |
| | | 98 | 55.1 |
| 10 | East Span, Max. + M | 101 | 22.8 |
| | | 102 | 28.6 |
| | | 103 | 34.7 |
| | | 104 | 39.1 |
| | | 105 | 42.8 |
| | | 106 | 46.8 |
| | | 107 | 50.5 |
| | | 108 | 54.3 |
| (c) | High Overloads | | |
| 11 | East Span, Max. + M | 111 | 24.3 |
| | | 112 | 51.4 |
| | | 113 | 55.5 |
| | | 114 | 59.3 |
| | | 115 | 62.5 |
| | | 116 | 67.0 |
| | | 117* | 58.3 |
| | | 118 | 60.0 |
| | | 119 | 62.0 |
| | | 120 | 58.2 |
| | | 121 | 62.7 |
| 13 | East Span, Max. + M | 131 | 23.5 |
| | | 132 | 50.9 |
| | | 133 | 55.1 |
| | | 134 | 59.0 |
| | | 135 | 62.5 |
| | | 136 | 64.4 |
| | | 137 | 64.8 |
| 14 | West Splice, Shear | 141 | 23.2 |
| | | 142 | 50.5 |
| | | 143 | 55.0 |
| | | 144 | 58.6 |
| | | 145 | 63.2 |
| | | 146 | 67.3 |
| | | 147 | 71.0 |
| | | 148 | 74.6 |
| | | 149 | 78.4 |
| | | 150 | 79.3 |
| | | 151 | 82.8 |
| | | 152 | 85.2 |

* After Load Loss

| Test | Load Position | Increment No. | Total Load, Kips |
|---|---|---|---|
| 16 | West Spice, Shear | 161 | 23.6 |
| | | 162 | 51.0 |
| | | 163 | 54.7 |
| | | 164 | 59.3 |
| | | 165 | 63.5 |
| | | 166 | 67.1 |
| | | 167 | 71.4 |
| | | 168 | 75.1 |
| | | 169 | 78.6 |
| | | 170 | 82.5 |
| | | 171 | 86.0 |
| | | 172 | 87.8 |
| | | 173 | 89.9 |
| 18 | West Splice, Shear | 181 | 22.6 |
| | | 182 | 50.0 |
| | | 183 | 54.0 |
| | | 184 | 58.4 |
| | | 185 | 62.4 |
| | | 186 | 66.3 |
| | | 187 | 70.4 |
| | | 188 | 74.0 |
| | | 189 | 78.2 |
| | | 190 | 82.4 |
| | | 191 | 85.9 |
| | | 192 | 88.2 |
| | | 193 | 56.6 |

Note: 1 kip force = 4.448 kN

Table 6.1 Results of Tests of Spliced #7 Bars

| Bar | Ult. Stress, K/in.$^2$ | Location of Fracture | Notes |
|---|---|---|---|
| Plain -1 | 109.0 | Near bar Center | 12.5% elongation in. 8" |
| Plain -2 | 108.9 | Near bar Center | 13.3% elongation in. 8" |
| Cadweld Test -1 | 102.6 | Center of Sleeve | Bar not preheated |
| Cadweld Test -2 | 88.3 | Center of Sleeve | Slag in fill hole |
| Cadweld Test -3 | 108.8 | 6 1/2 in. from Sleeve | |
| W. Splice bars | | | |
| S. Bottom Outside | 107.5 | Center of Sleeve | |
| S. Top Bar | 95.5 | Center of Sleeve | |
| N. Top Bar | 105.0 | Center of Sleeve | |
| N. Bottom Inside | 107.7 | Center of Sleeve | |
| E. Splice bars | | | |
| S. Bottom Outside | 85.4 | Center of Sleeve | |
| S. Bottom Inside | 108.5 | 1 3/4 in. from Sleeve | In area flattened for strain gage |
| S. Top | 99.4 | Center of Sleeve | |
| N. Top | 107.6 | 2 1/2 in. from Sleeve | In area flattened for strain gage |
| N. Bottom Inside | 94.6 | Center of Sleeve | |
| N. Bottom Outside | 91.6 | Center of Sleeve | |

1 Kip force/in.$^2$ = 6.89 N/mm$^2$

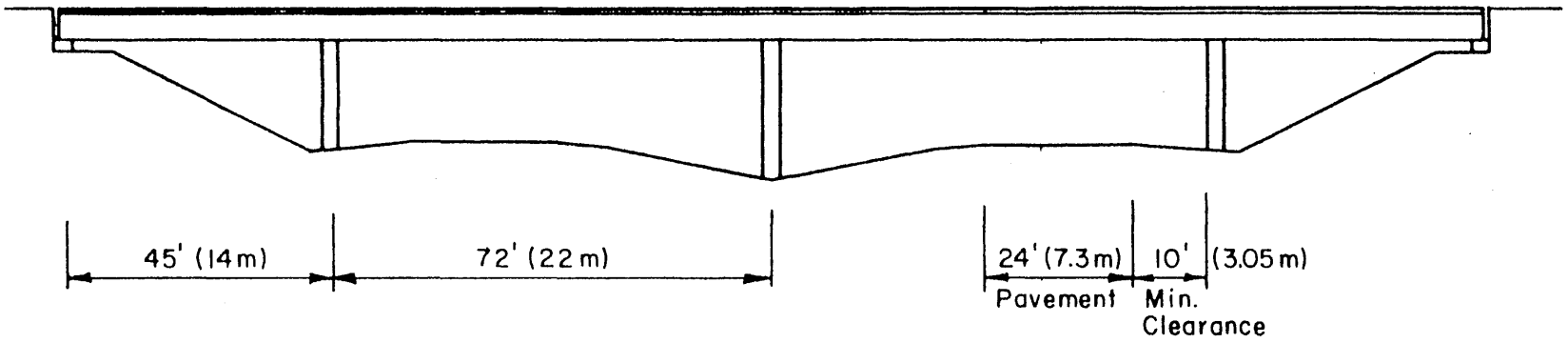


FIG. 1.1 OLDER FOUR-SPAN GRADE SEPARATION STRUCTURE

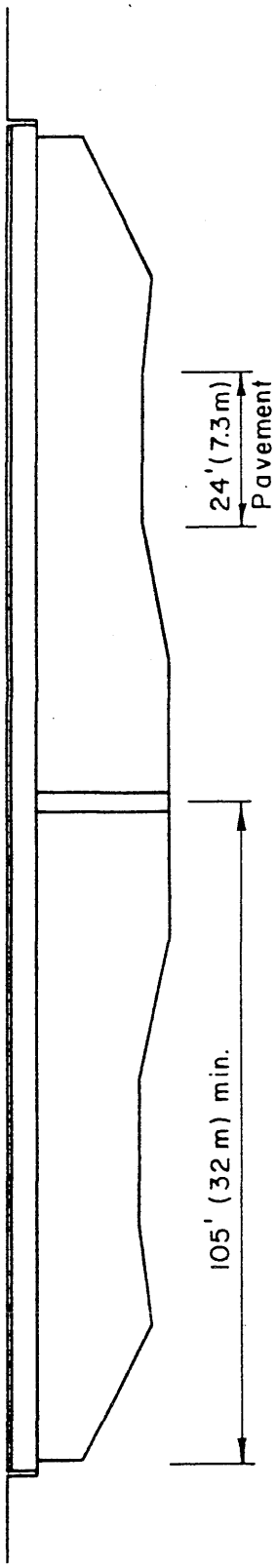


FIG. 1.2 NEW TWO-SPAN GRADE SEPARATION STRUCTURE

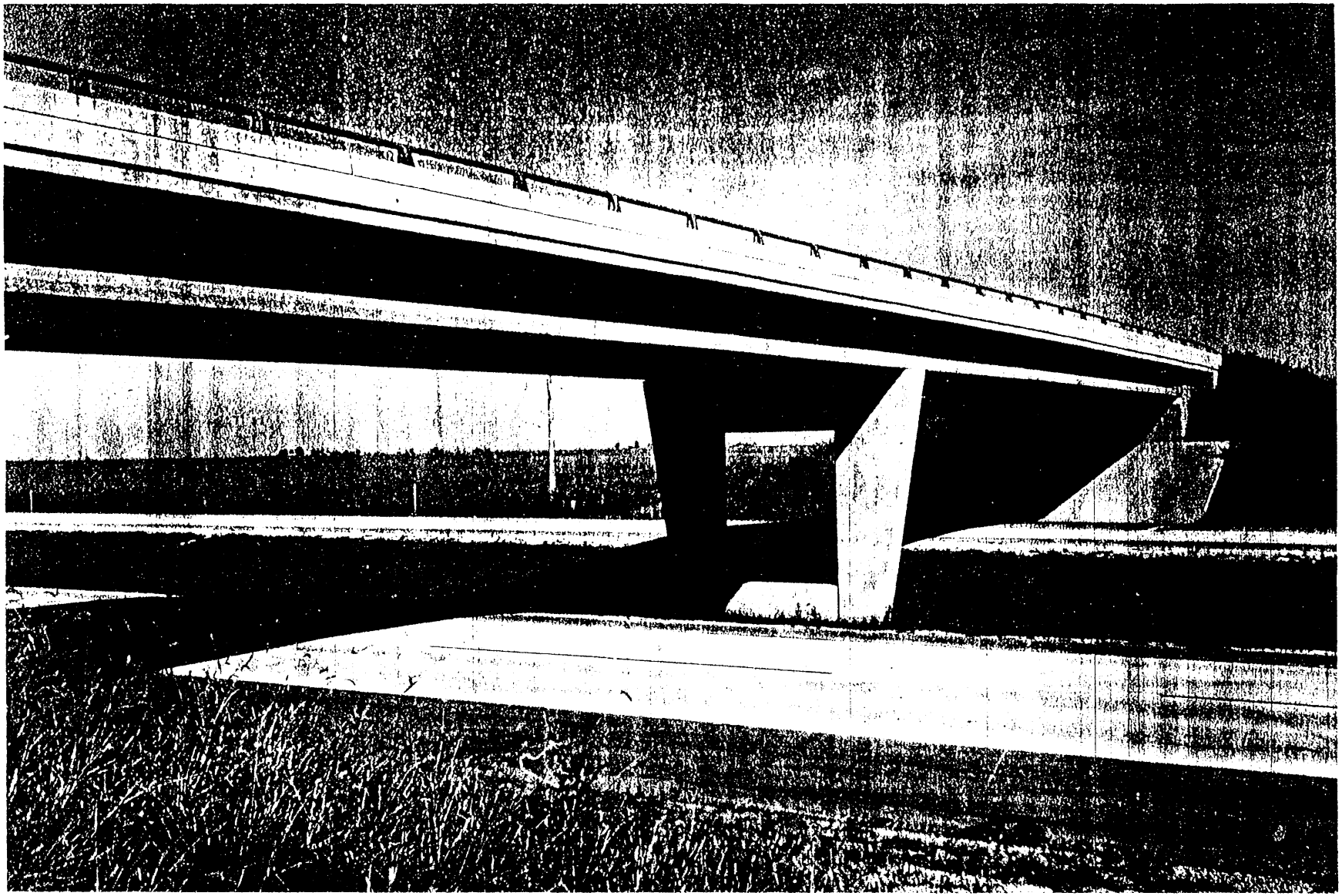

FIG. 1.3 PHOTO OF FIRST TWO-SPAN LONG-SEGMENT STRUCTURE IN ILLINOIS

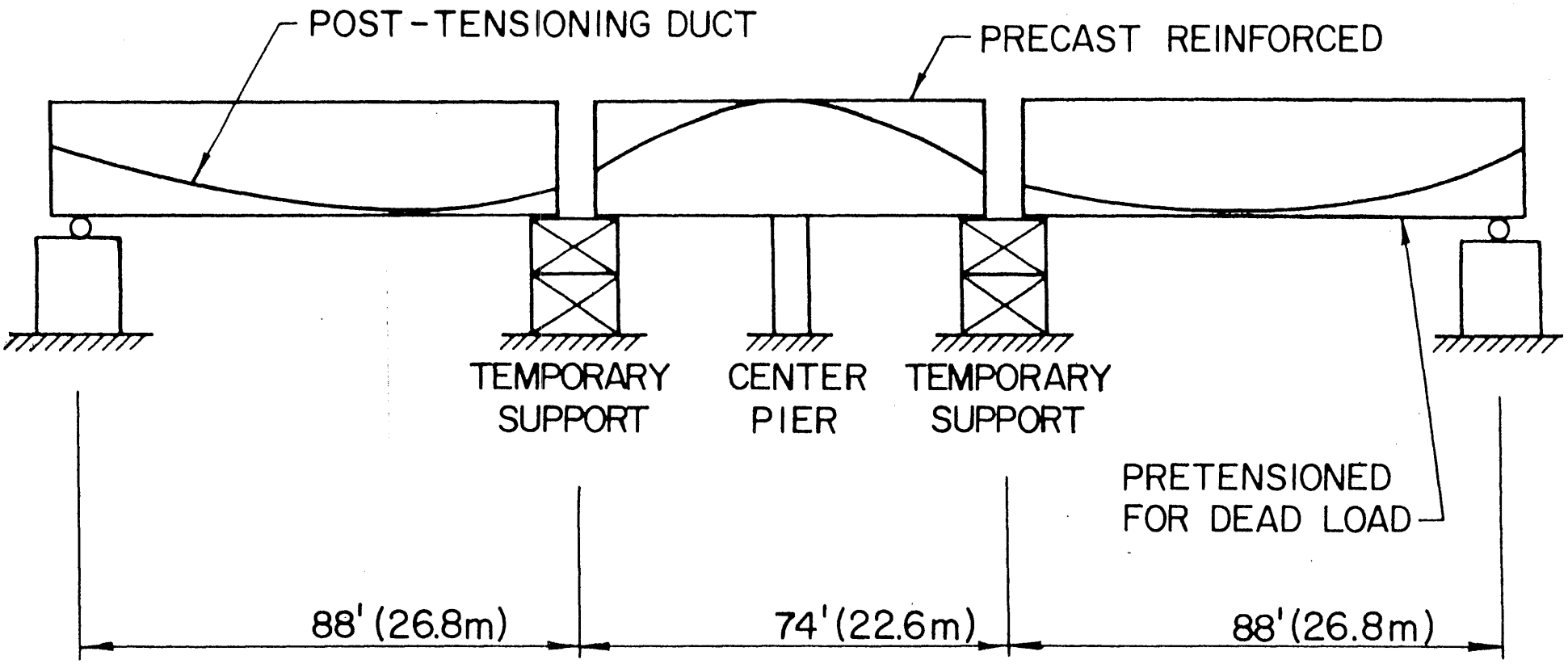


FIG. 1.4 SEGMENTAL GIRDERS PLACED ON FINAL AND TEMPORARY SUPPORTS

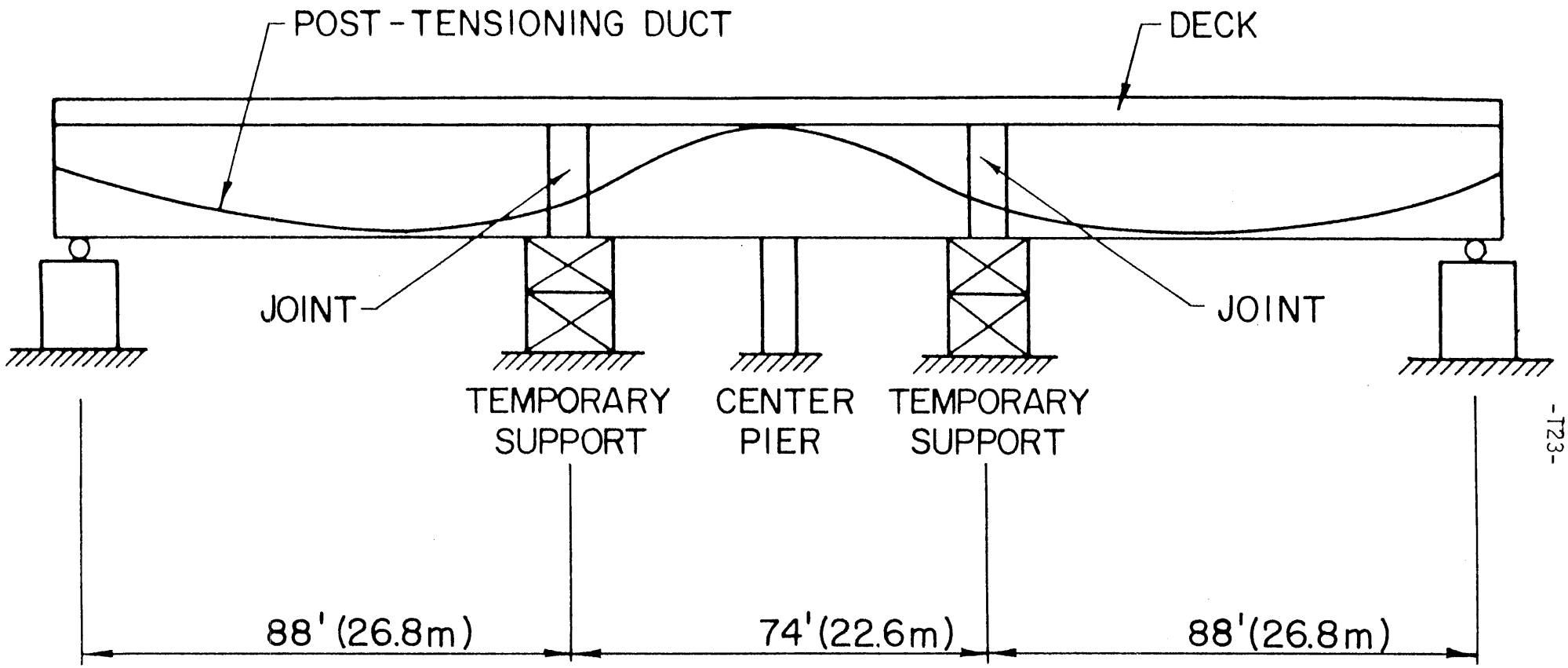


FIG. 1.5 DECK AND JOINT CONCRETE CAST-IN-PLACE

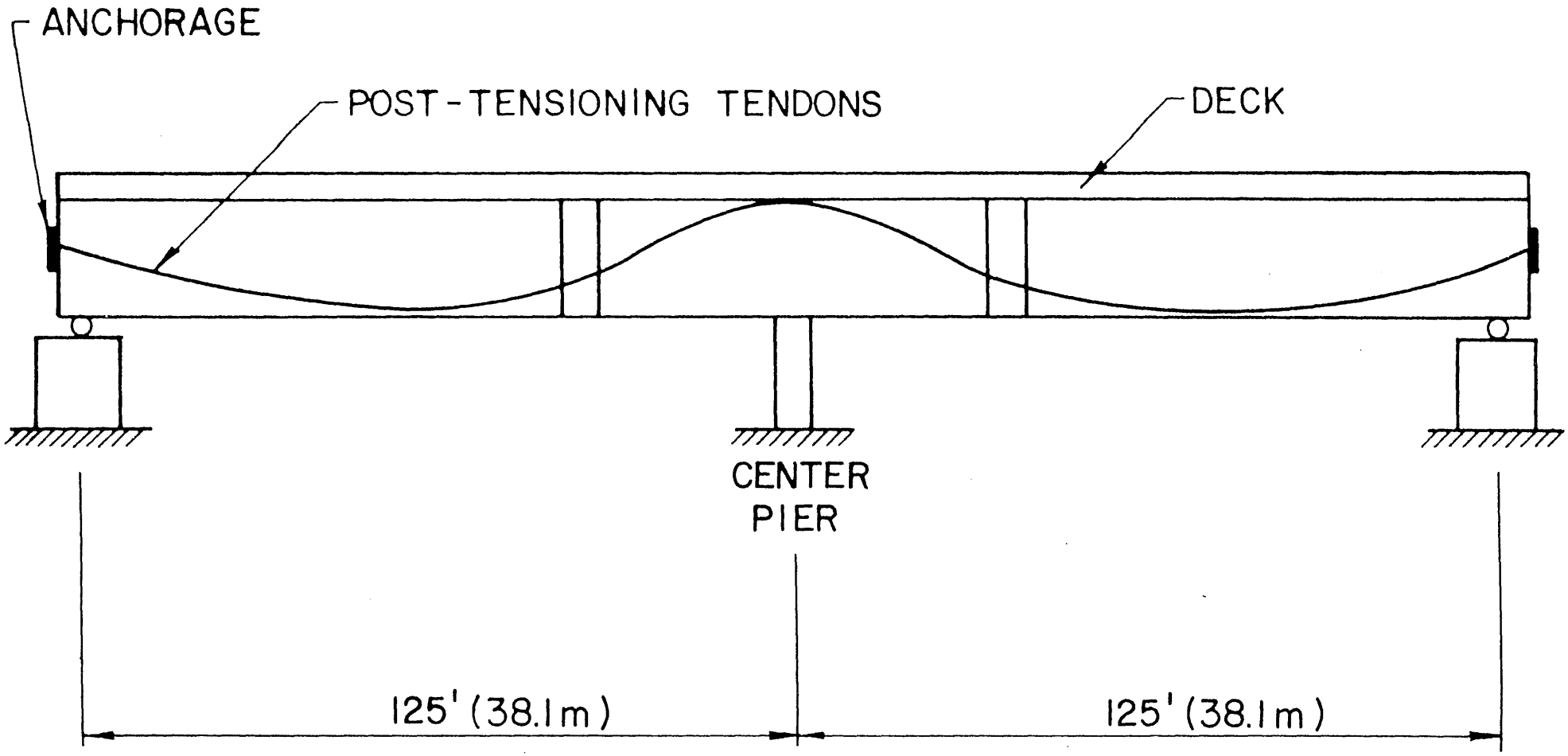


FIG. 1.6 STRUCTURE AFTER POST-TENSIONING AND REMOVAL OF TEMPORARY SUPPORTS

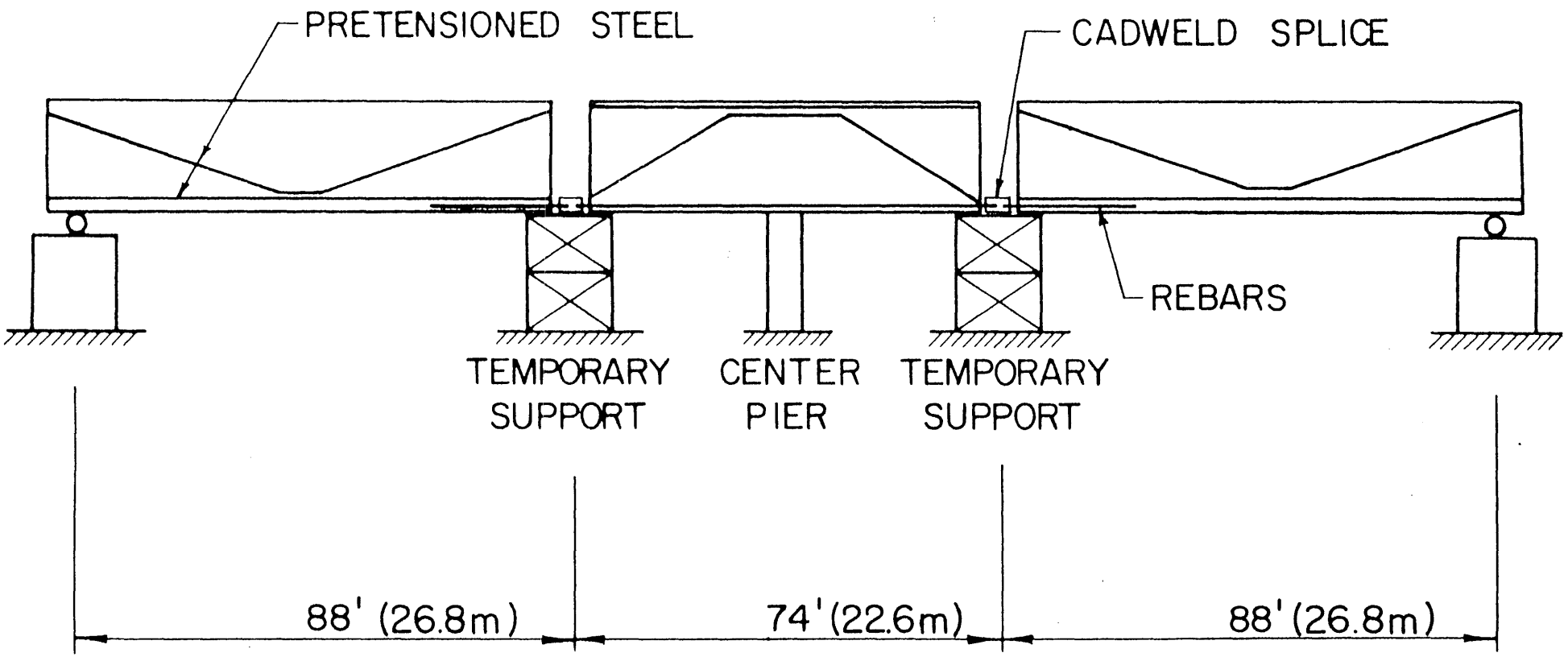


FIG. 1.7 FULLY PRETENSIONED SEGMENTS PLACED ON TEMPORARY AND FINAL SUPPORTS

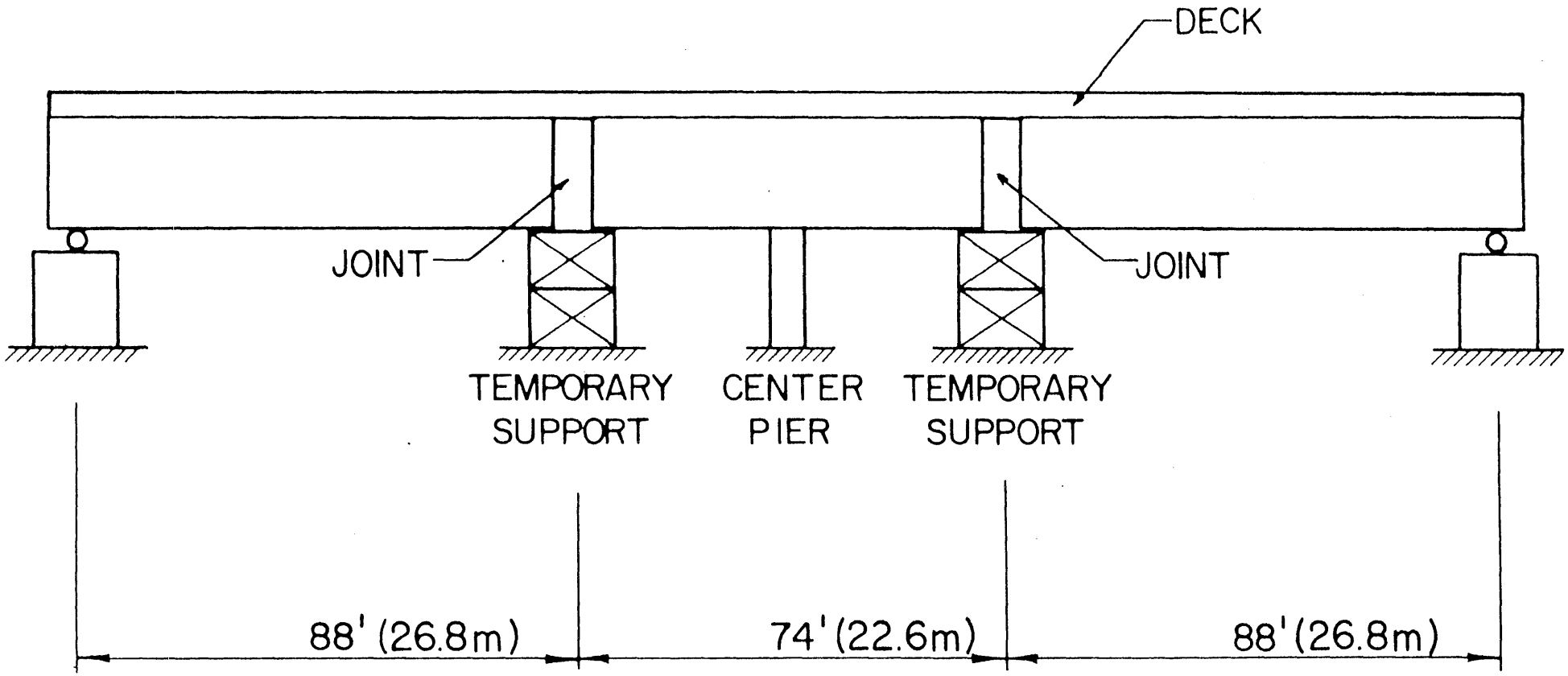


FIG. 1.8 DECK AND JOINT CONCRETE CAST AFTER JOINT REINFORCEMENT IS SPLICED

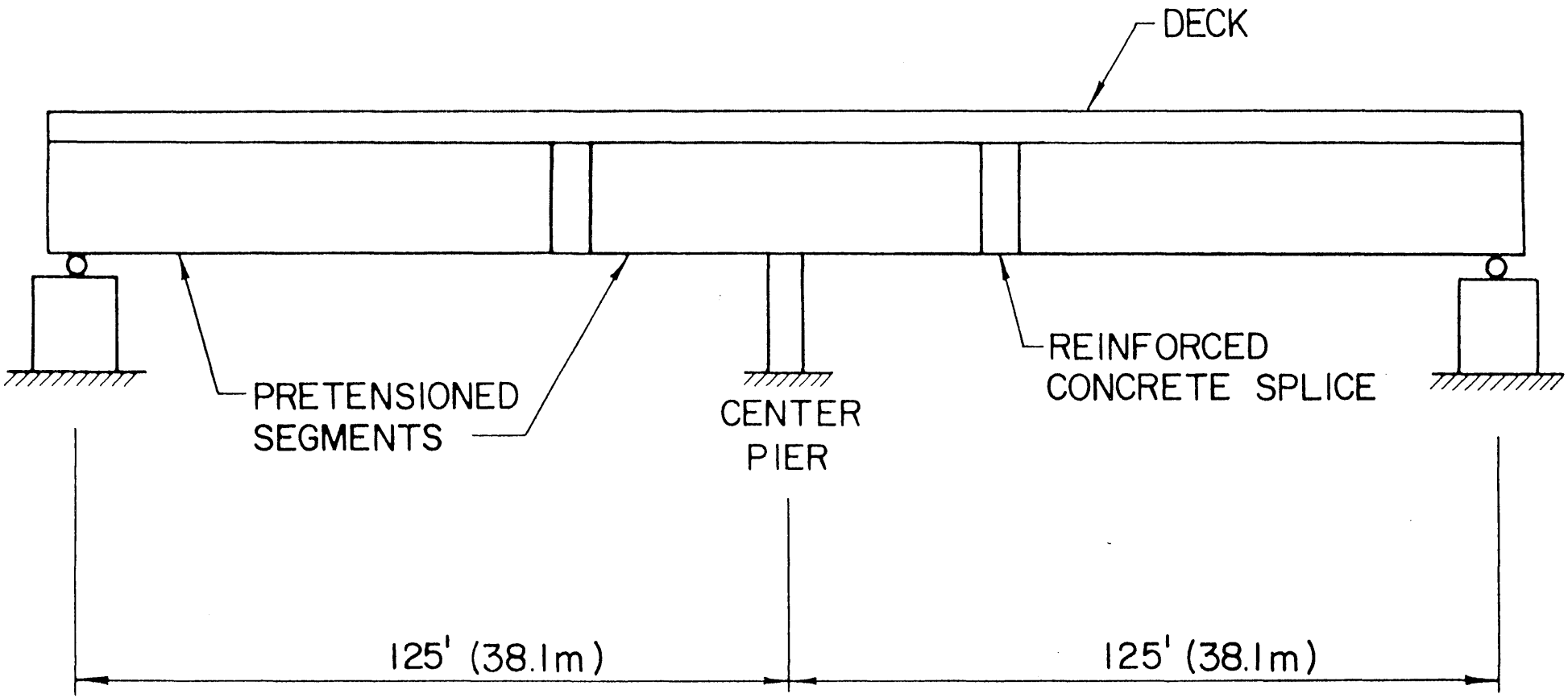


FIG. 1.9 TEMPORARY SUPPORTS REMOVED AFTER DECK AND JOINT CONCRETE IS CURED

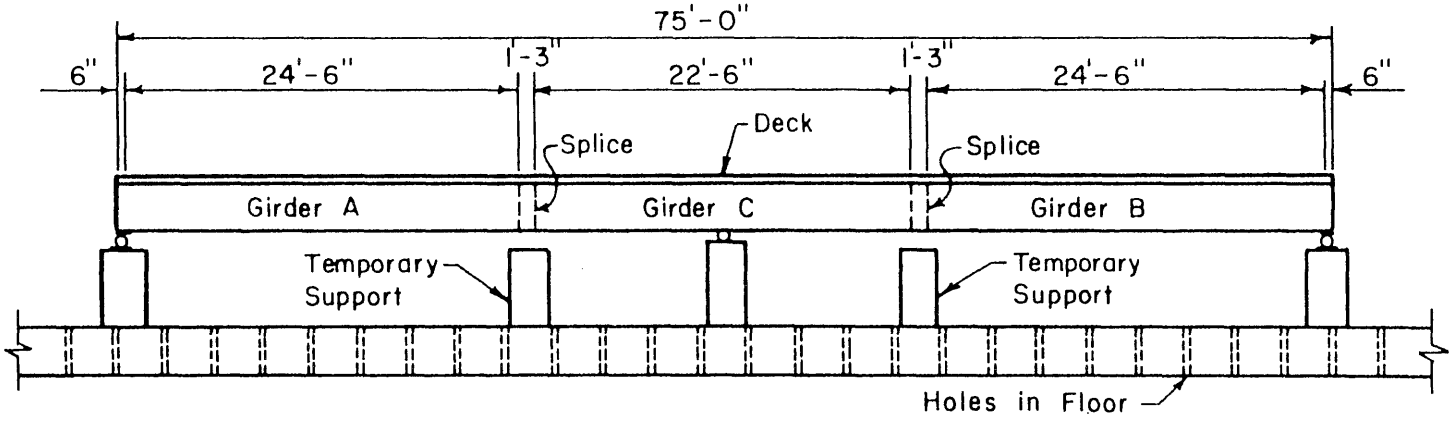


FIG. 2.1 LAYOUT AND DIMENSIONS OF MODEL 1

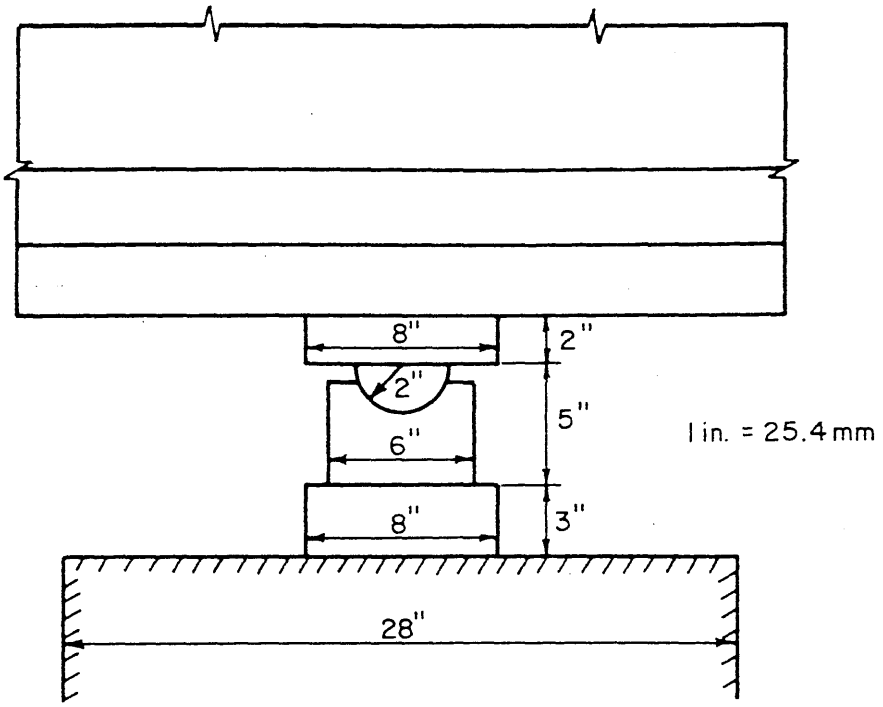


(a) Hinged Reaction At Center Pier

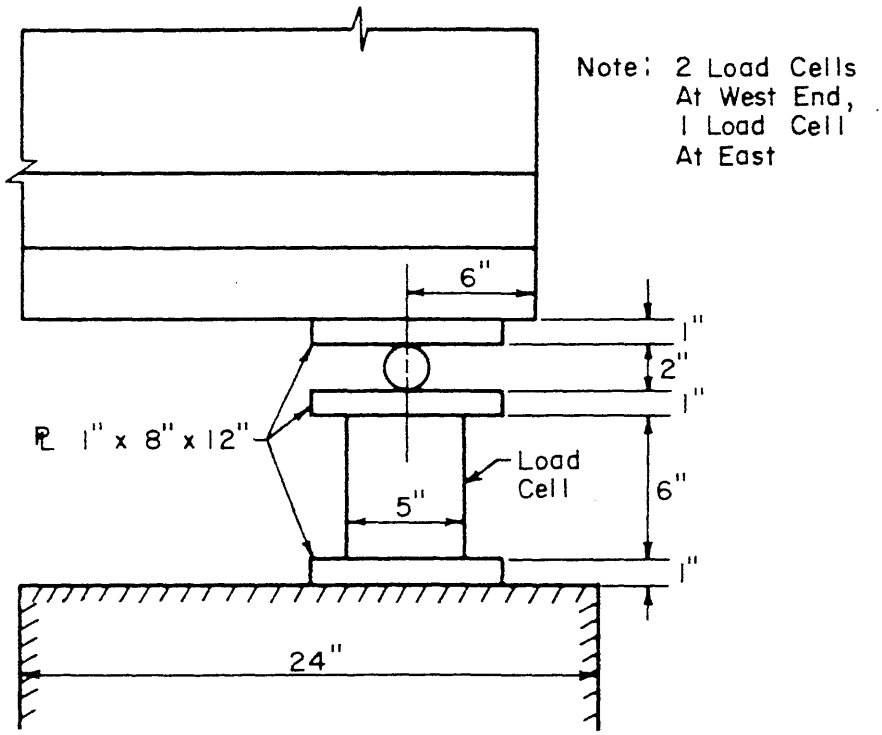


(b) Roller Reaction At End Abutments

FIG. 2.2 DETAILS OF SUPPORTS FOR MODELS 1 AND 2

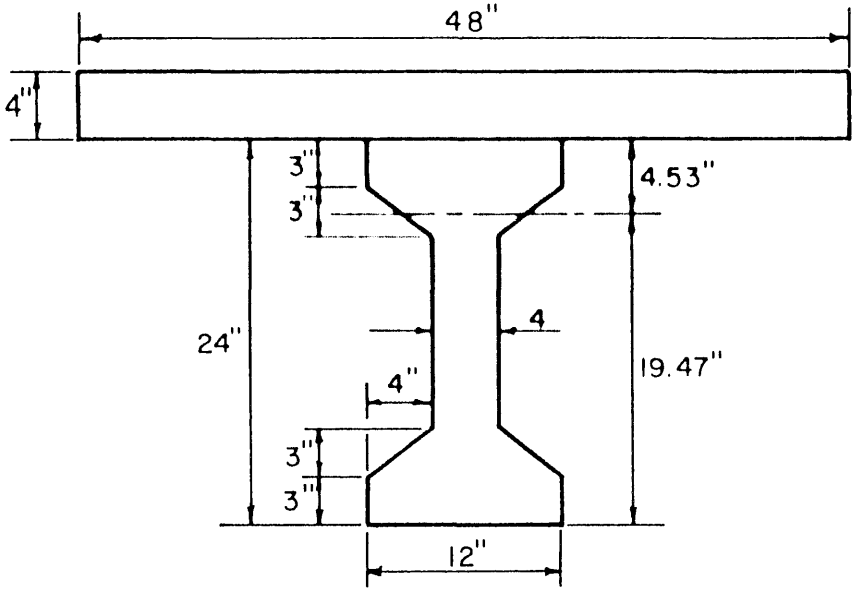


**Beam Properties**

| | |
|---|---|
| $A_b$ = 168 in.$^2$ | $I_b$ = 11,484 in.$^4$ |
| $y_t$ = 12" | $y_b$ = 12" |
| $I_b/y_t$ = 957 in.$^3$ | $I_b/y_t$ = 957 in.$^3$ |

**Composite - Section Properties**

| | |
|---|---|
| $A_c$ = 360 in.$^2$ | $I_c$ = 29,300 in.$^4$ |
| $y_t$ = 4.53 in. | $y_b$ = 19.47 in. |
| $I_c/y_t$ = 6470 in. | $I_c/y_b$ = 1500 in. |
| $E_{beam} = E_{deck}$ | |

1 in. = 25.4 mm

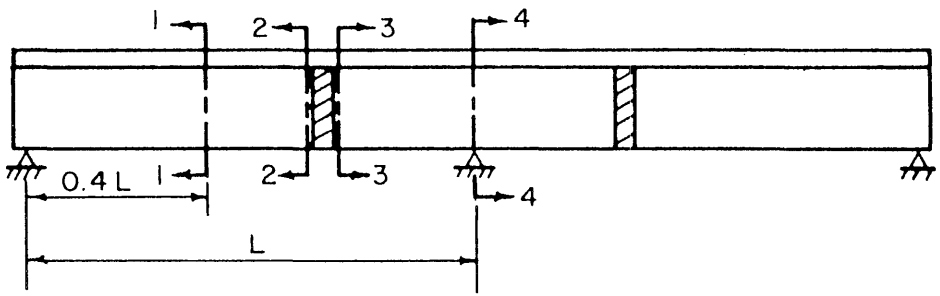


**Cross-Sections For Stress Calculations**

| Section | Property |
|---|---|
| 1-1 | Max. Pos. Moment |
| 2-2 | Splice Face |
| 3-3 | Splice Face |
| 4-4 | Max. Neg. Moment |

FIG. 2.3 CROSS SECTION PROPERTIES AND LOCATIONS OF CRITICAL SECTIONS

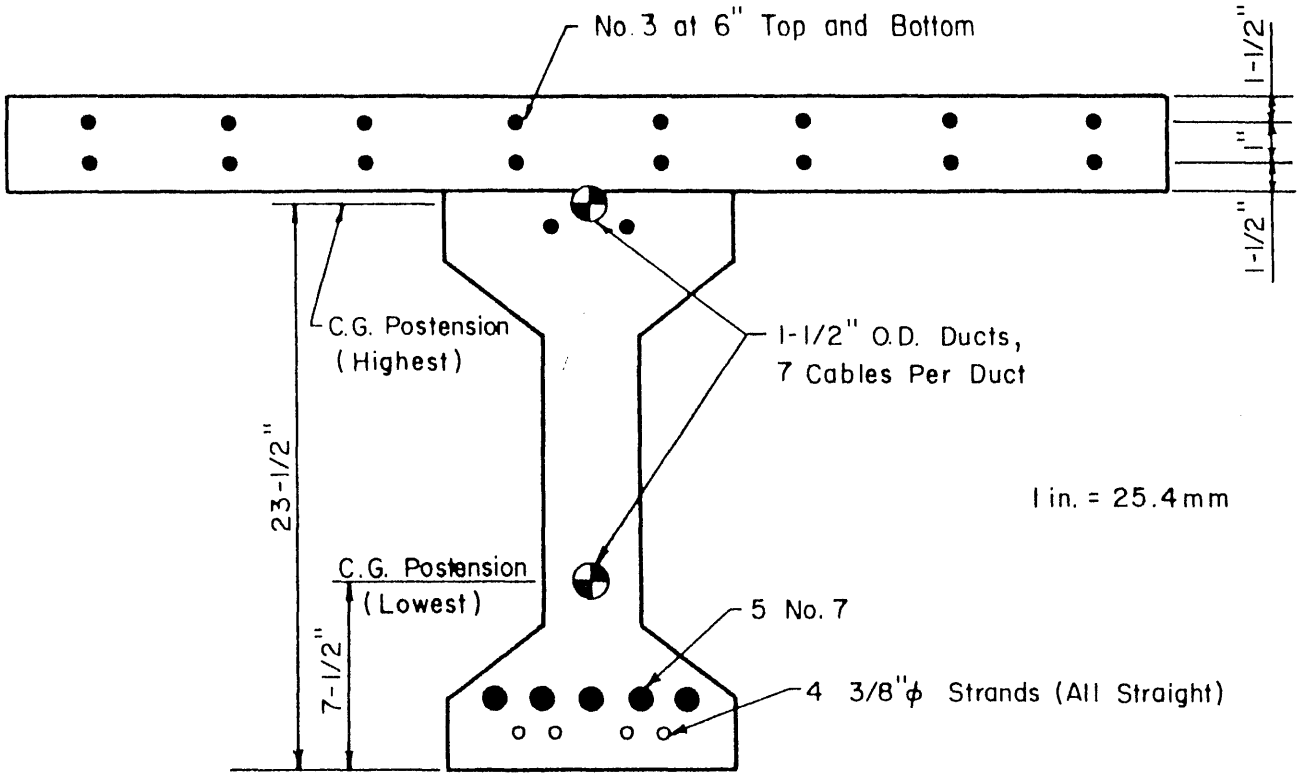


FIG. 2.4 LOCATION OF REINFORCEMENT IN CENTRAL SEGMENT OF MODEL 1

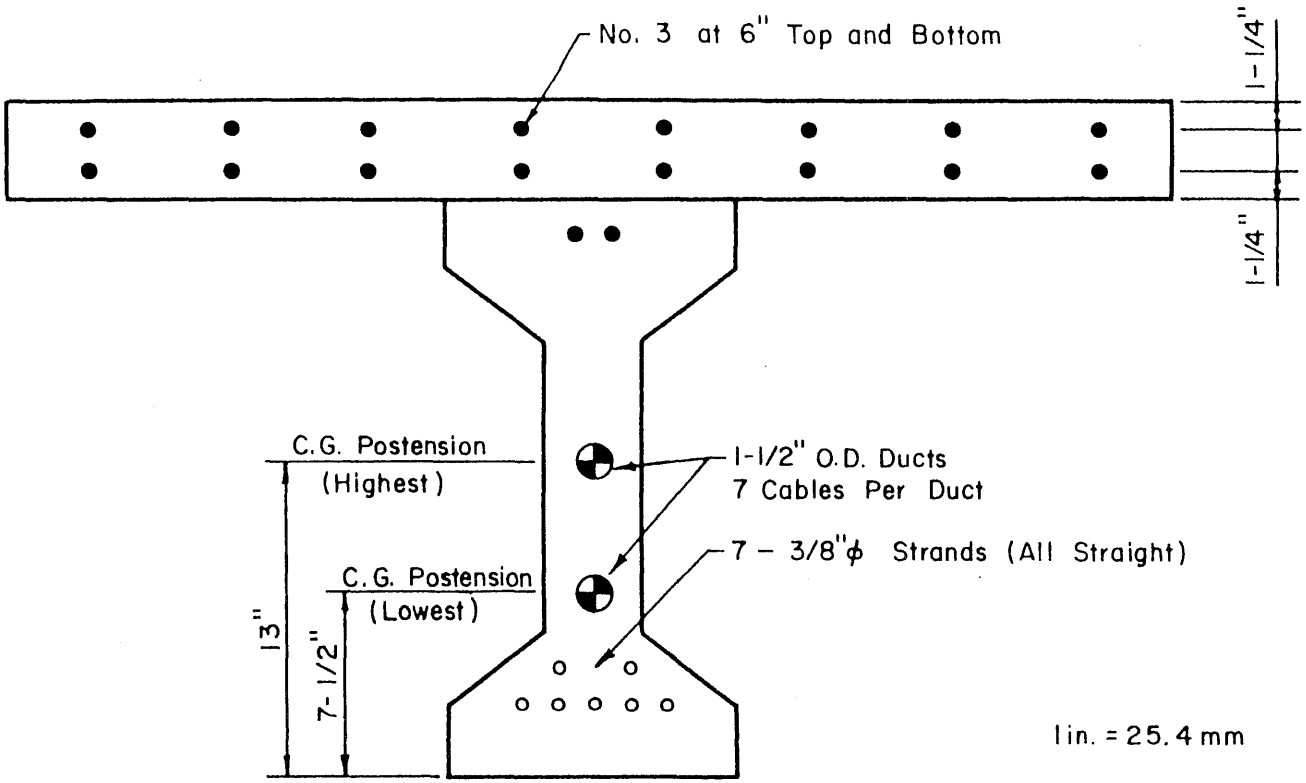


FIG. 2.5 LOCATIONS OF REINFORCEMENT IN END SEGMENTS OF MODEL 2

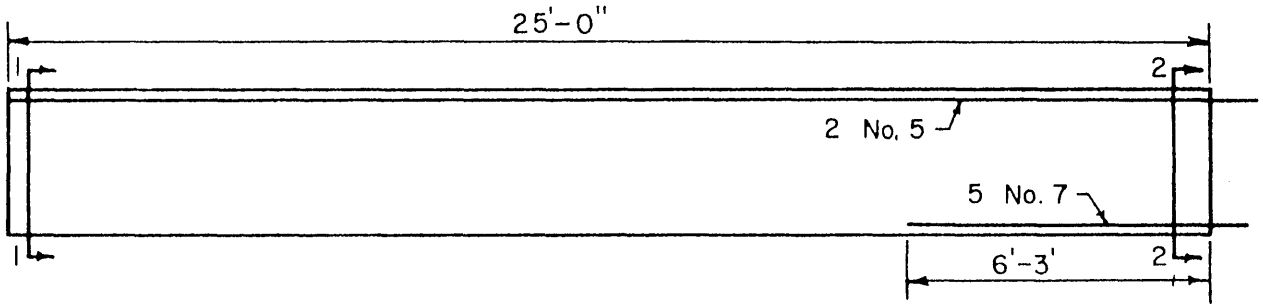


End Beam A ( Beam B Opposite Hand )

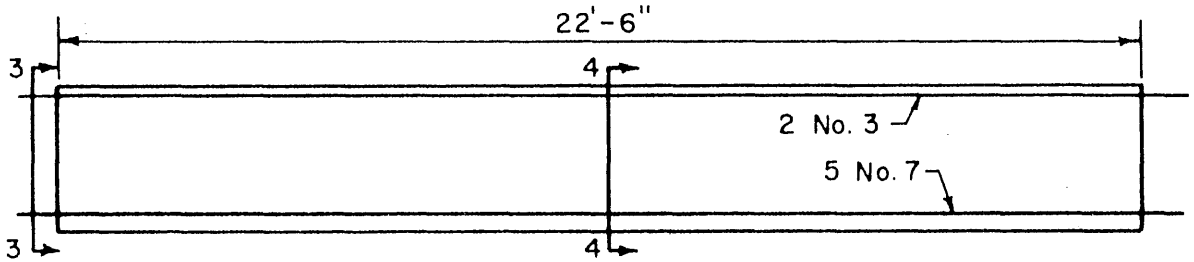


Center Beam C

1 ft. = 0.305 m
1 in. = 25.4 mm

FIG. 2.6 LOCATIONS OF DEFORMED REINFORCING BARS AND SECTION IDENTIFICATIONS, MODEL 1

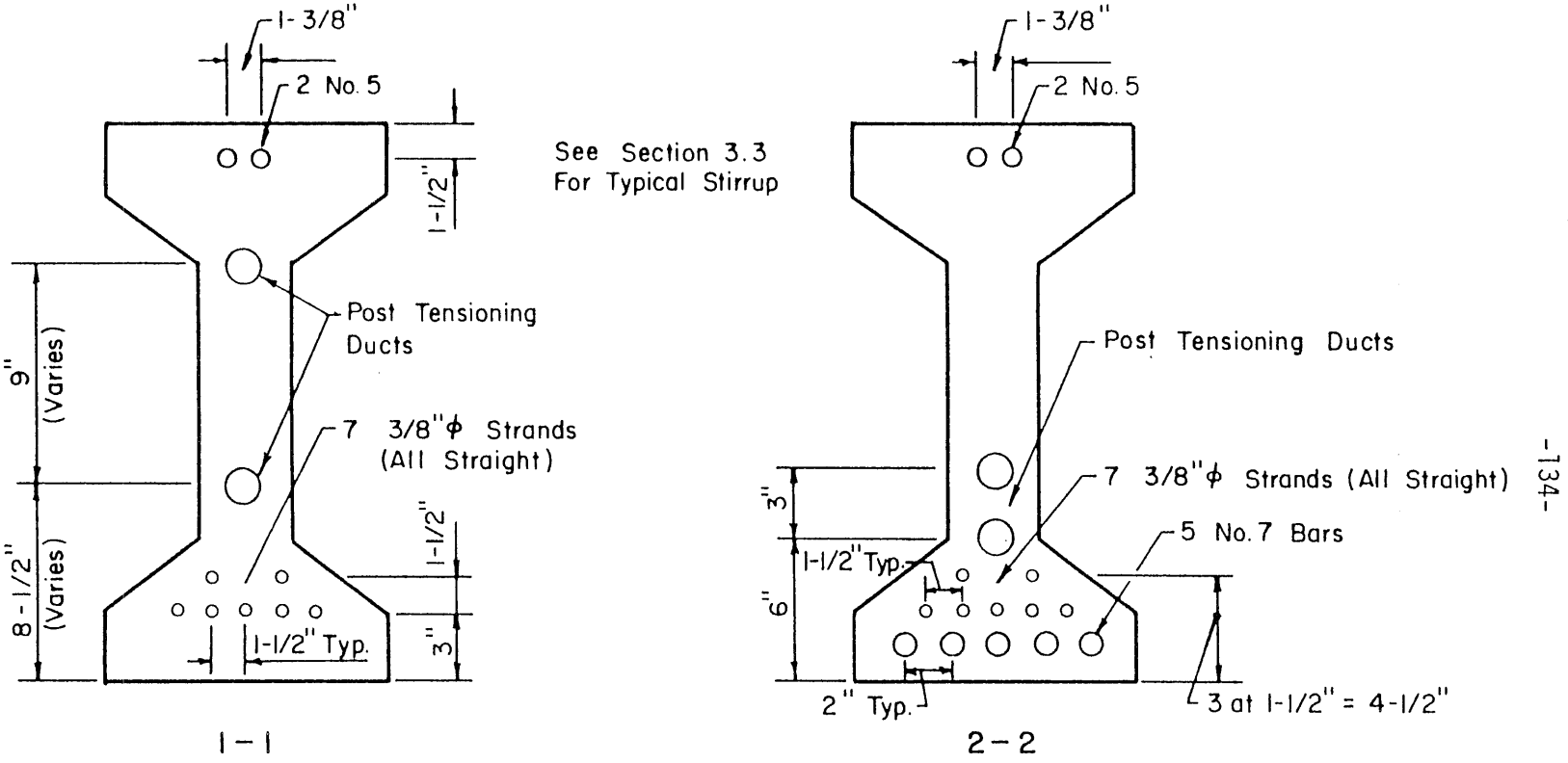


Note: Duct Dimensions Shown Apply at End of Beam Only.

FIG. 2.7 LOCATIONS OF REINFORCEMENT AT ENDS OF END SEGMENTS, MODEL 1

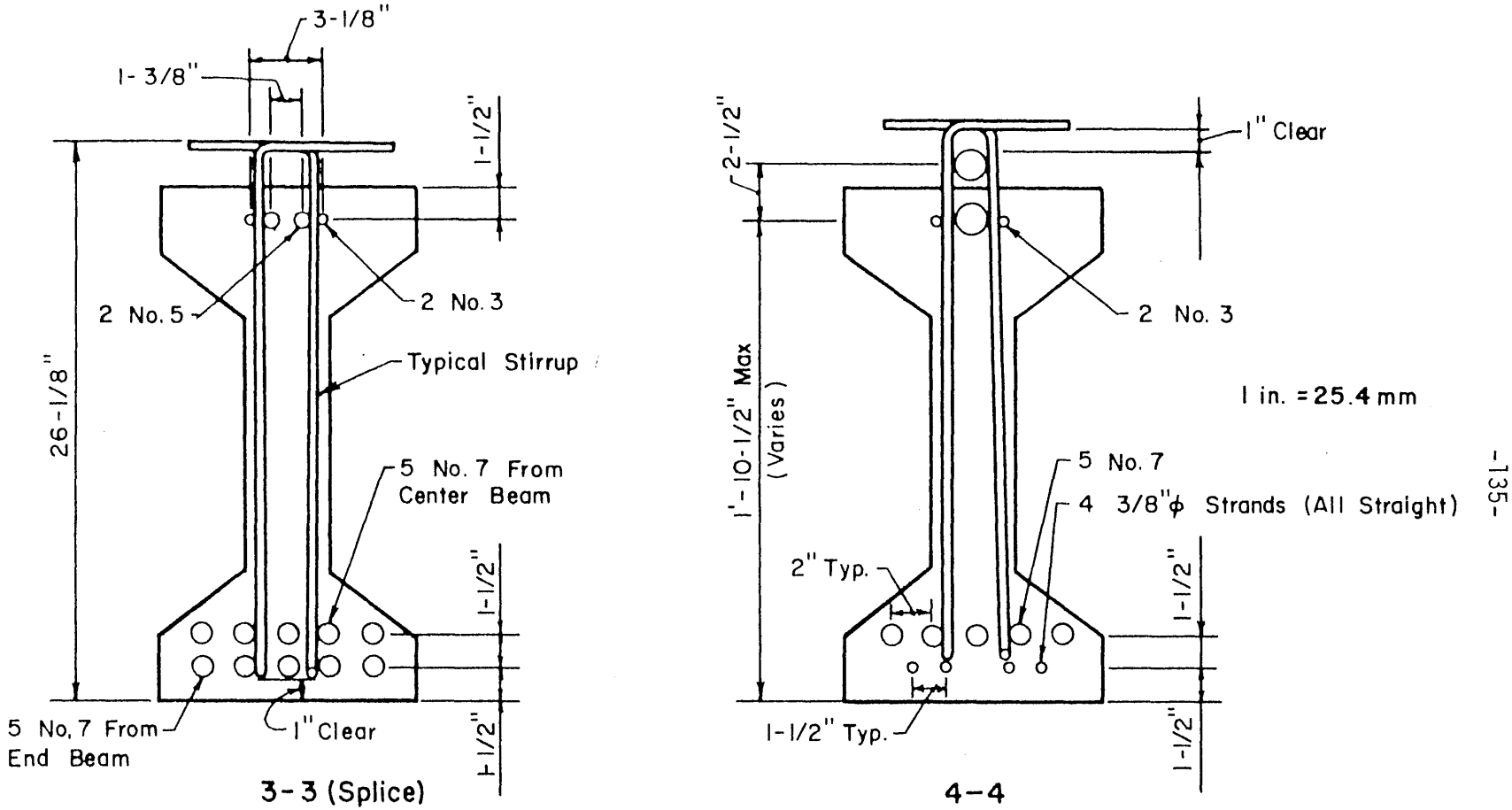


FIG. 2.8 LOCATIONS OF REINFORCEMENT IN SPLICE AND MIDDLE OF CENTRAL SEGMENT, MODEL 1

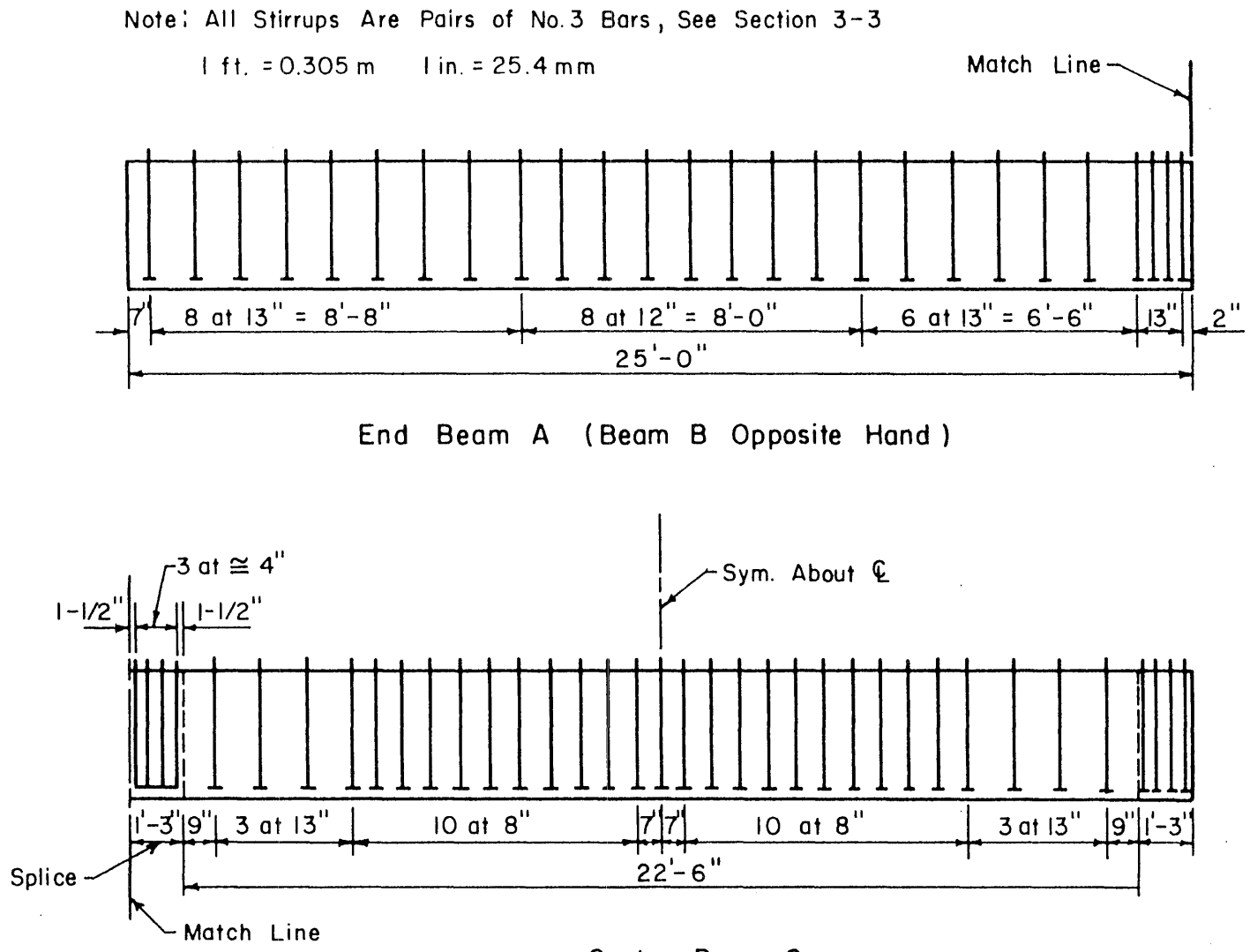


FIG. 2.9 WEB REINFORCEMENT IN MODEL 1

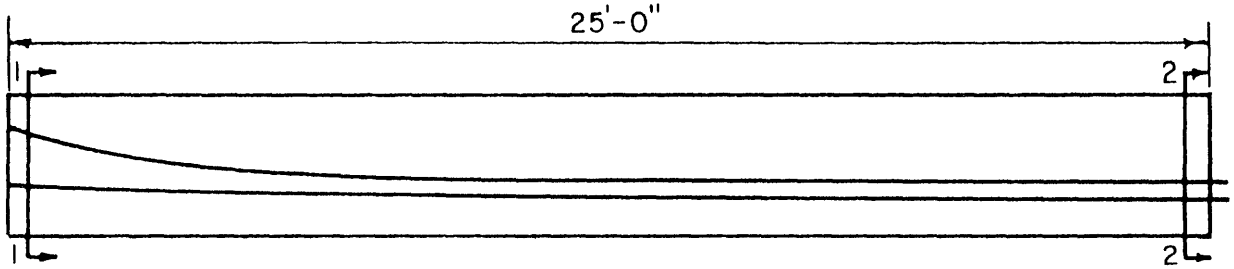


(a) End Beam A (Beam B Opposite Hand)

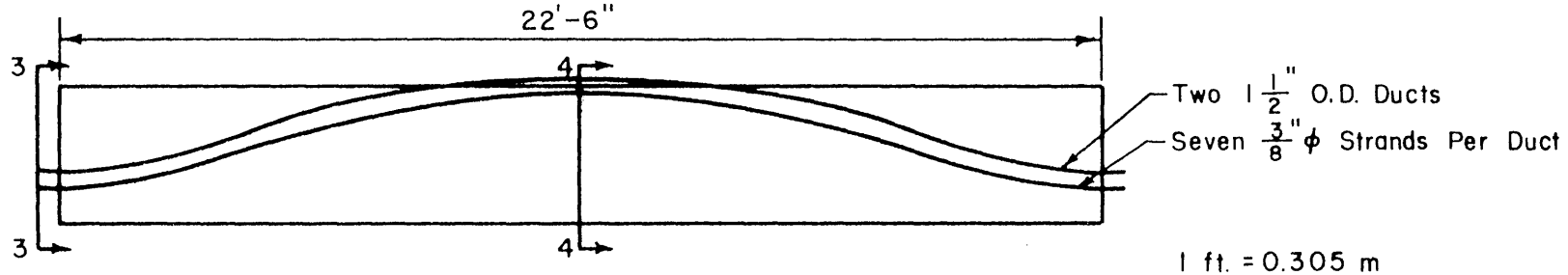


(b) Center Beam C

FIG. 2.10 GENERAL ARRANGEMENT OF POST-TENSIONING DUCTS IN MODEL 1

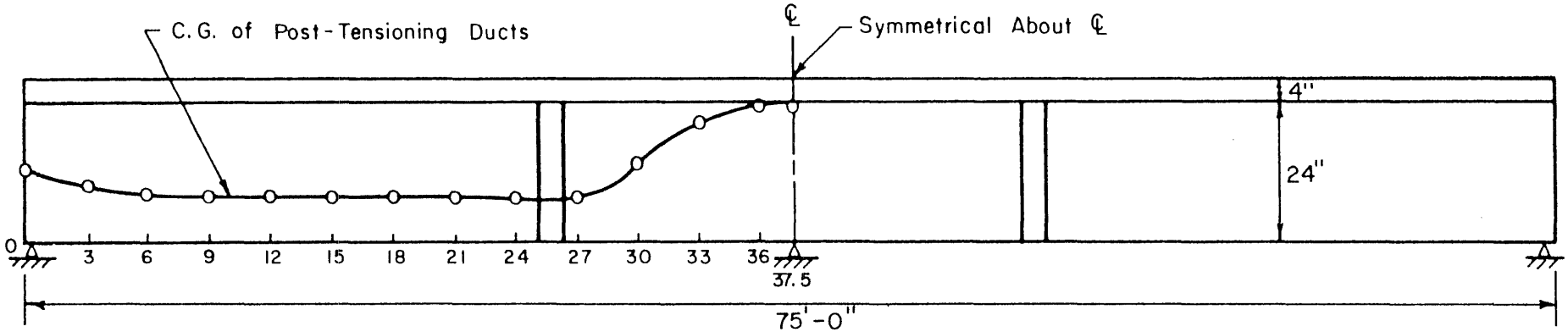


x — Distance From End of Bridge

y — Distance From Bottom of Beams To Center of Gravity of Post-Tensioned Steel

Curve Composed of Two 4th. Degree Curves

| x-ft | 0 | 3 | 6 | 9 | 12 | 15 | 18 | 21 | 24 | 27 | 30 | 33 | 36 | 37.5 |
|---|---|---|---|---|---|---|---|---|---|---|---|---|---|---|
| y-in. | 13.00 | 10.12 | 8.68 | 8.12 | 7.99 | 8.00 | 7.95 | 7.79 | 7.58 | 7.89 | 14.02 | 20.63 | 23.37 | 23.5 |

1 ft. = 0.305 m

1 in. = 25.4 mm

FIG. 2.11 COORDINATES OF POINTS AT CENTER OF GRAVITY OF POST-TENSIONED REINFORCEMENT

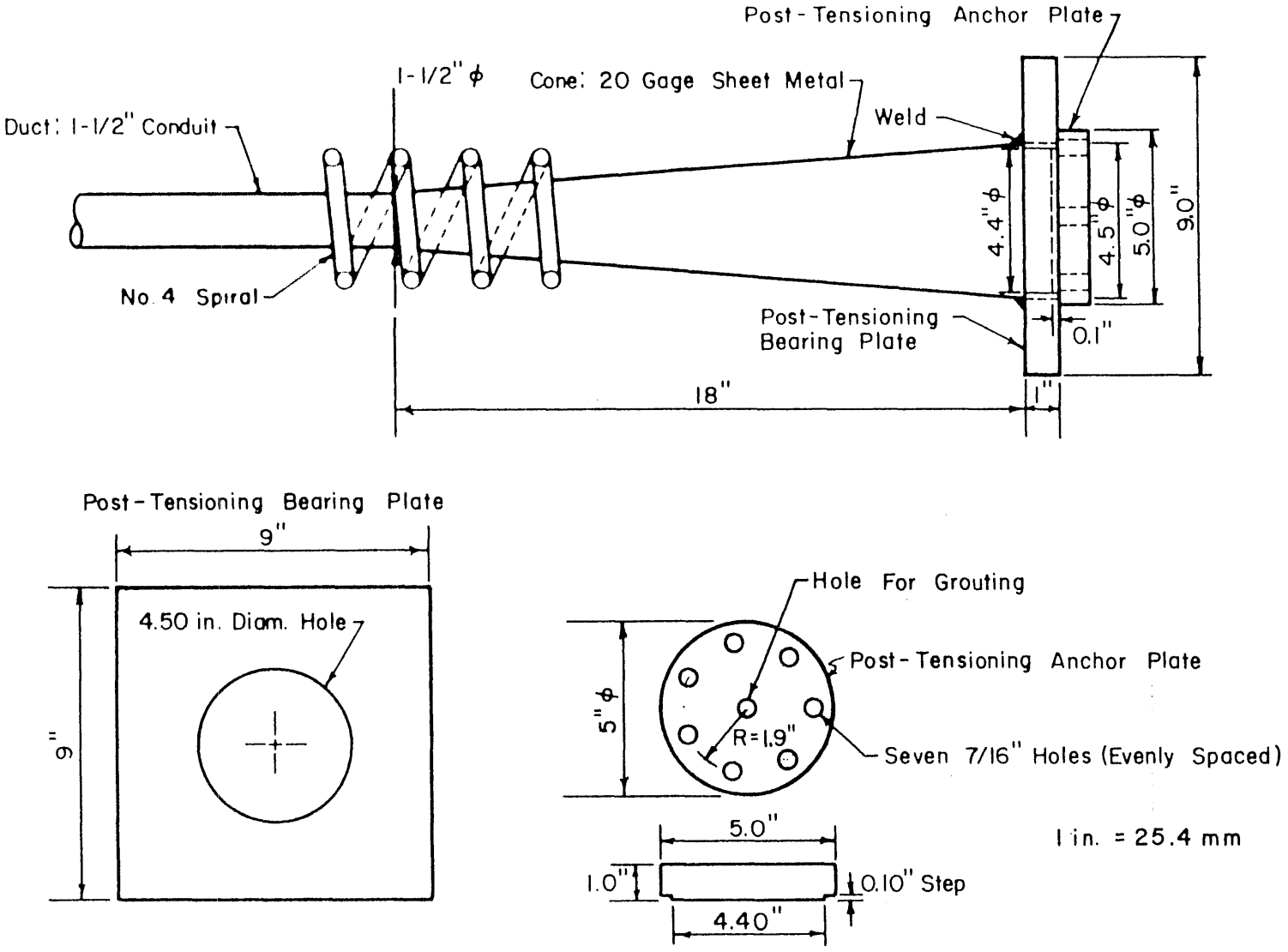


FIG. 2.12 DETAILS OF POST-TENSIONING ANCHOR PLATES AND DUCT TRANSITIONS

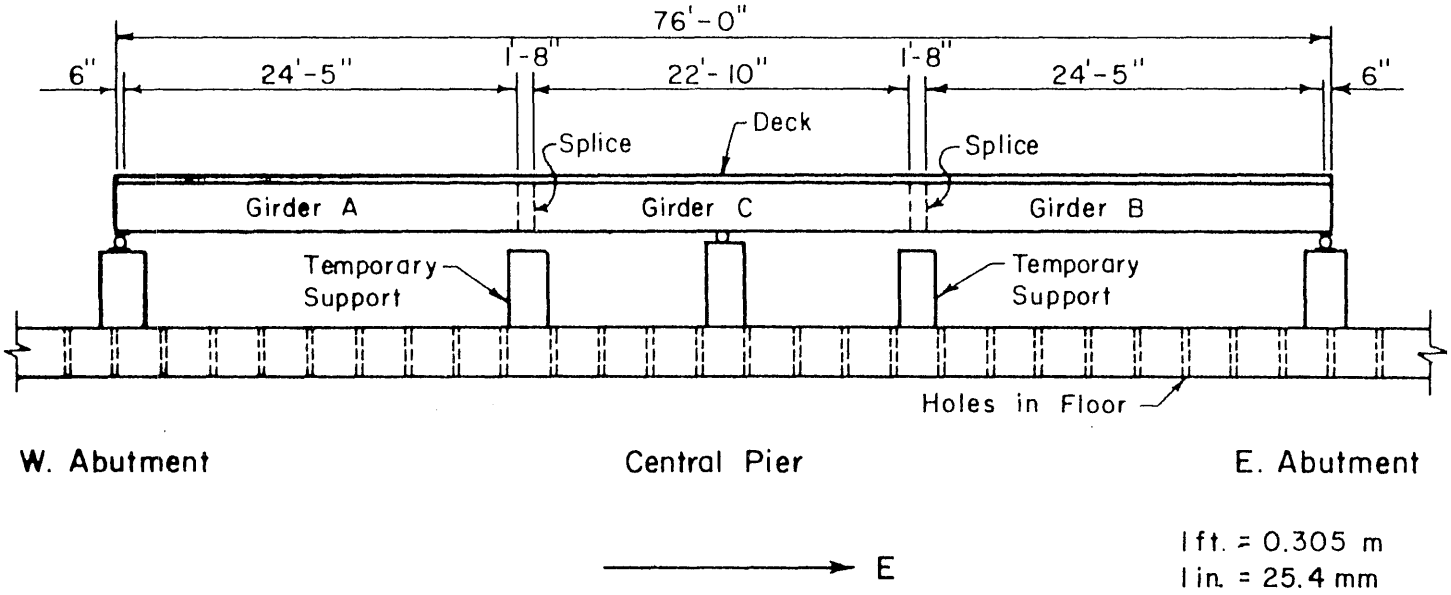


FIG. 2.13 LAYOUT AND DIMENSIONS OF MODEL 2

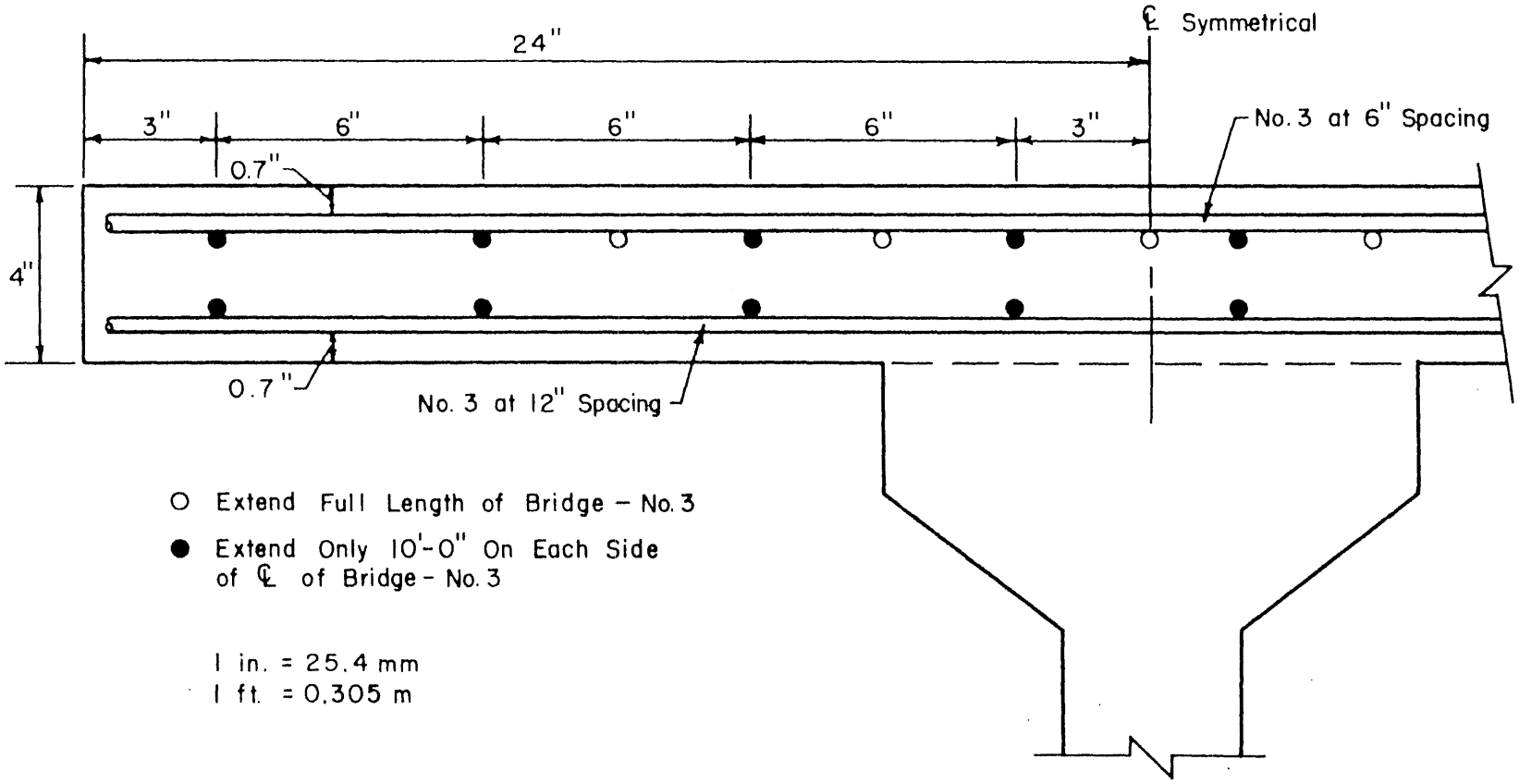


FIG. 2.14 DECK REINFORCEMENT IN MODEL 2

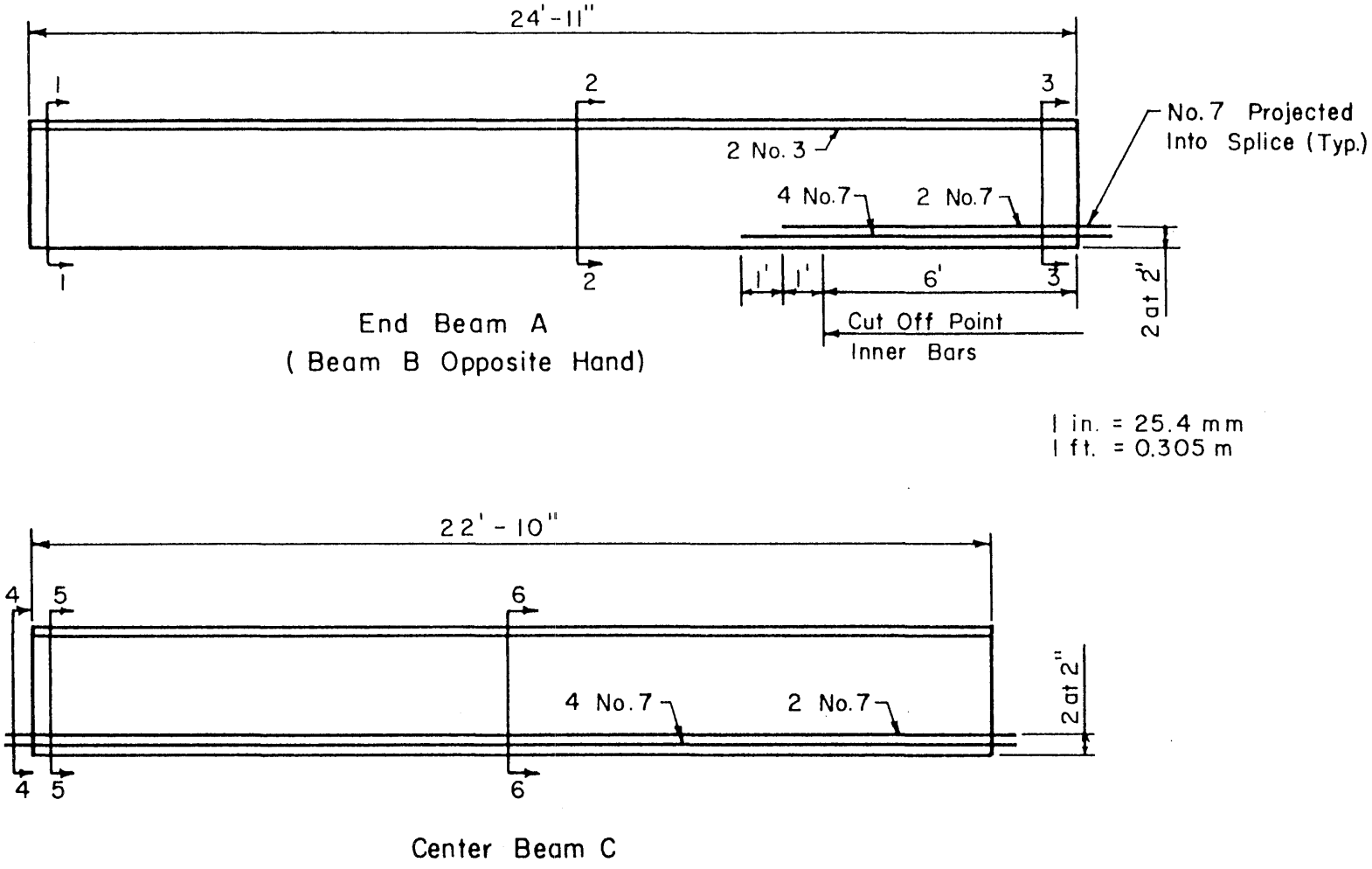


FIG. 2.15 ARRANGEMENT OF LONGITUDINAL DEFORMED REINFORCEMENT IN MODEL 2

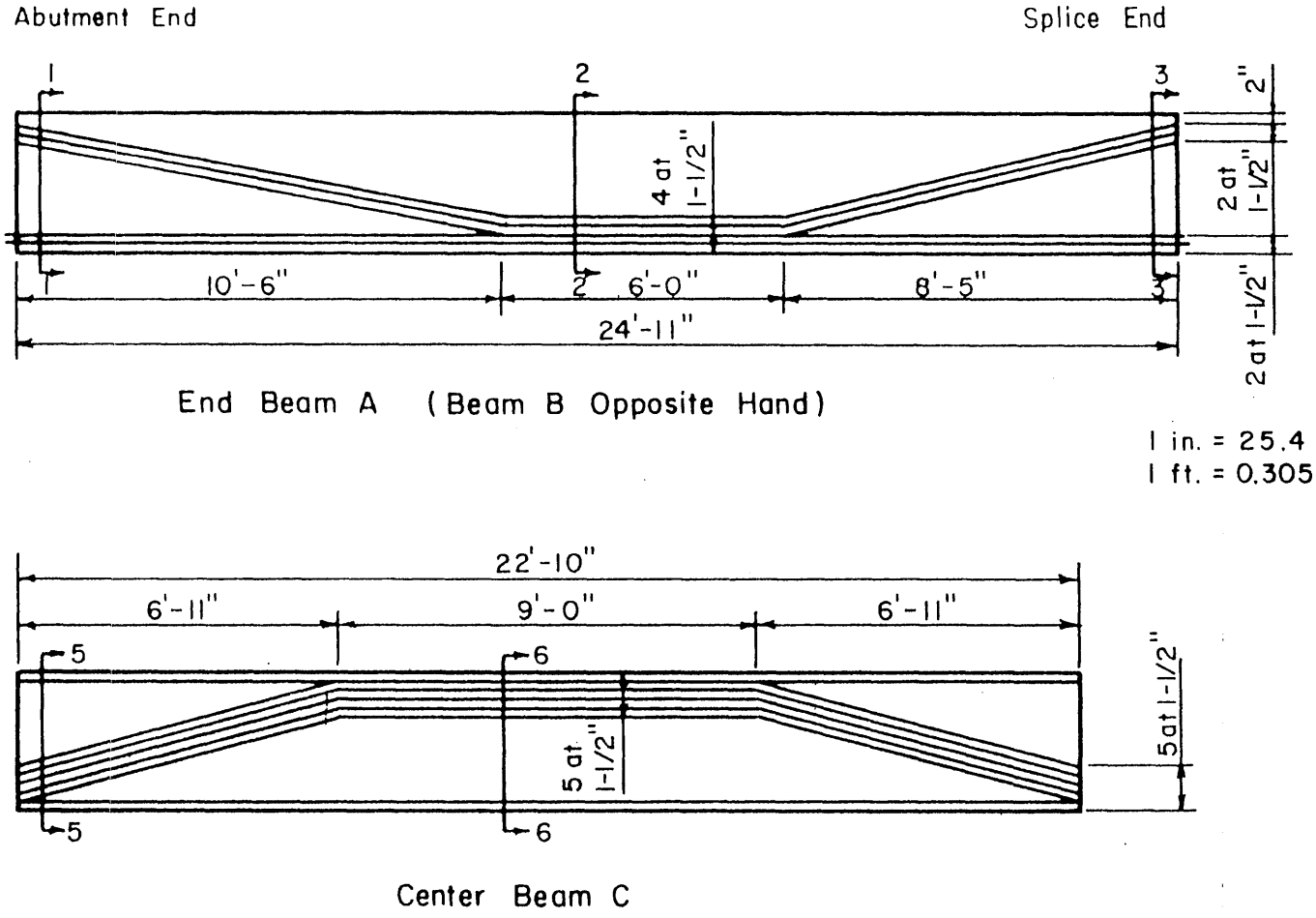


FIG. 2.16 ELEVATION OF PRETENSIONED REINFORCEMENT AND IDENTIFICATION OF SECTIONS IN MODEL 2

Matz Reference Room
Civil Engineering Department
B106 C. E. Building
University of Illinois
Urbana, Illinois 61801

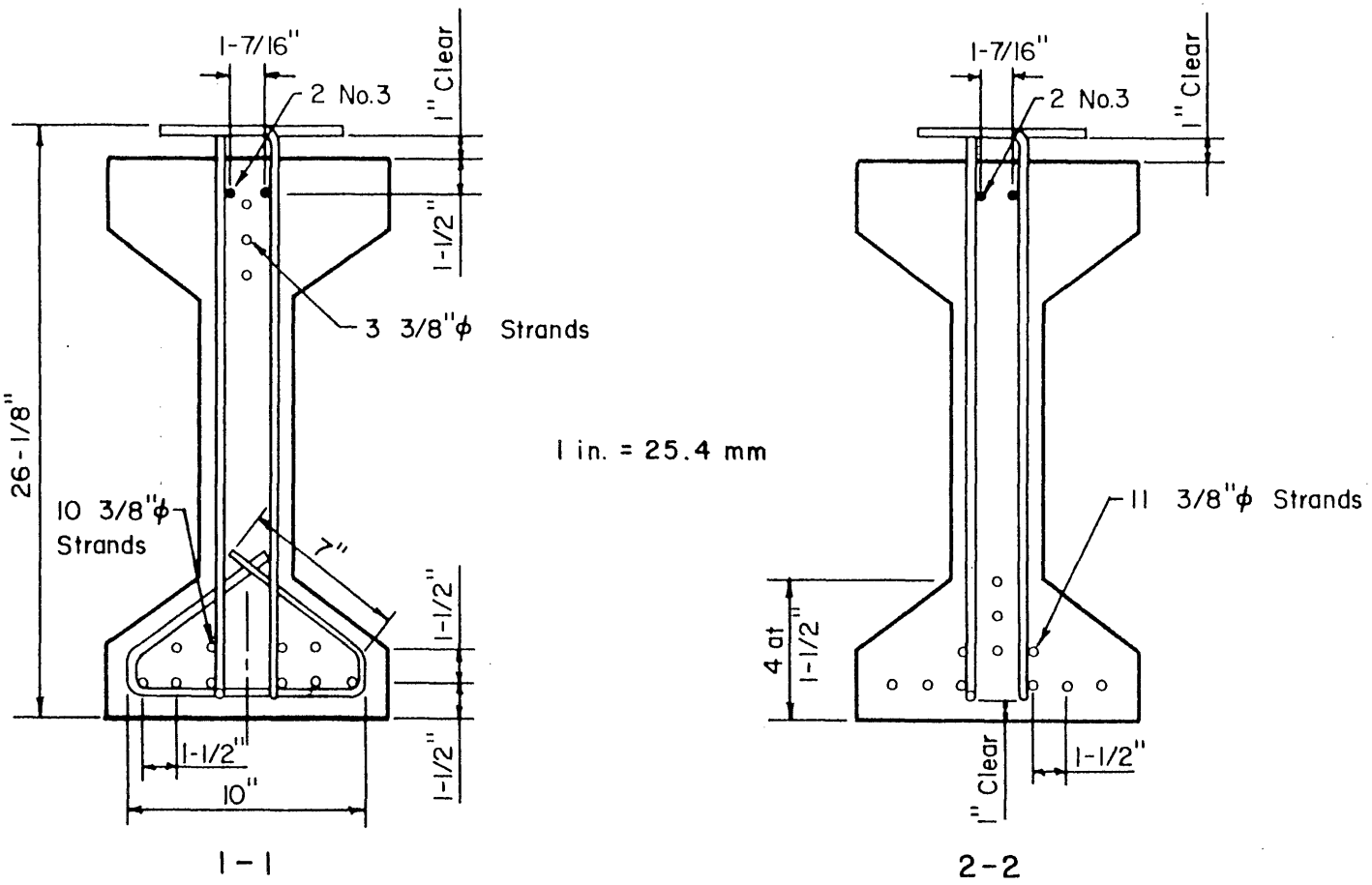


FIG. 2.17 CROSS SECTIONS OF GIRDER AT ABUTMENT END AND MIDSPAN OF END SEGMENT, MODEL 2

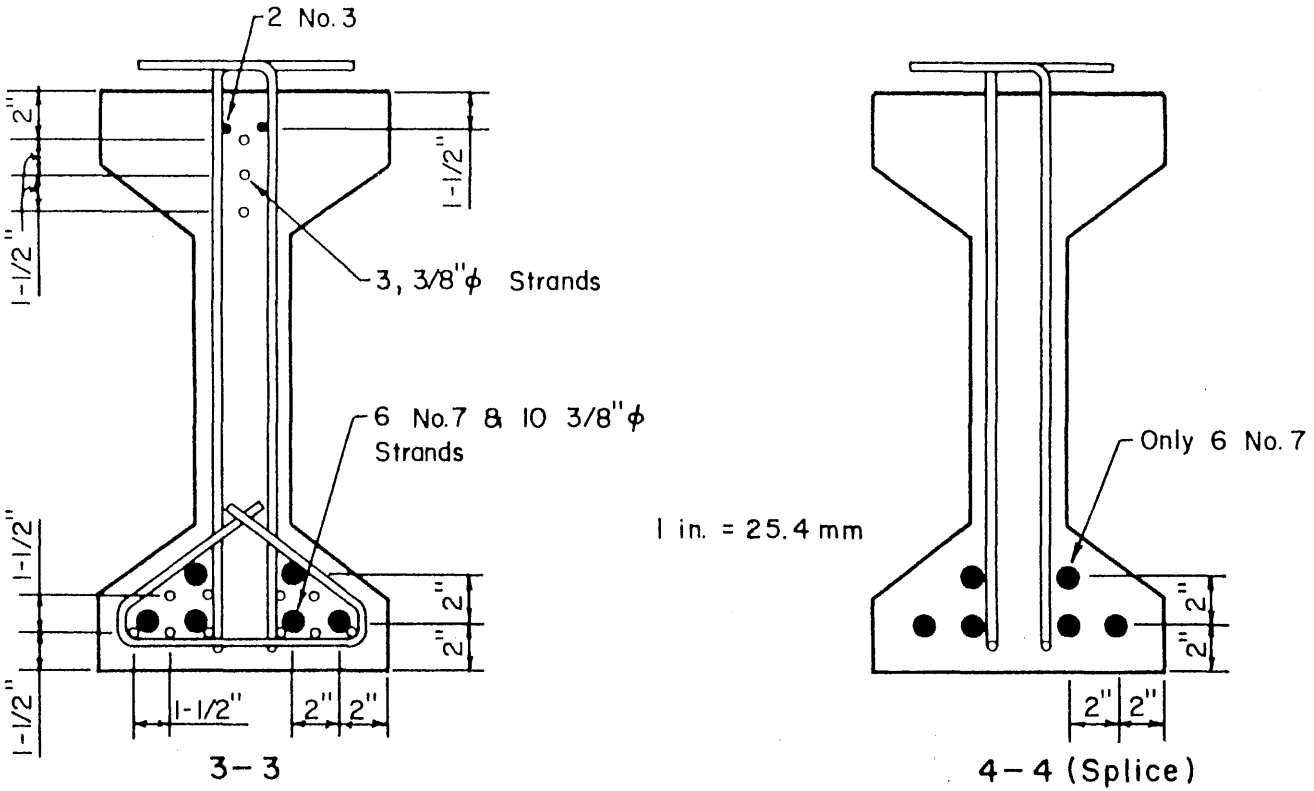


FIG. 2.18 CROSS SECTIONS OF GIRDER AT EACH END OF SPLICE, MODEL 2

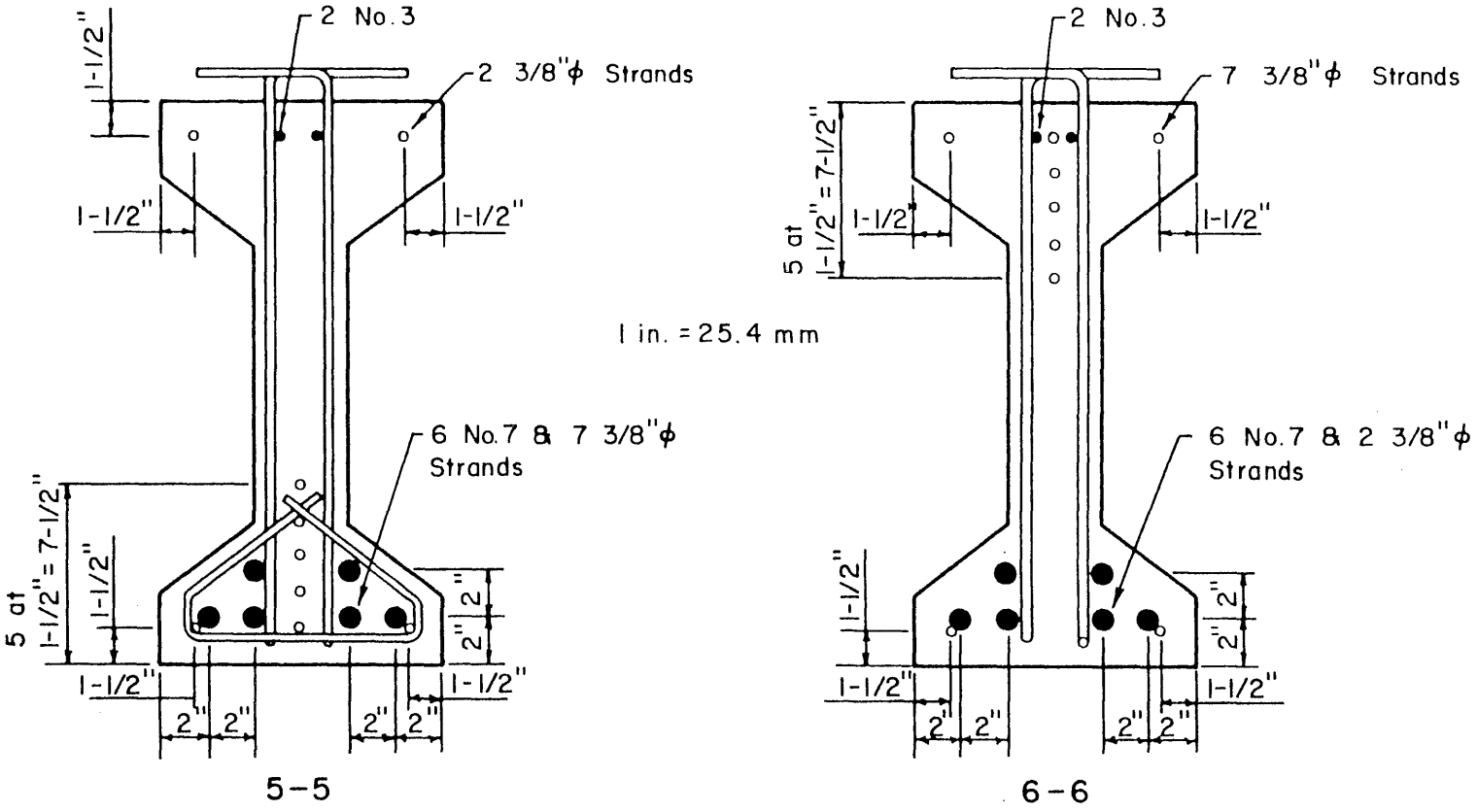


FIG. 2.19 CROSS SECTIONS OF CENTRAL GIRDER SEGMENT, MODEL 2

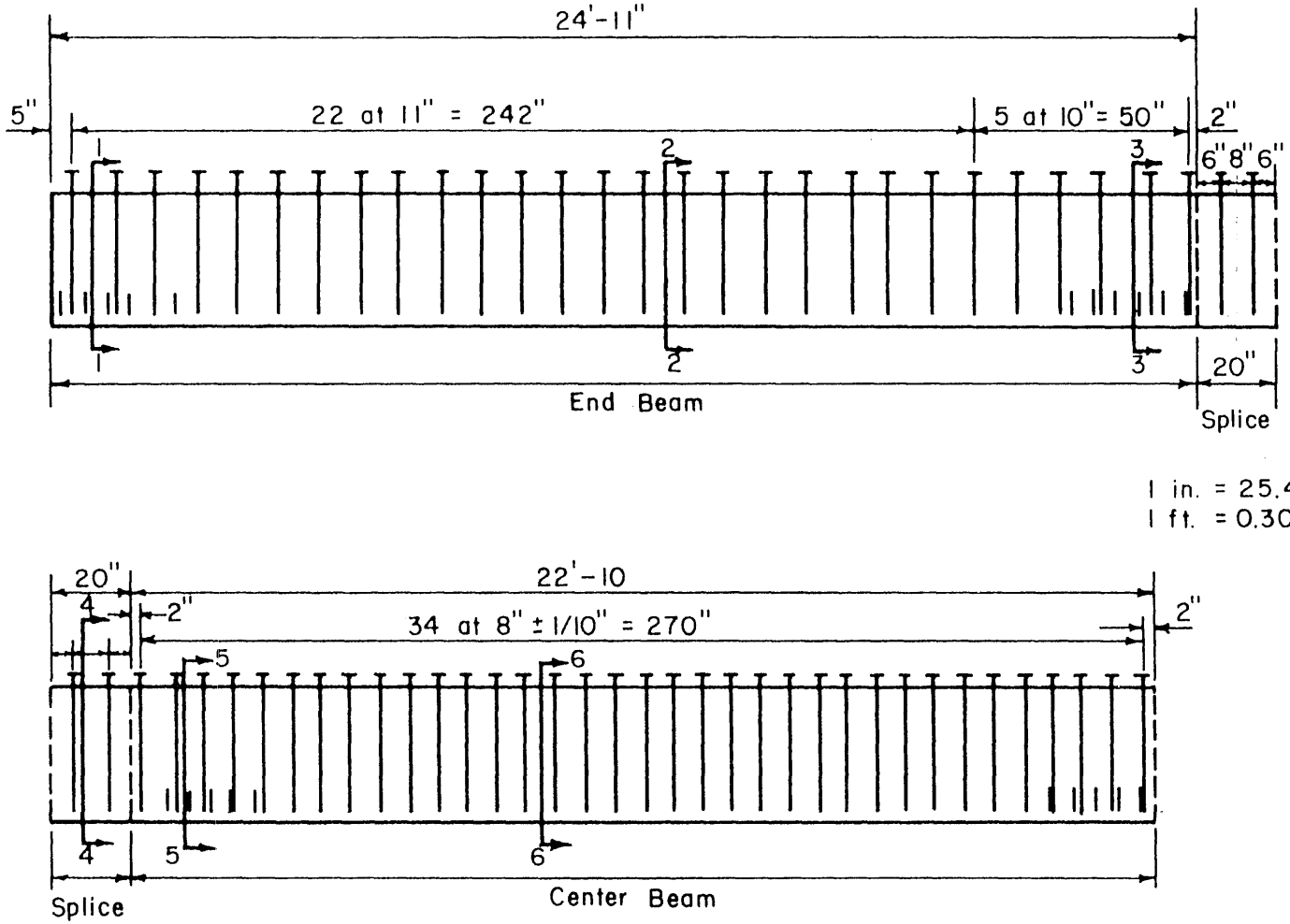


Note: All Stirrups are Pairs of No. 3 Bars, See Sec. 1-1

FIG. 2.20 SHEAR REINFORCEMENT IN MODEL 2

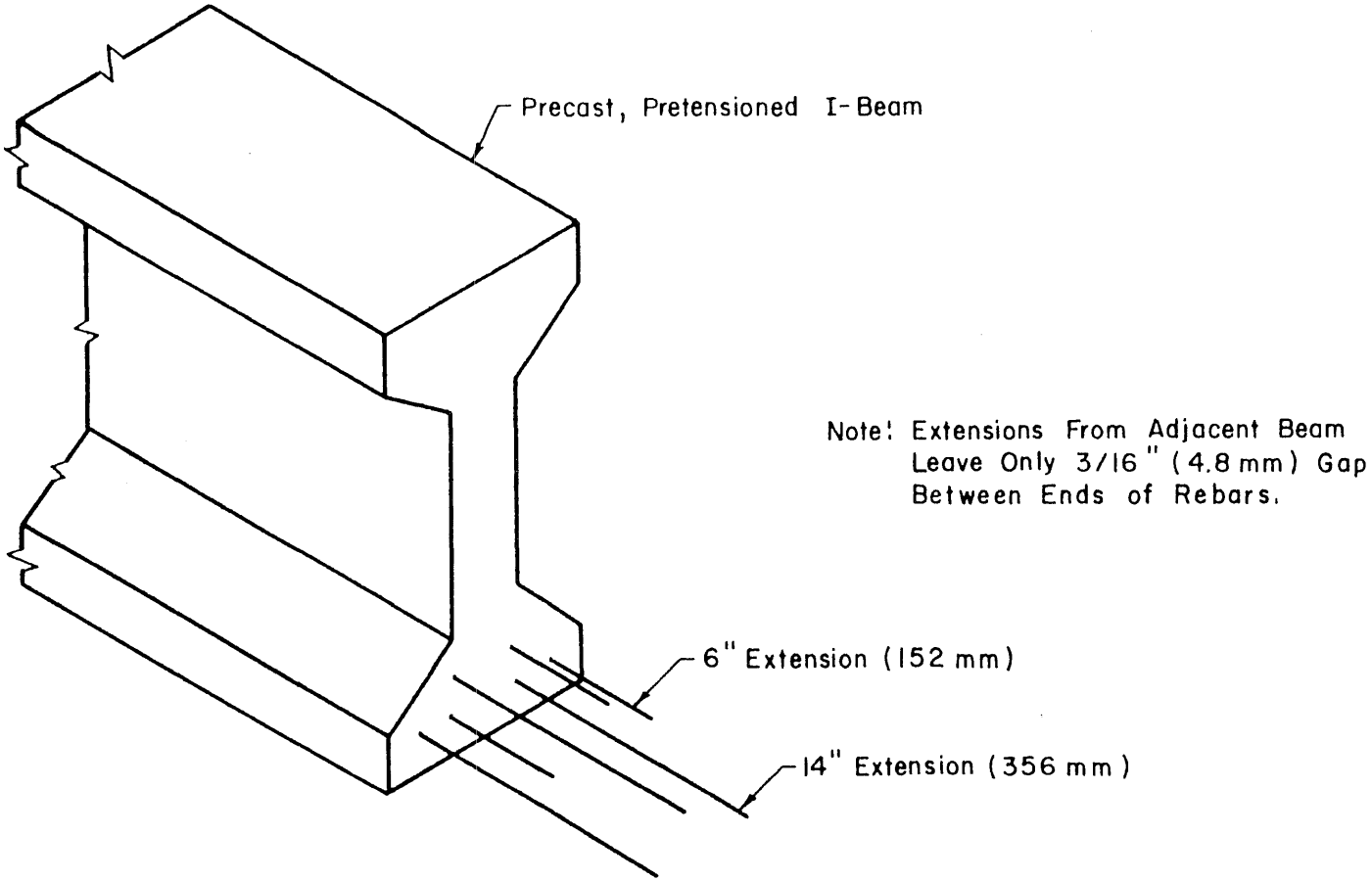


FIG. 2.21 EXTENSIONS OF #7 DEFORMED REINFORCING BARS INTO SPLICE REGION, MODEL 2

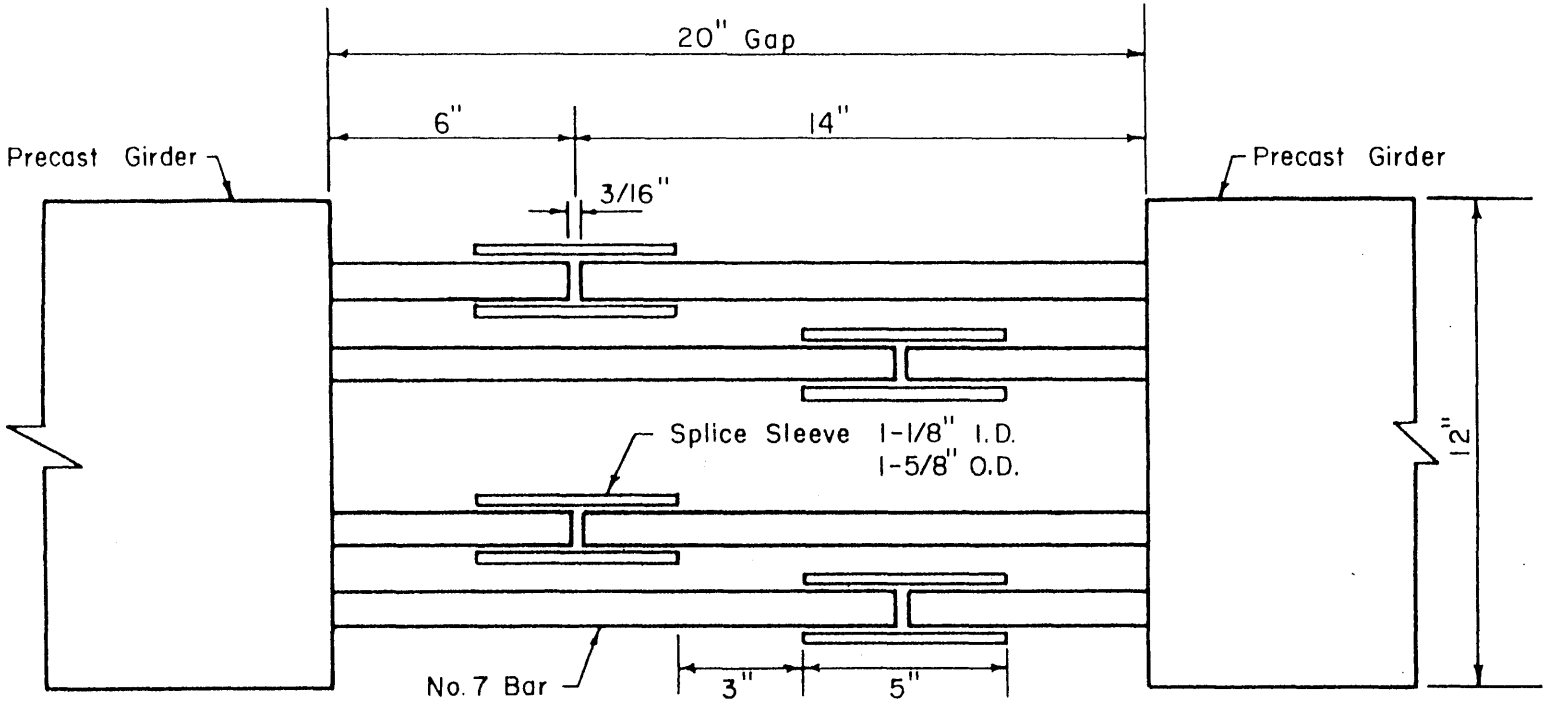


(a) Plan View of No.7 Rebar Splicing in Bottom Layer

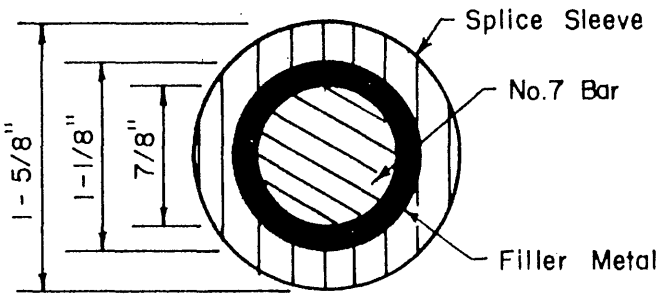


1 in. = 25.4 mm

(b) Cross-Section of A Splice

FIG. 2.22 TYPICAL LOCATIONS OF CADWELD SPLICES IN JOINTS, MODEL 2

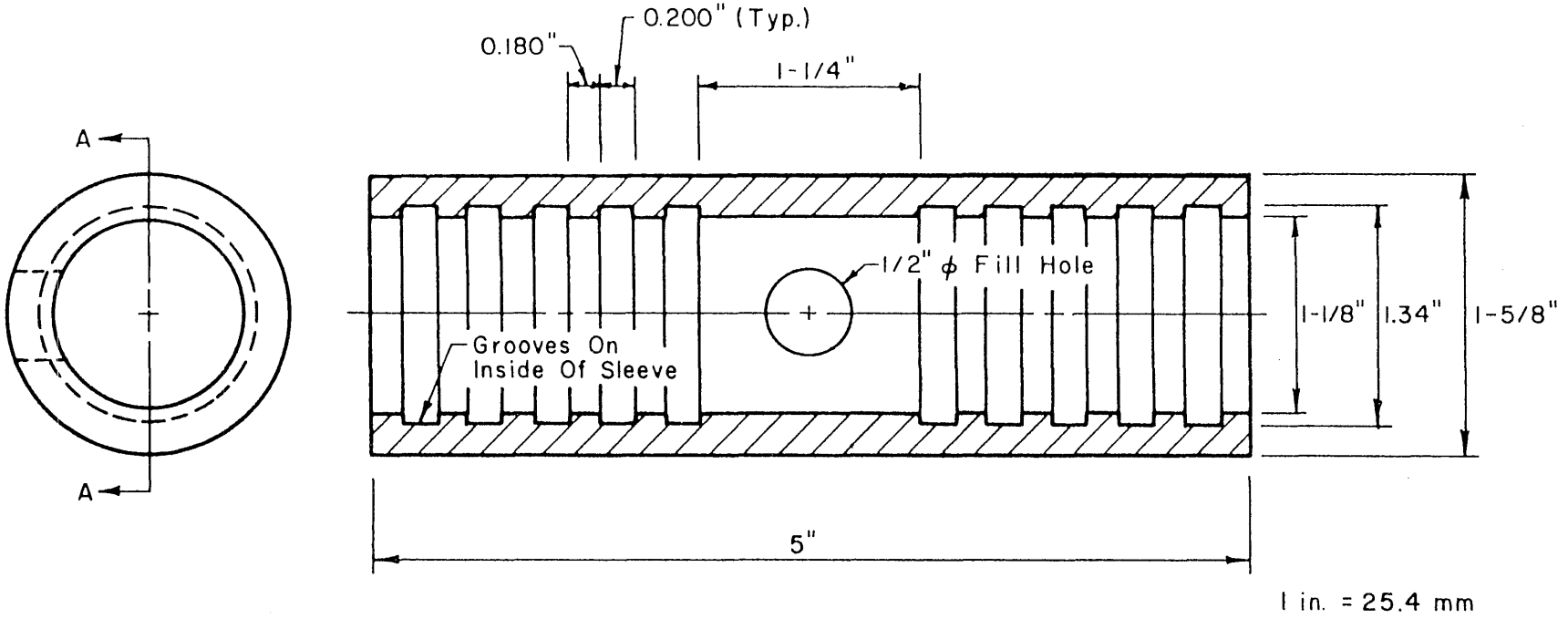


FIG. 2.23 DIMENSIONS OF CADWELD SPLICE SLEEVES USED IN MODEL 2

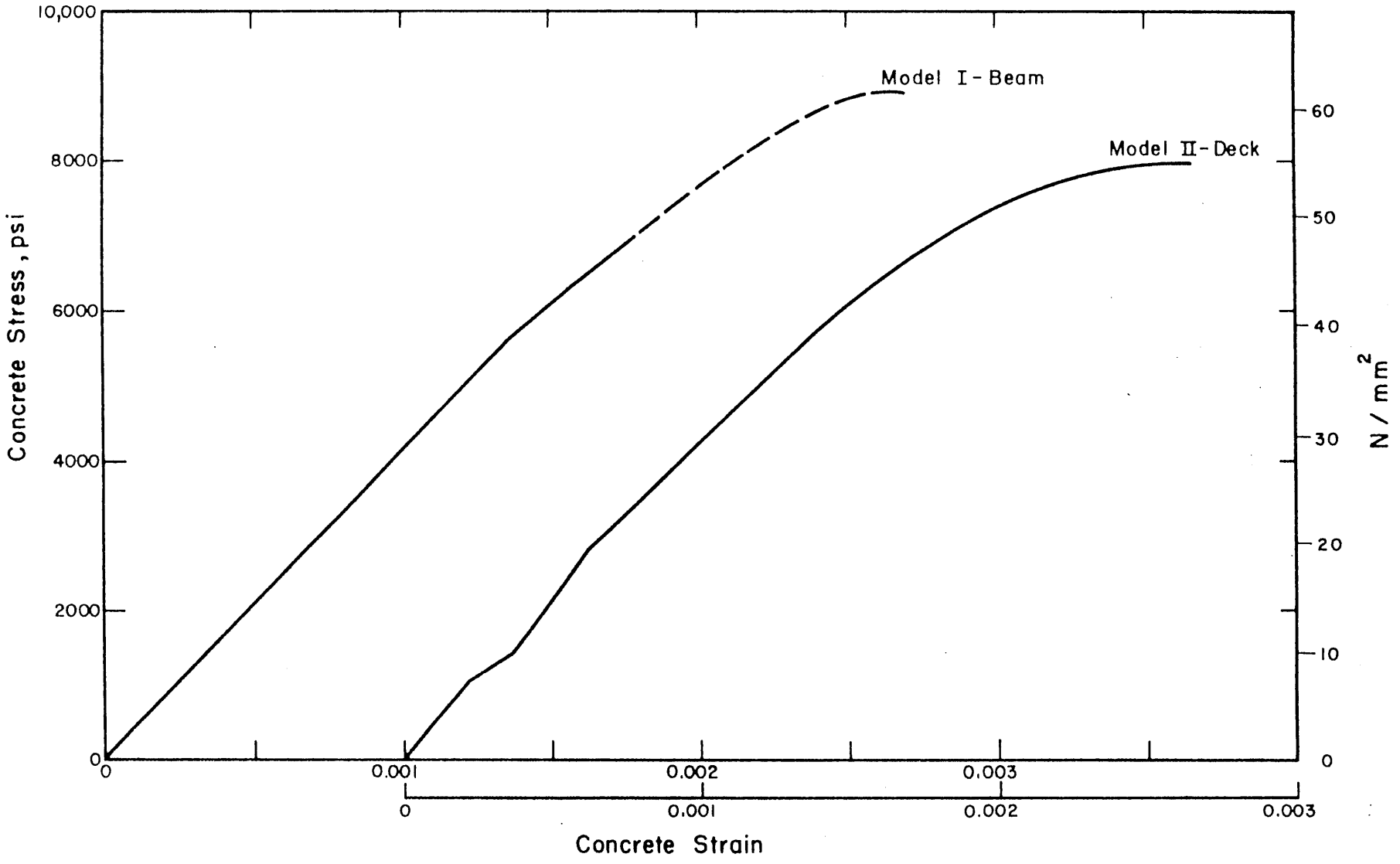


FIG. 2.24 TYPICAL STRESS-STRAIN CURVES FOR CONCRETE USED IN MODELS

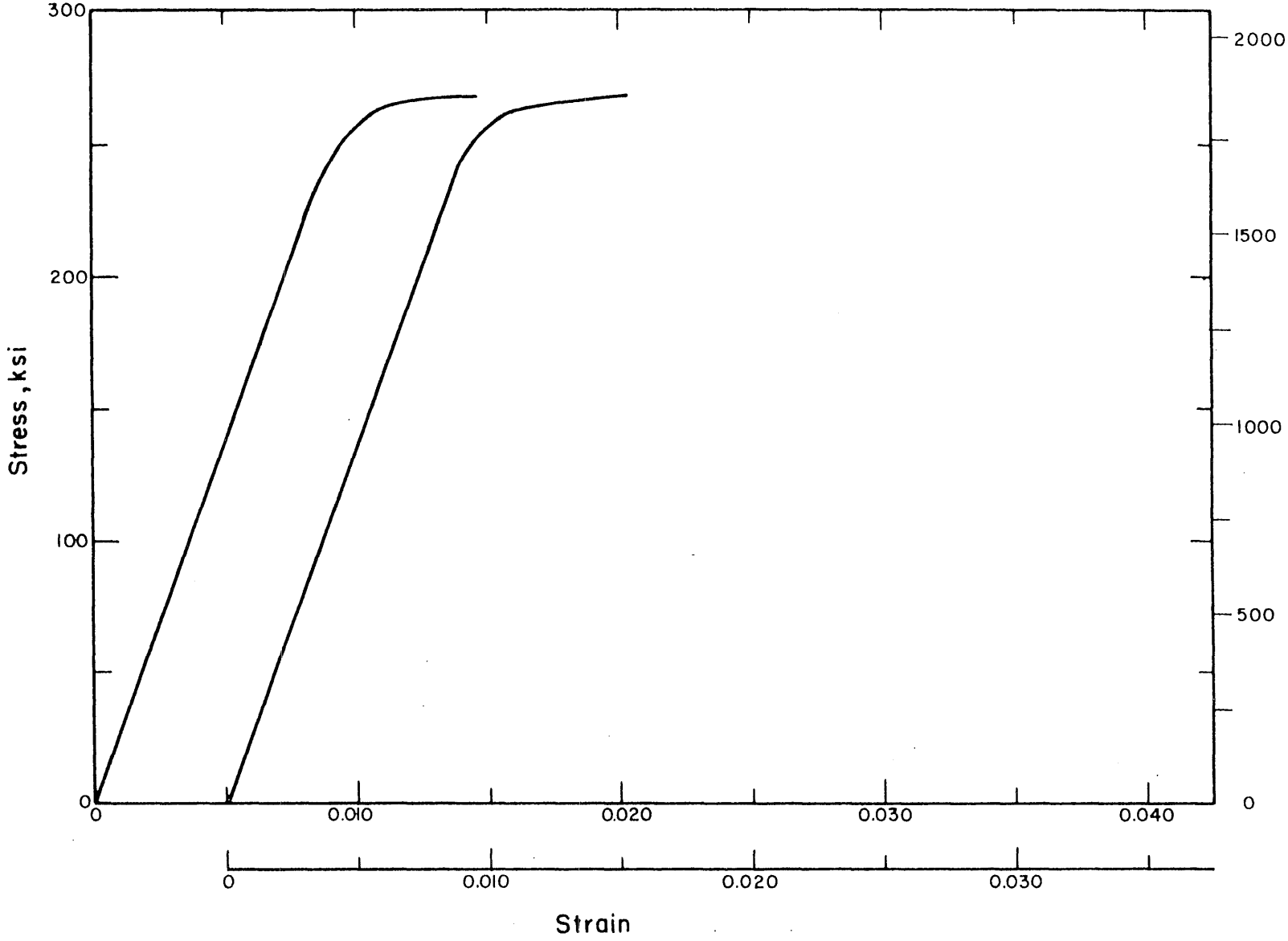


FIG. 2.25 STRESS-STRAIN CURVES FOR 3/8 IN. DIAM (9.5 mm) 7-STRAND PRESTRESSING STRANDS

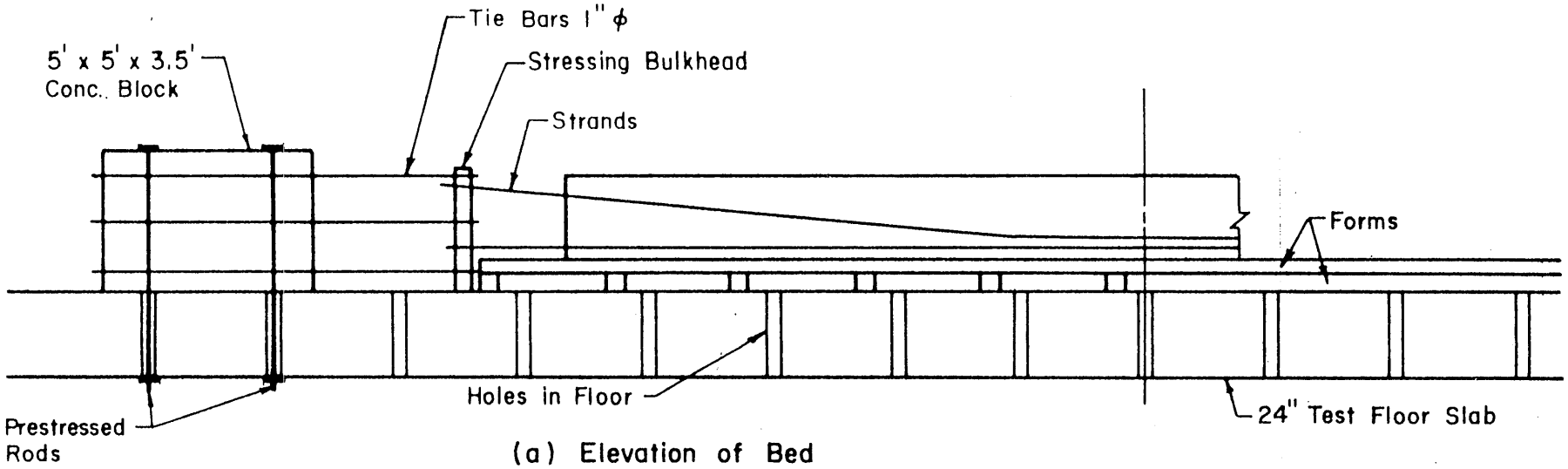


(a) Elevation of Bed

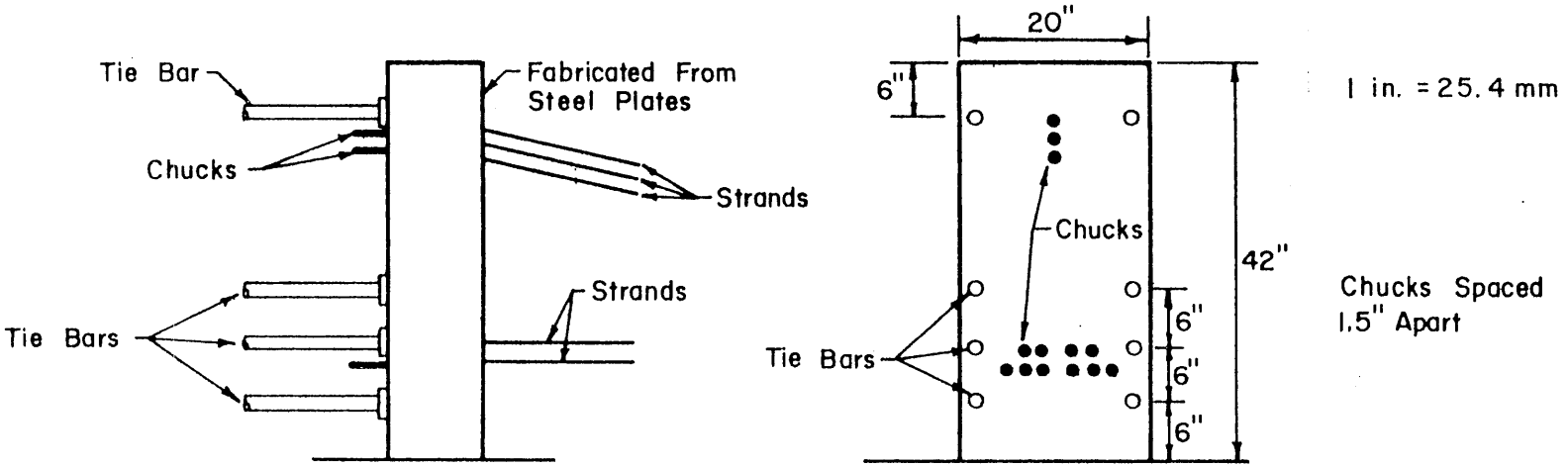


(b) Stressing Bulkhead

FIG. 2.26 GENERAL ARRANGEMENT OF COMPONENTS OF PRESTRESSING BED IN LABORATORY

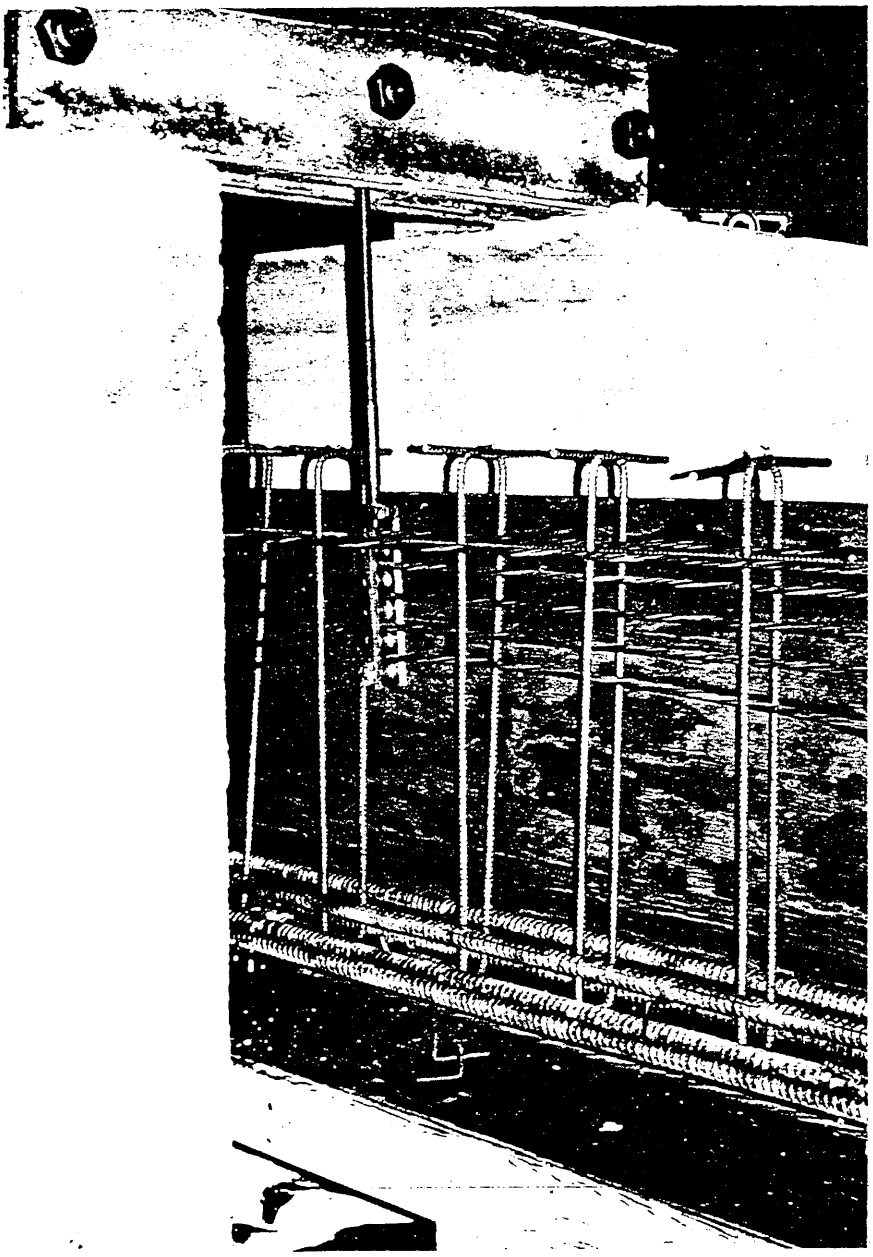

FIG. 2.27 PHOTO OF STRAND HOLD-UP DEVICE, CENTRAL SEGMENT, MODEL 2

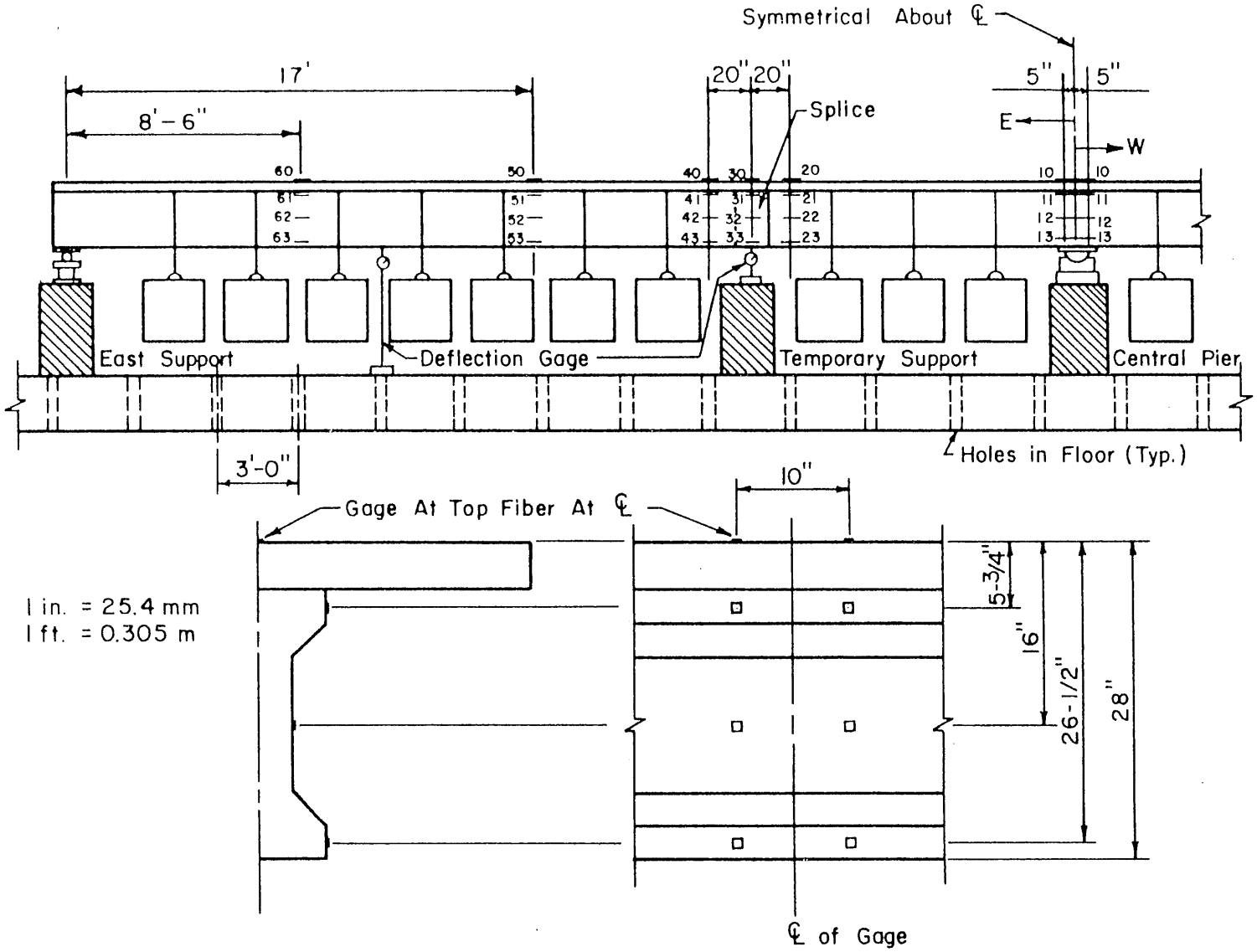


FIG. 2.28 LOCATIONS OF MECHANICAL STRAIN GAGE LINES AND OF DEAD LOAD COMPENSATION BLOCKS

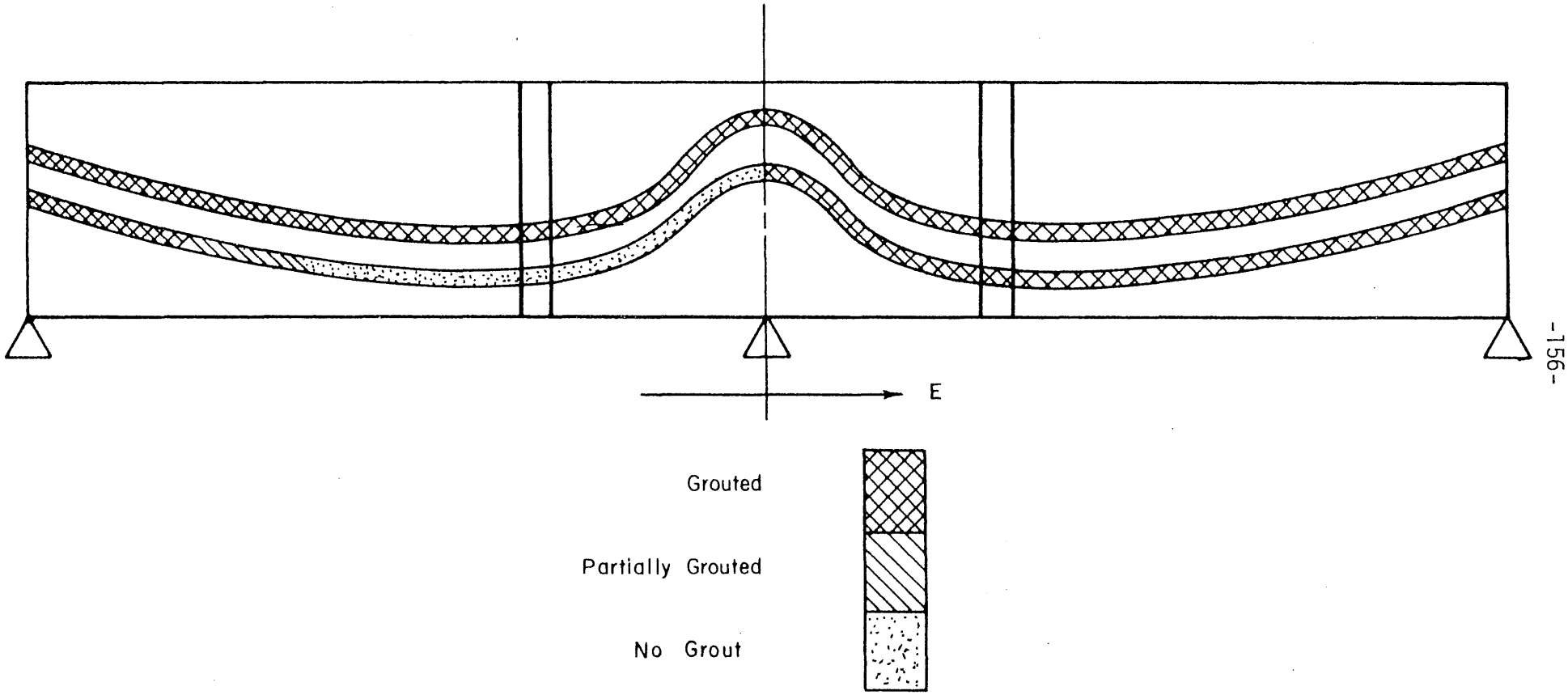


FIG. 2.29 DIAGRAM SHOWING DUCT AREAS WITH INCOMPLETE AND COMPLETE GROUTING, MODEL 1

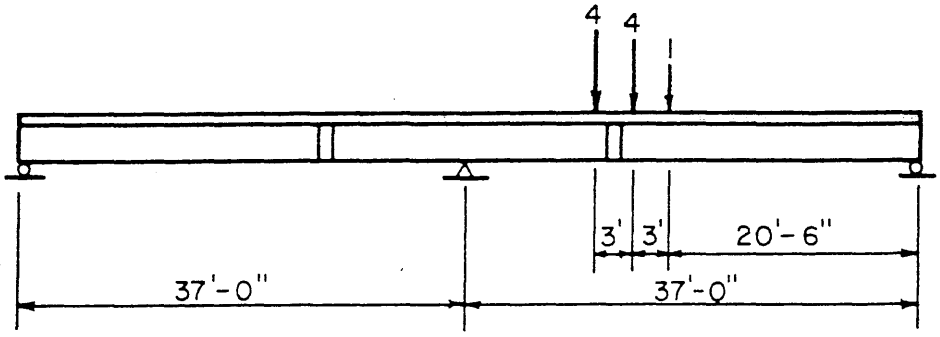


(a) Maximum Moment at Splice

1 in. = 25.4 mm
1 ft. = 0.305 m

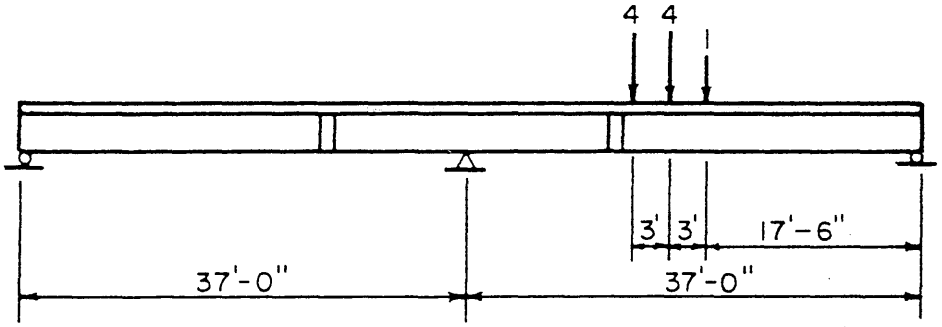


(b) Maximum Shear at Splice

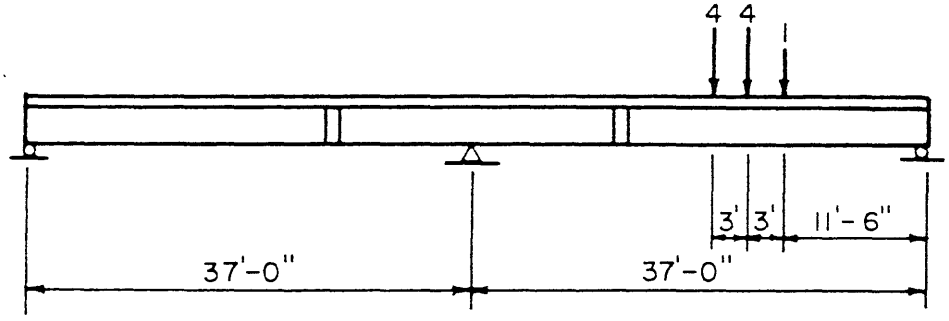


(c) Maximum Moment at Midspan

FIG. 3.1 LOCATIONS OF LOAD APPLICATIONS, MODEL 1

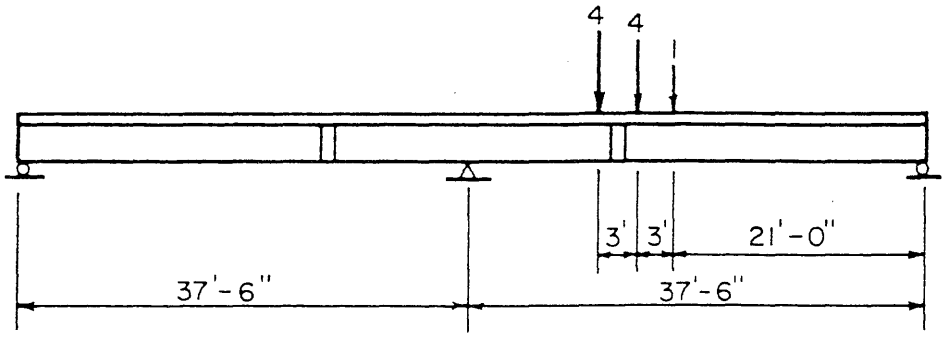


(a) Maximum Moment at Splice

1 in = 25.4 mm
1 ft. = 0.305 m

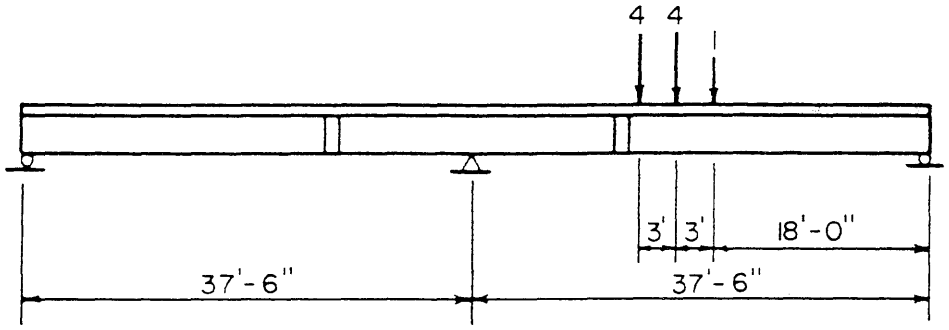


(b) Maximum Shear at Splice

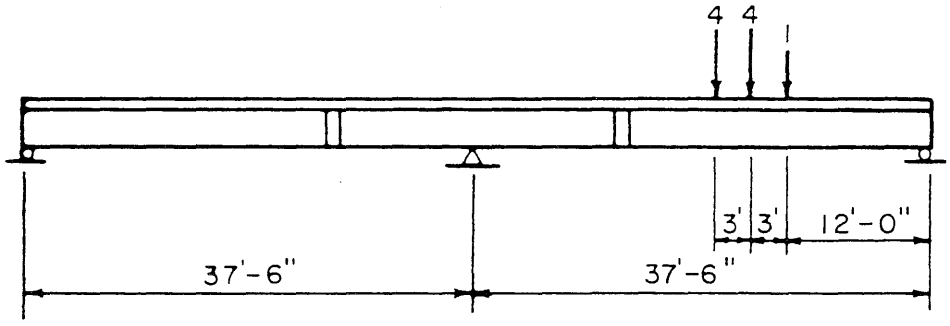


(c) Maximum Moment at Midspan

FIG. 3.2 LOCATIONS OF LOAD APPLICATIONS, MODEL 2

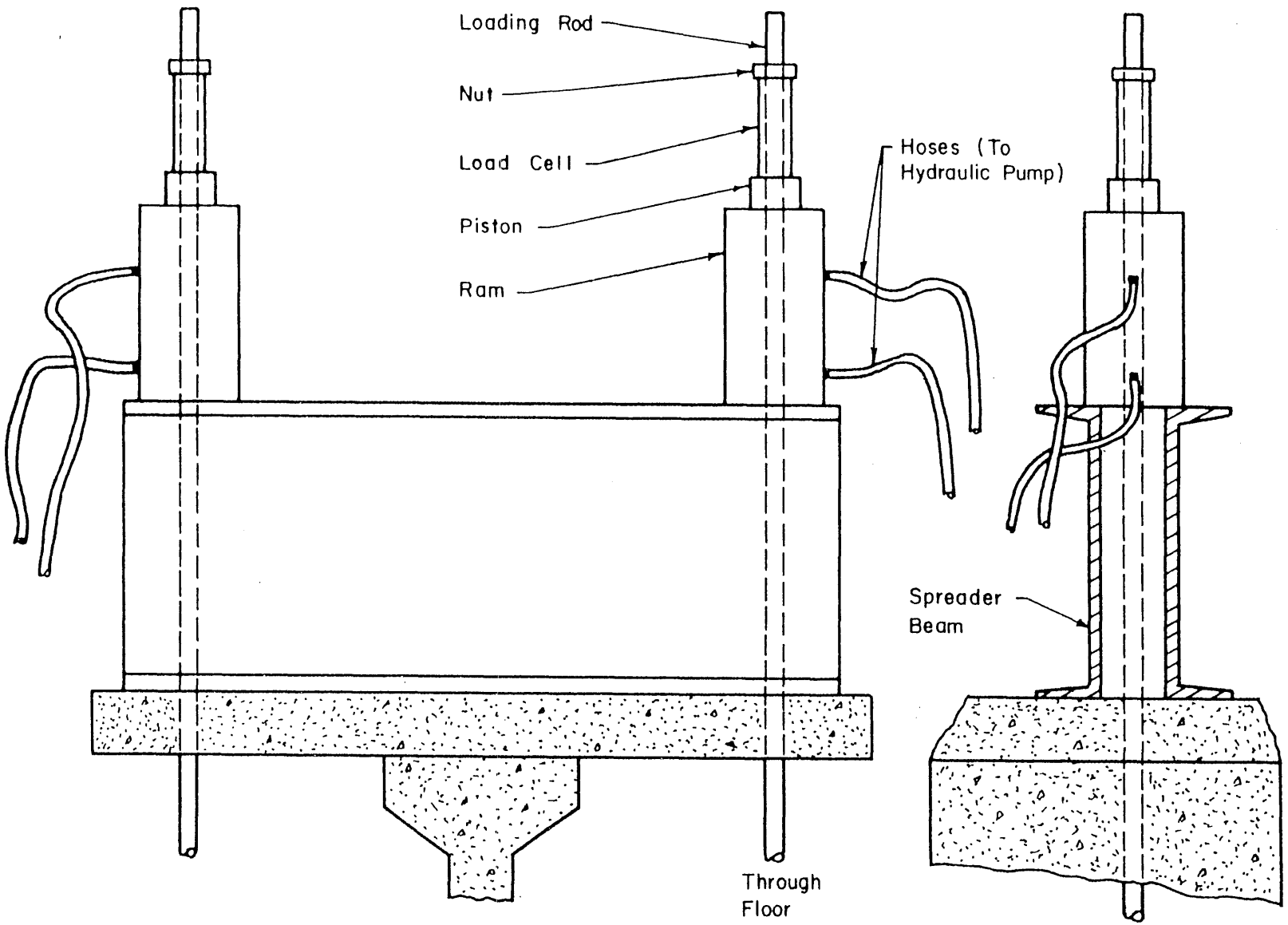


FIG. 3.3 ARRANGEMENT OF LOADING BEAMS, HYDRAULIC RAMS, AND LOAD CELLS ON TOP OF STRUCTURES

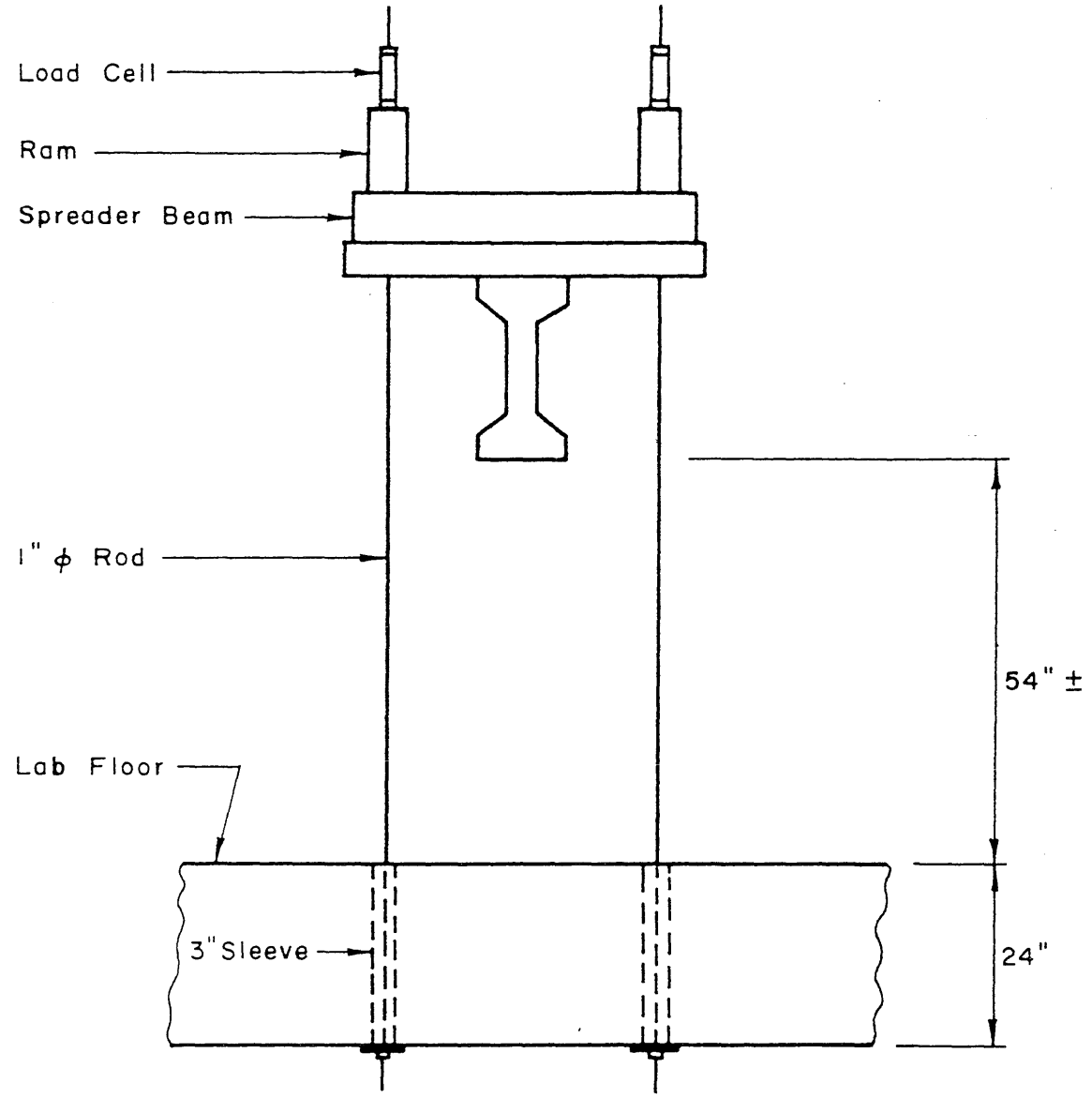


1 in. = 25.4 mm

FIG. 3.4 ANCHORAGE OF LOADING EQUIPMENT TO LABORATORY FLOOR

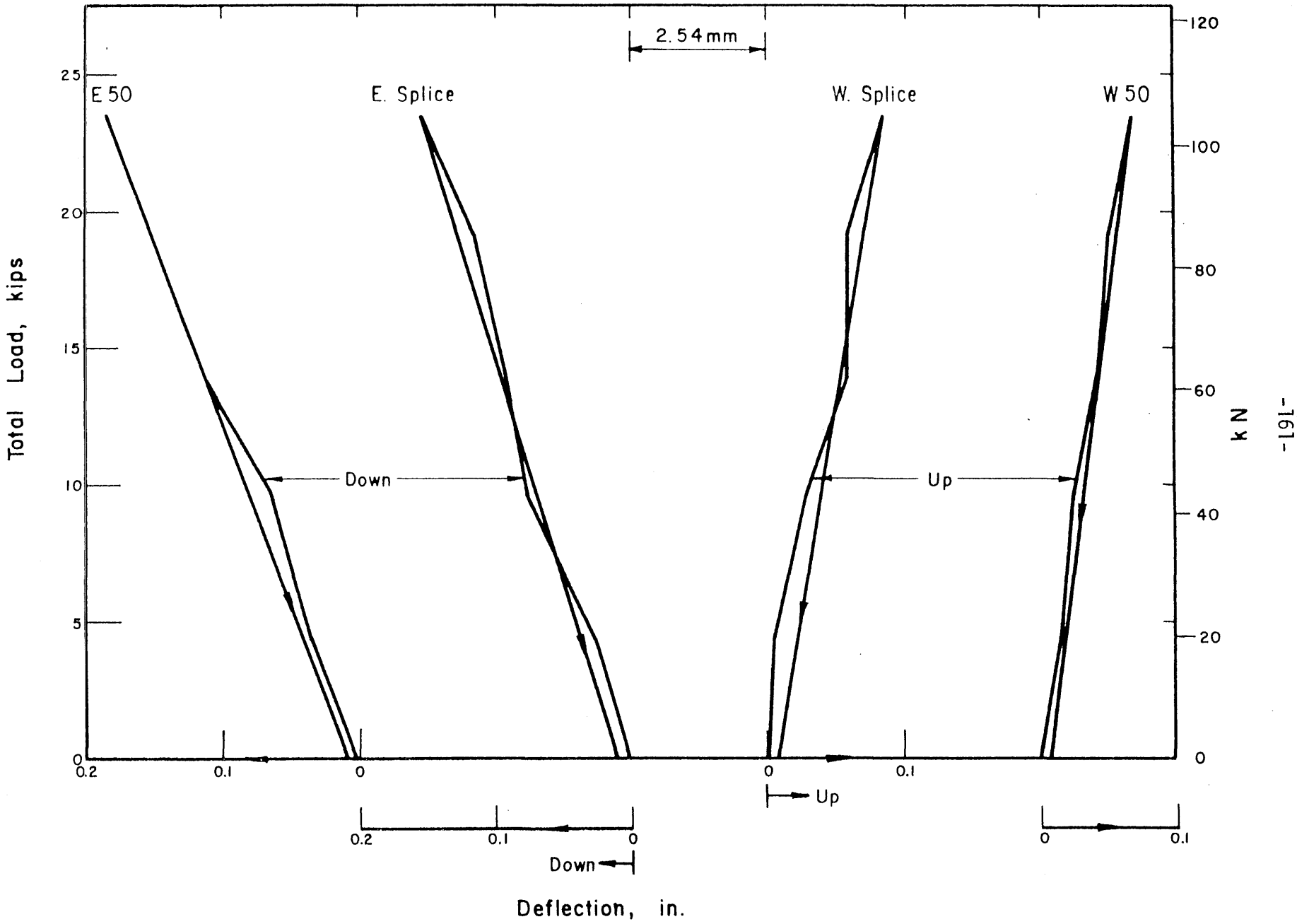


FIG. 4.1 LOAD-DEFLECTION CURVES FOR TEST 1, MODEL 1

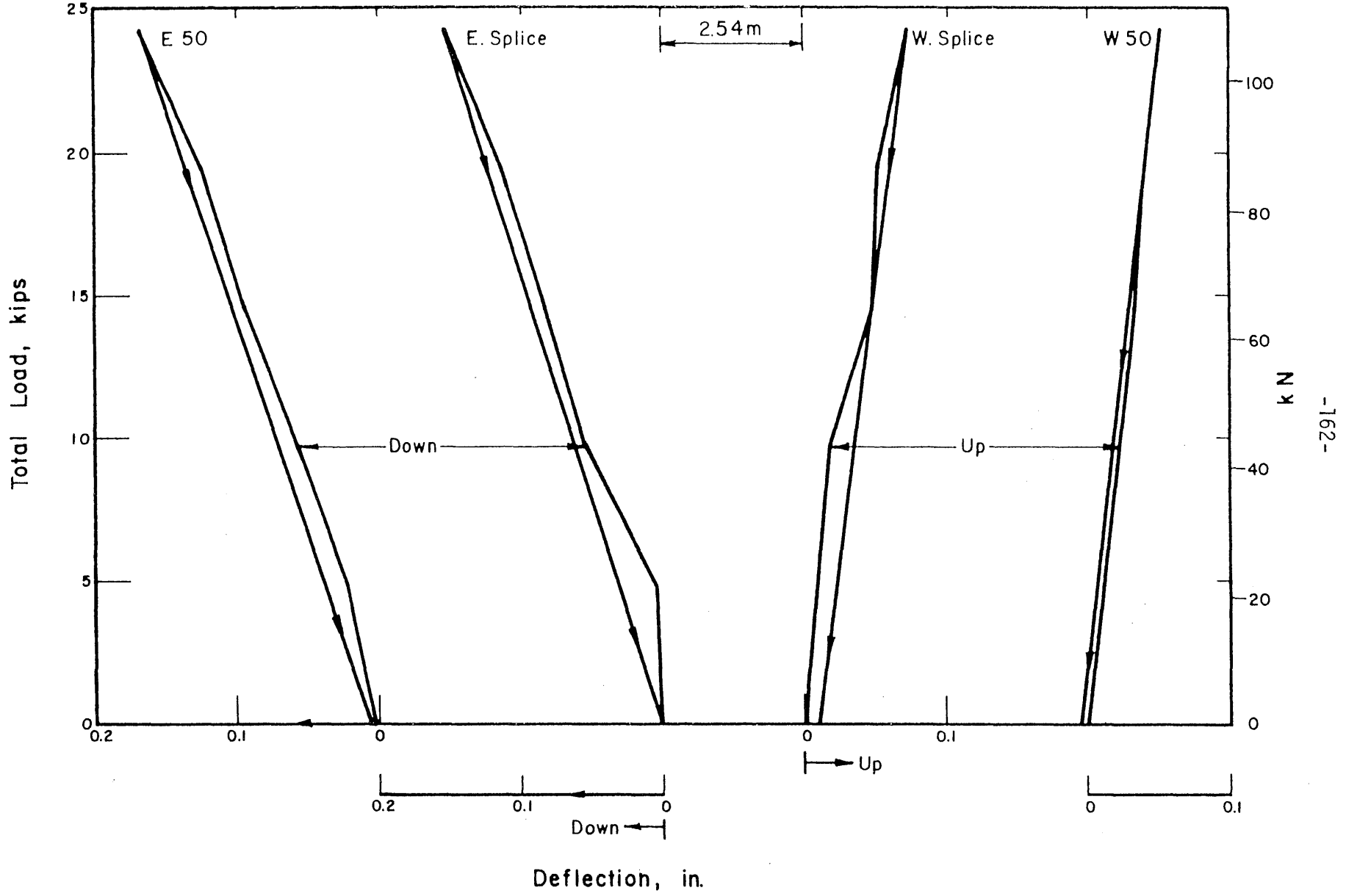


FIG. 4.2 LOAD-DEFLECTION CURVES FOR TEST 2, MODEL 1

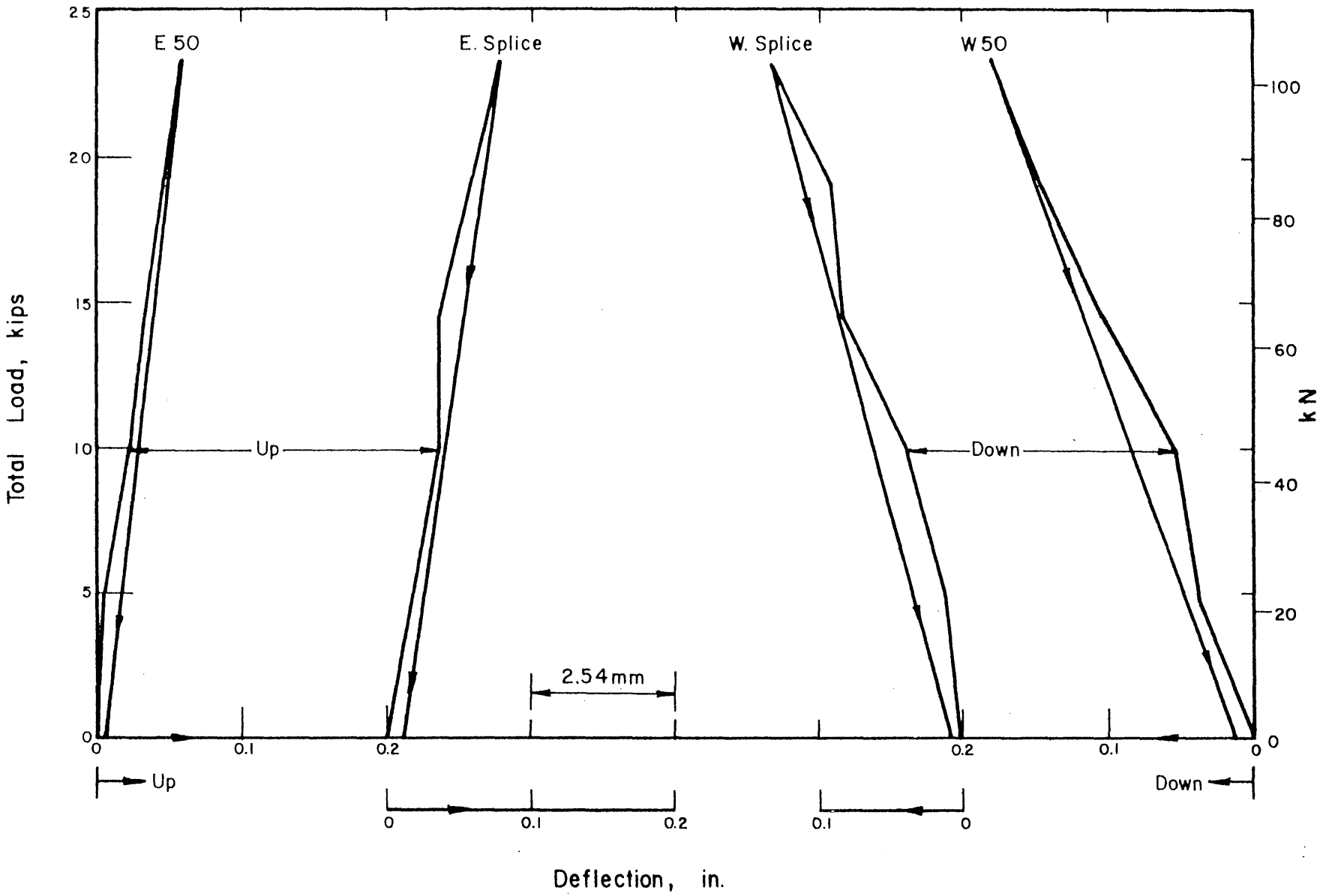


FIG. 4.3 LOAD-DEFLECTION CURVES FOR TEST 3, MODEL 1

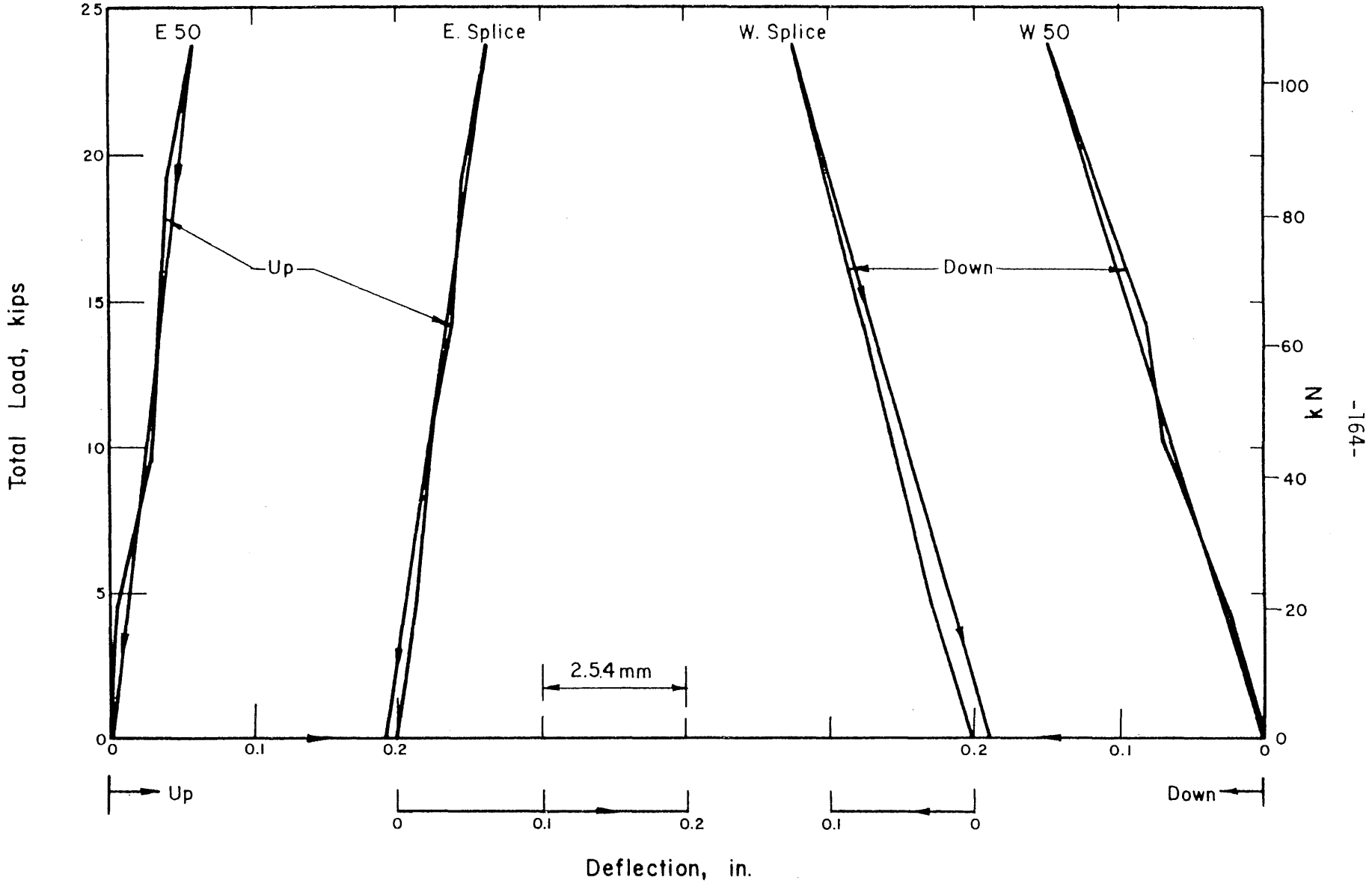


FIG. 4.4 LOAD-DEFLECTION CURVES FOR TEST 4, MODEL 1

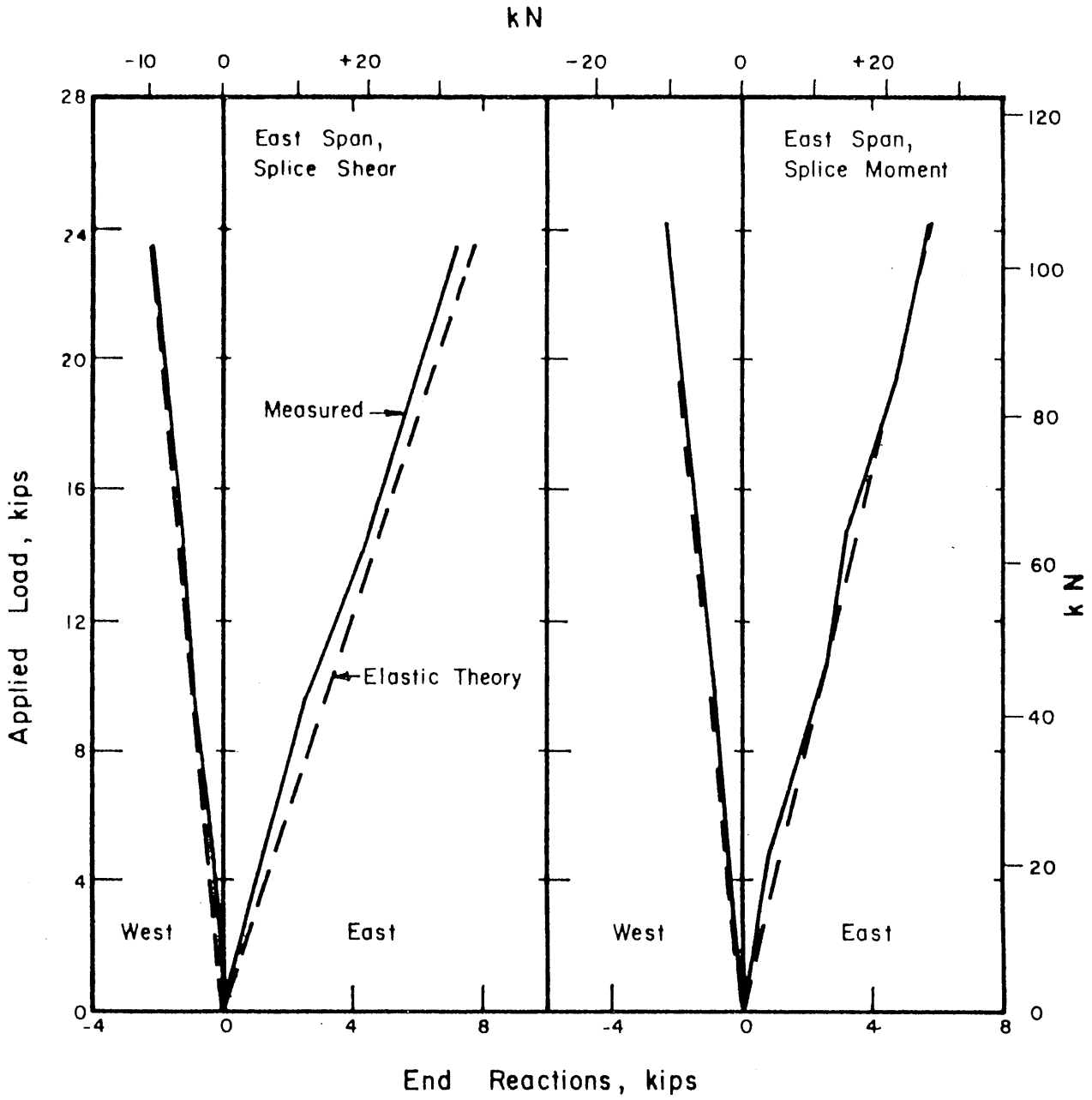


FIG. 4.5 LOAD-END REACTION CURVES FOR TESTS 1 AND 2, MODEL 1

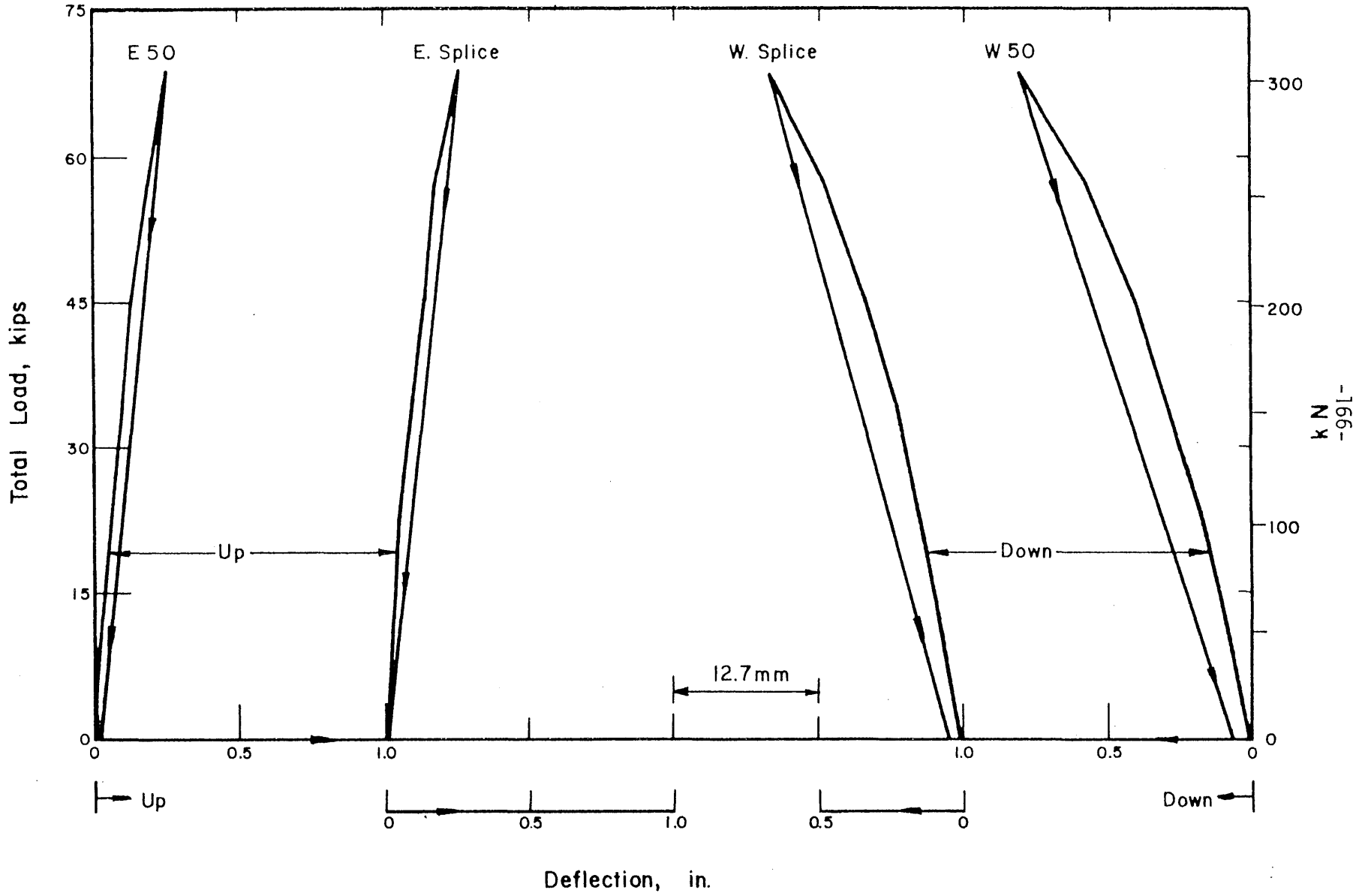


FIG. 4.6 LOAD-DEFLECTION CURVES FOR TEST 5, MODEL 1

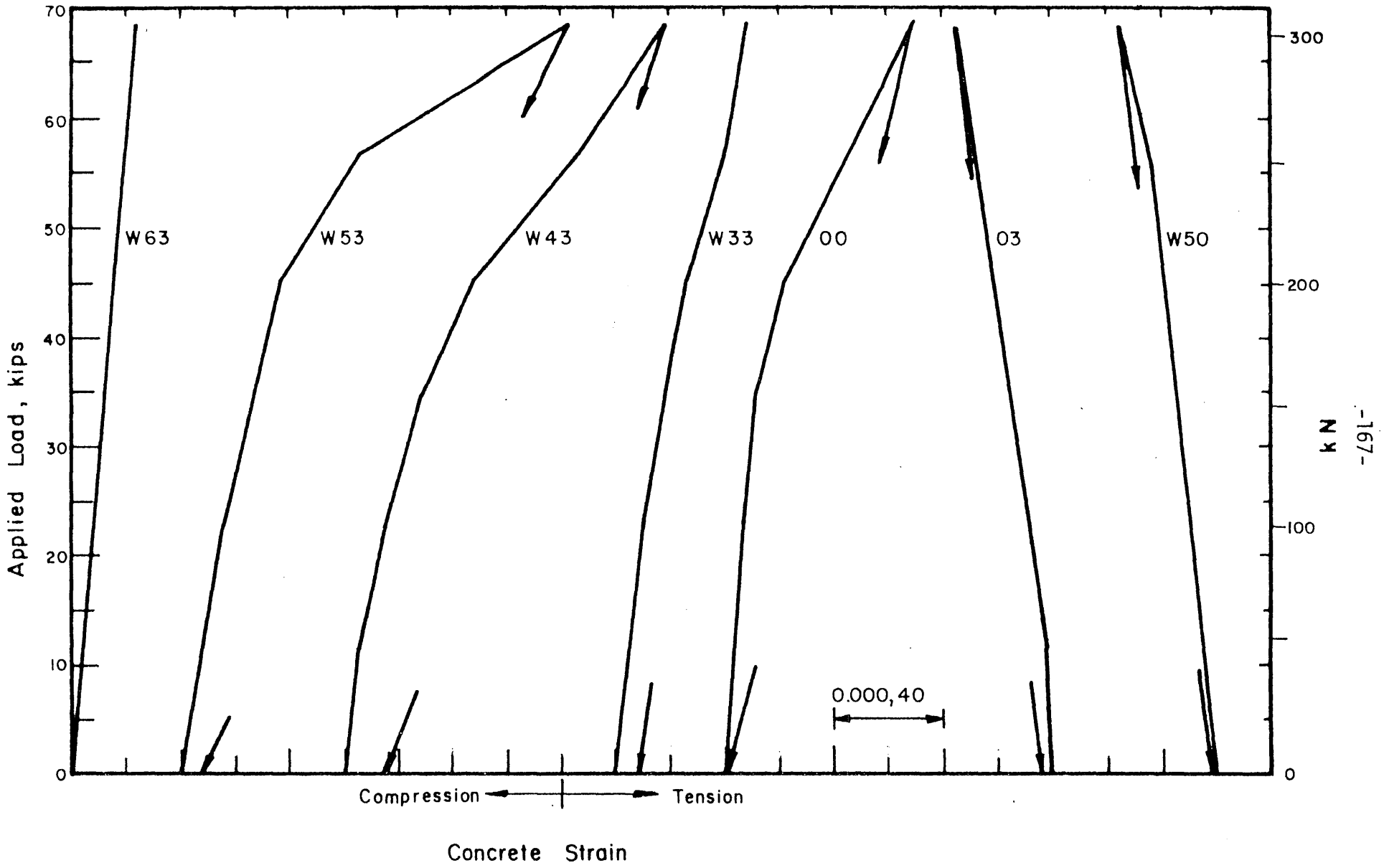


FIG. 4.7 LOAD-CONCRETE STRAIN CURVES FOR TEST 5, MODEL 1

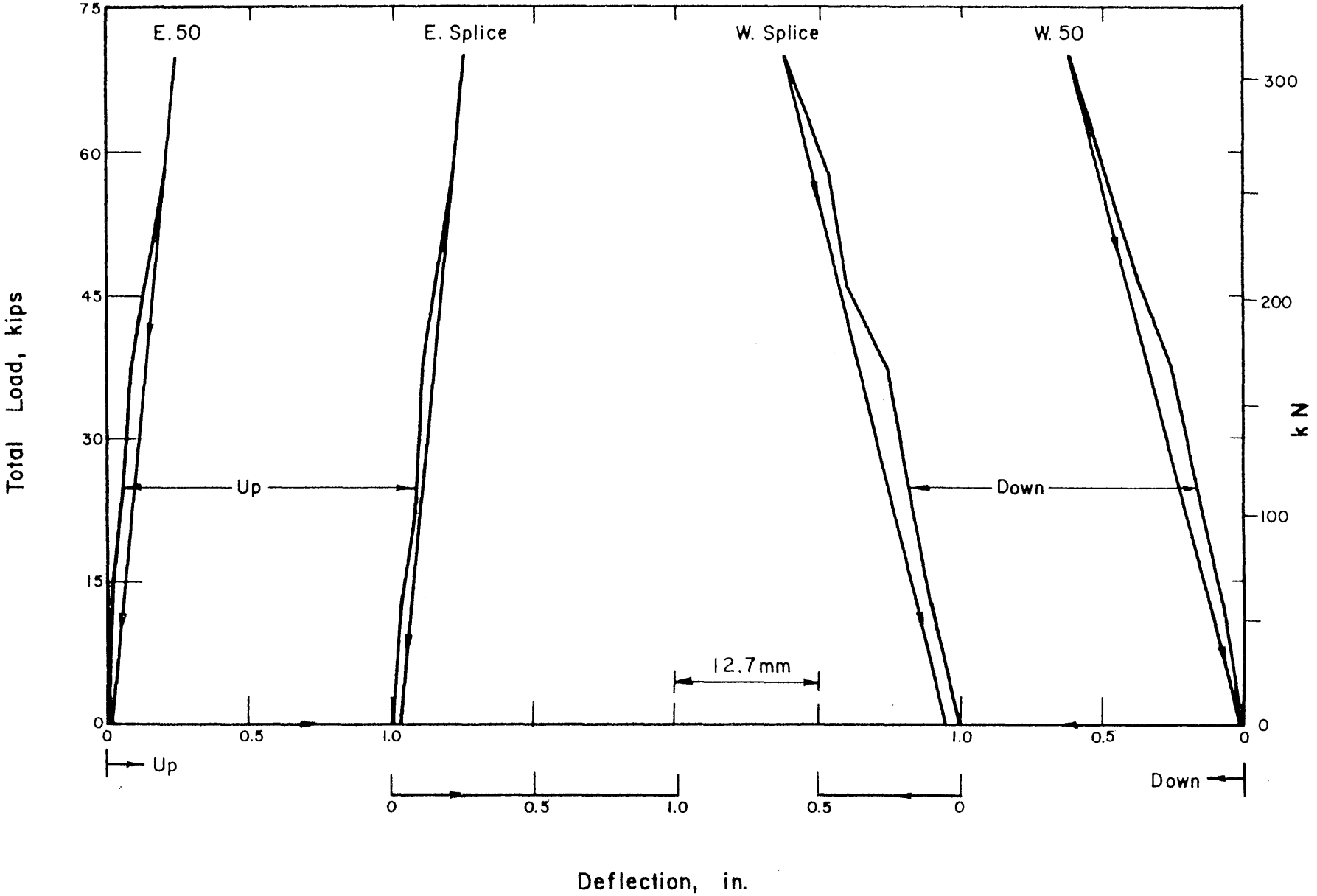


FIG. 4.8 LOAD-DEFLECTION CURVES FOR TEST 6, MODEL 1

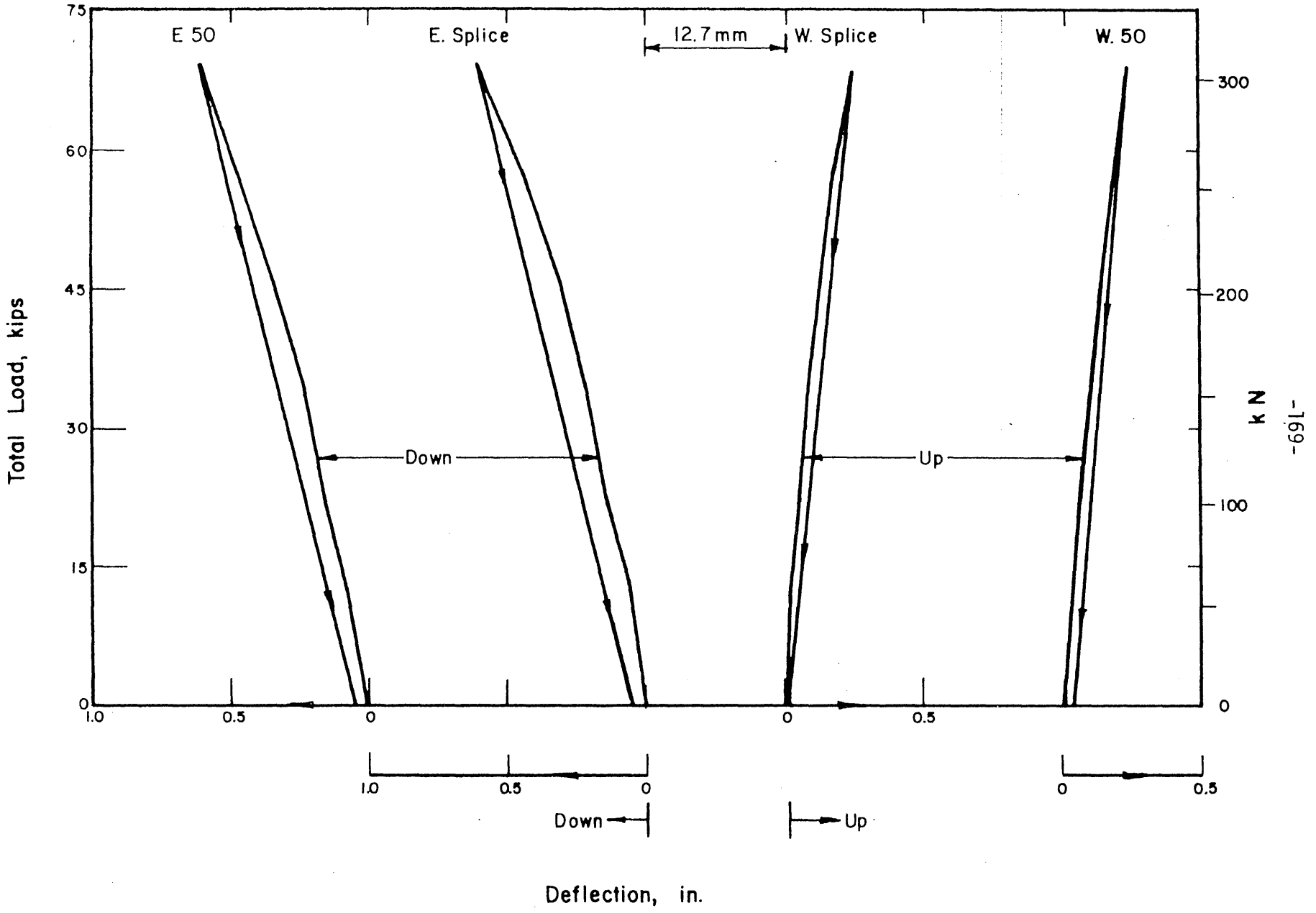


FIG. 4.9 LOAD-DEFLECTION CURVES FOR TEST 7, MODEL 1

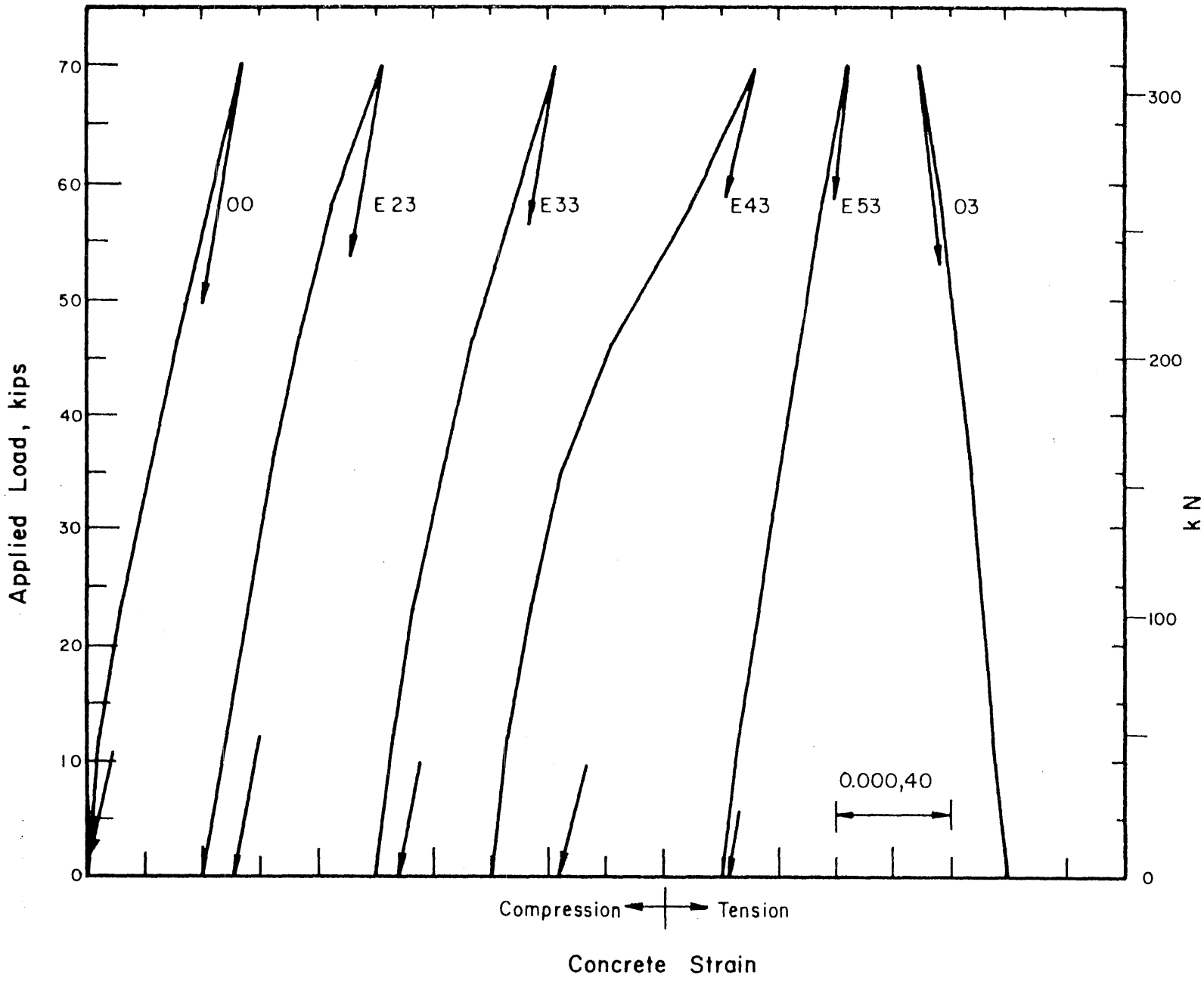


FIG. 4.10 LOAD-CONCRETE STRAIN CURVES FOR TEST 7, MODEL 1

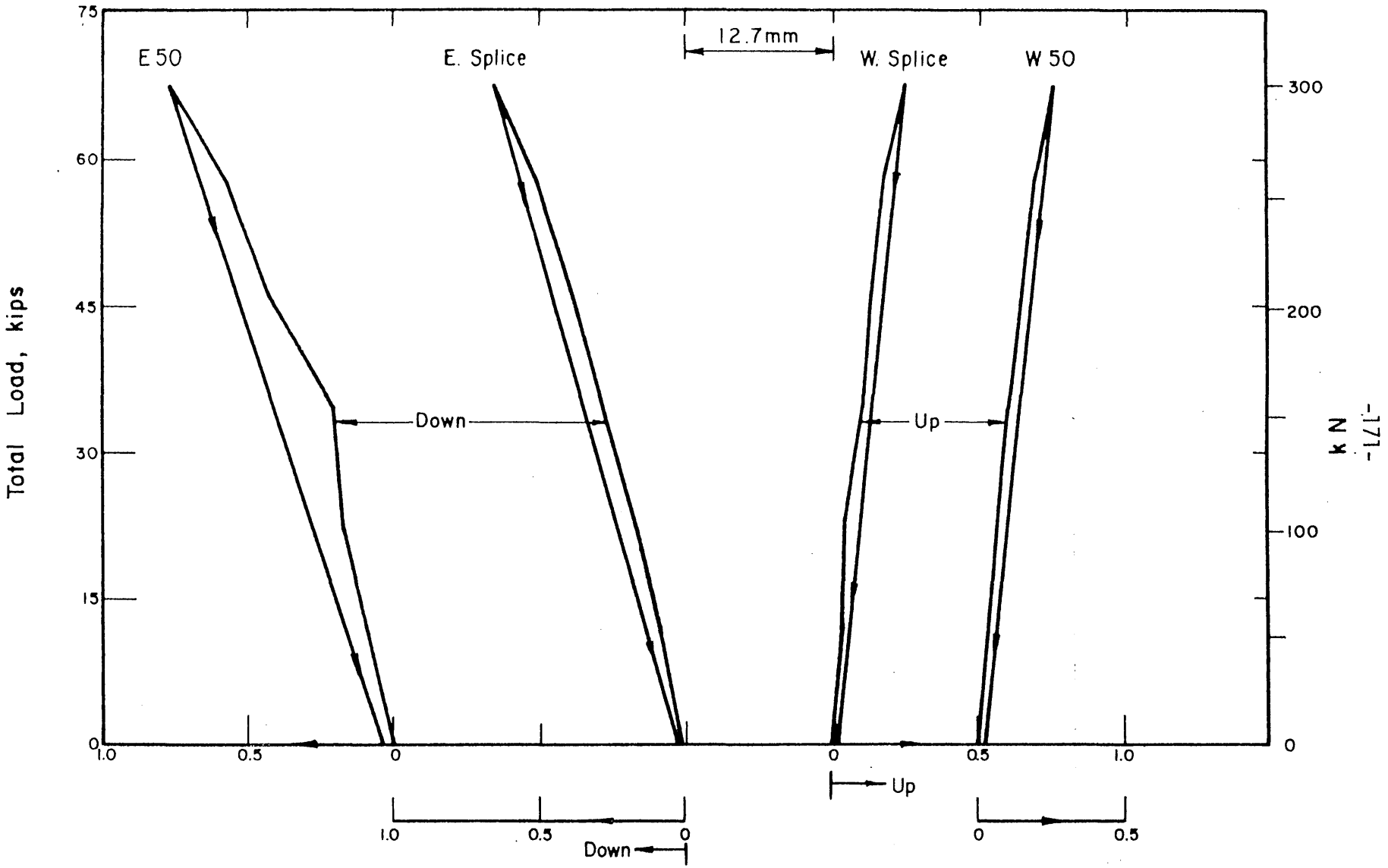


FIG. 4.11 LOAD-DEFLECTION CURVES FOR TEST 8, MODEL 1

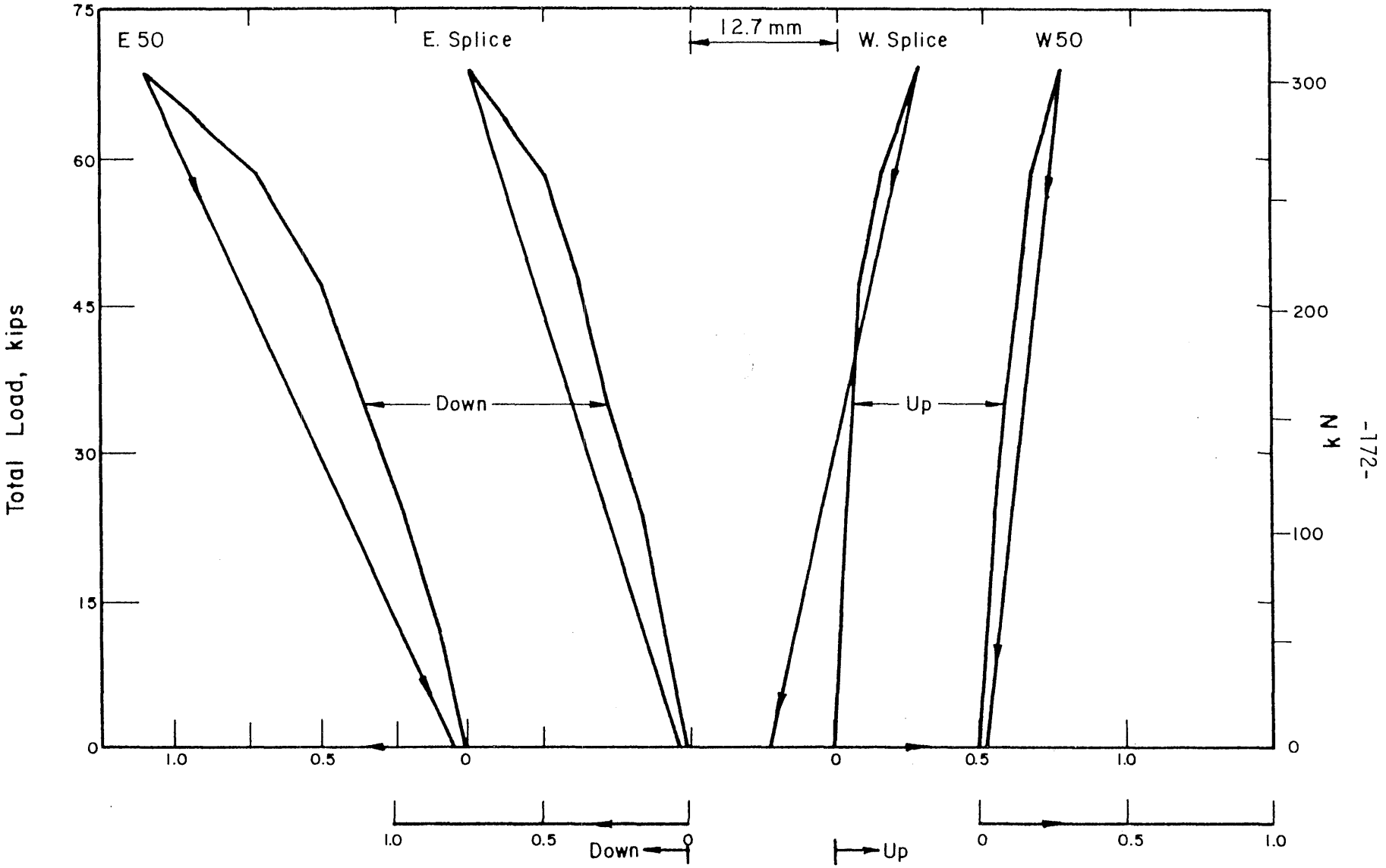


FIG. 4.12 LOAD-DEFLECTION CURVES FOR TEST 9, MODEL 1

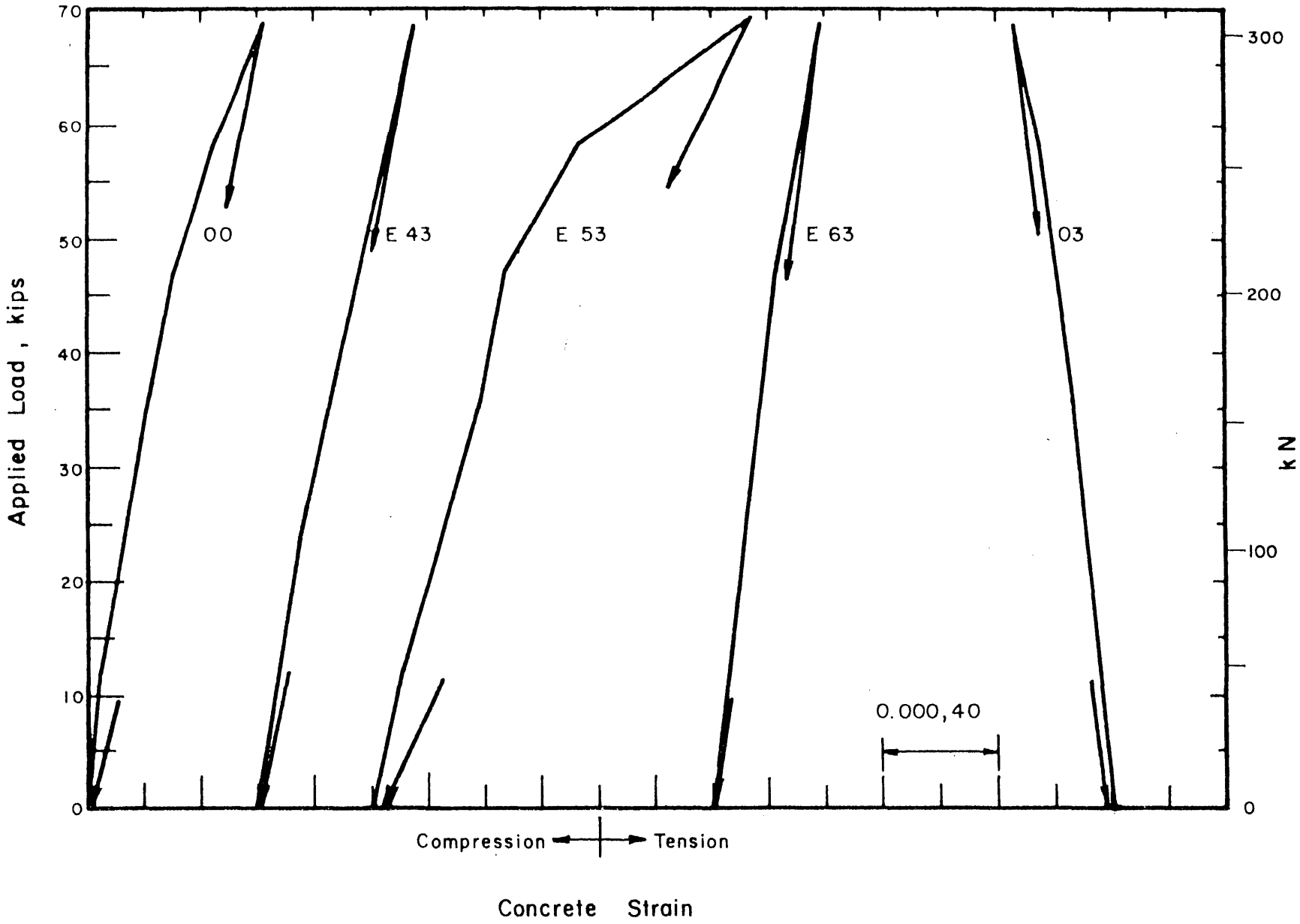


FIG. 4.13 LOAD-CONCRETE STRAIN CURVES FOR TEST 9, MODEL 1

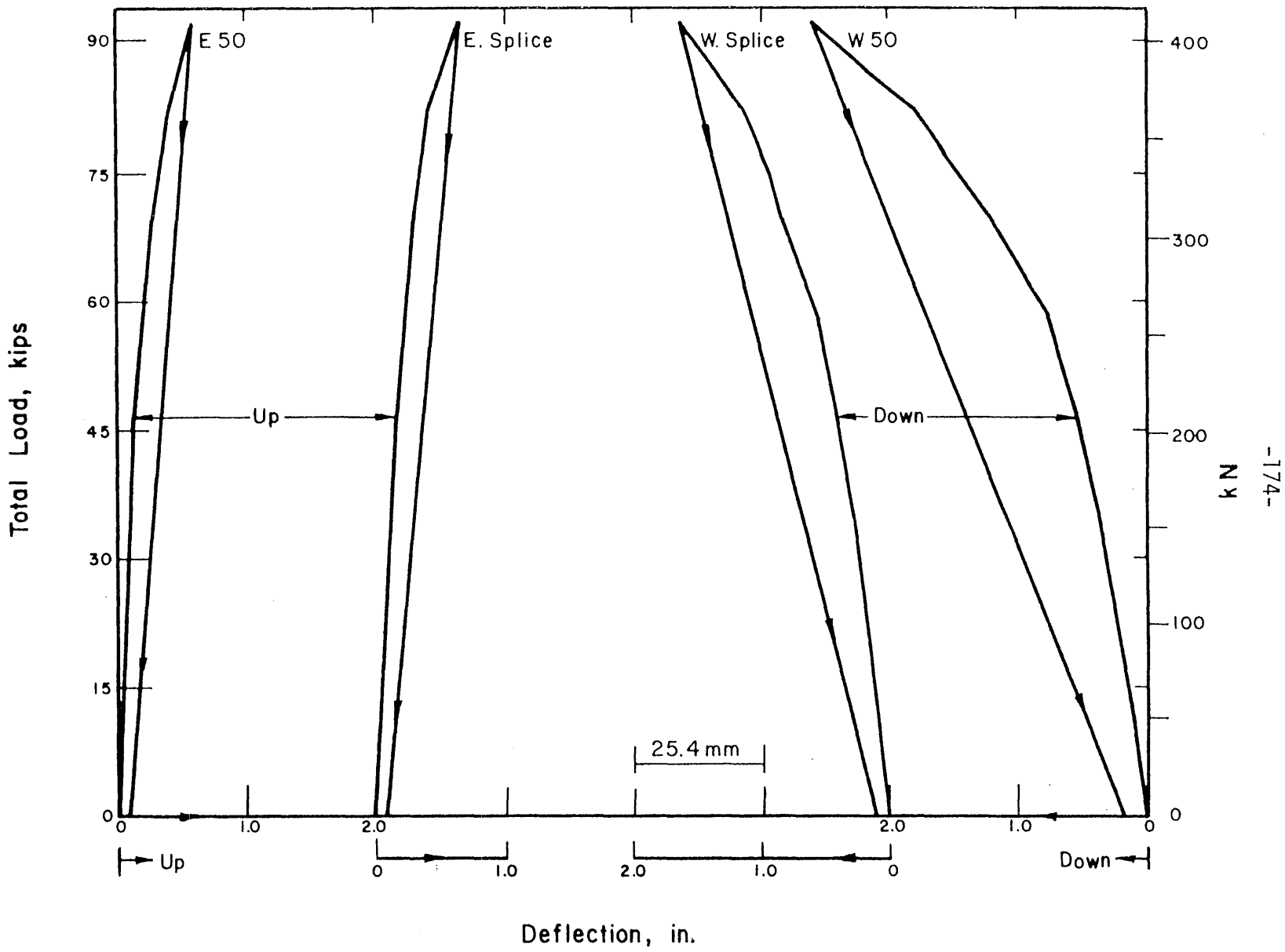


FIG. 4.14 LOAD-DEFLECTION CURVES FOR TEST 10, MODEL 1

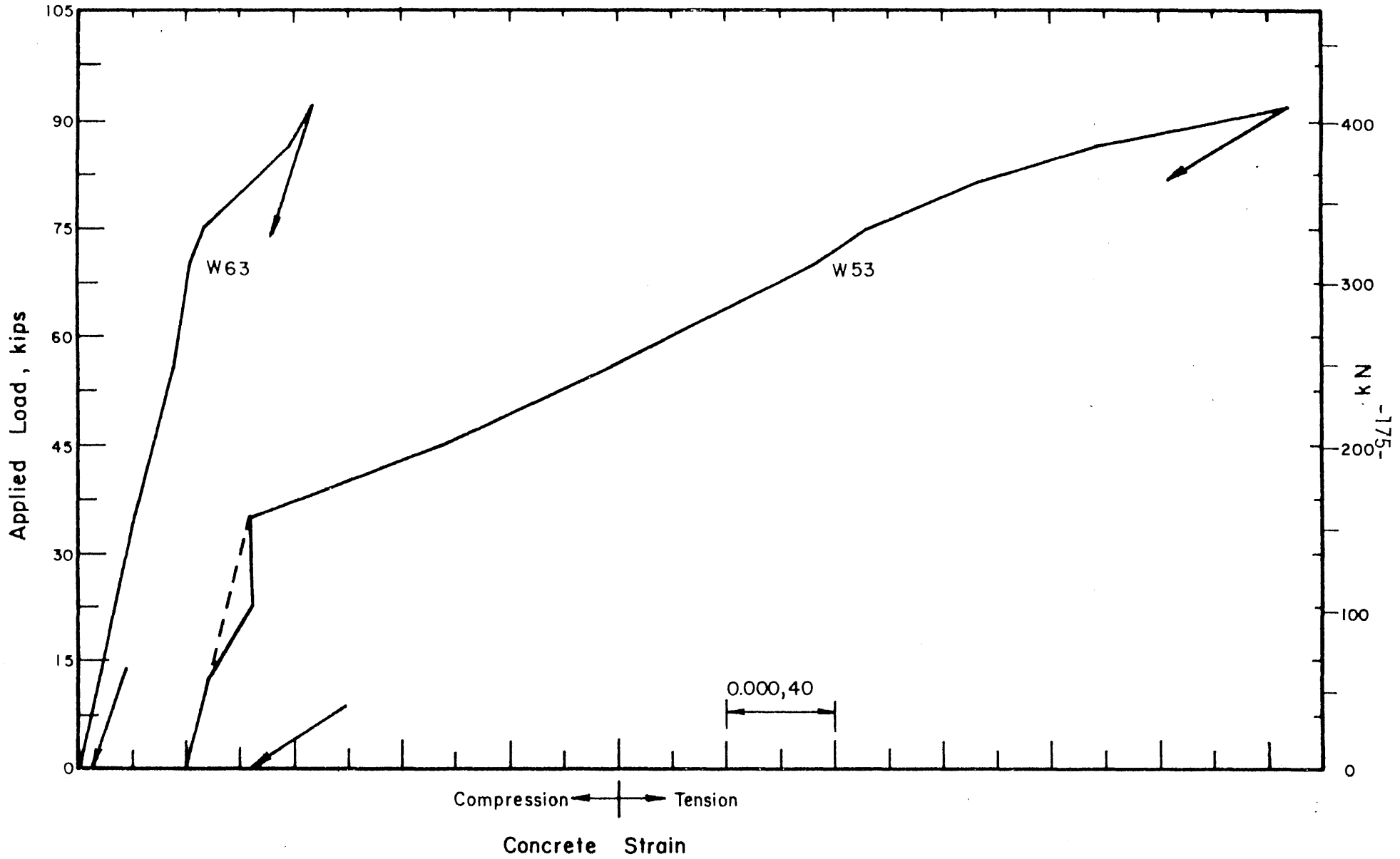


FIG. 4.15 LOAD-CONCRETE STRAIN CURVES NEAR MIDDLE OF WEST SPAN, TEST 10, MODEL 1

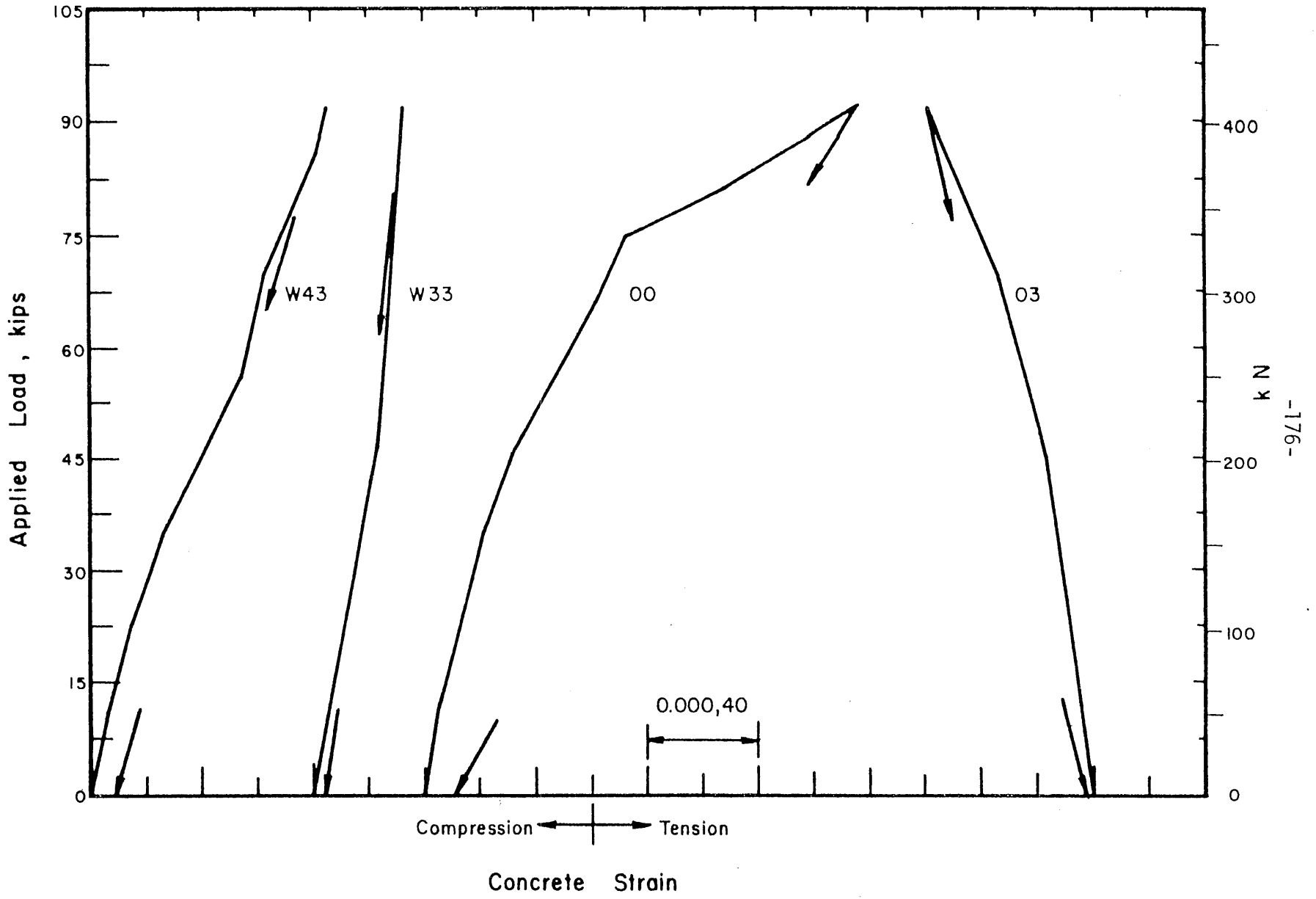


FIG. 4.16 LOAD-CONCRETE STRAIN CURVES NEAR SPLICE AND CENTRAL SUPPORT, TEST 10, MODEL 1

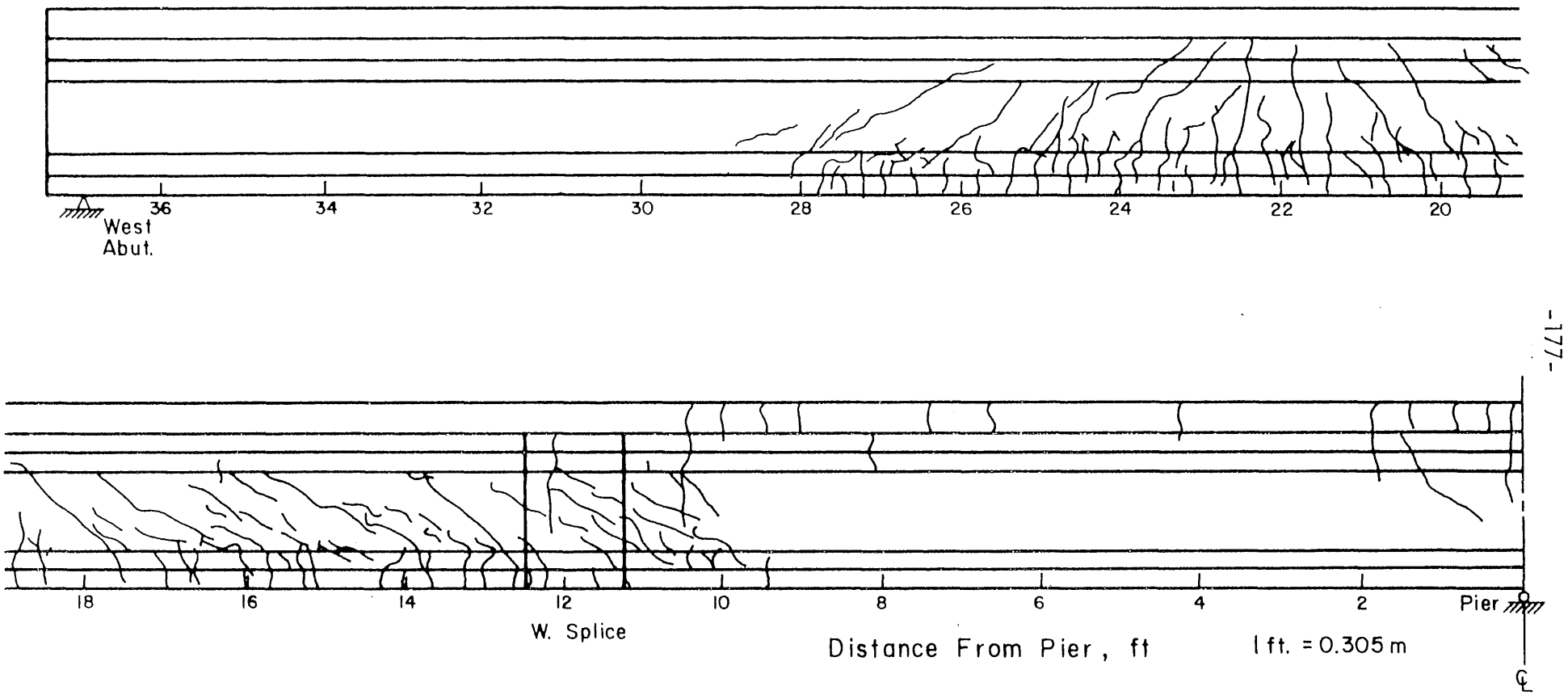


FIG. 4.17 CRACKS IN WEST SPAN AT END OF TEST 10, MODEL 1

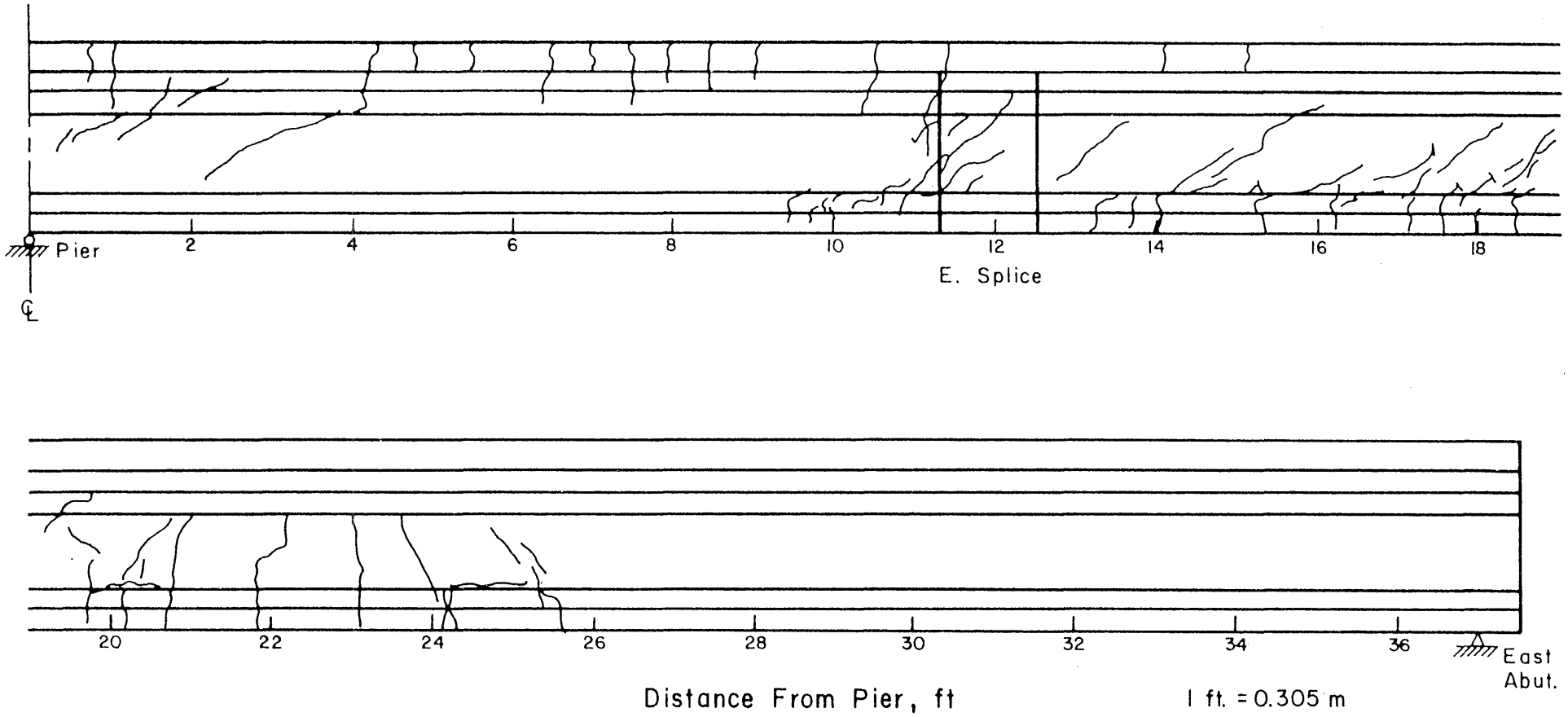


FIG. 4.18 CRACKS IN EAST SPAN AT END OF TEST 10, MODEL 1

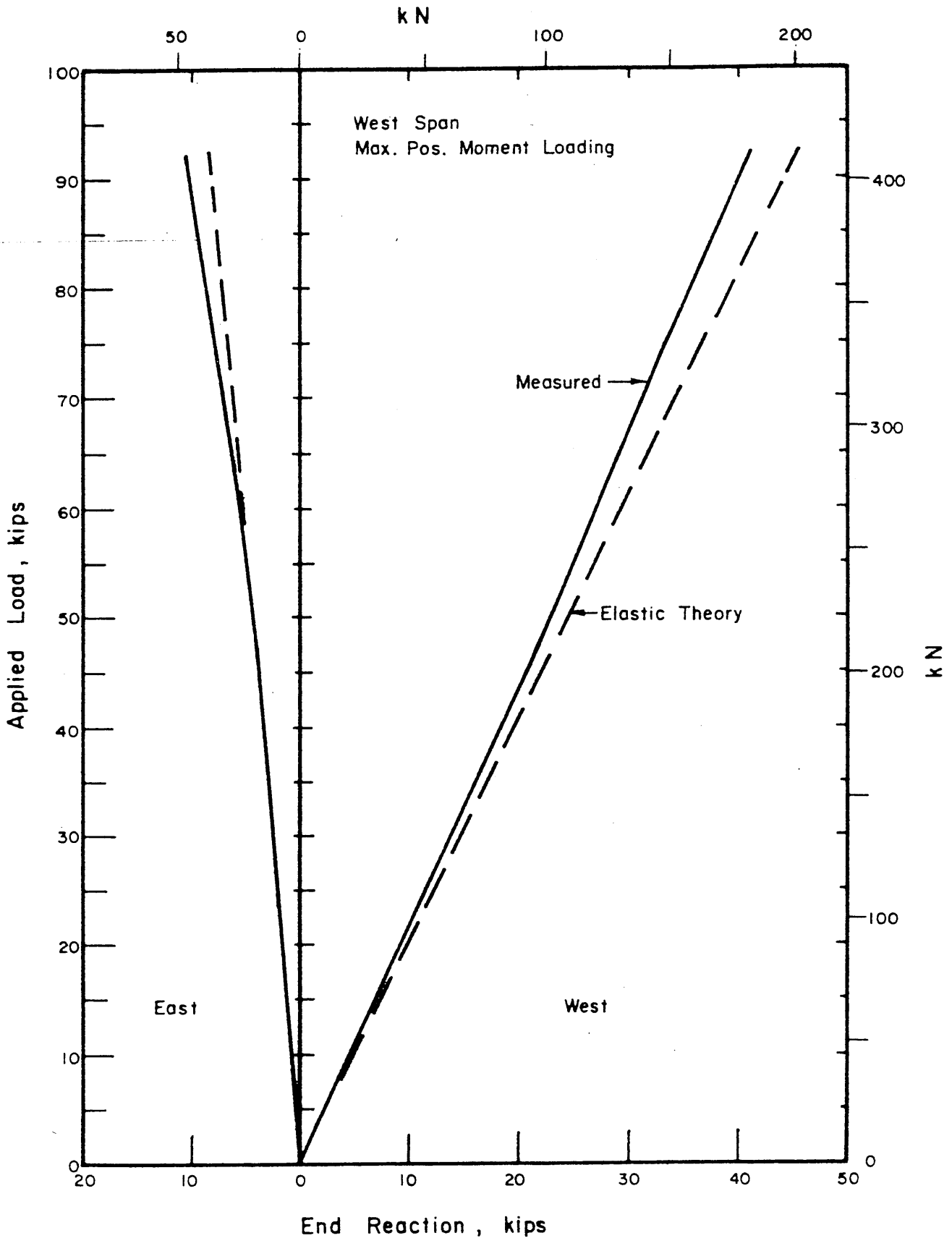


FIG. 4.19 LOAD-END REACTION CURVES FOR TEST 10, MODEL 1

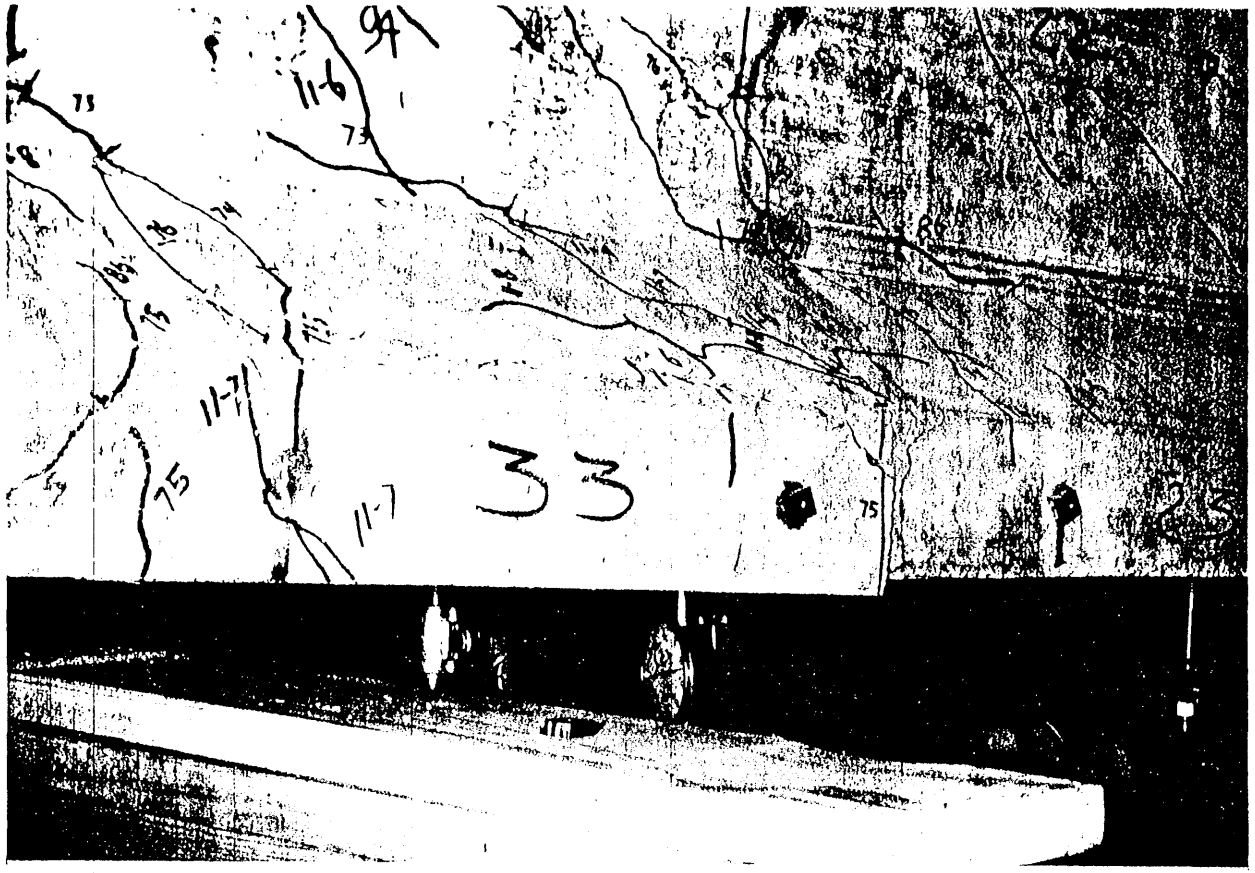

FIG. 4.20 PHOTO OF LOWER PART OF EAST SPLICE AFTER LAP SPLICE FAILURE, MODEL 1

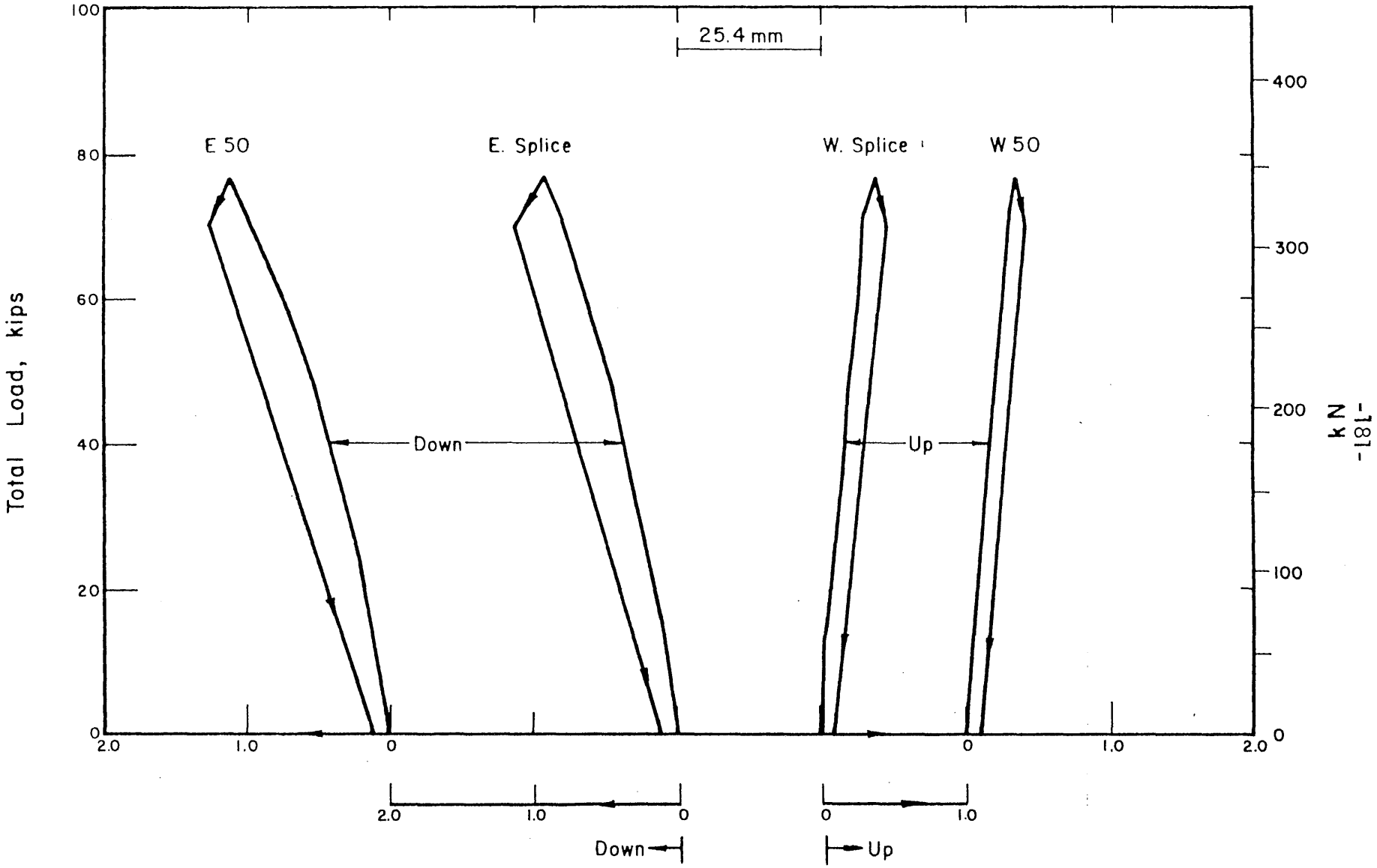


FIG. 4.21 LOAD-DEFLECTION CURVES FOR TEST 11, MODEL 1

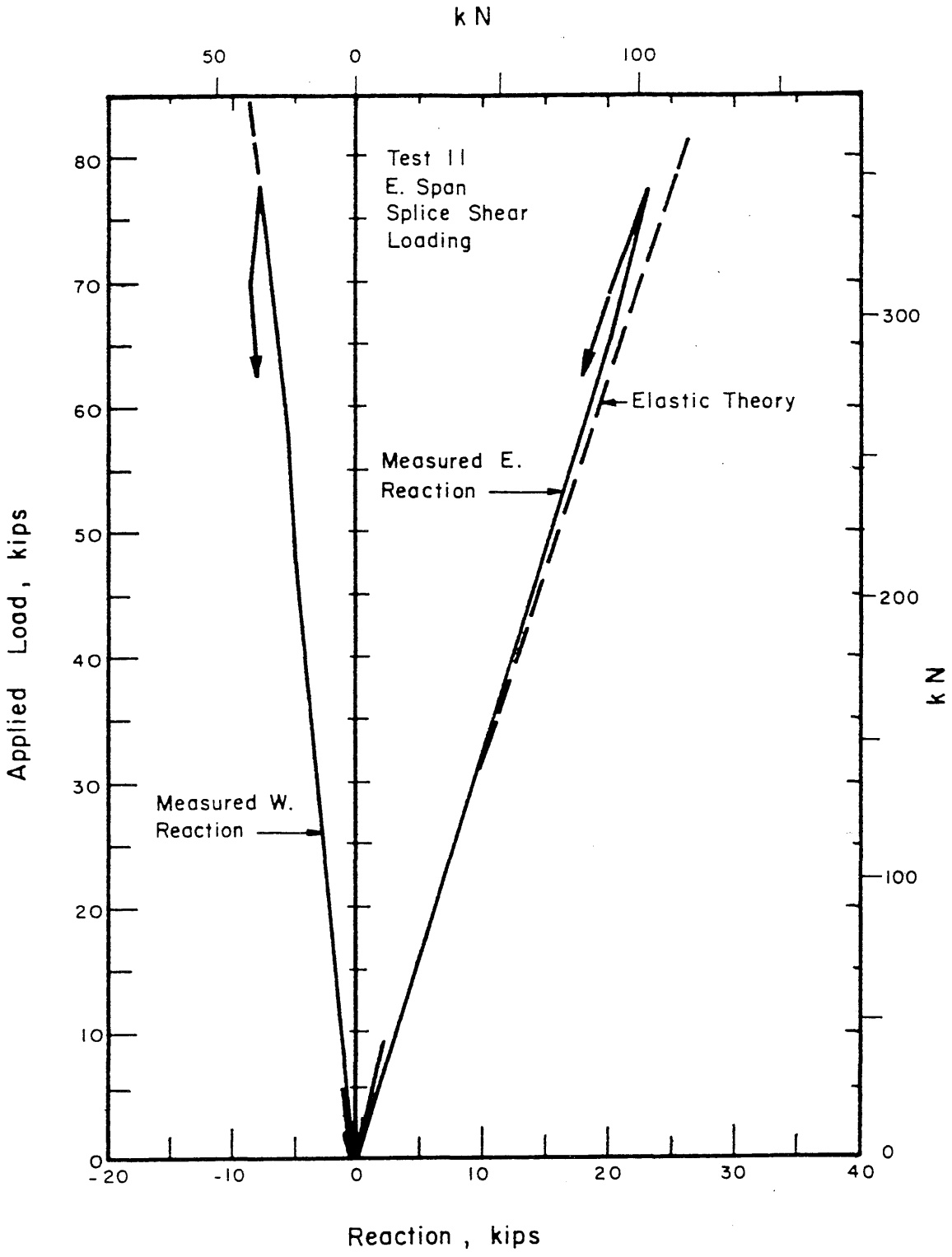


FIG. 4.22 LOAD-END REACTION CURVES FOR TEST 11, MODEL 1

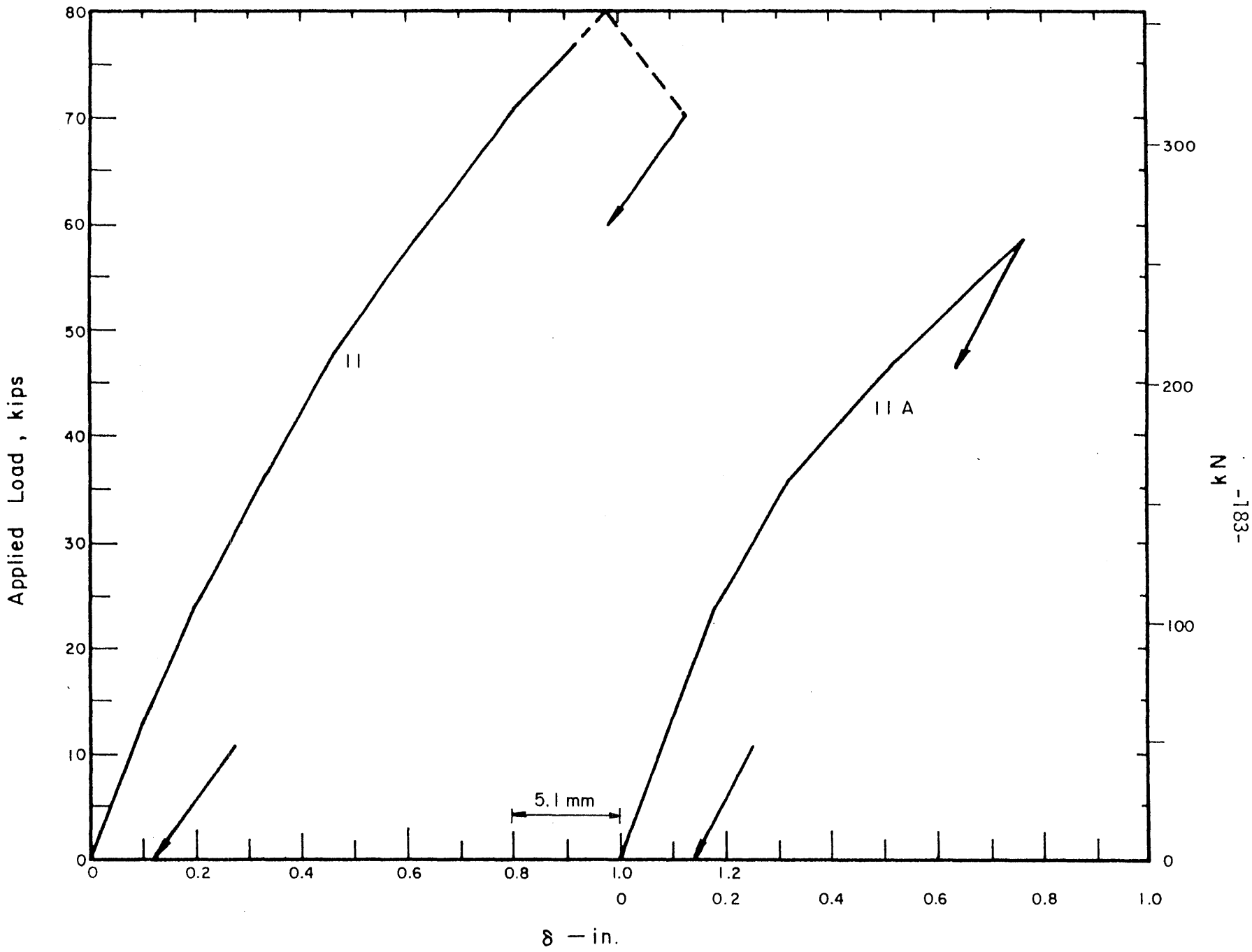


FIG. 4.23 LOAD-DEFLECTION CURVES FOR EAST SPLICE, TESTS 11 AND 11A, MODEL 1

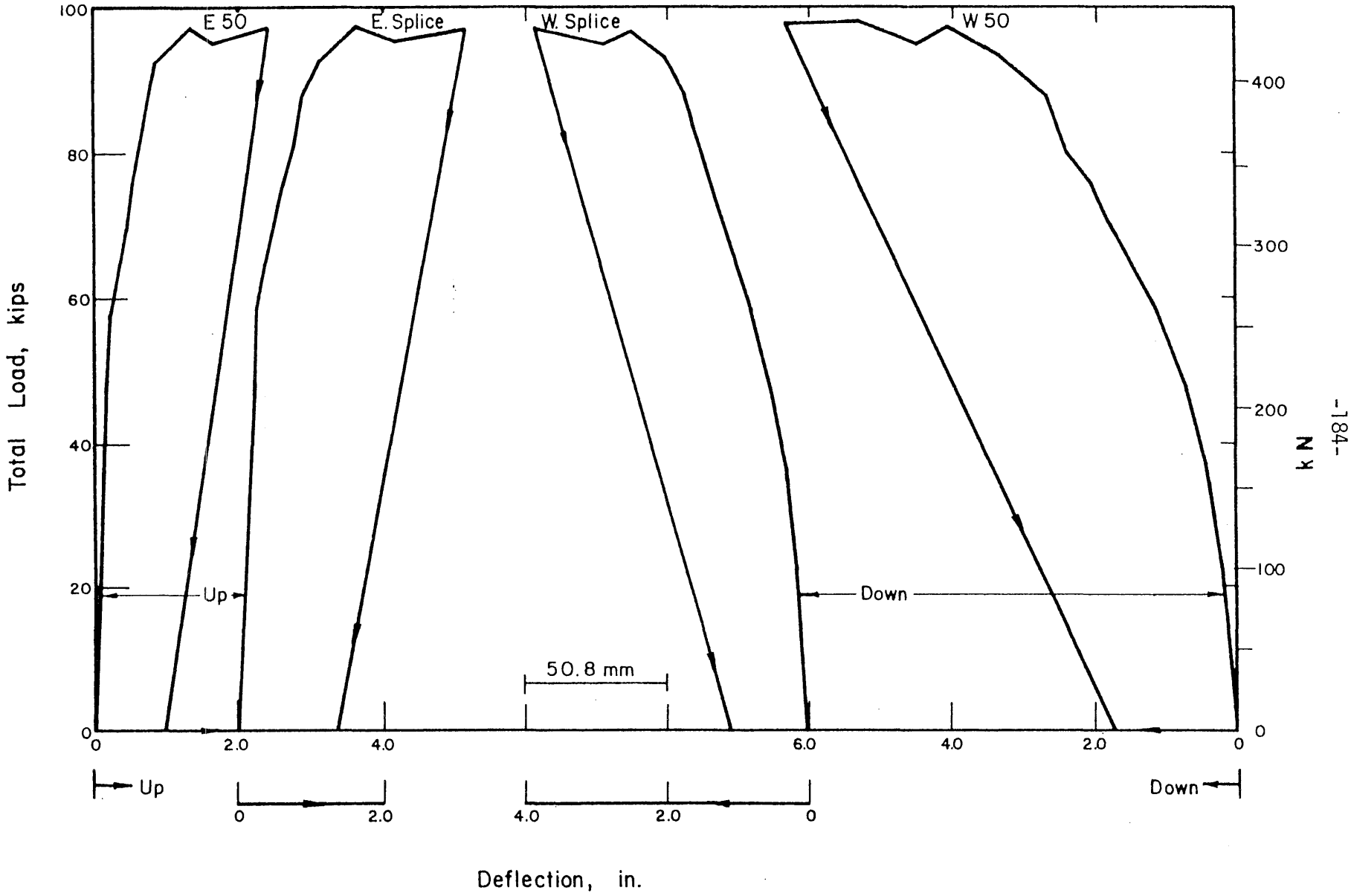


FIG. 4.24 LOAD-DEFLECTION CURVES FOR TEST 12, MODEL 1

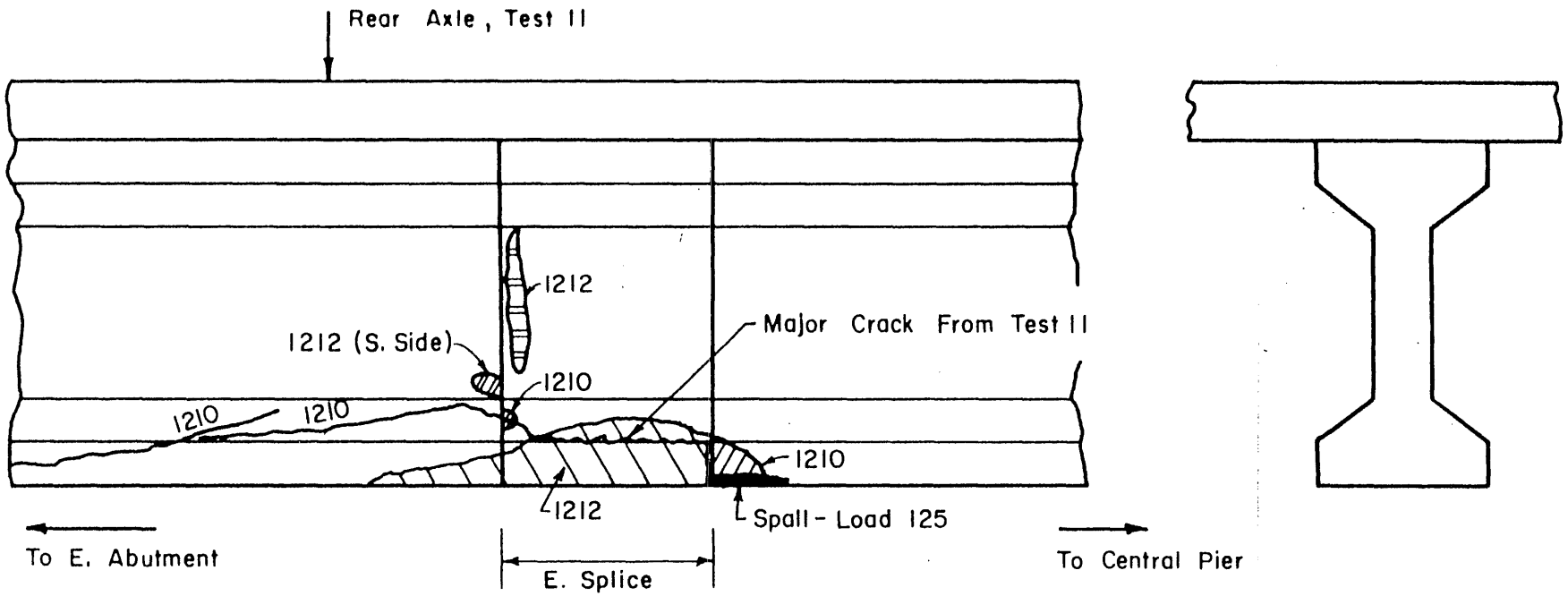


FIG. 4.25 SKETCH OF DAMAGE IN EAST SPLICE DUE TO TESTS 11 AND 12

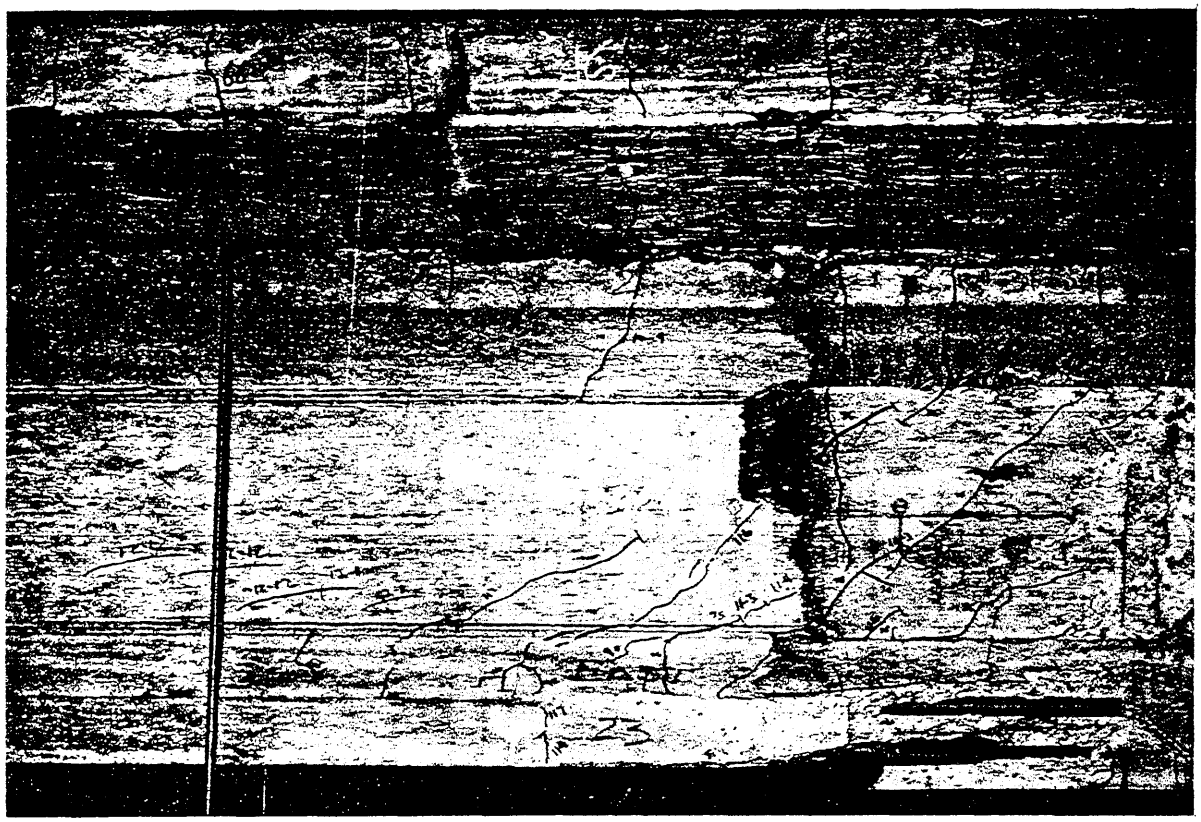

FIG. 4.26 PHOTOGRAPH OF EAST SPLICE AND ADJACENT PIER MODULE, MODEL 1

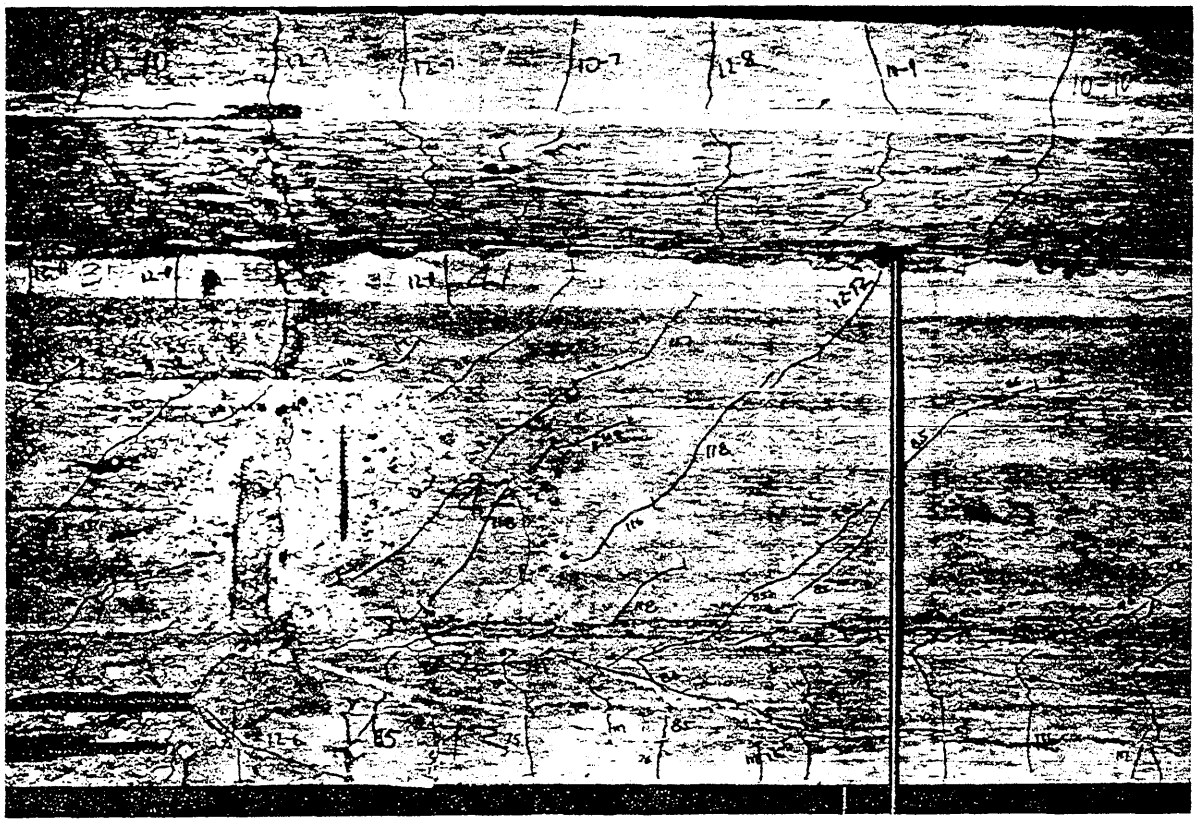

FIG. 4.27 PHOTO OF EAST SPLICE AND ADJACENT END SEGMENT, MODEL 1

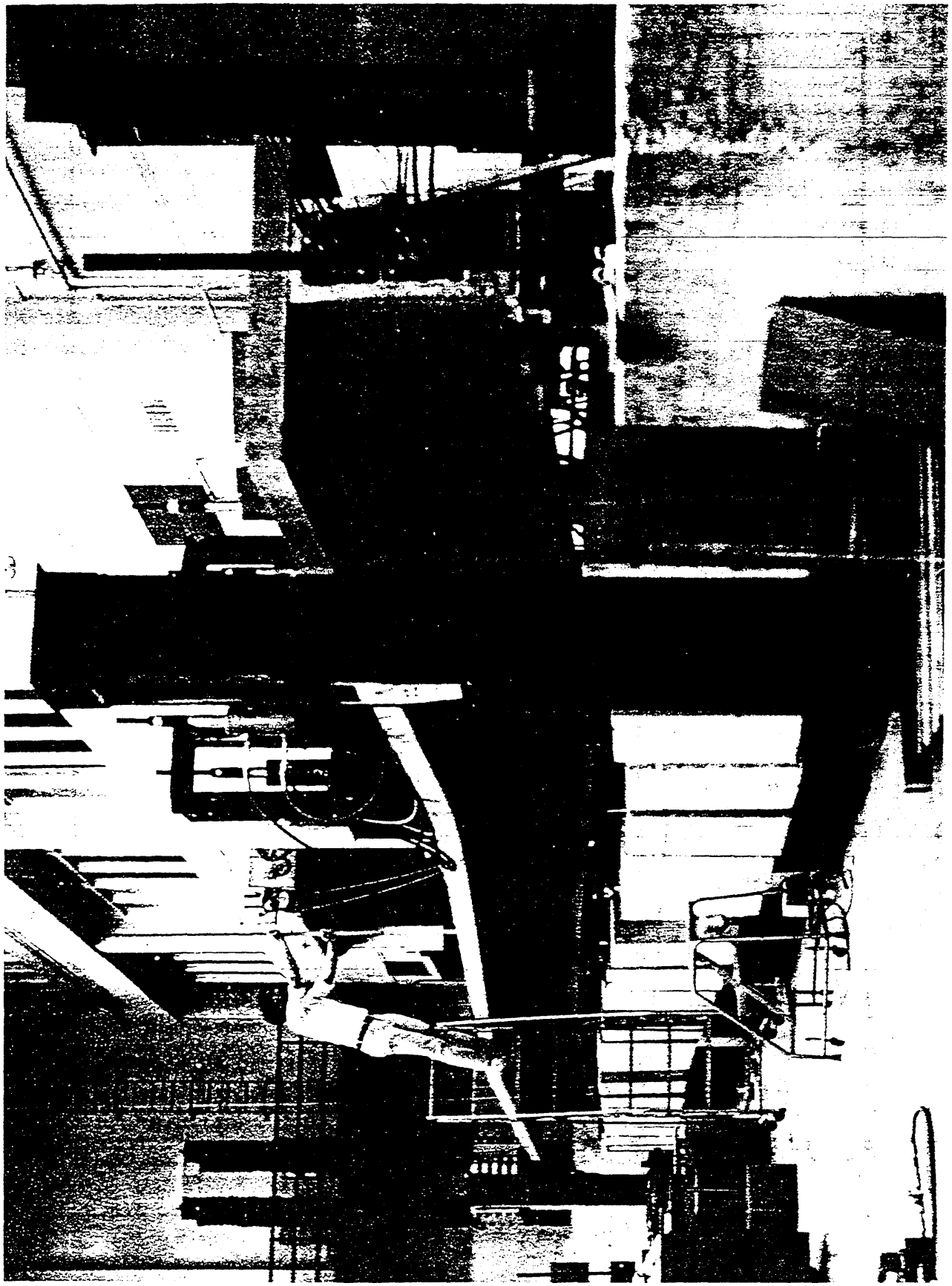

FIG. 4.28 OVERALL PHOTO OF MODEL 1 NEAR END OF TESTING

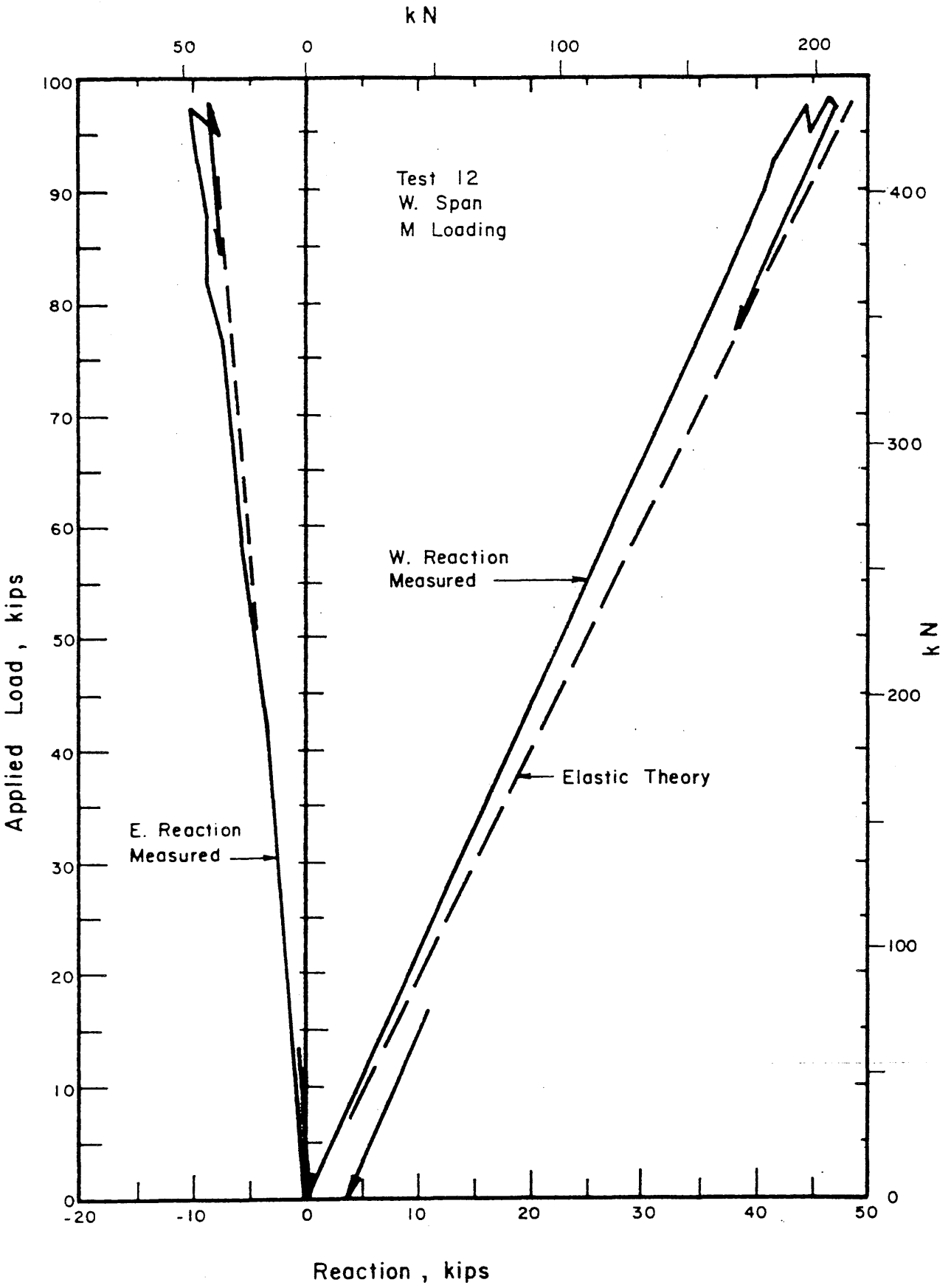


FIG. 4.29 LOAD-END REACTION CURVES FOR TEST 12, MODEL 1

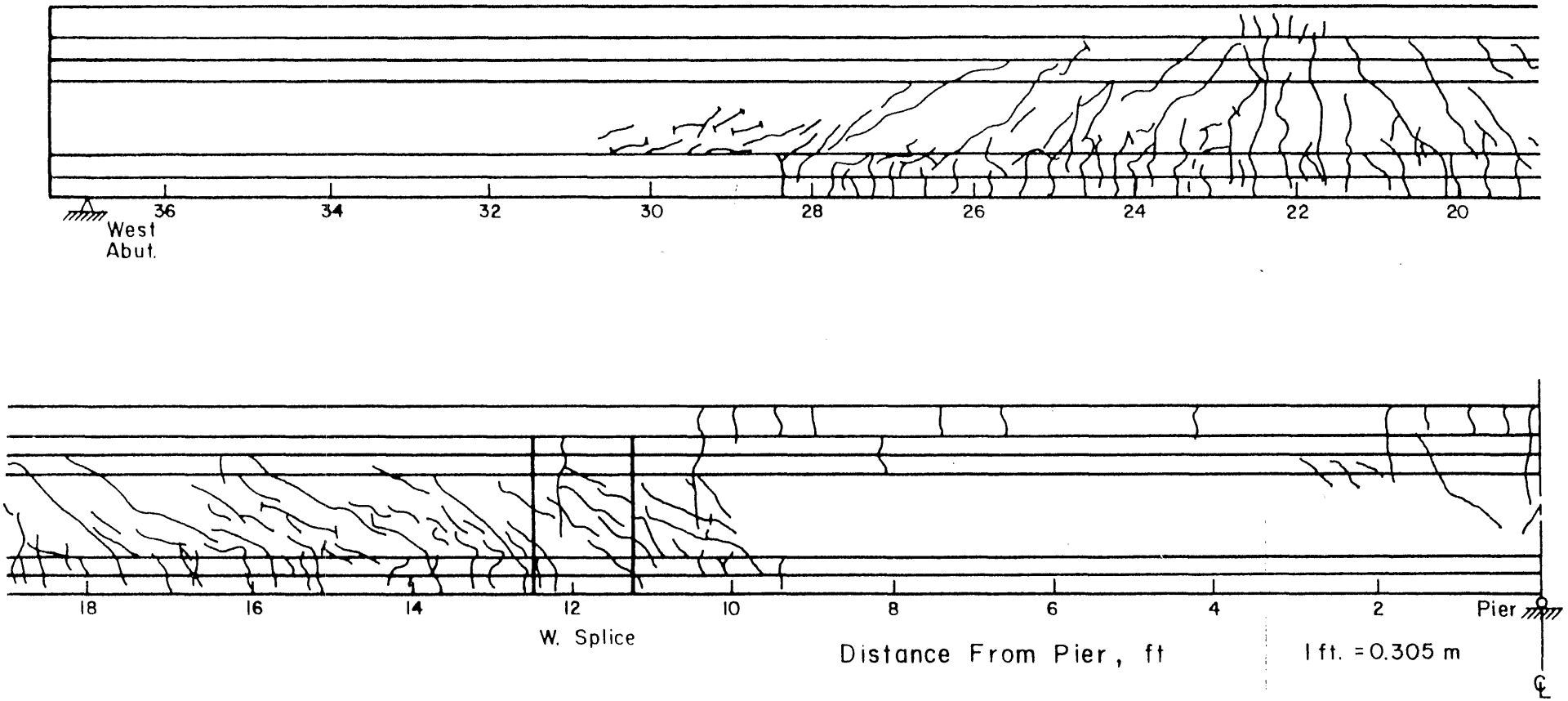


FIG. 4.30 CRACKS IN THE WEST SPAN AT THE END OF TESTING, MODEL 1

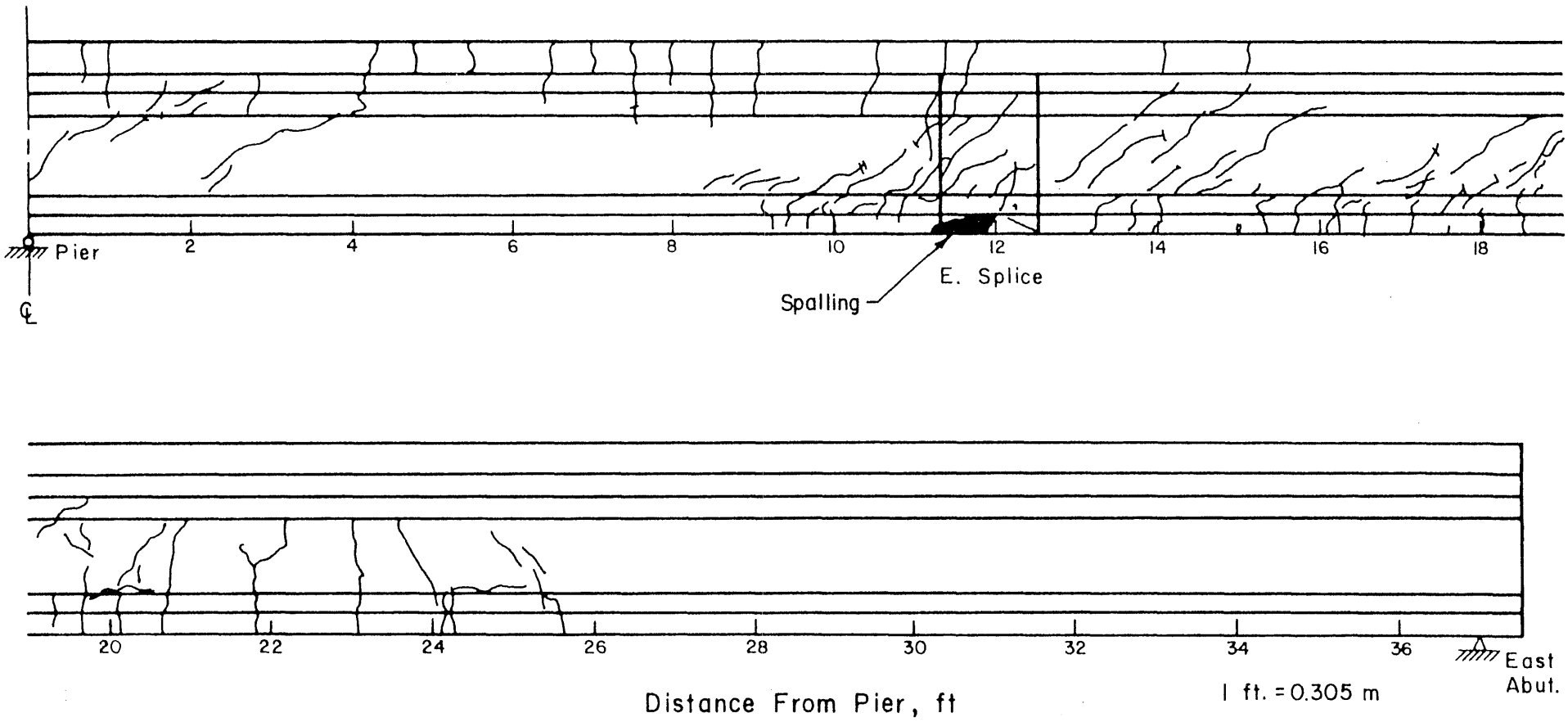


FIG. 4.31 CRACKS IN THE EAST SPAN AT THE END OF TESTING, MODEL 1

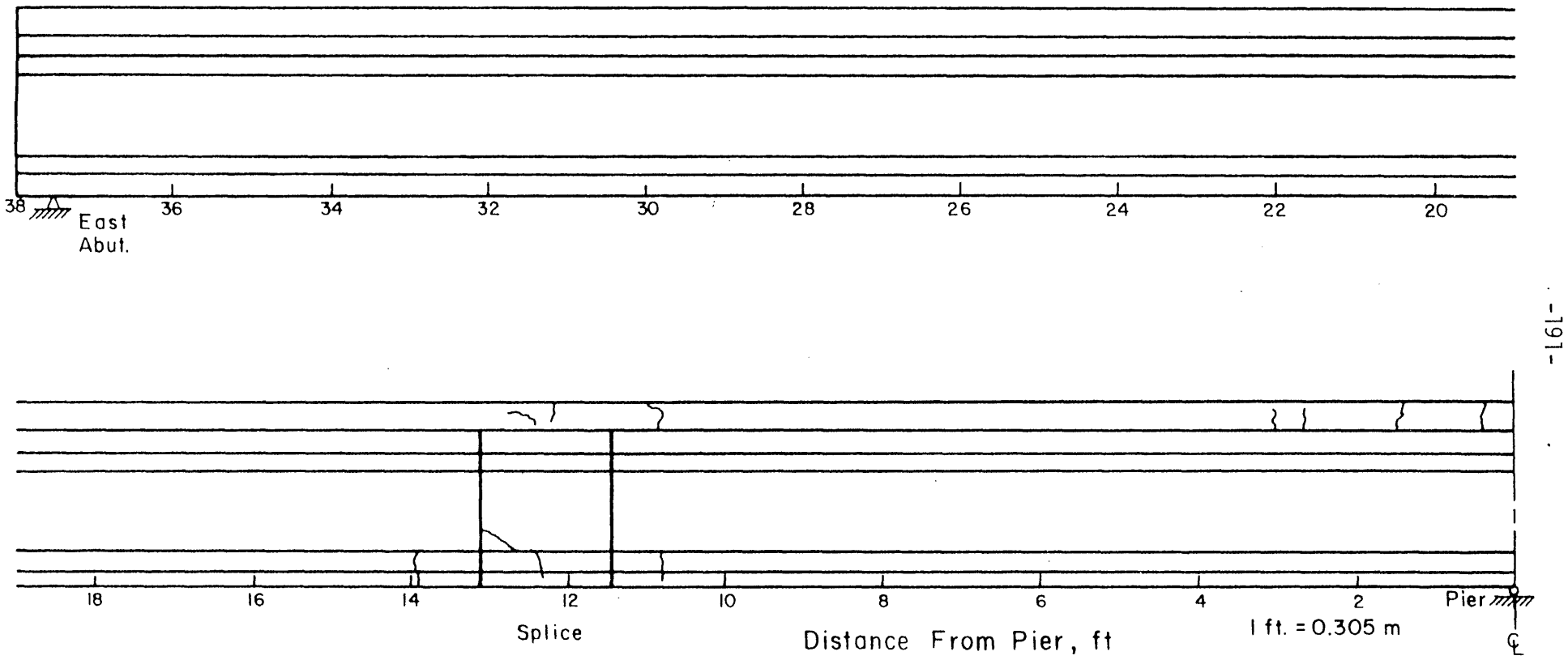




FIG. 5.1 CRACKS IN EAST SPAN OF MODEL 2 DUE TO DEAD LOAD

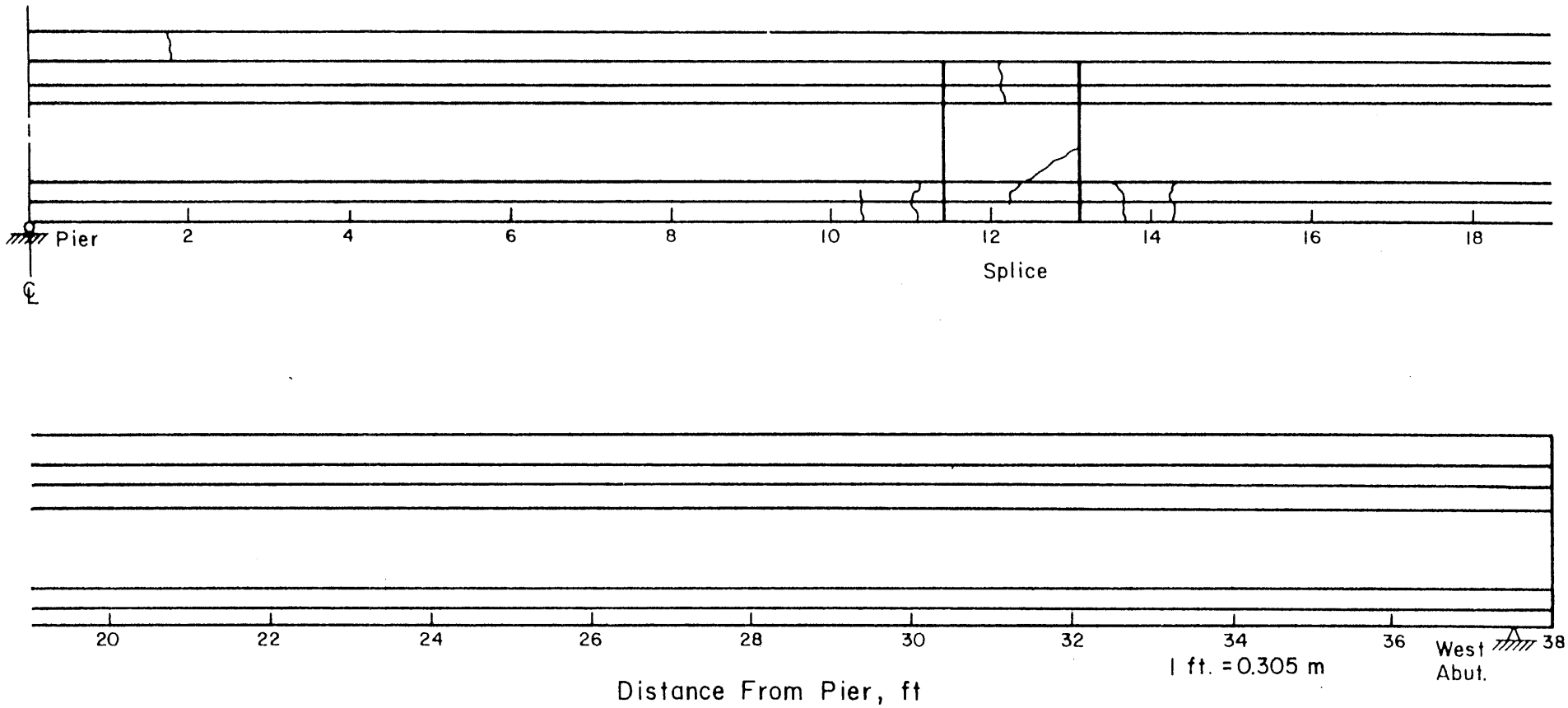


FIG. 5.2 CRACKS IN WEST SPAN OF MODEL 2 DUE TO DEAD LOAD

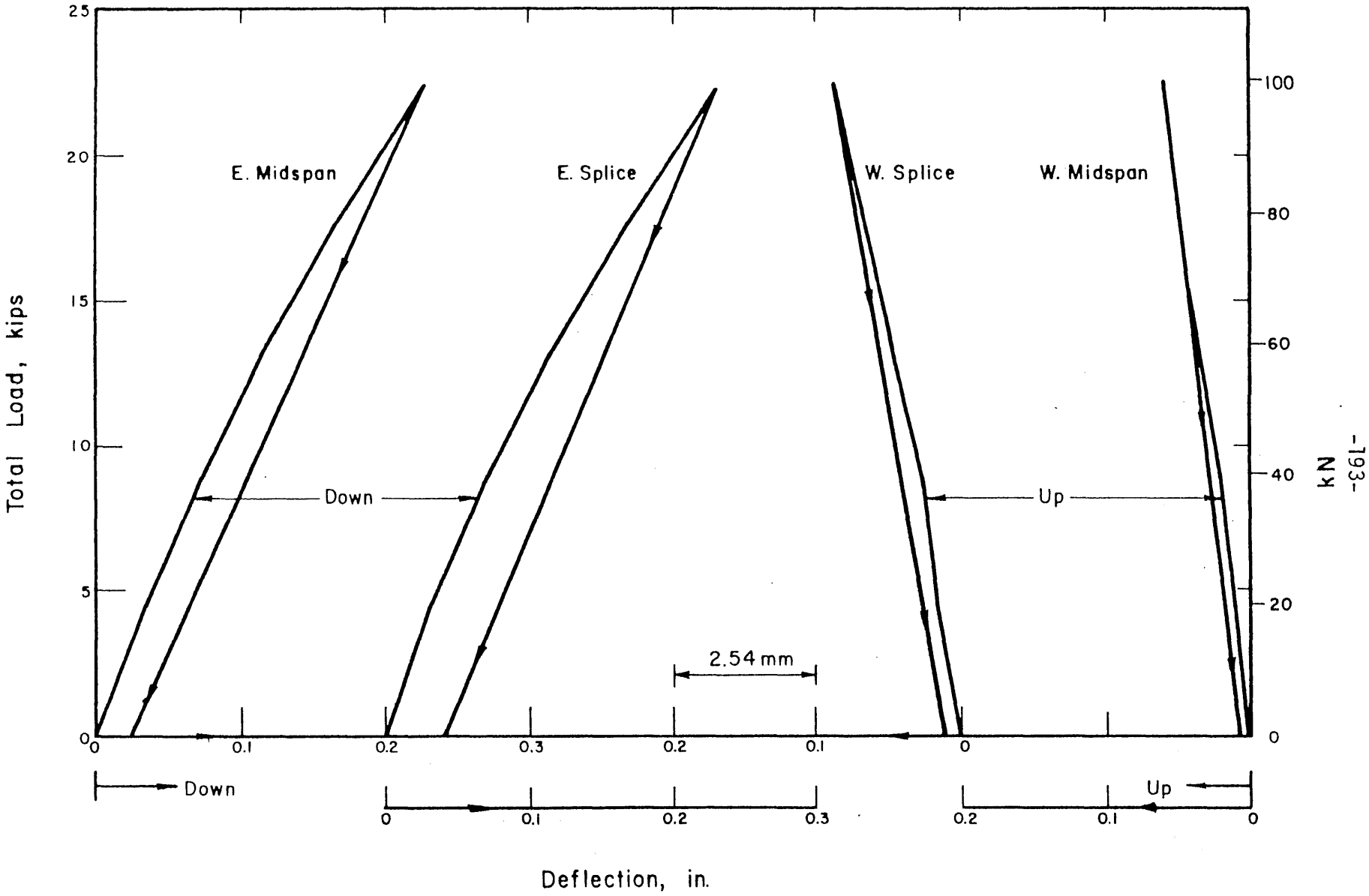


FIG. 5.3 LOAD-DEFLECTION CURVES FOR TEST 1, MODEL 2

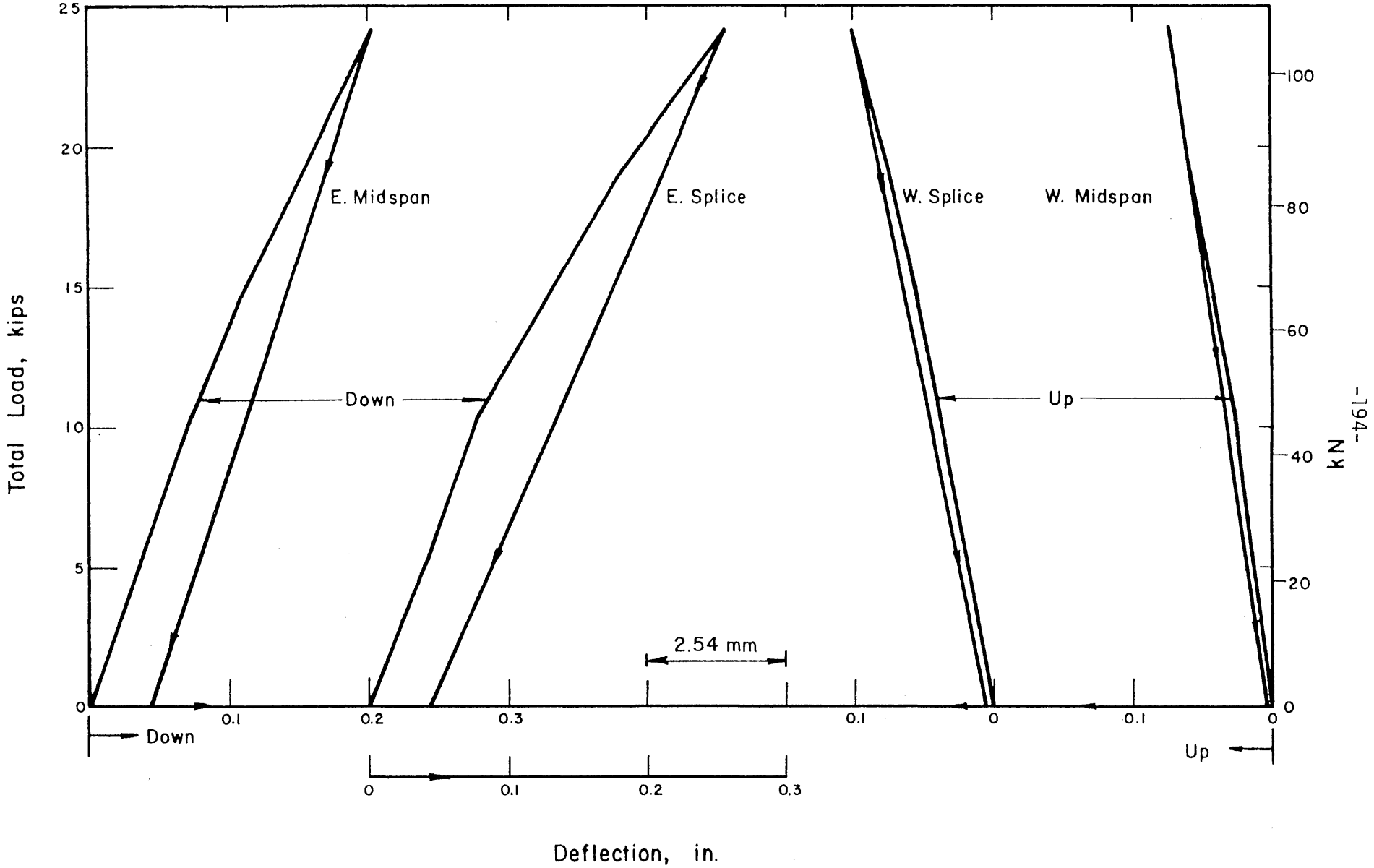


FIG. 5.4 LOAD-DEFLECTION CURVES FOR TEST 2, MODEL 2

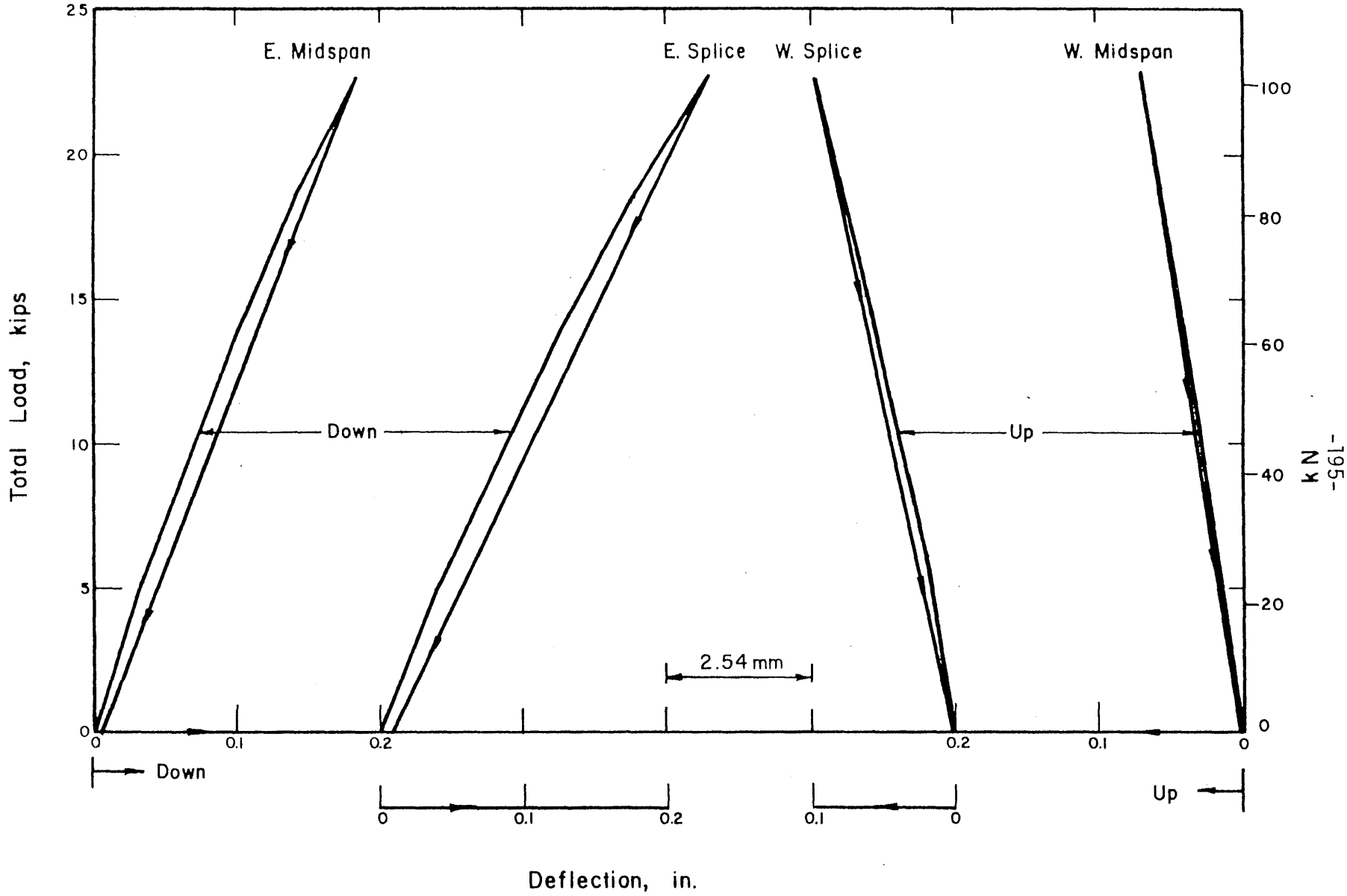


FIG. 5.5 LOAD-DEFLECTION CURVES FOR TEST 3, MODEL 2

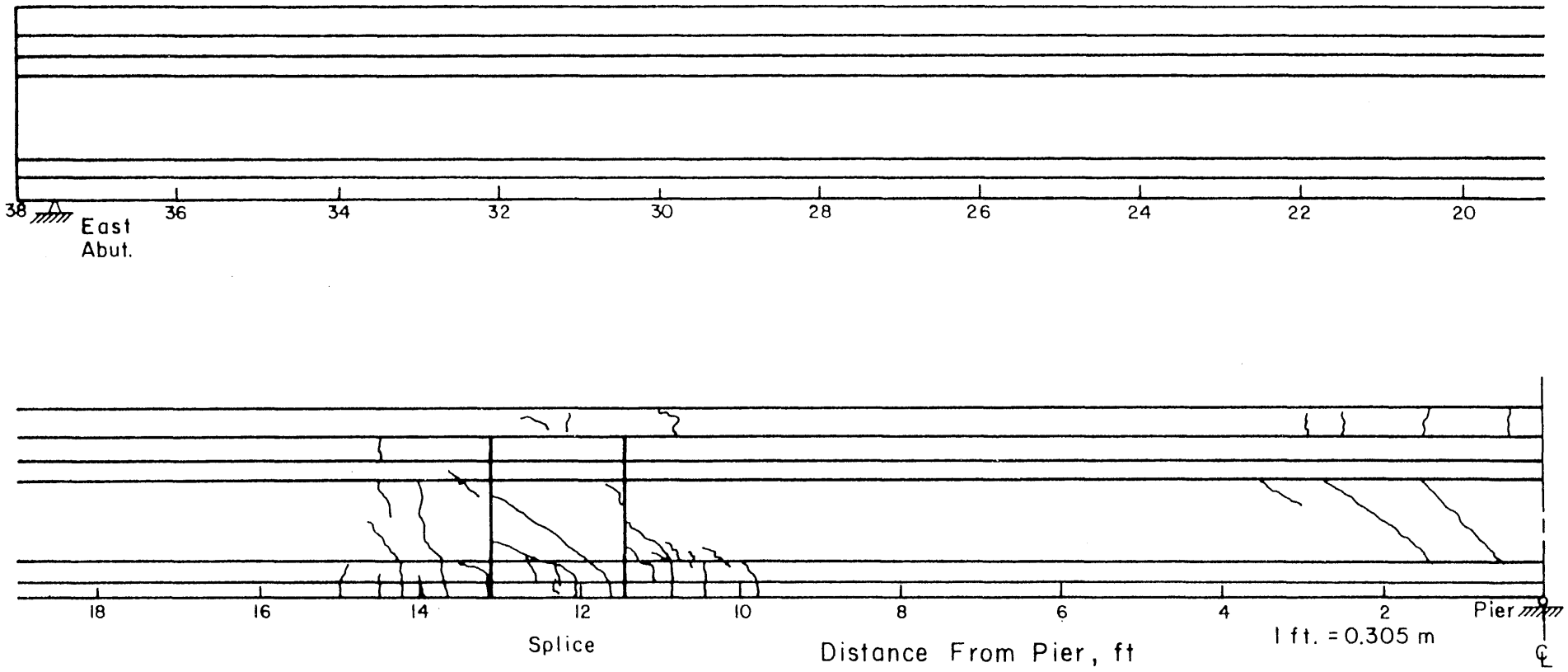


FIG. 5.6 CRACKS IN EAST SPAN AFTER SERVICE LOAD TESTS, MODEL 2

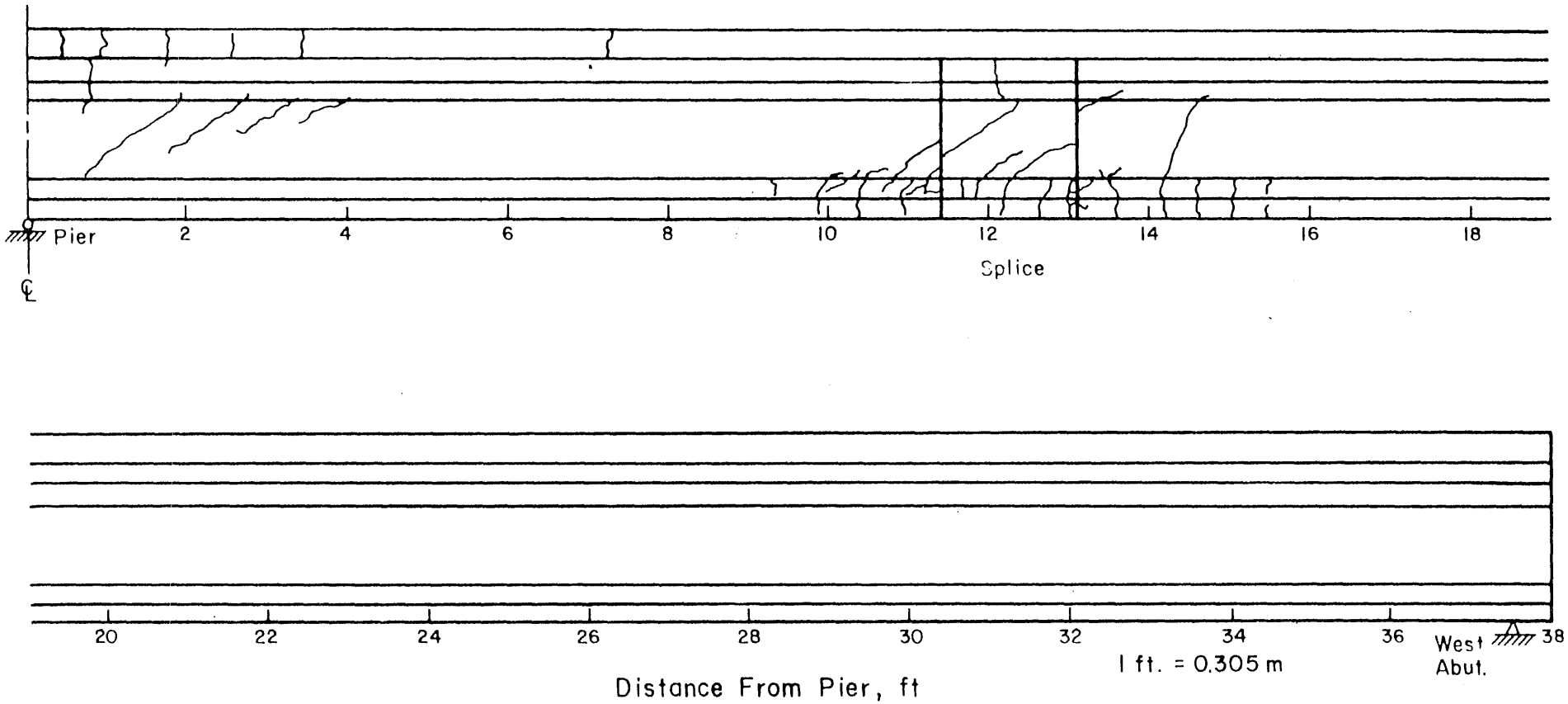


FIG. 5.7 CRACKS IN WEST SPAN AFTER SERVICE LOAD TESTS, MODEL 2

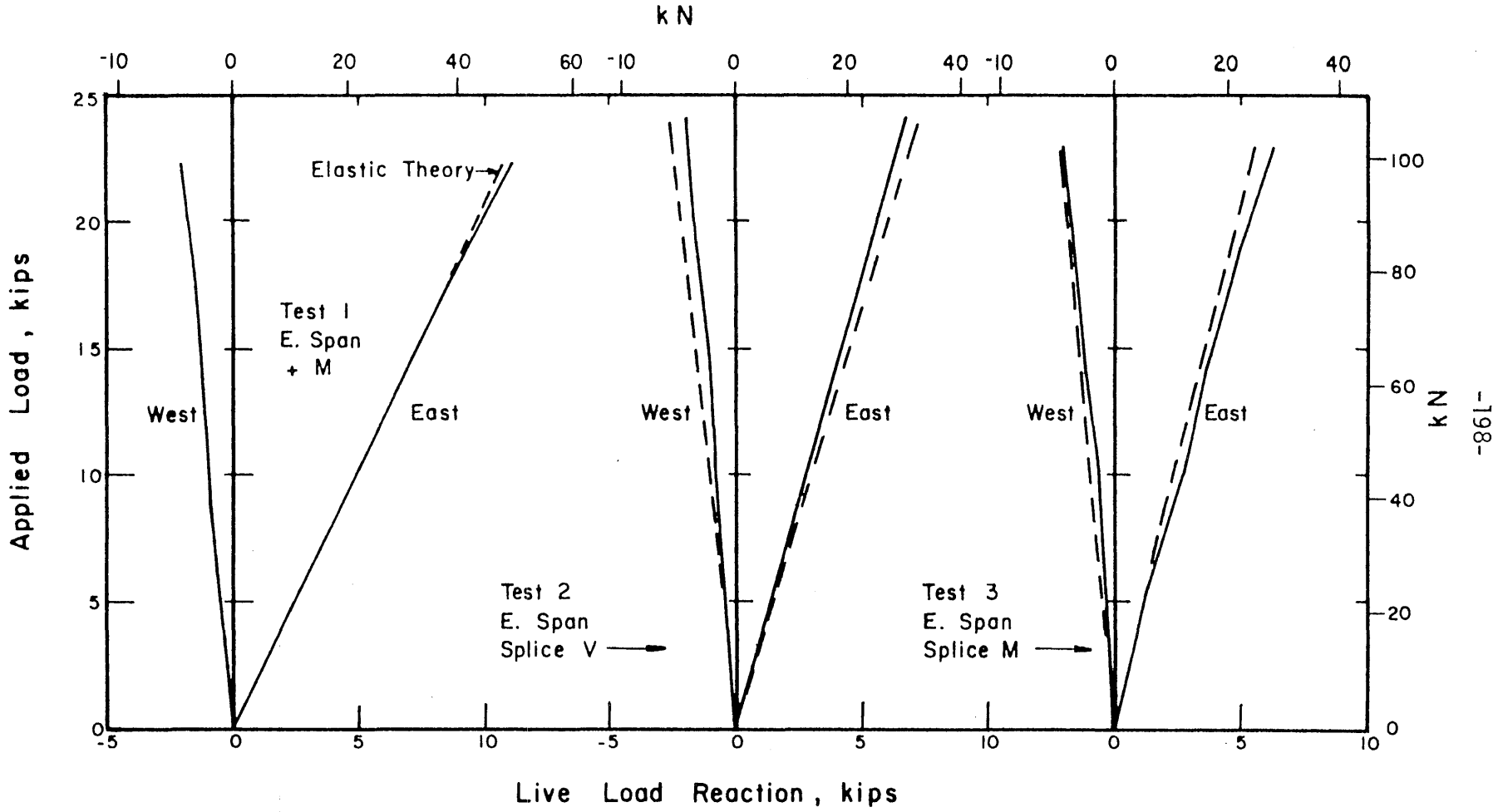


FIG. 5.8 LOAD-END REACTION CURVES FOR TESTS 1, 2 AND 3, MODEL 2

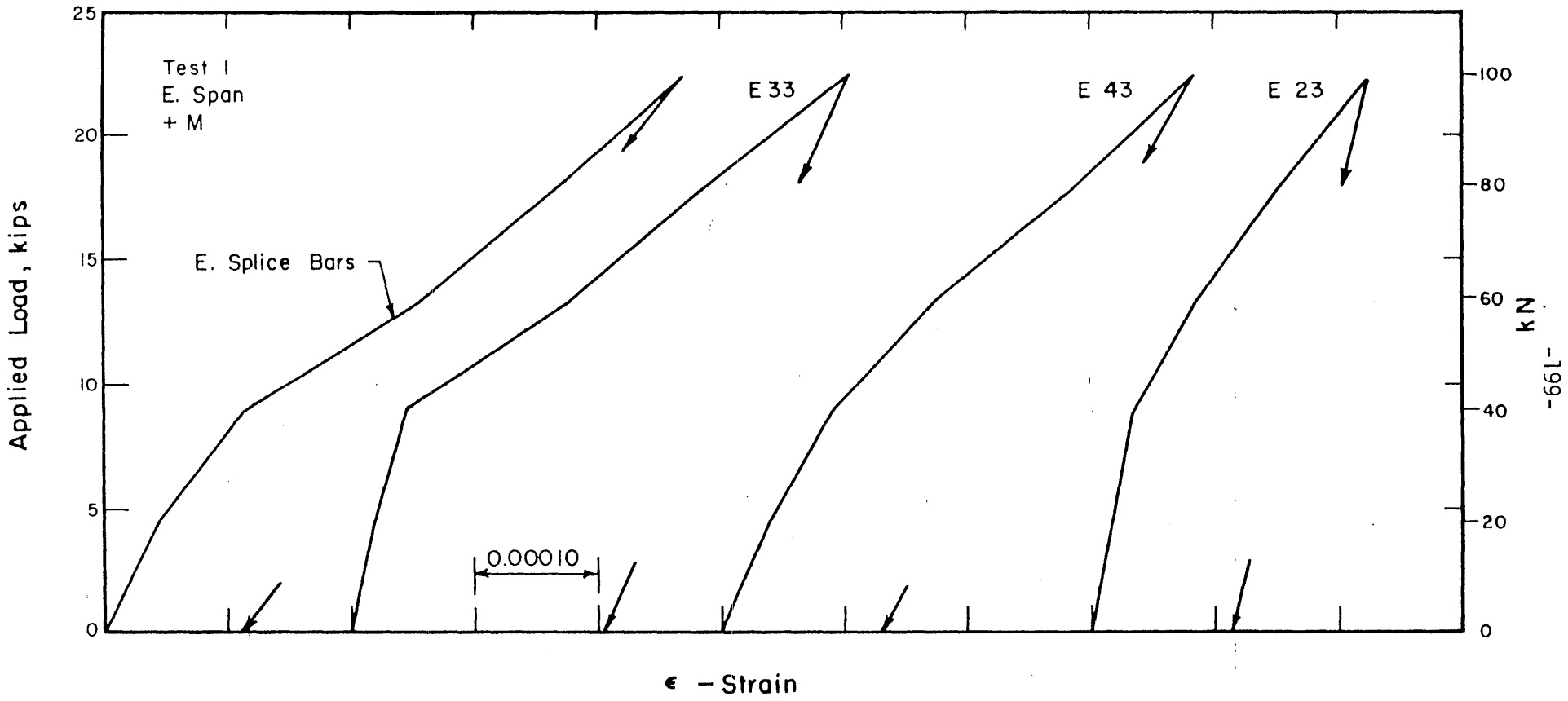


FIG. 5.9 LOAD-STRAIN CURVES FOR TEST 1, MODEL 2

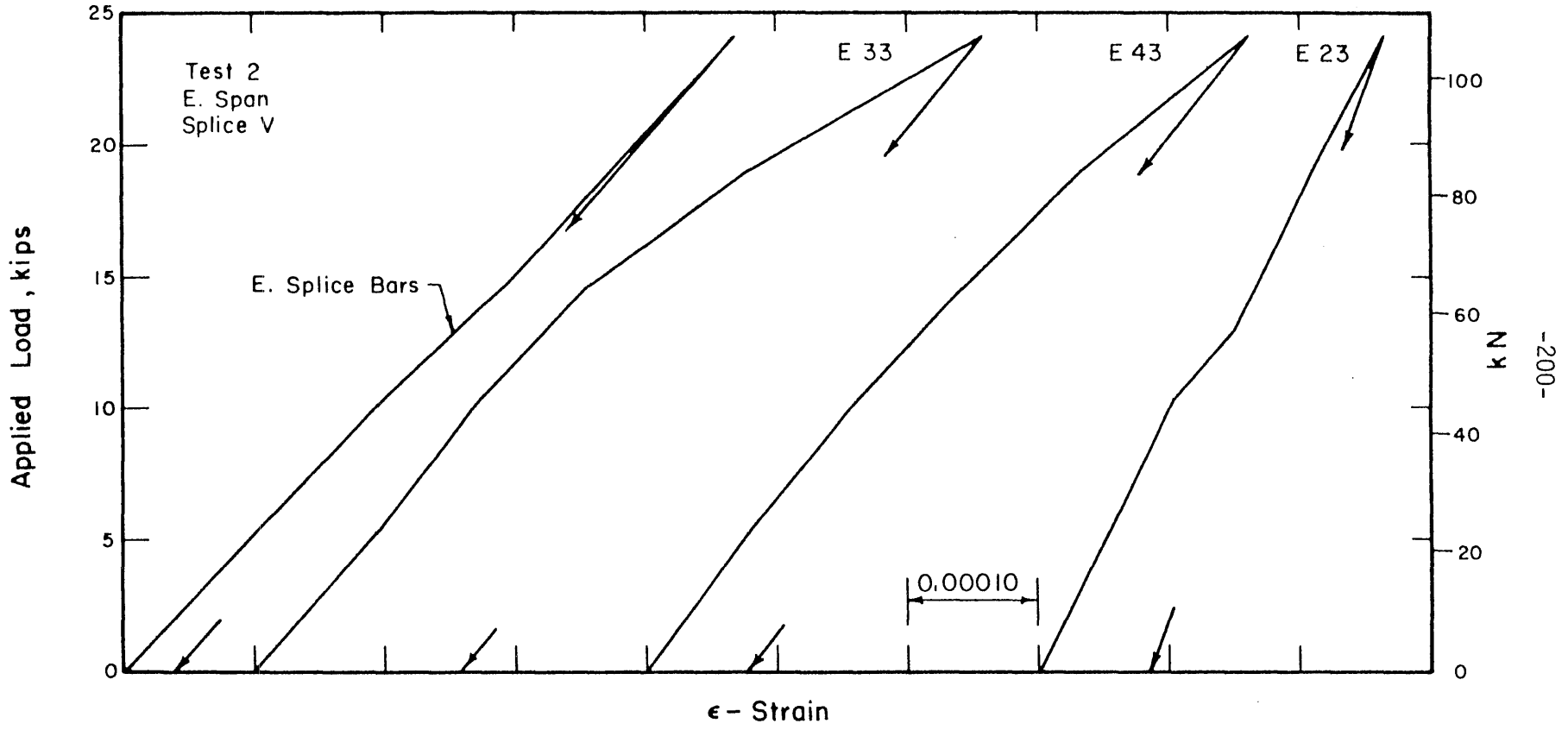


FIG. 5.10 LOAD-STRAIN CURVES FOR TEST 2, MODEL 2

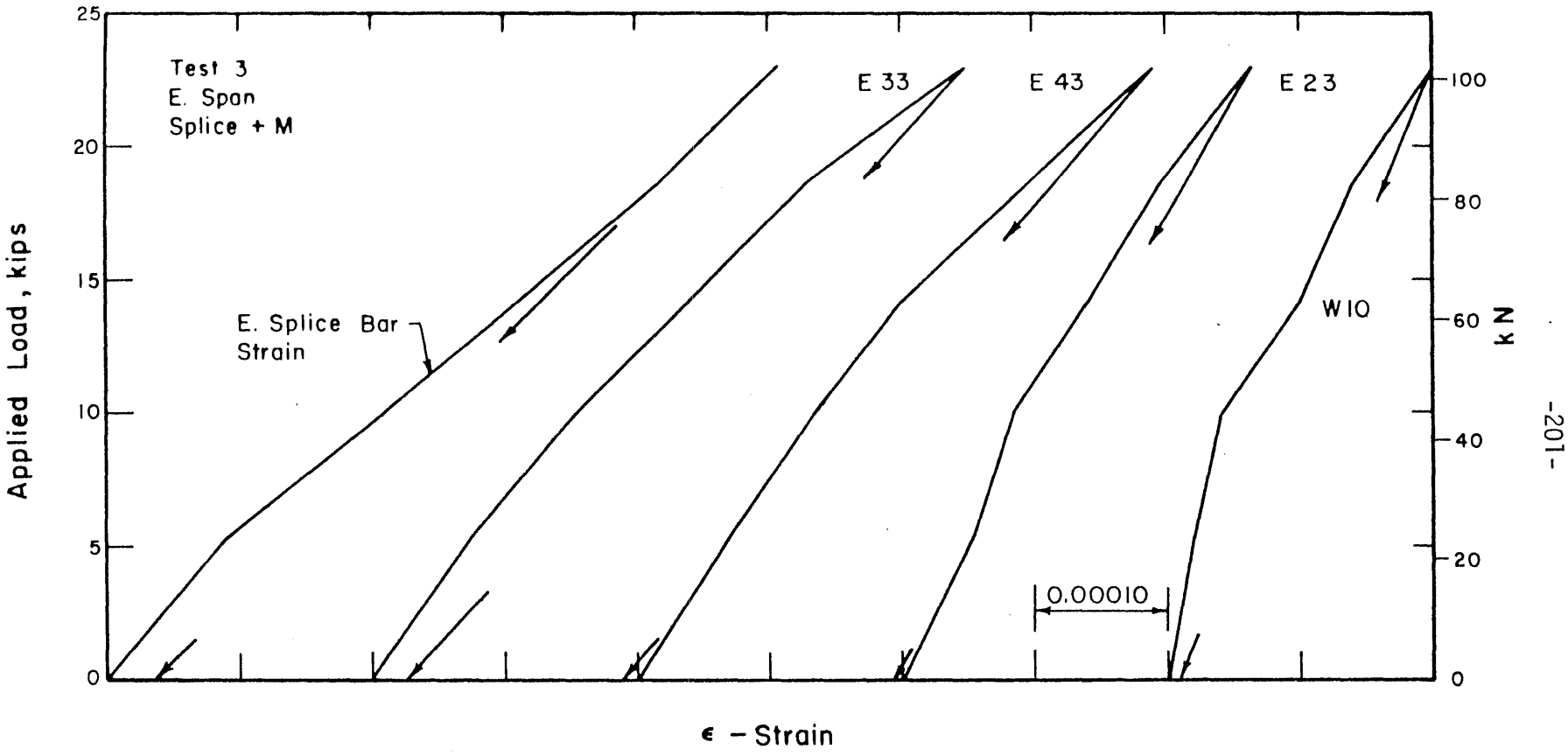


FIG. 5.11 LOAD-STRAIN CURVES FOR TEST 3, MODEL 2

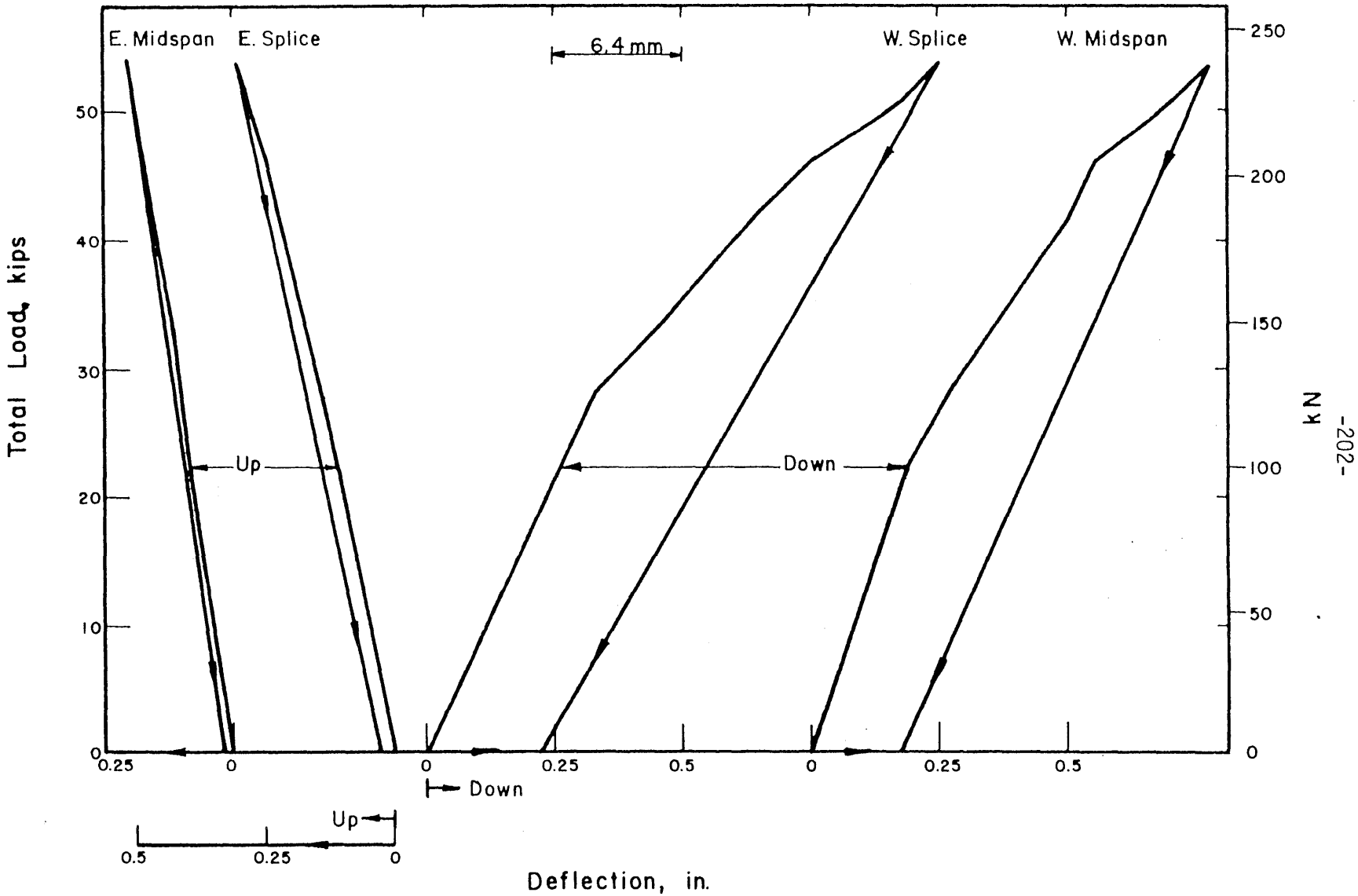


FIG. 5.12 LOAD-DEFLECTION CURVES FOR TEST 7, MODEL 2

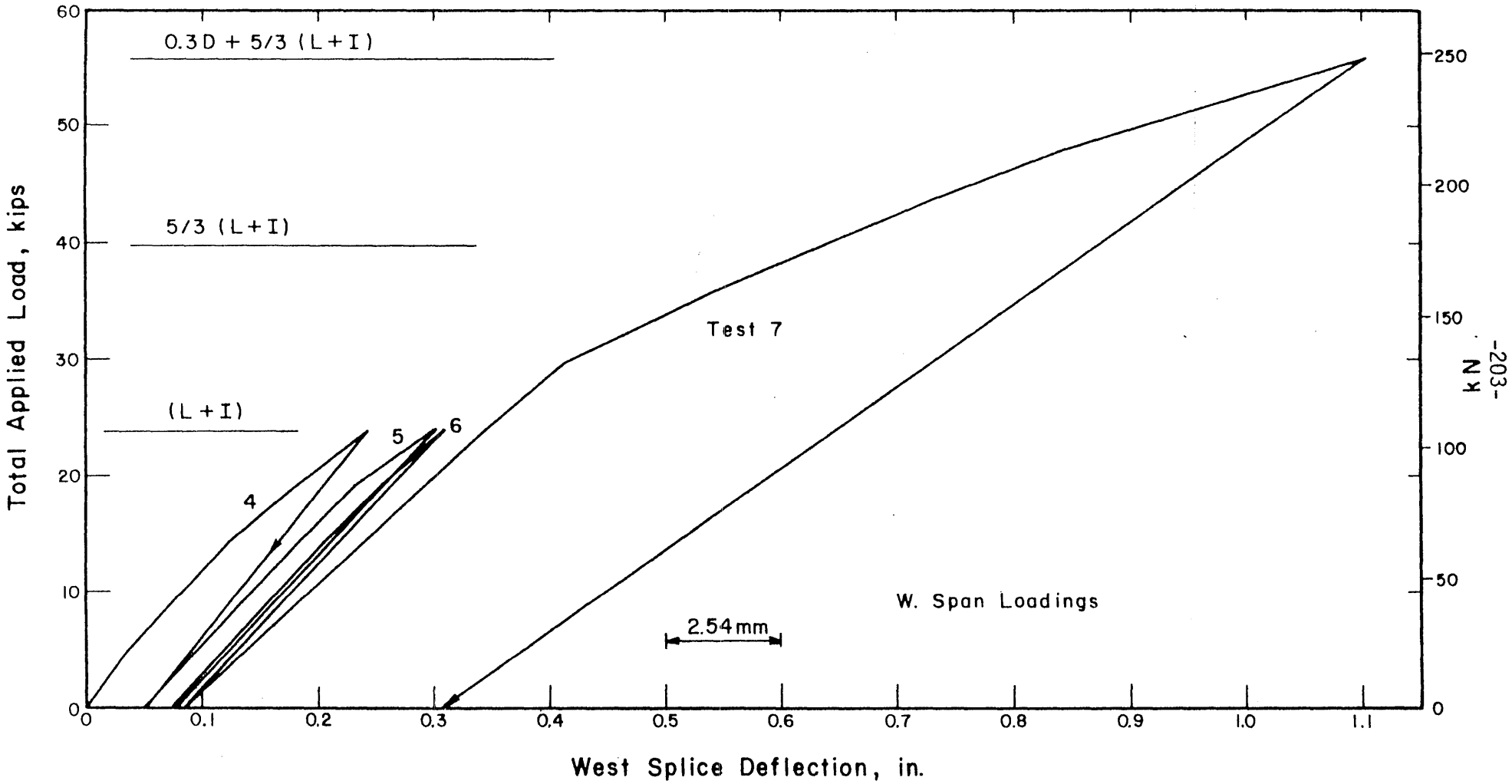


FIG. 5.13 LOAD-CUMULATIVE DEFLECTION CURVES AT WEST SPLICE OF MODEL 2, TESTS 4, 5, 6, AND 7

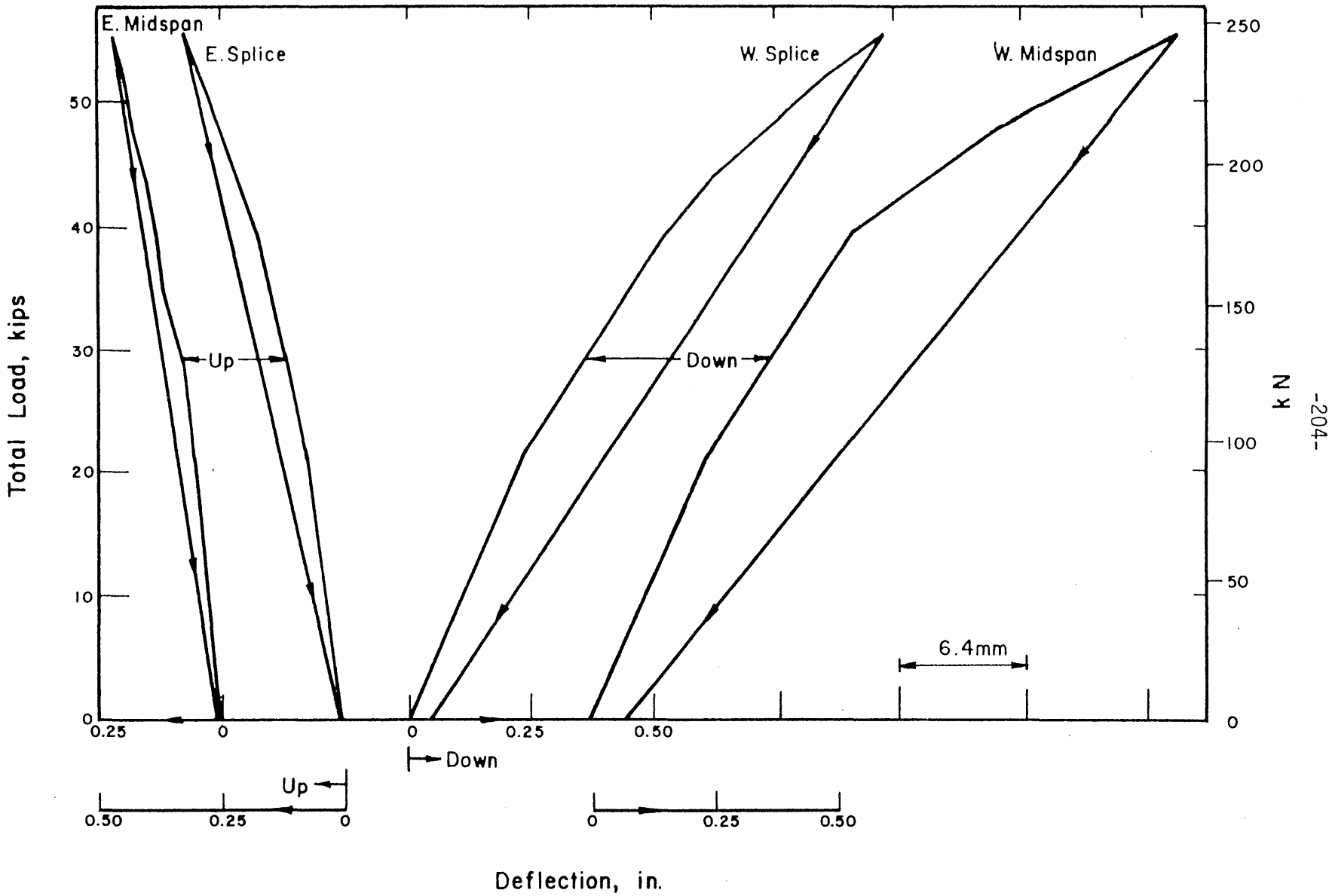


FIG. 5.14 LOAD-DEFLECTION CURVES FOR TEST 8, MODEL 2

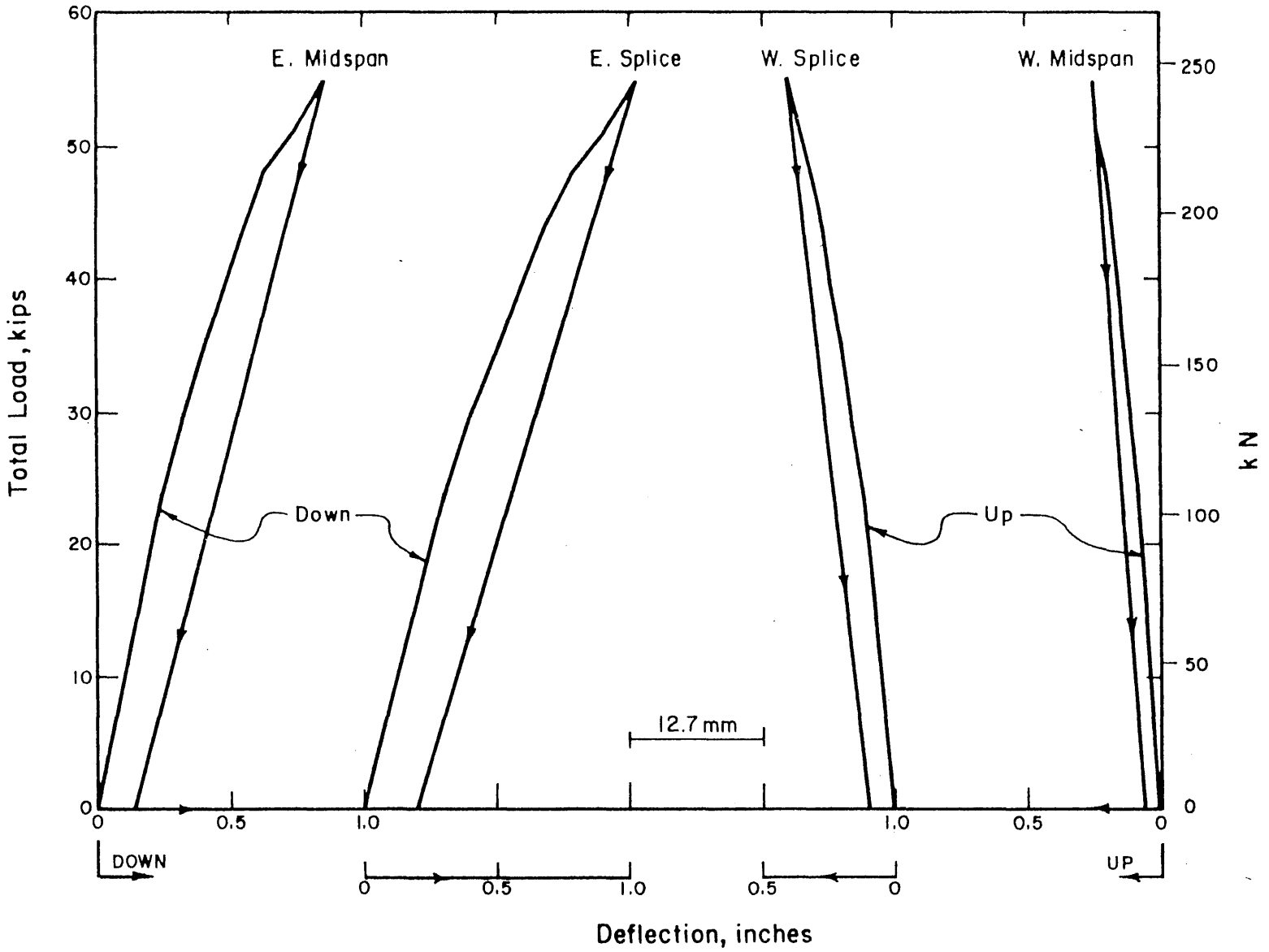


FIG. 5.15 LOAD-DEFLECTION CURVES FOR TEST 9, MODEL 2

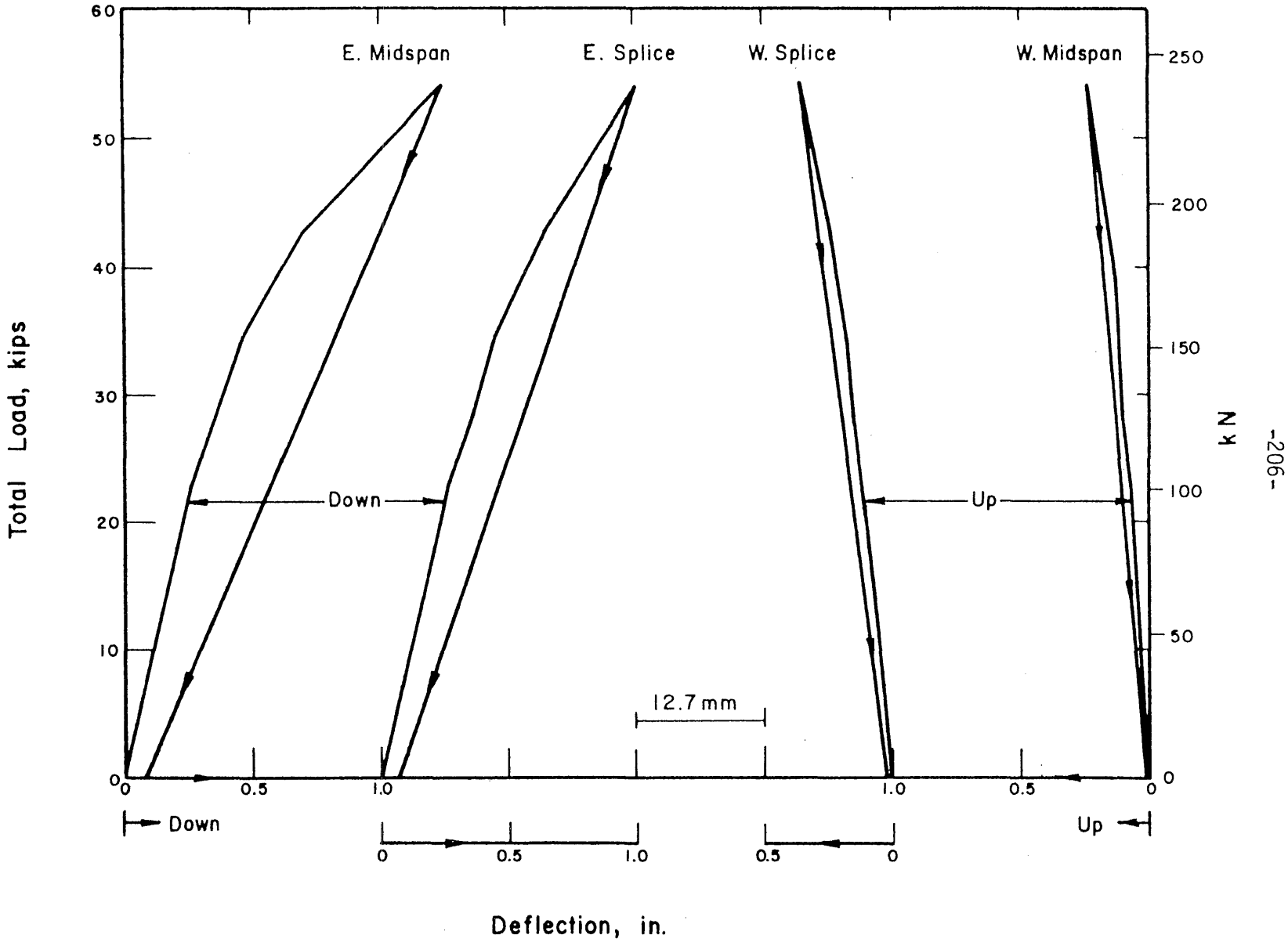


FIG. 5.16 LOAD-DEFLECTION CURVES FOR TEST 10, MODEL 2

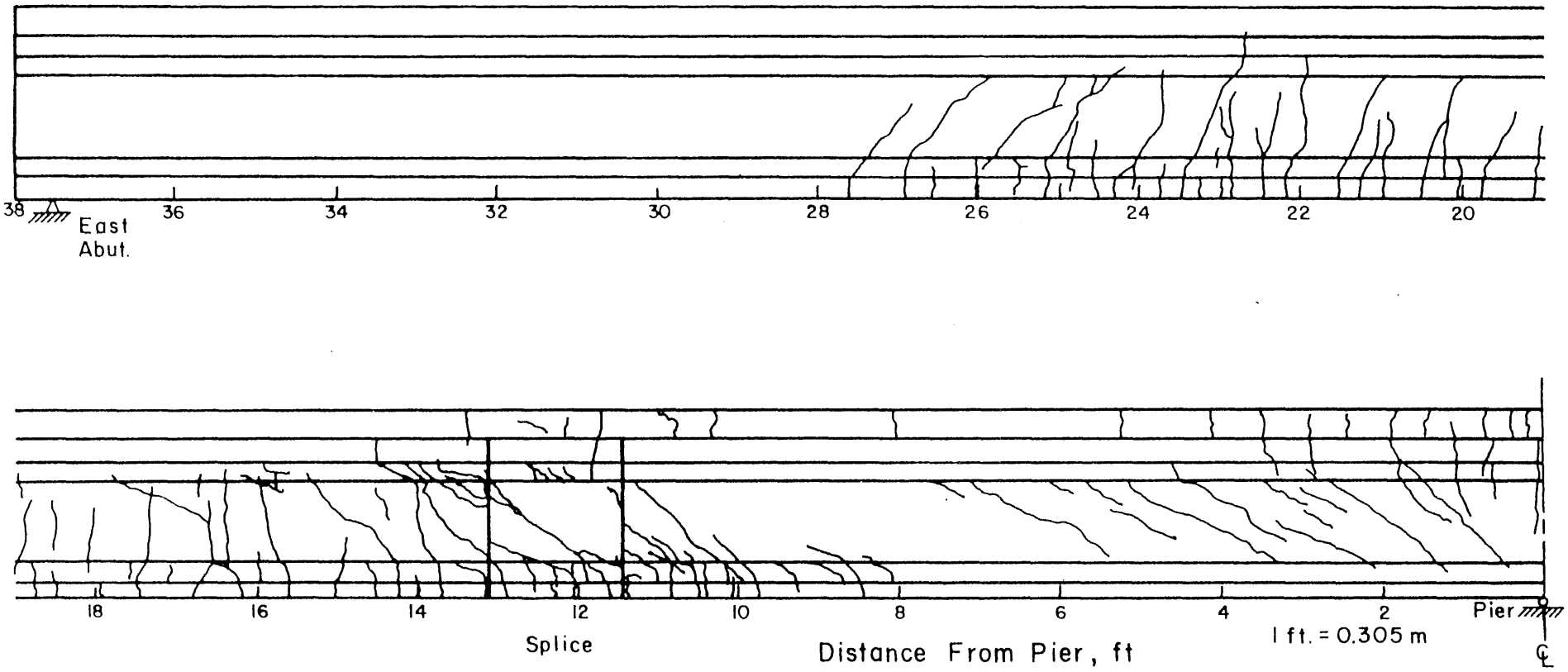


FIG. 5.17 CRACKS IN EAST SPAN AT END OF DESIGN ULTIMATE LOAD TESTS, MODEL 2

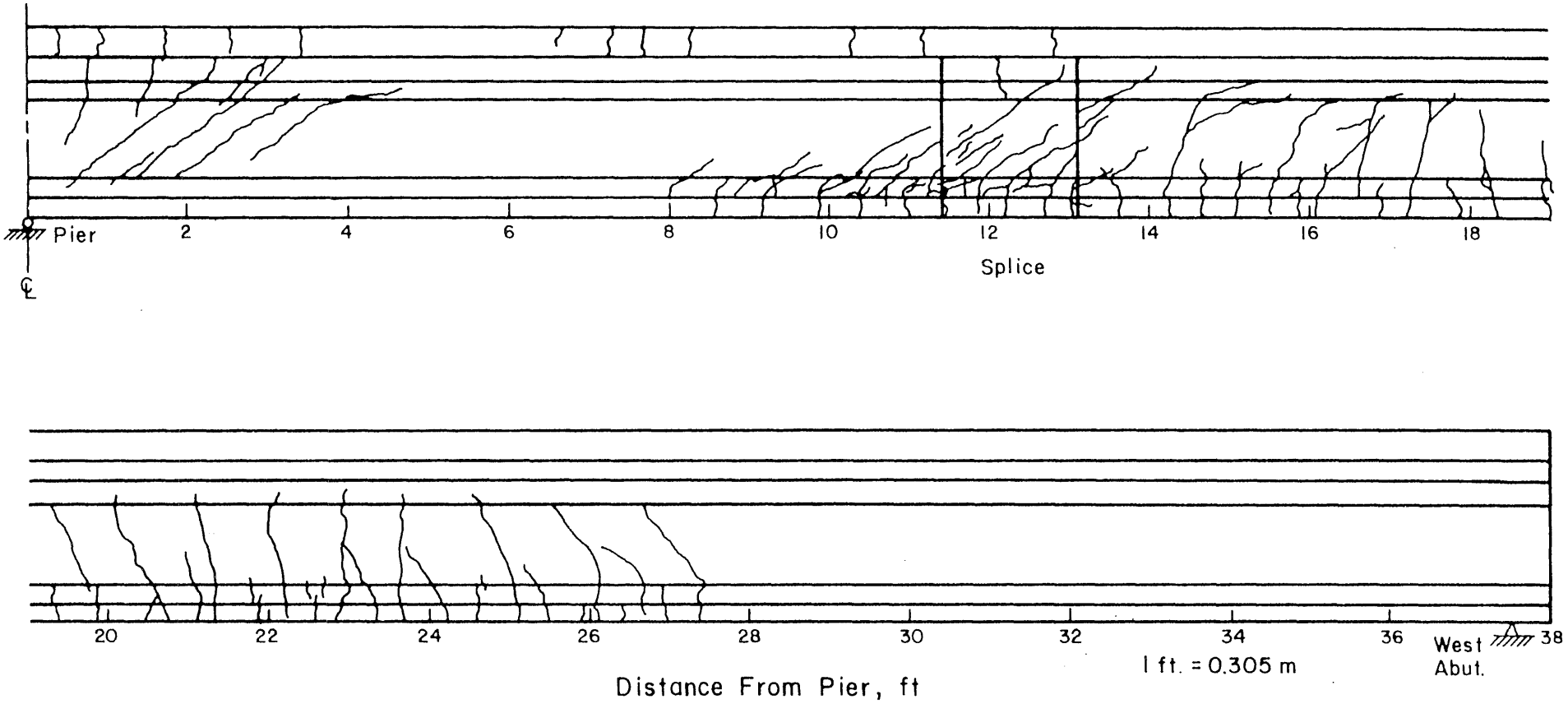


FIG. 5.18 CRACKS IN WEST SPAN AT END OF DESIGN ULTIMATE LOAD TESTS, MODEL 2

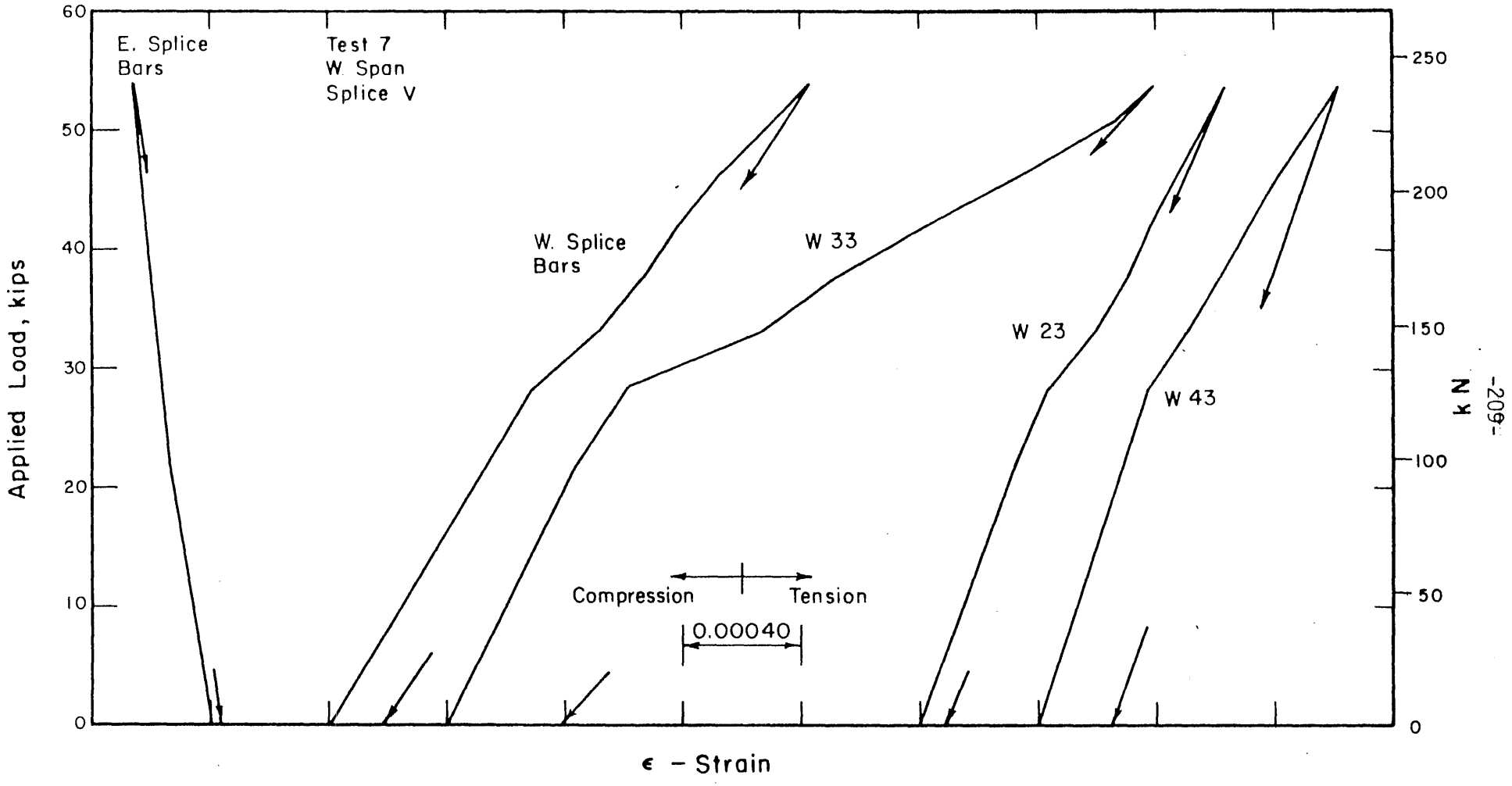


FIG. 5.19 LOAD-STRAIN CURVES IN AND NEAR SPLICES IN TEST 7, MODEL 2

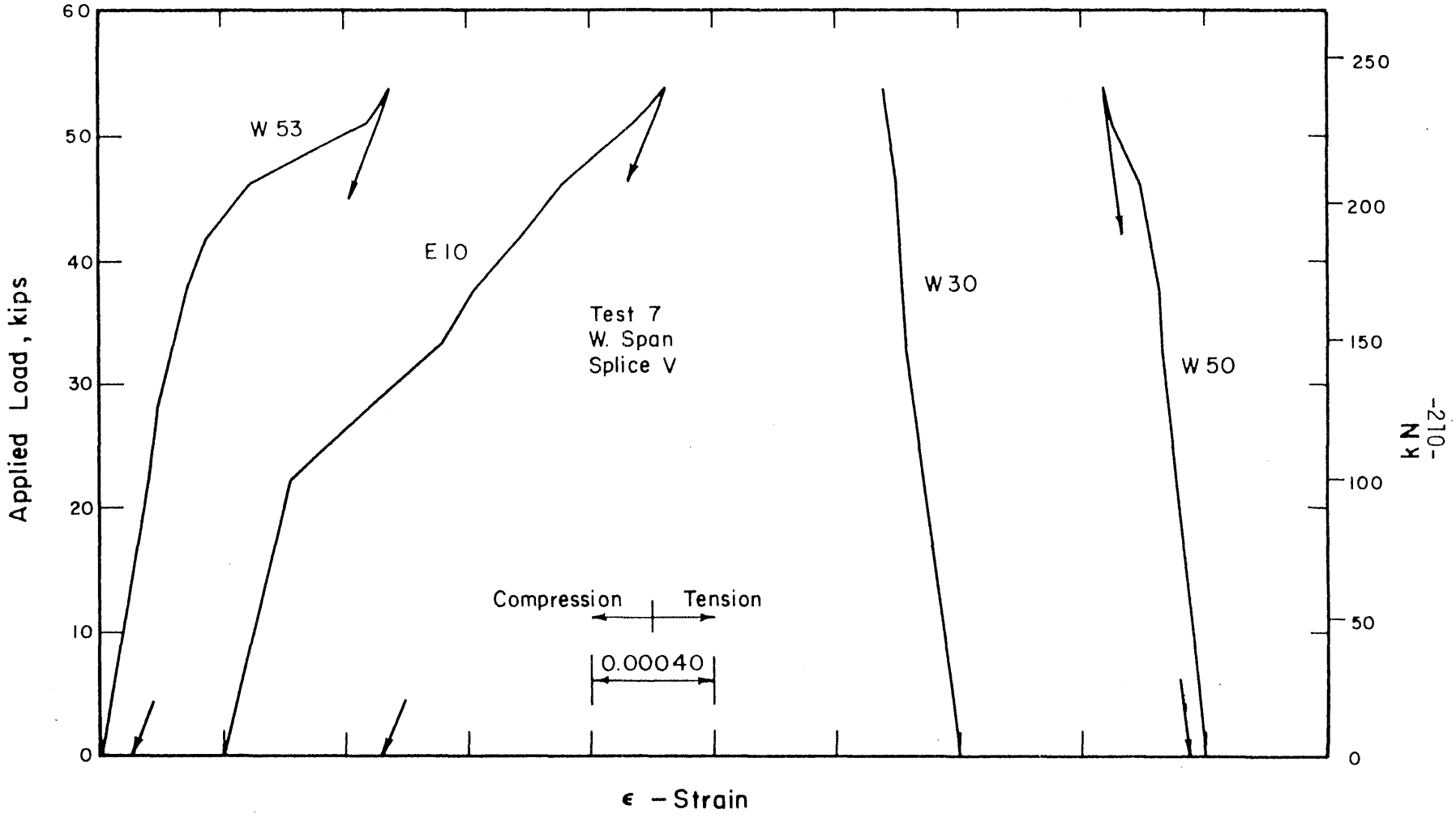


FIG. 5.20 LOAD-STRAIN CURVES FOR VARIOUS SECTIONS IN TEST 7, MODEL 2

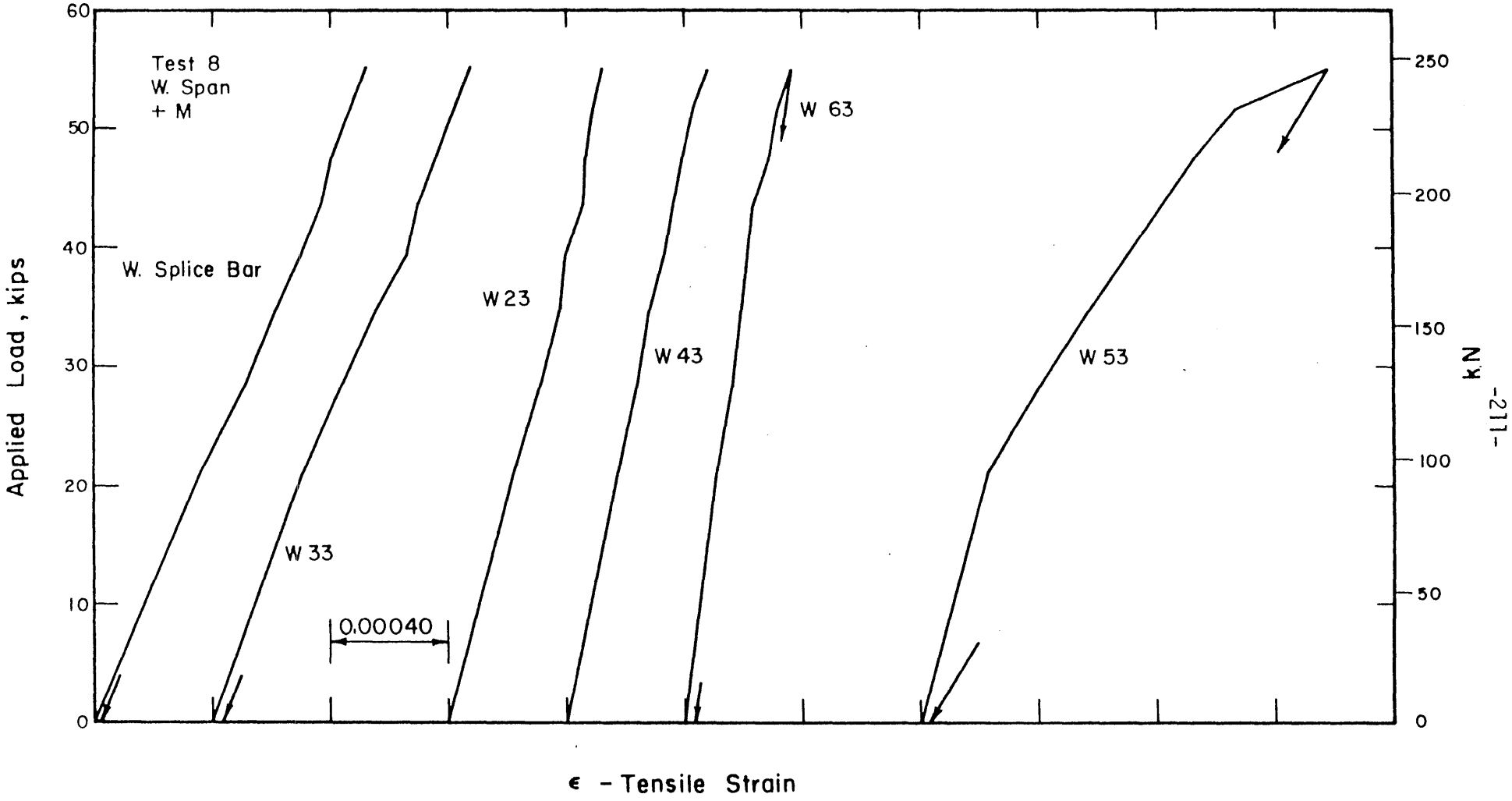


FIG. 5.21 LOAD-STRAIN CURVES FOR TEST 8, MODEL 2

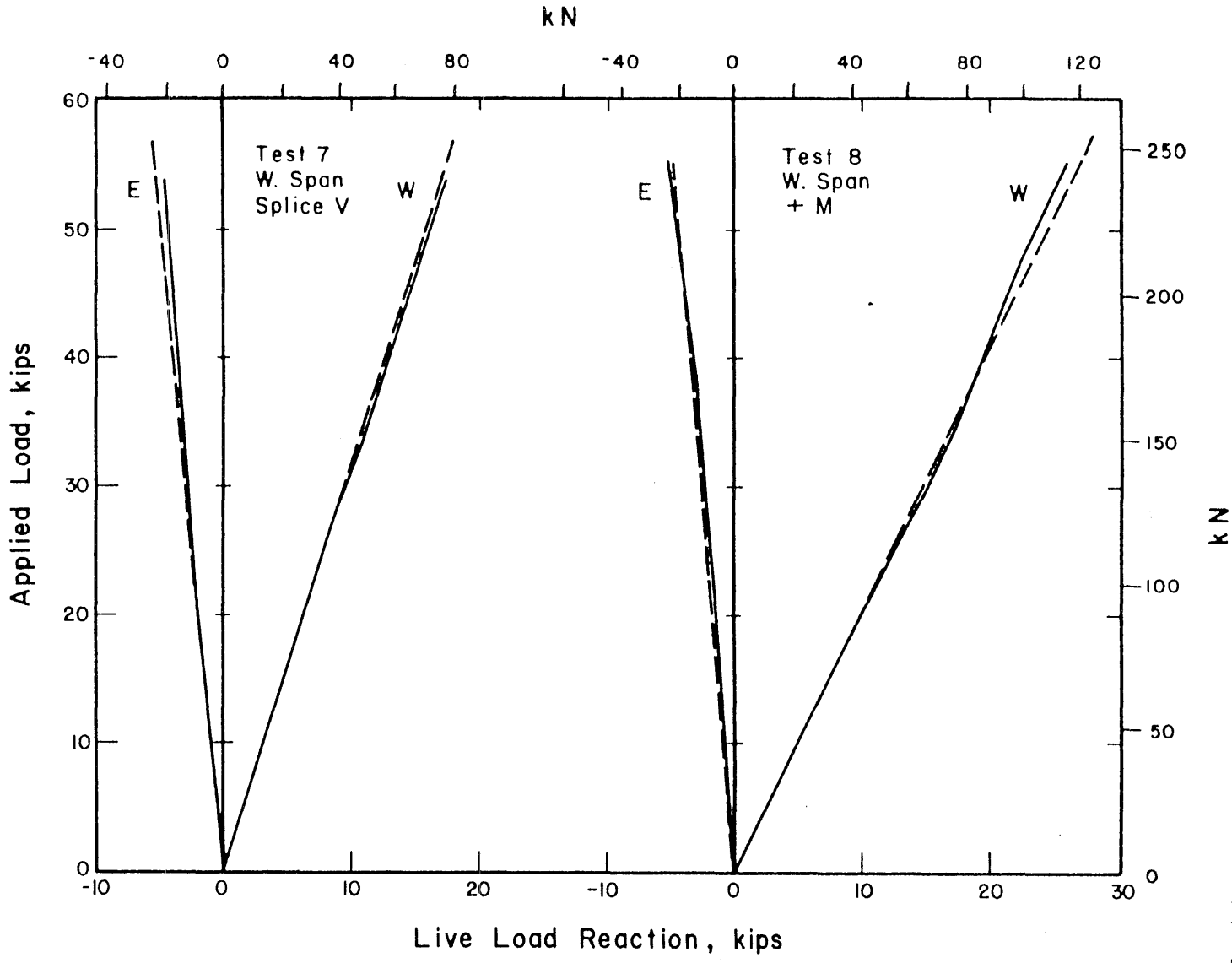


FIG. 5.22 LOAD-END REACTION CURVES FOR TESTS 7 AND 8, MODEL 2

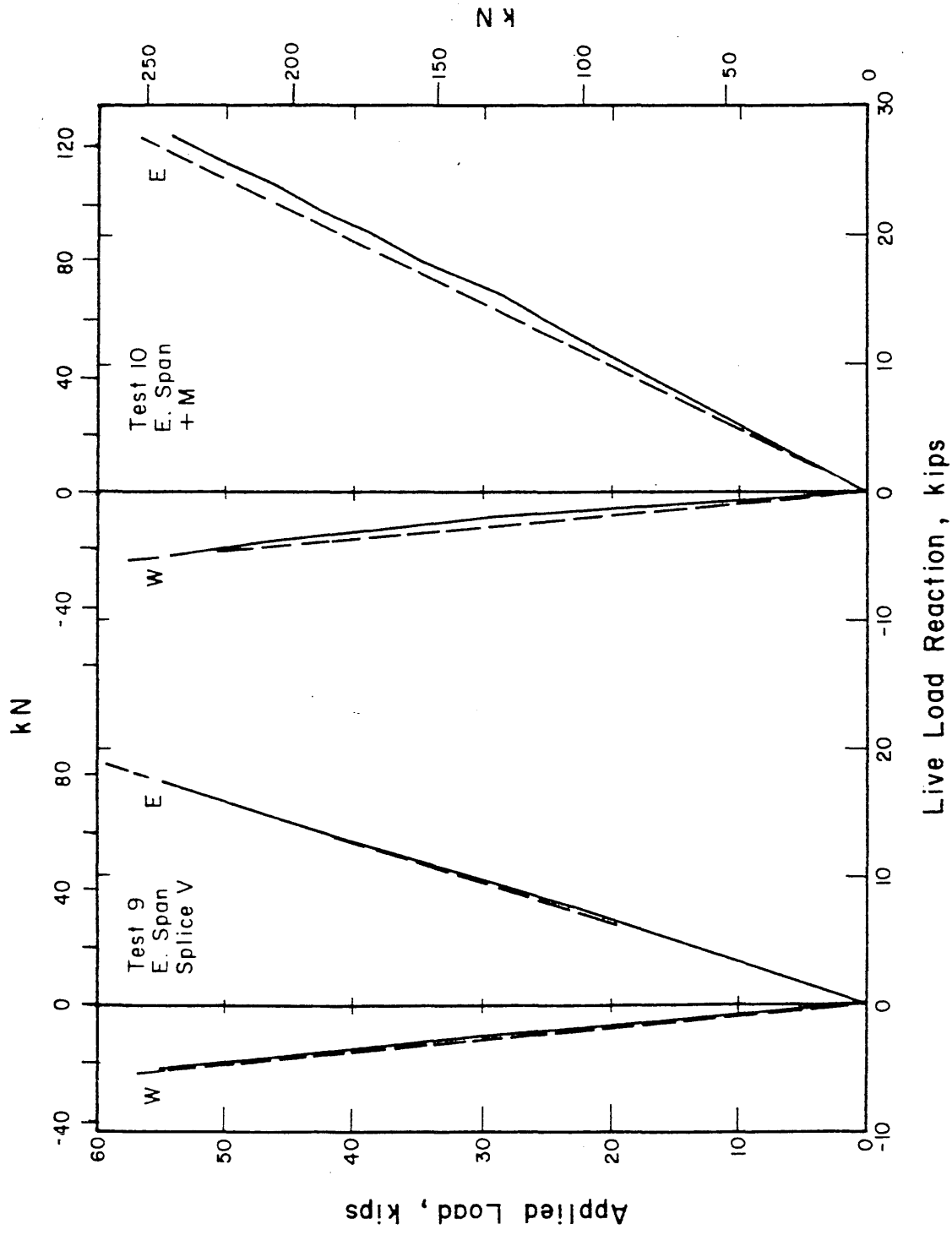


FIG. 5.23 LOAD-END REACTION CURVES FOR TESTS 9 AND 10, MODEL 2

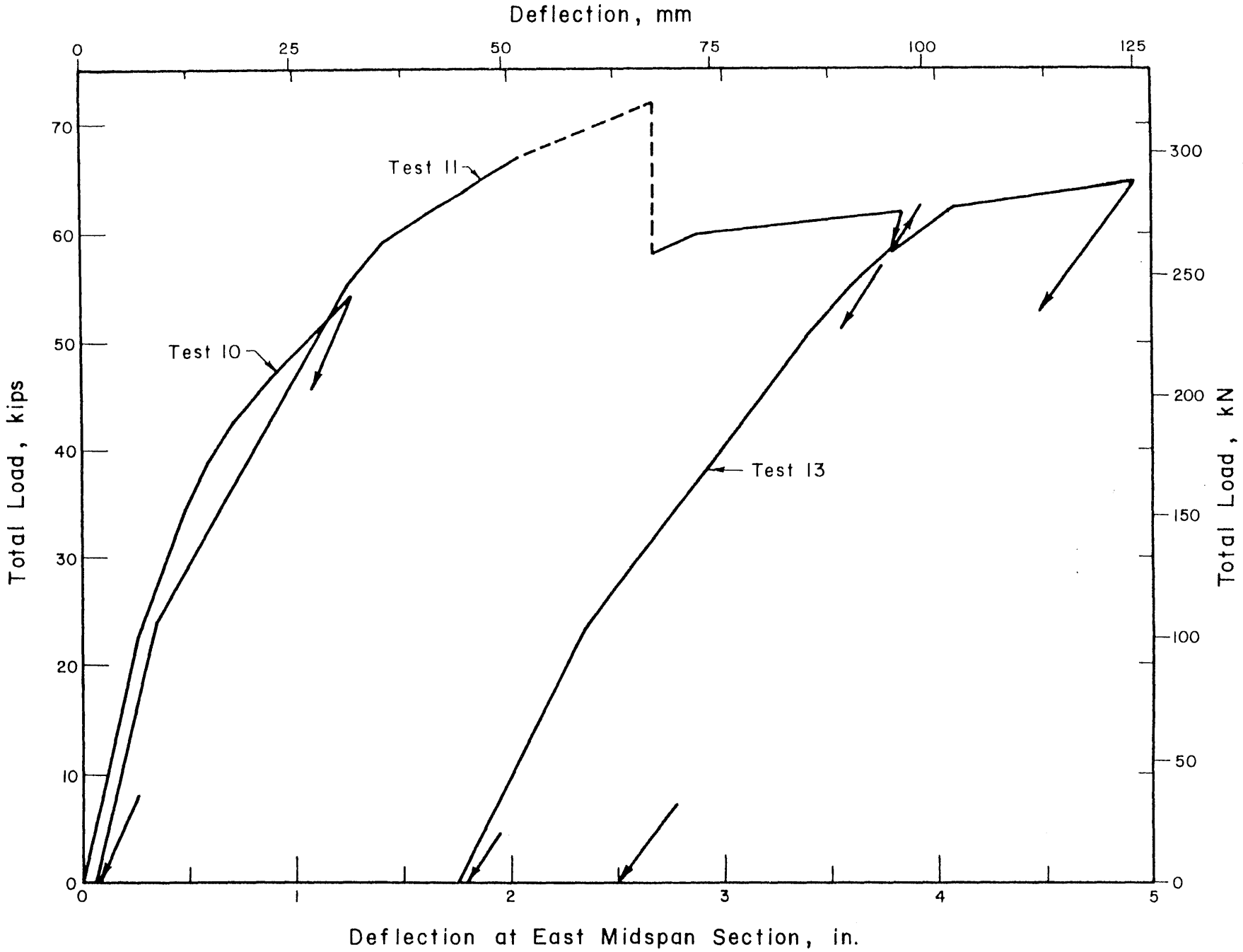


FIG. 5.24 LOAD-DEFLECTION CURVES FOR FINAL THREE TESTS ON EAST SPAN, MODEL 2

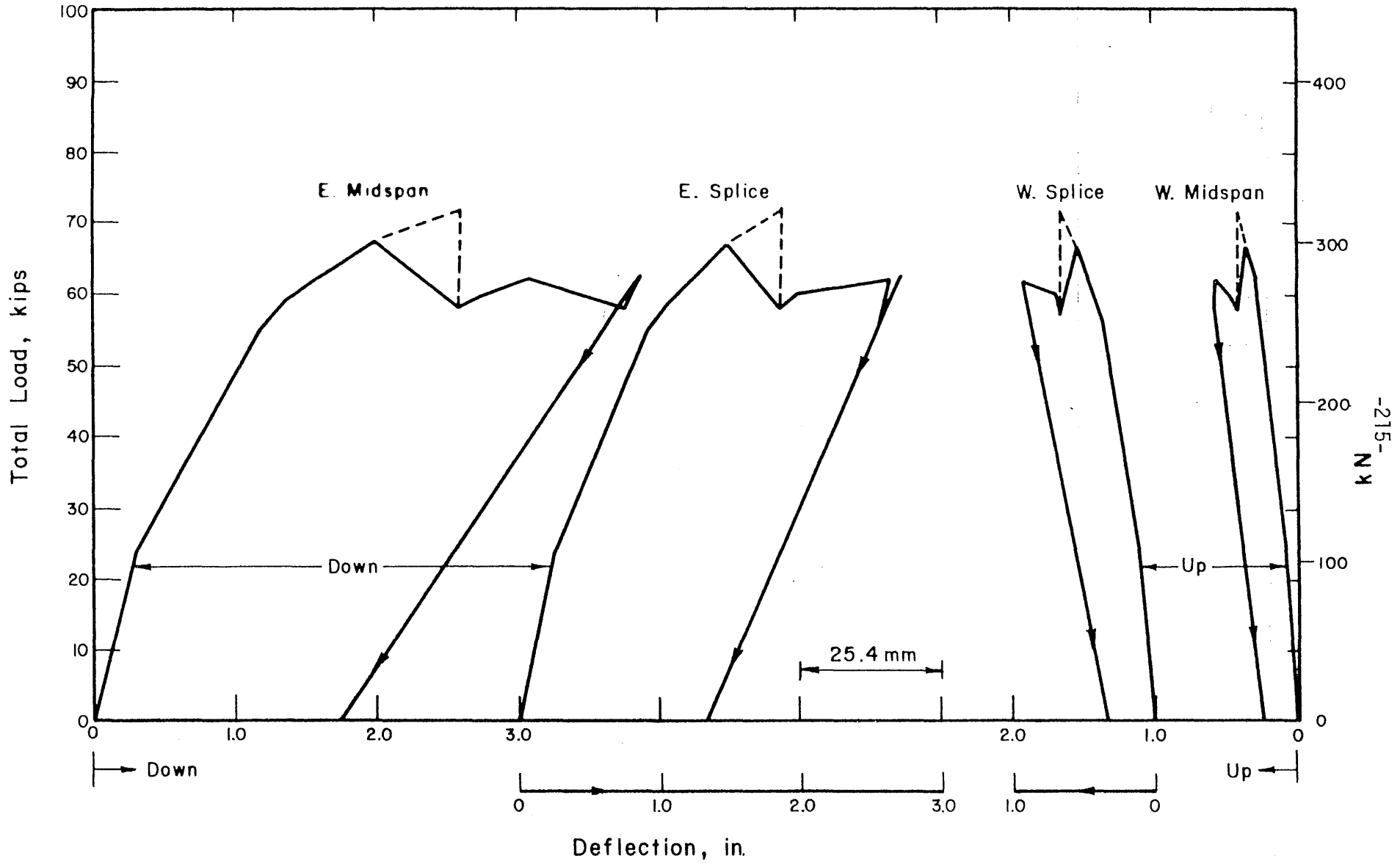


FIG. 5.25 LOAD-DEFLECTION CURVES FOR TEST 11, MODEL 2

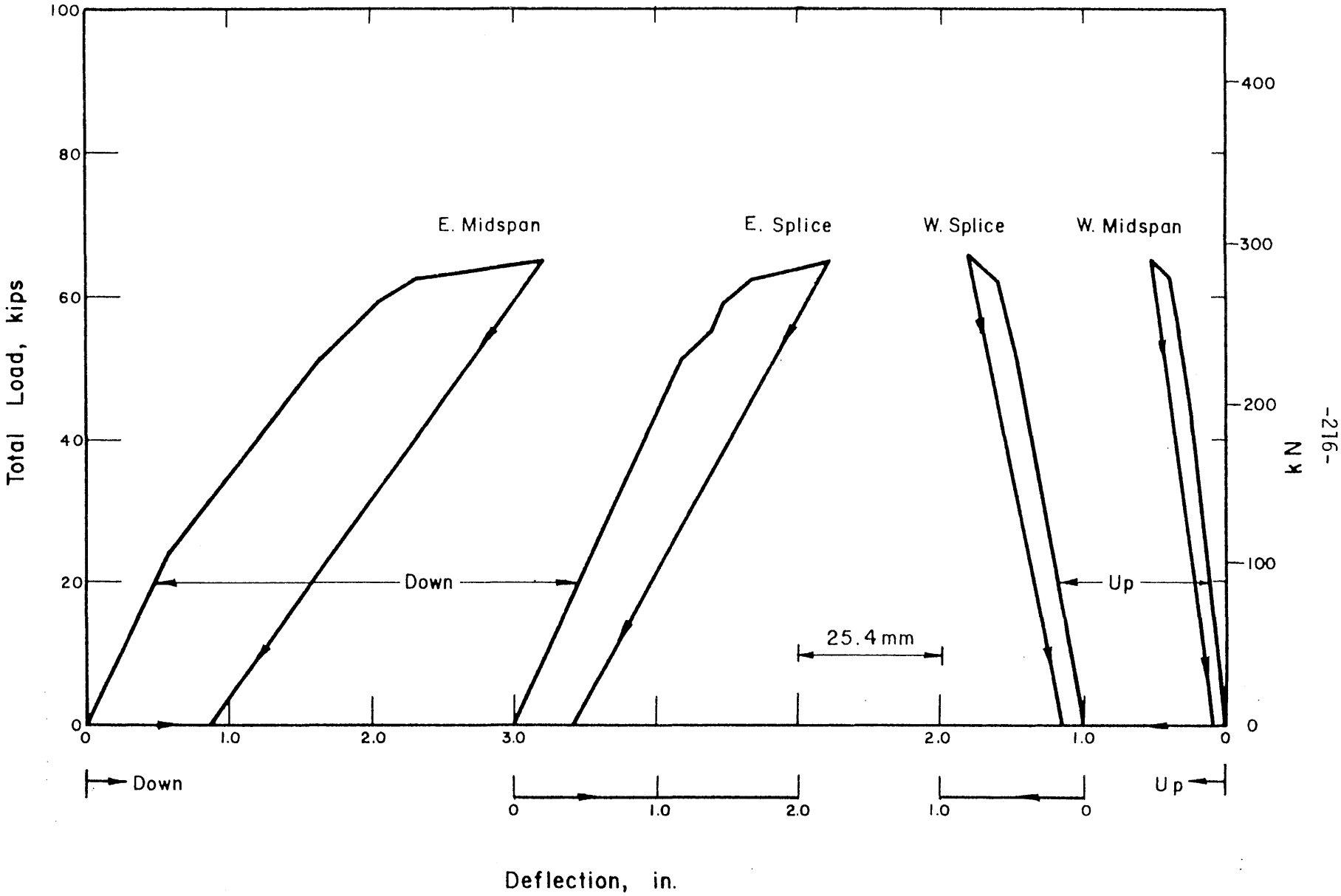


FIG. 5.26 LOAD-DEFLECTION CURVES FOR TEST 13, MODEL 2

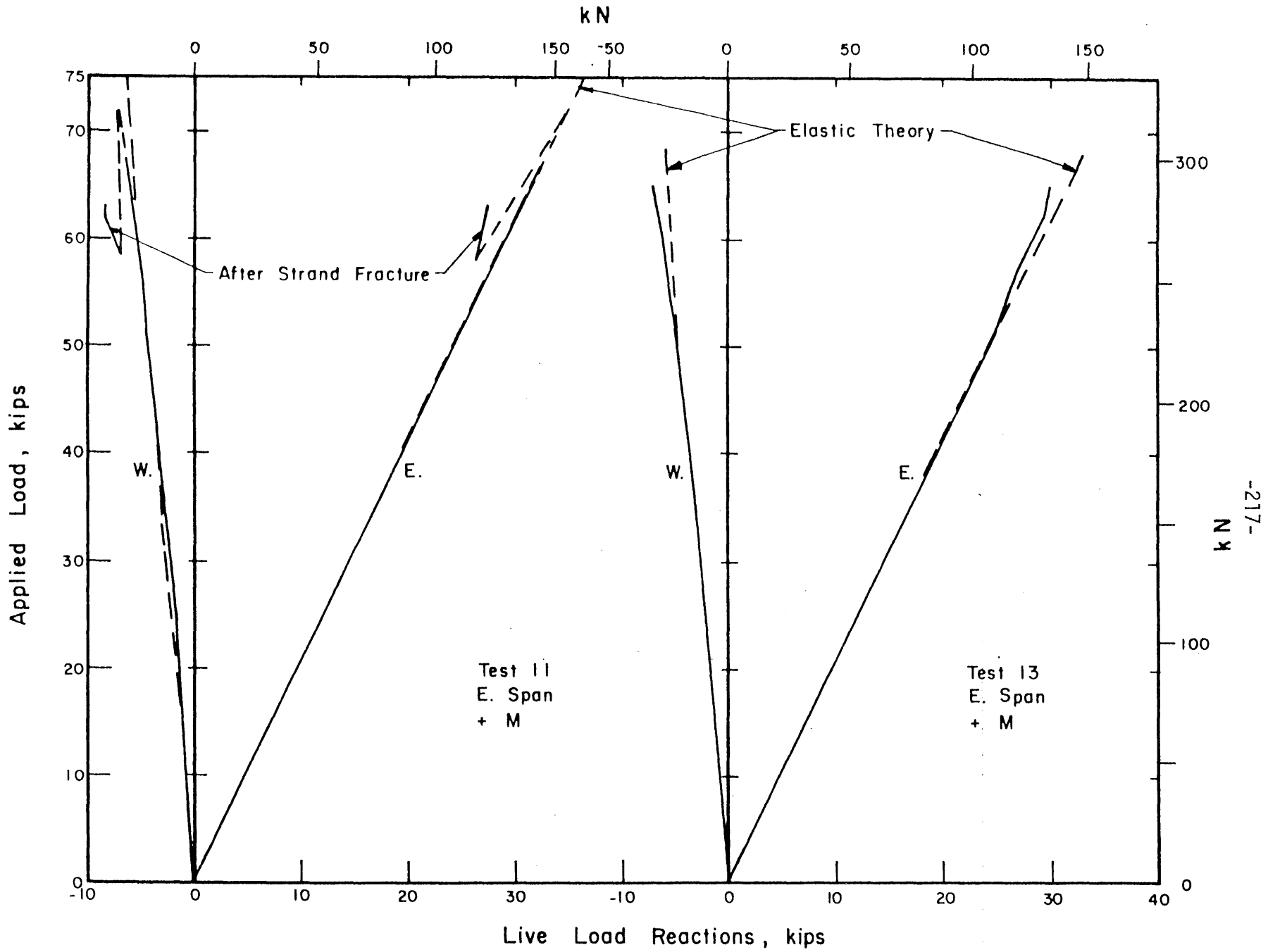


FIG. 5.27 LOAD-END REACTION CURVES FOR TESTS 11 AND 13, MODEL 2

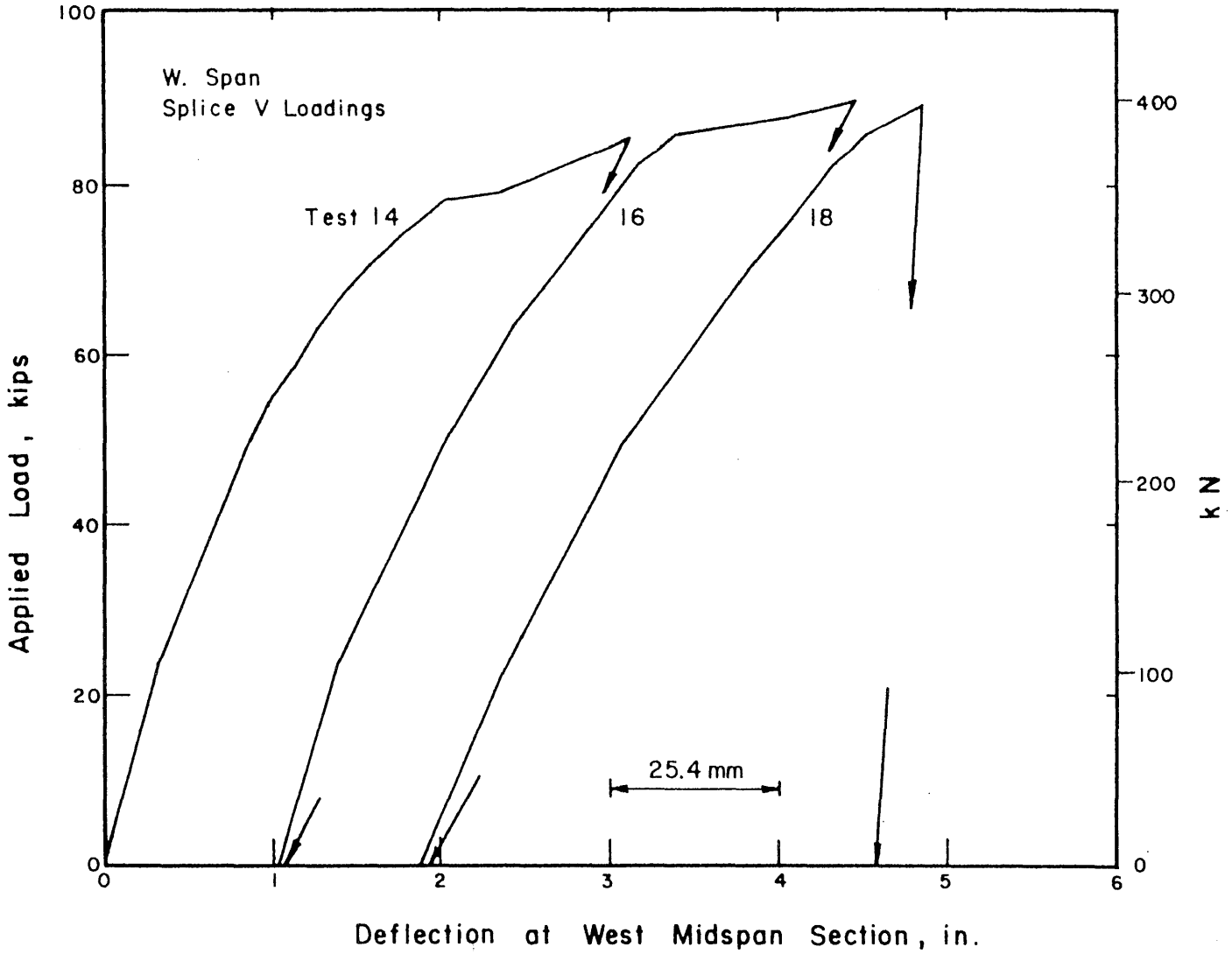


FIG. 5.28 LOAD-CUMULATIVE DEFLECTION CURVES FOR WEST SPLICE DURING FINAL THREE TESTS, MODEL 2

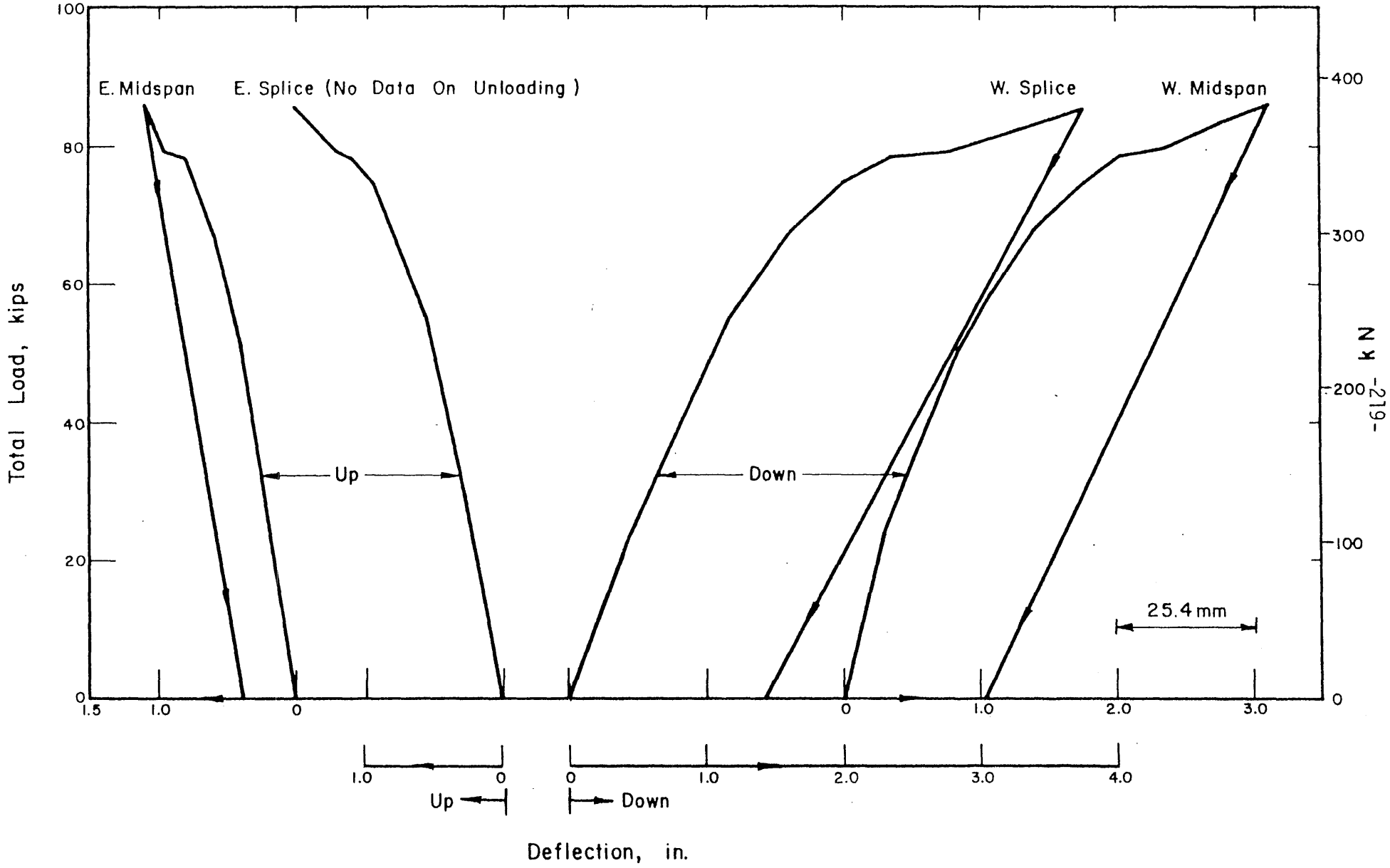


FIG. 5.29 LOAD-DEFLECTION CURVES FOR TEST 14, MODEL 2

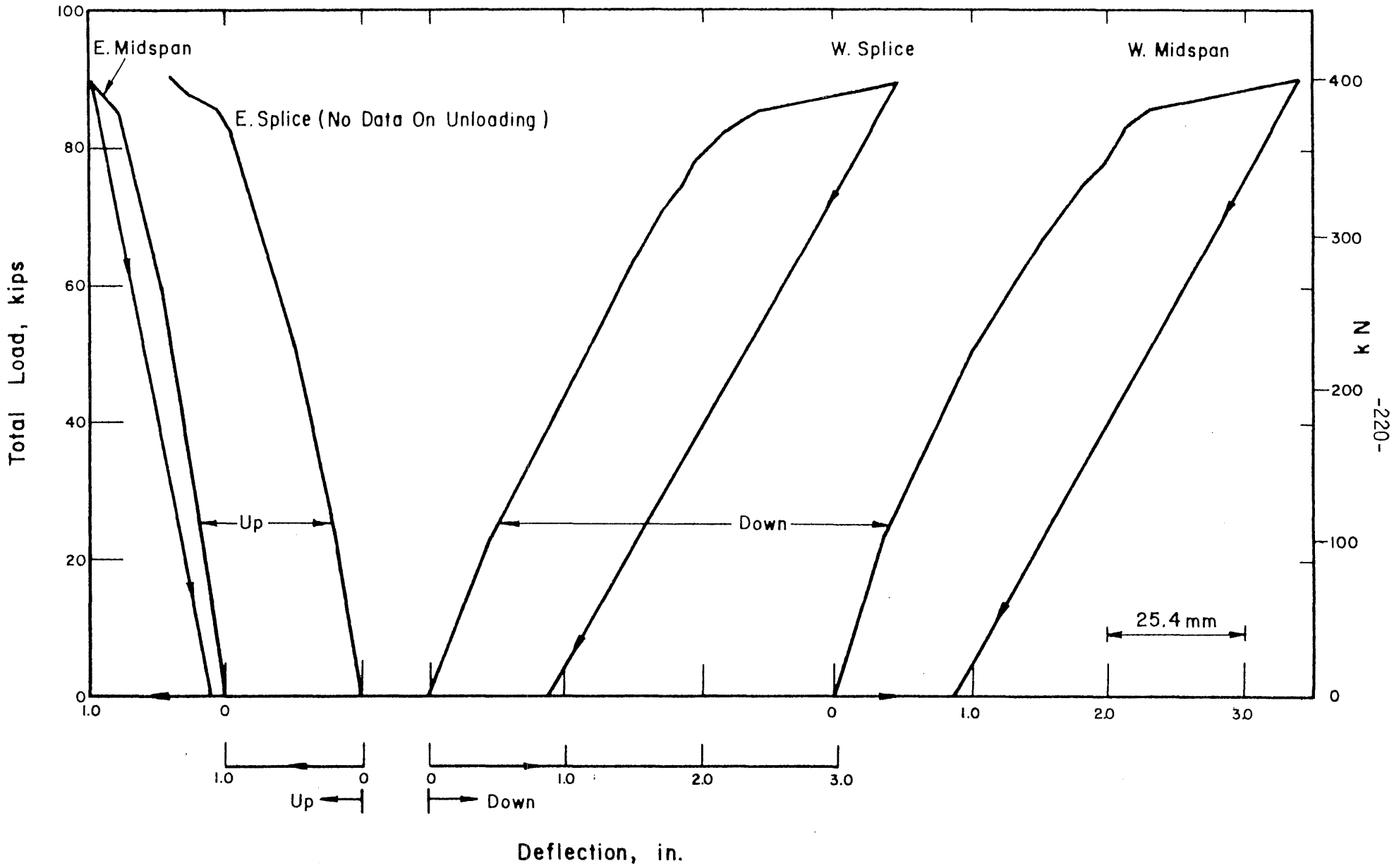


FIG. 5.30 LOAD-DEFLECTION CURVES FOR TEST 16, MODEL 2

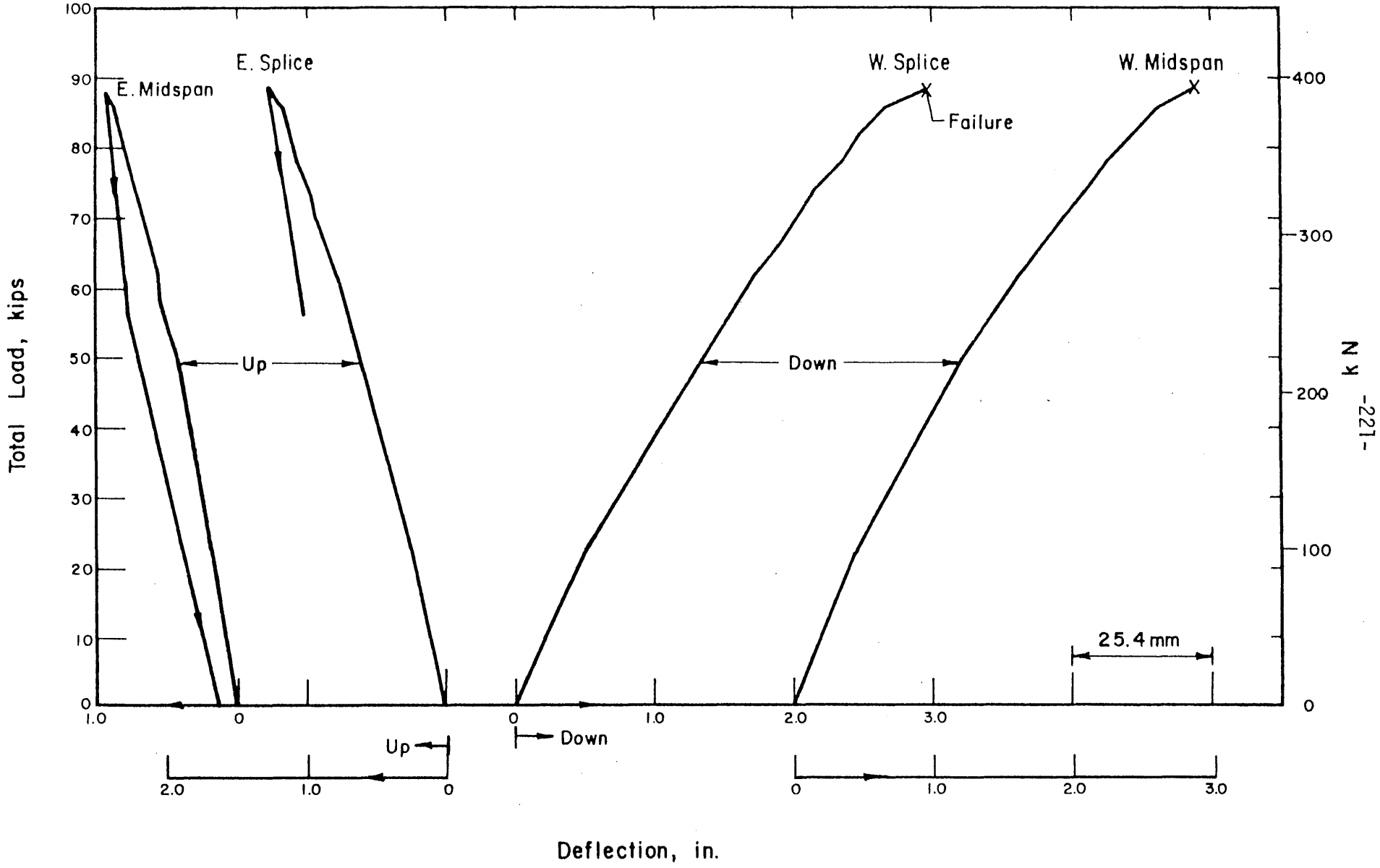


FIG. 5.31 LOAD-DEFLECTION CURVES FOR TEST 18, MODEL 2

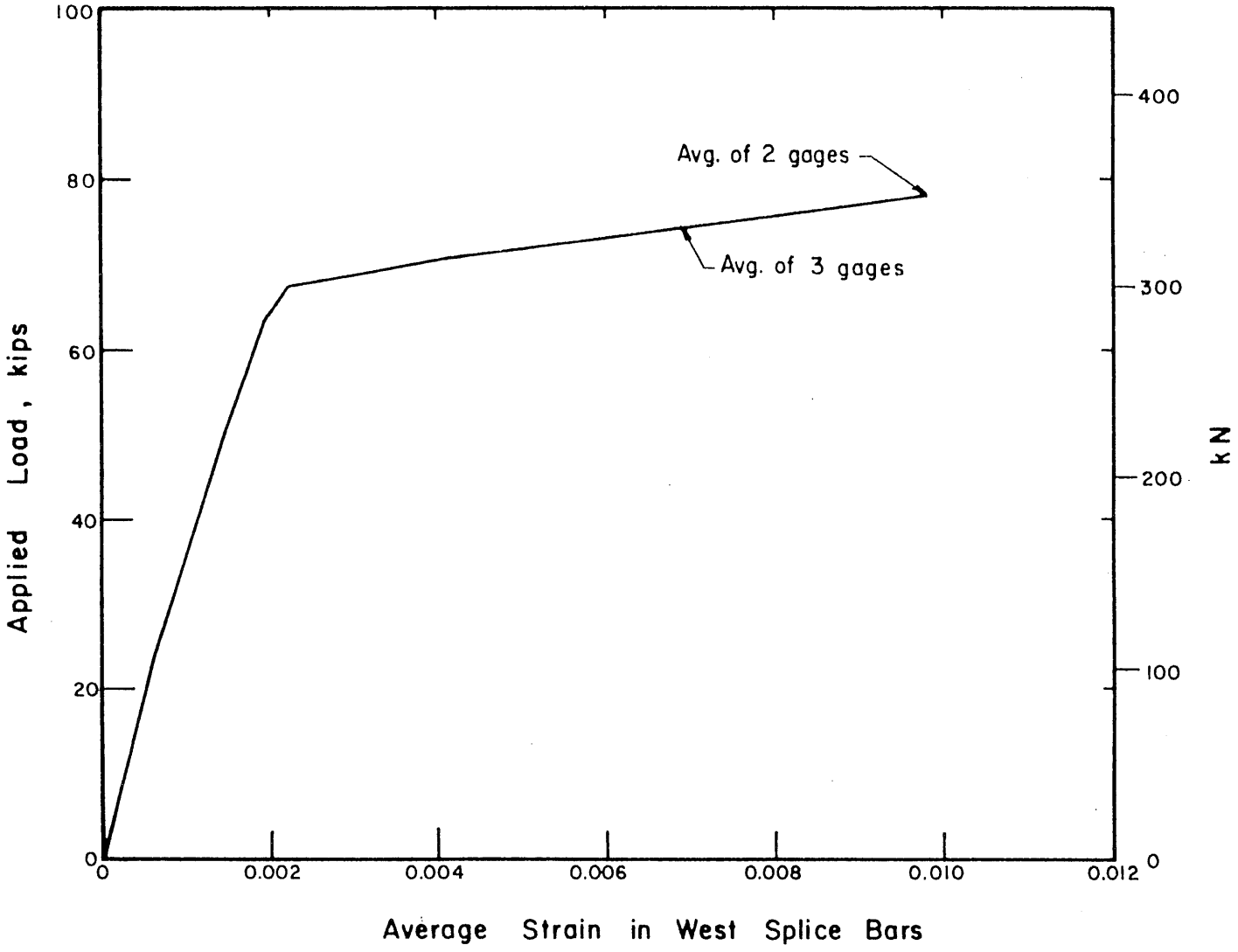


FIG. 5.32 LOAD-STEEL STRAIN CURVE FOR WEST SPLICE IN TEST 14, MODEL 2

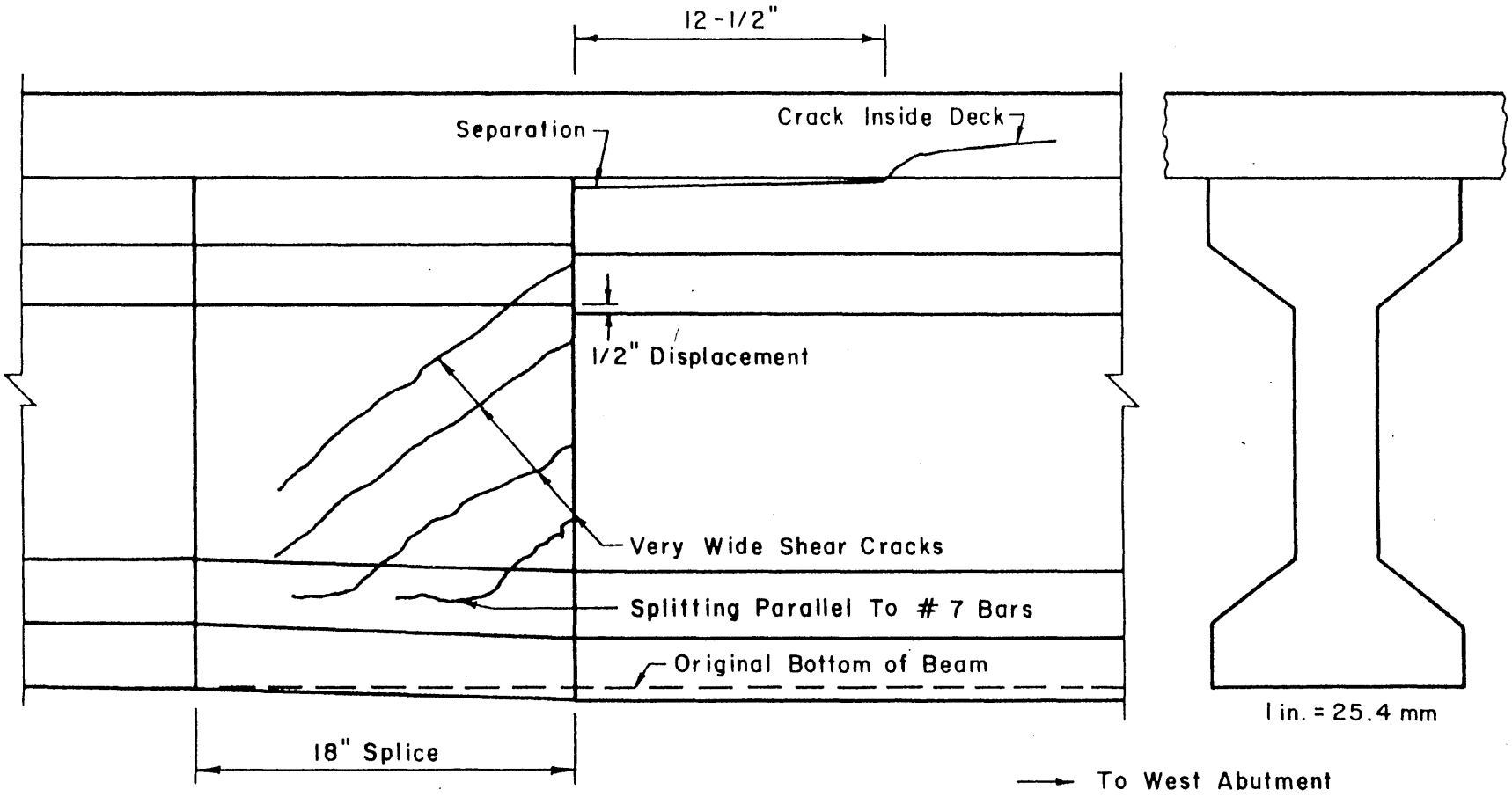


FIG. 5.33 SKETCH OF DEVELOPMENT OF CRACKING IN WEST SPLICE, MODEL 2

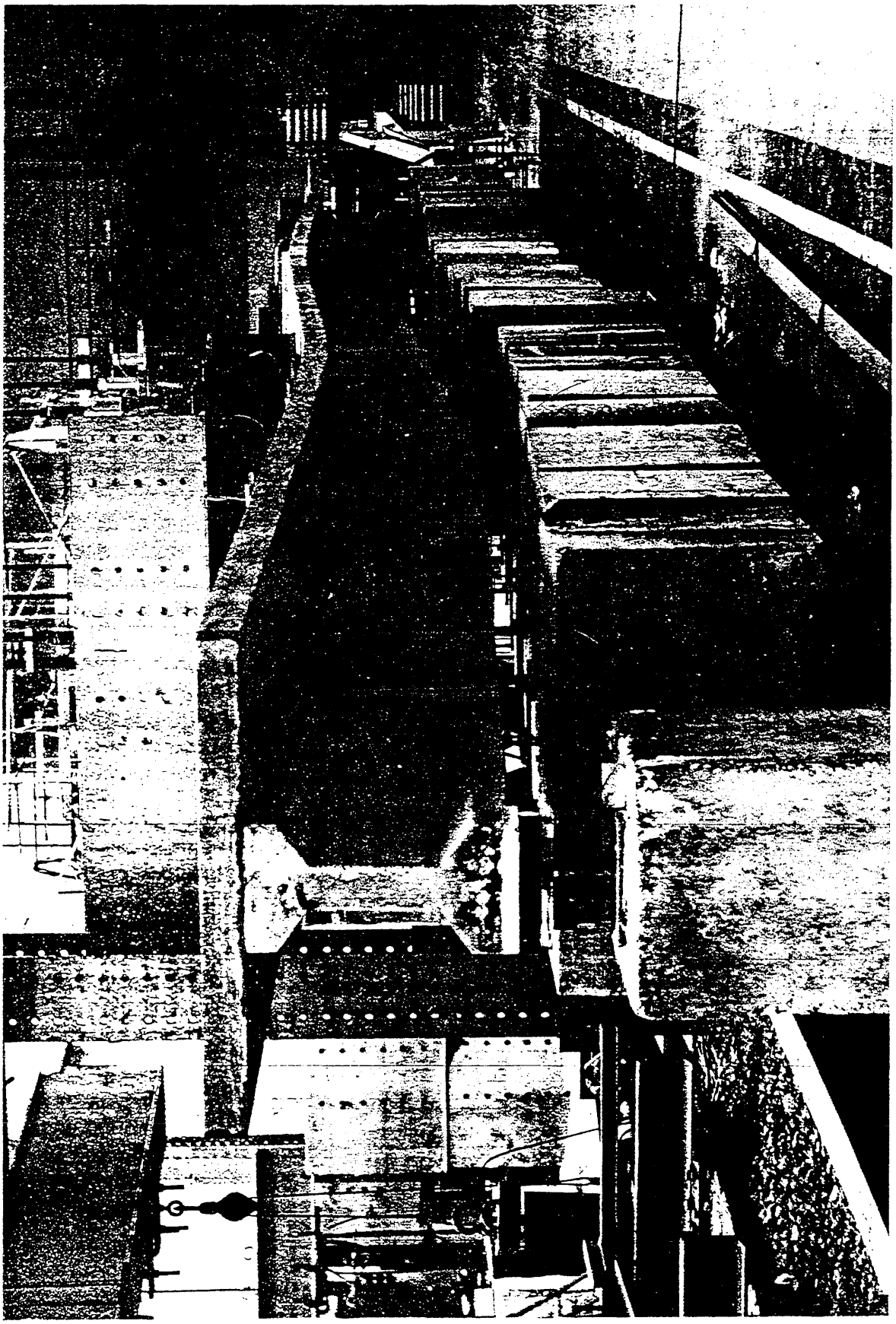

FIG. 5.34 OVERALL VIEW OF MODEL 2 AT LOAD 173

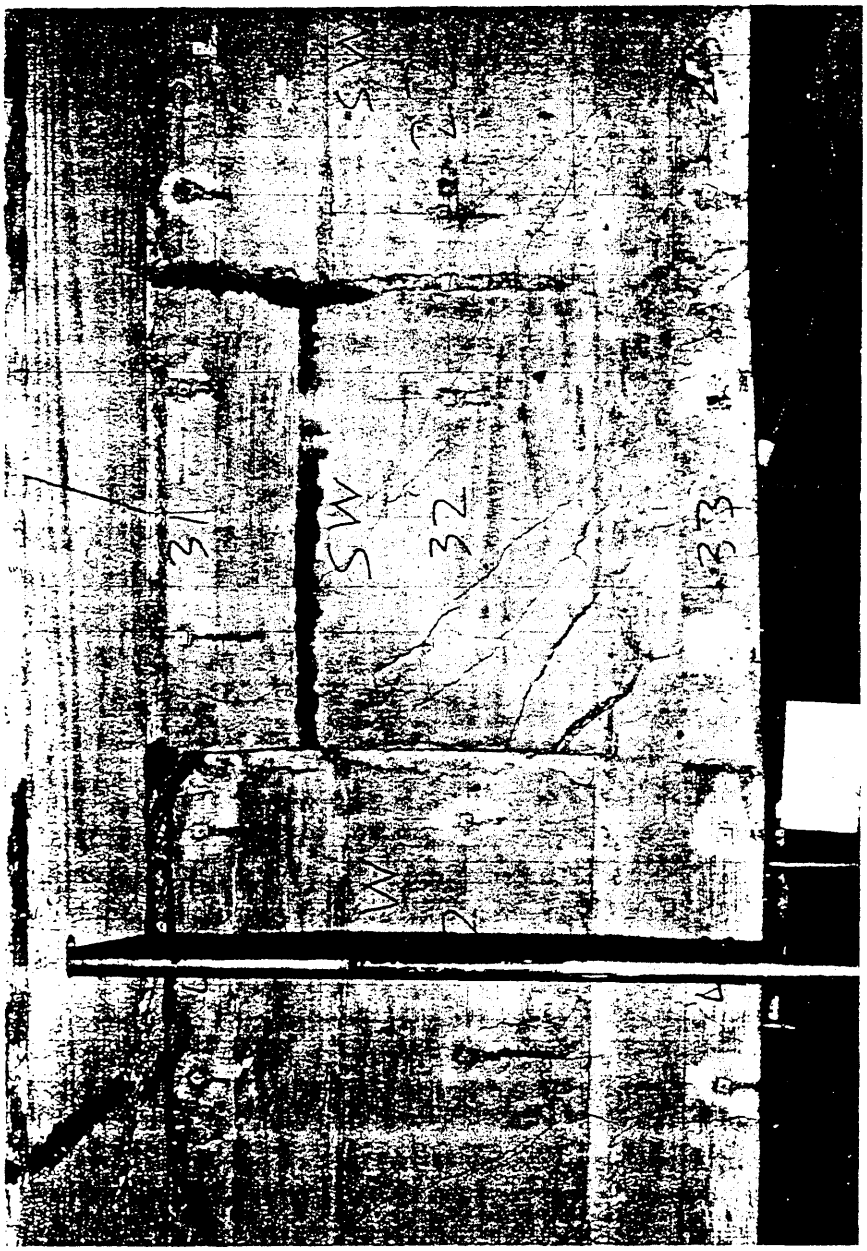


FIG. 5.35 PHOTO OF SOUTH SIDE OF WEST SPLICE OF MODEL 2, LOAD 173


FIG. 5.36 PHOTO OF SOUTH SIDE OF WEST SPLICE OF MODEL 2 AFTER FAILURE

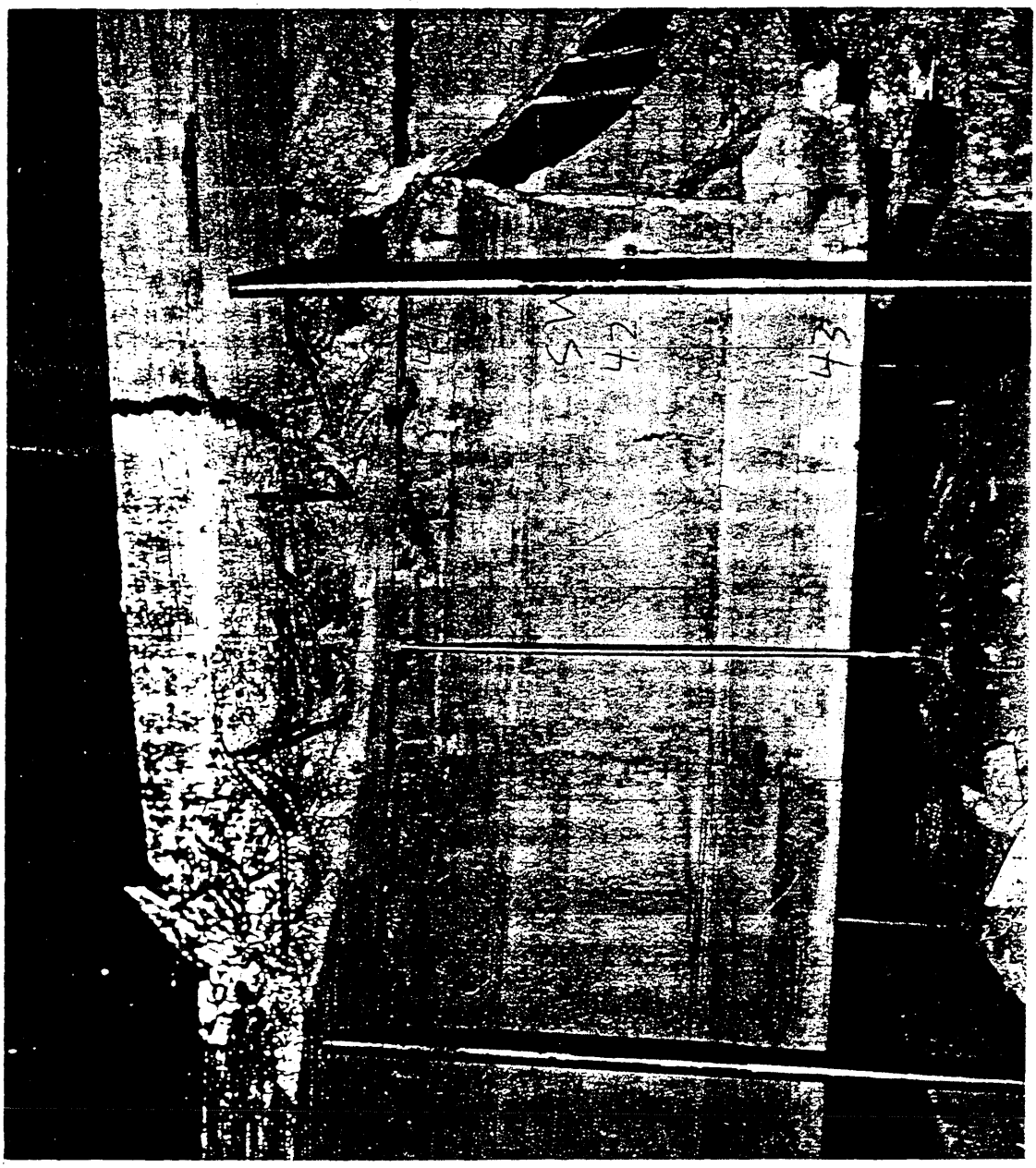


FIG. 5.37 PHOTO OF SOUTH SIDE OF WEST SEGMENT AND DECK ADJACENT TO SPLICE, MODEL 2

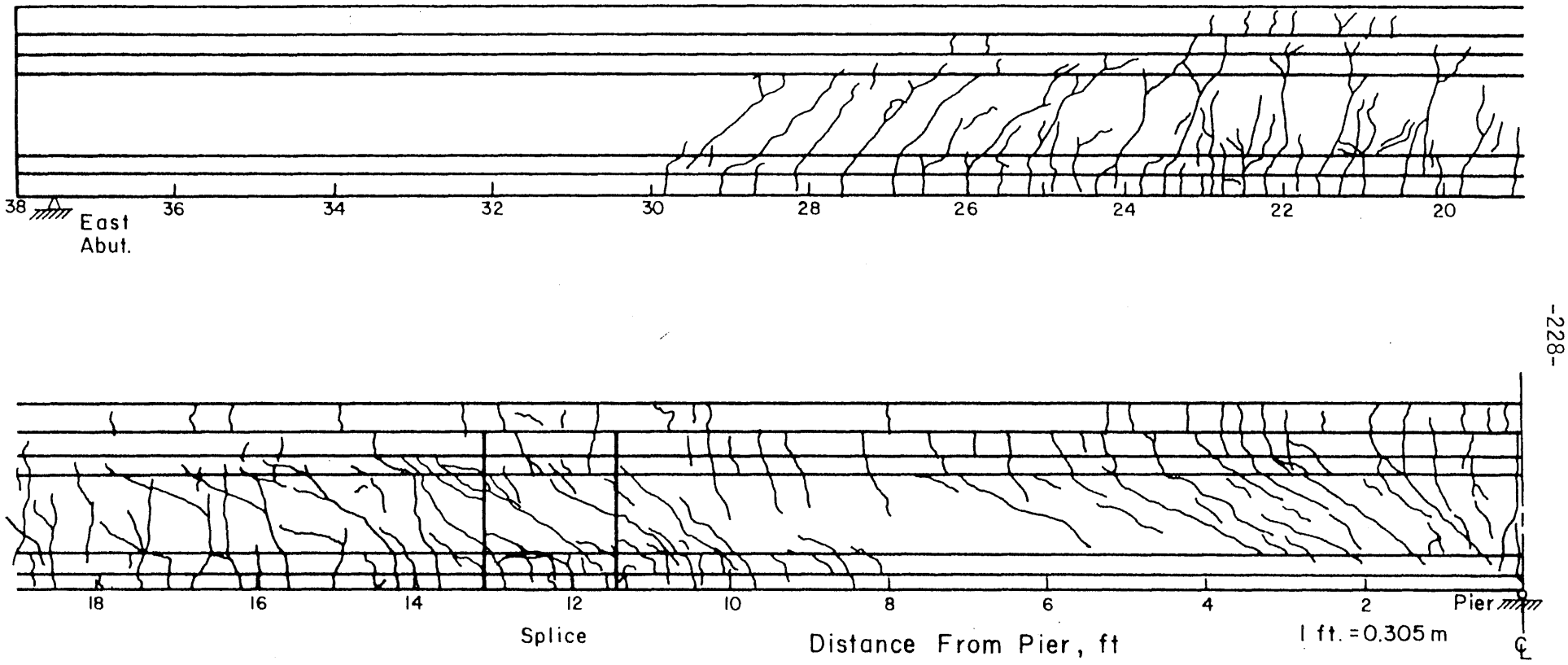




FIG. 5.38 CRACKS IN EAST SPAN AFTER COMPLETION OF TESTING, MODEL 2

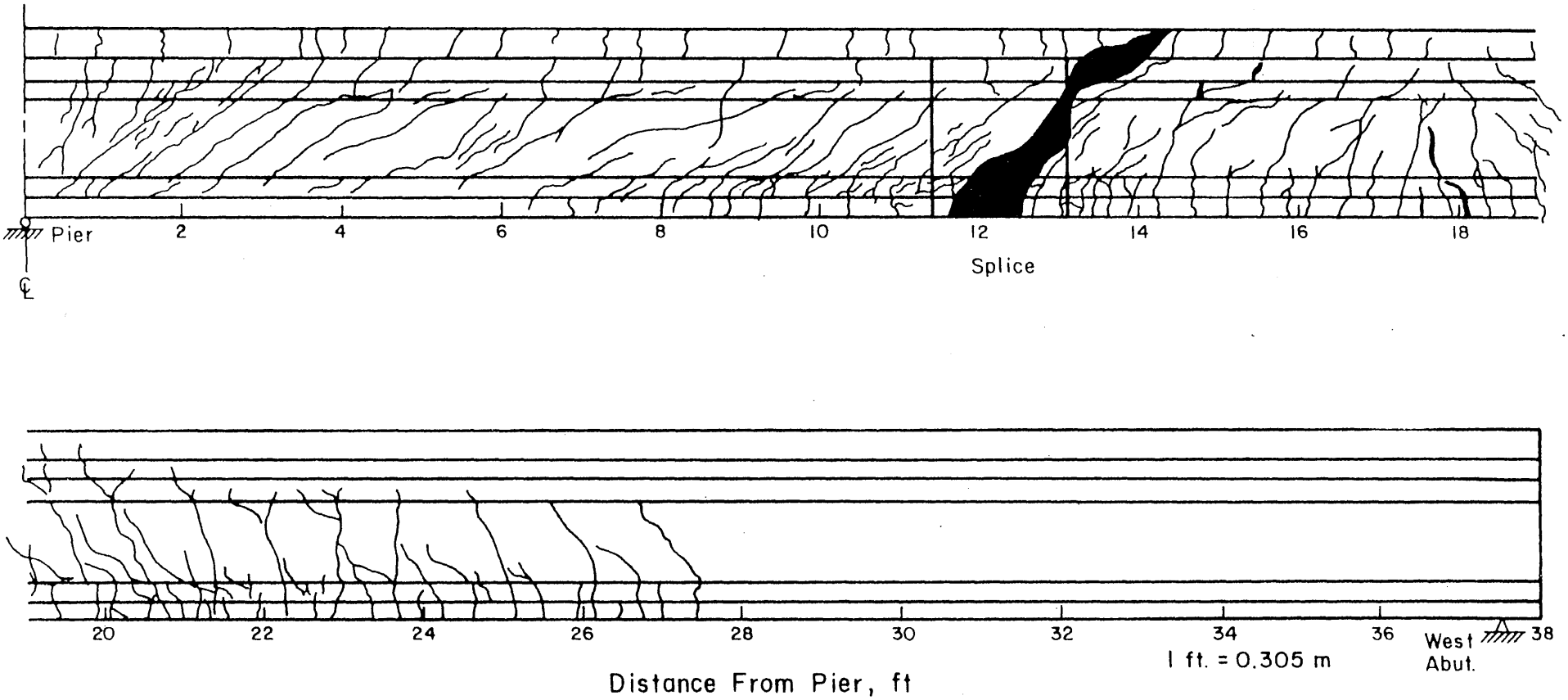


FIG. 5.39 CRACKS IN WEST SPAN AFTER COMPLETION OF TESTING, MODEL 2

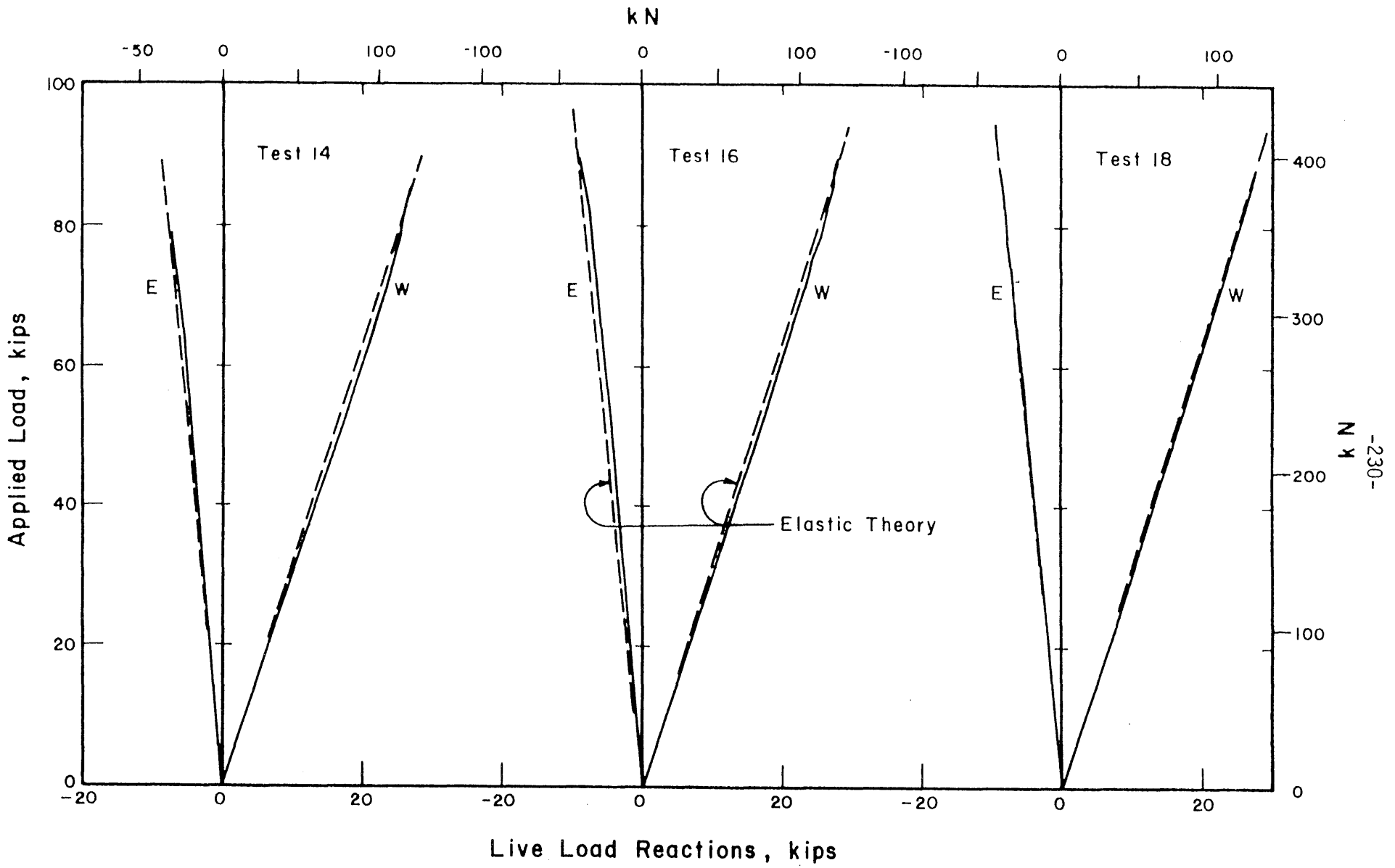


FIG. 5.40 LOAD-END REACTION CURVES FOR TESTS 14, 16, AND 18, MODEL 2

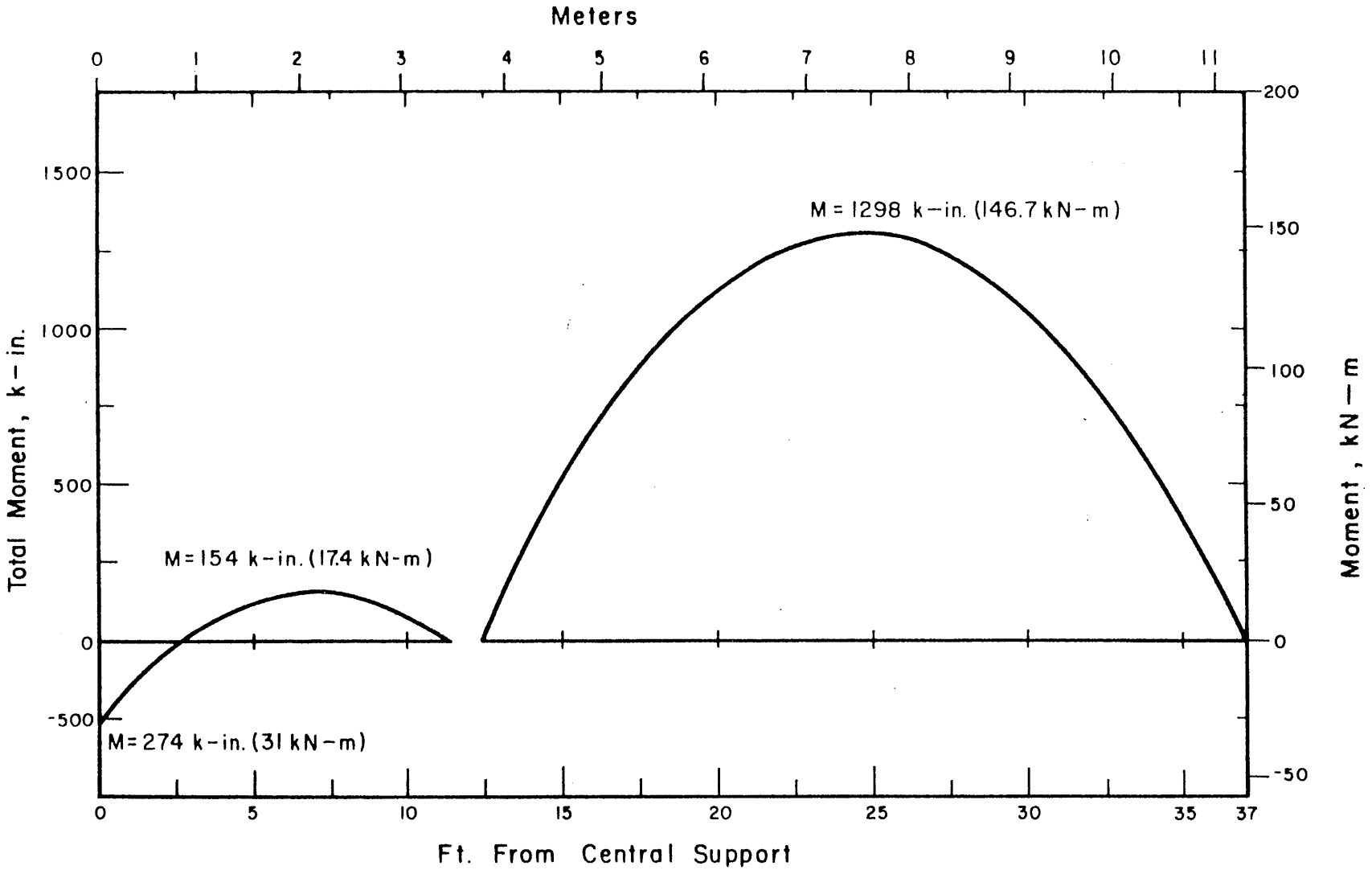


FIG. 6.1 DEAD LOAD MOMENT DIAGRAM IMMEDIATELY BEFORE POST-TENSIONING, MODEL 1

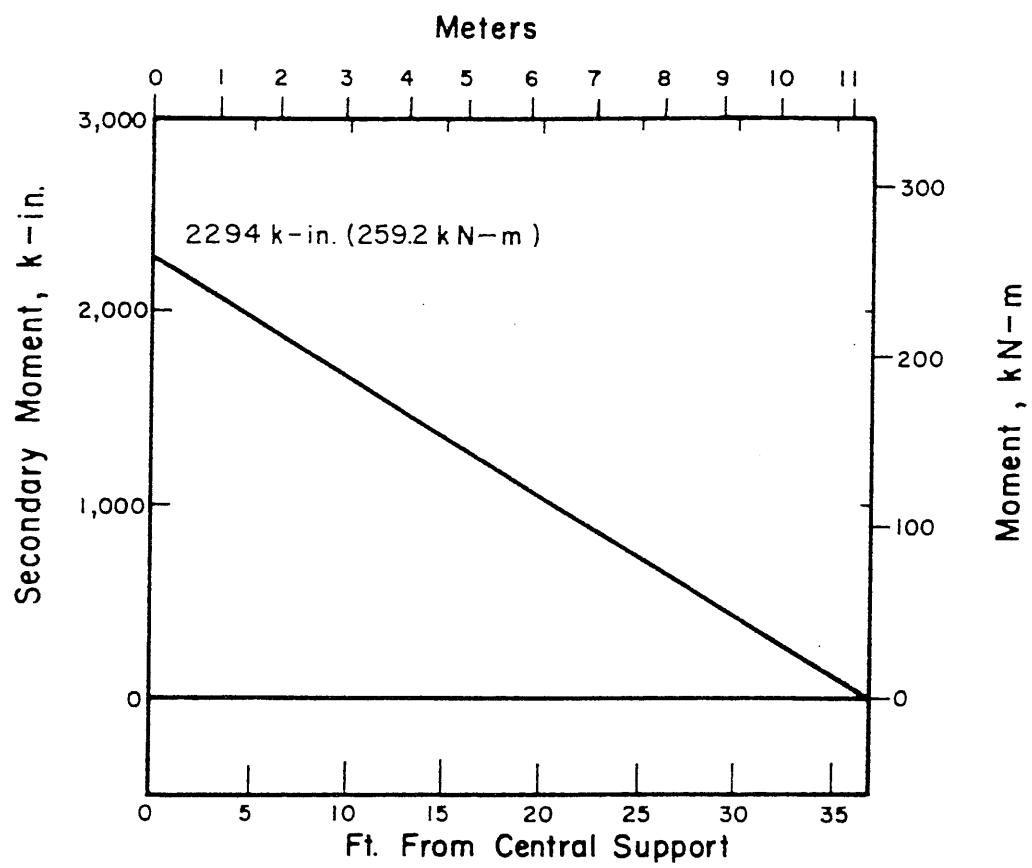


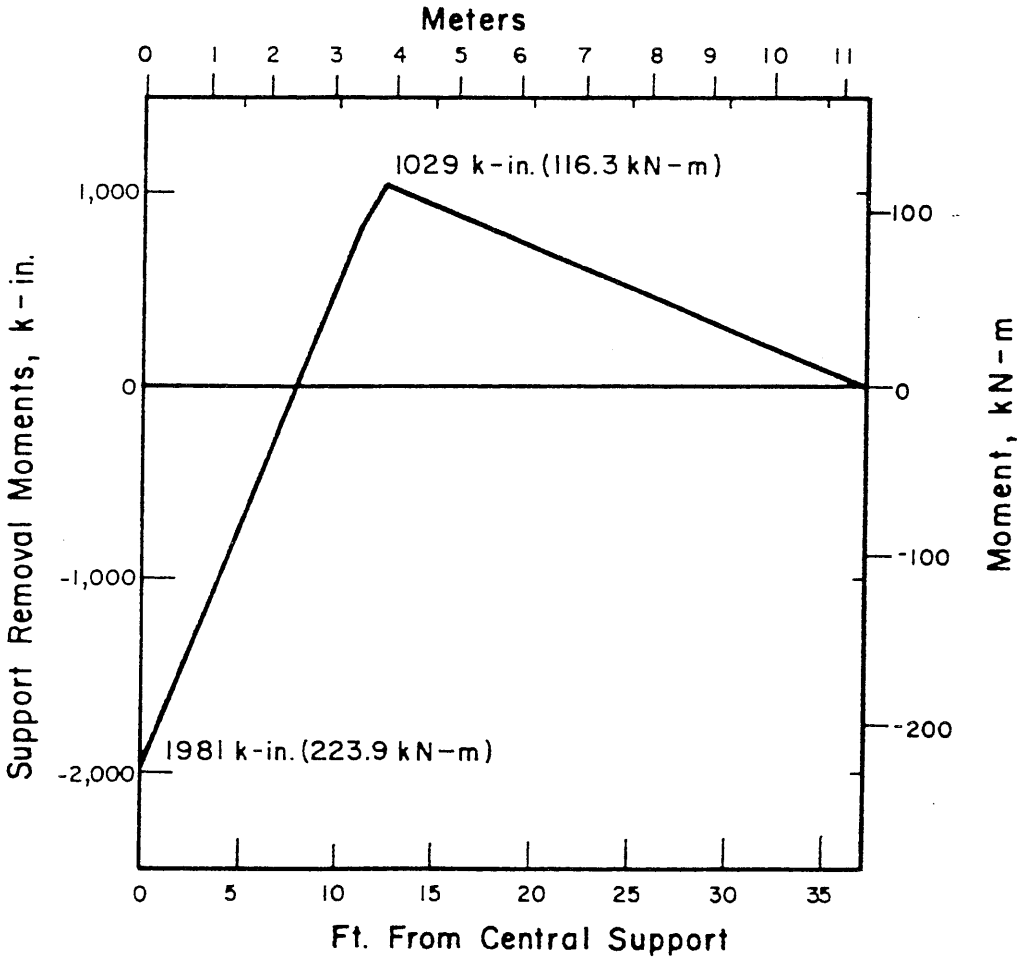


FIG. 6.2 MOMENT DIAGRAMS DUE TO POST-TENSIONING AND SUPPORT REMOVAL, MODEL 1

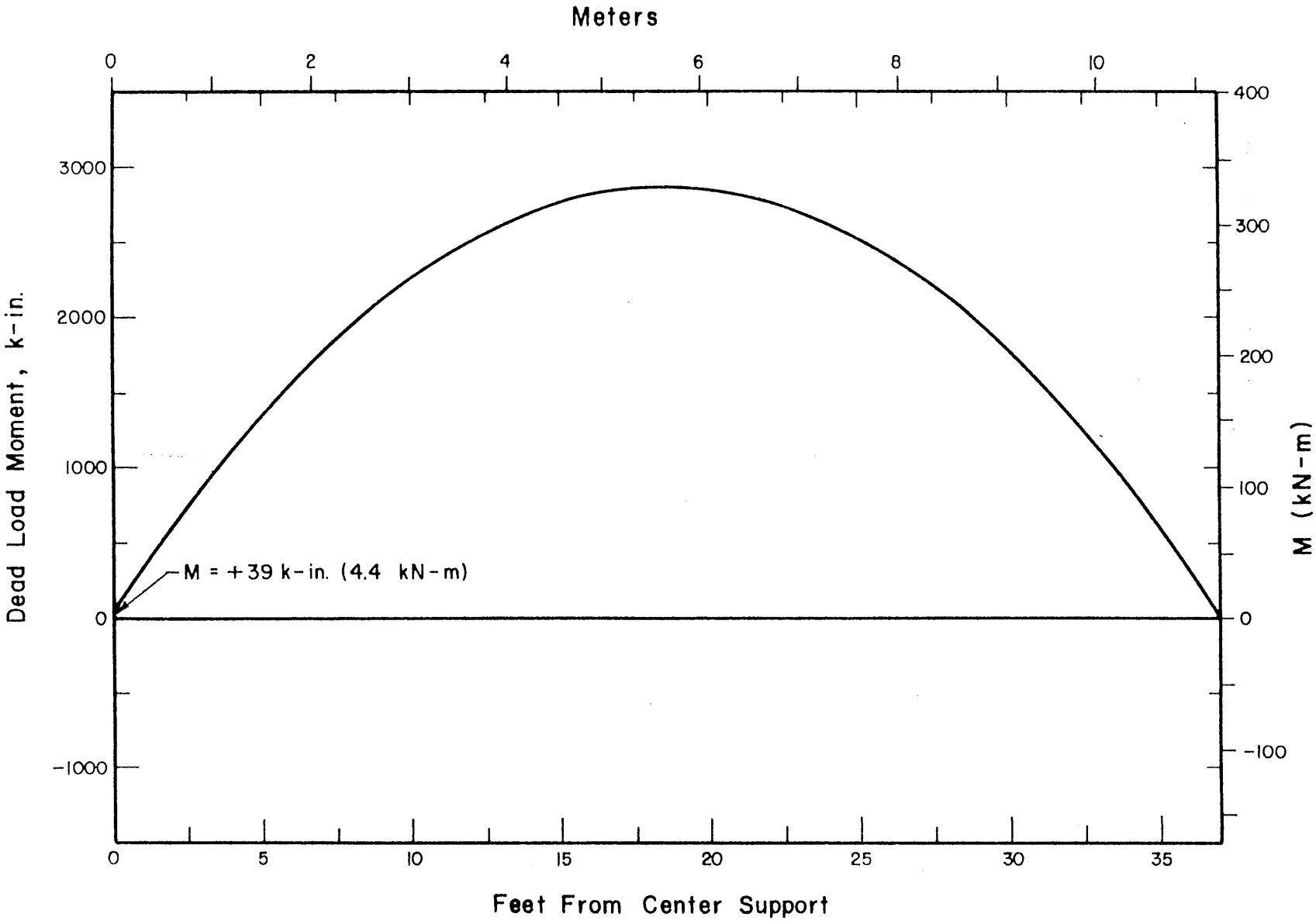


FIG. 6.3 MOMENT DIAGRAM FOR MODEL 1 IMMEDIATELY AFTER POST-TENSIONING AND SUPPORT REMOVAL

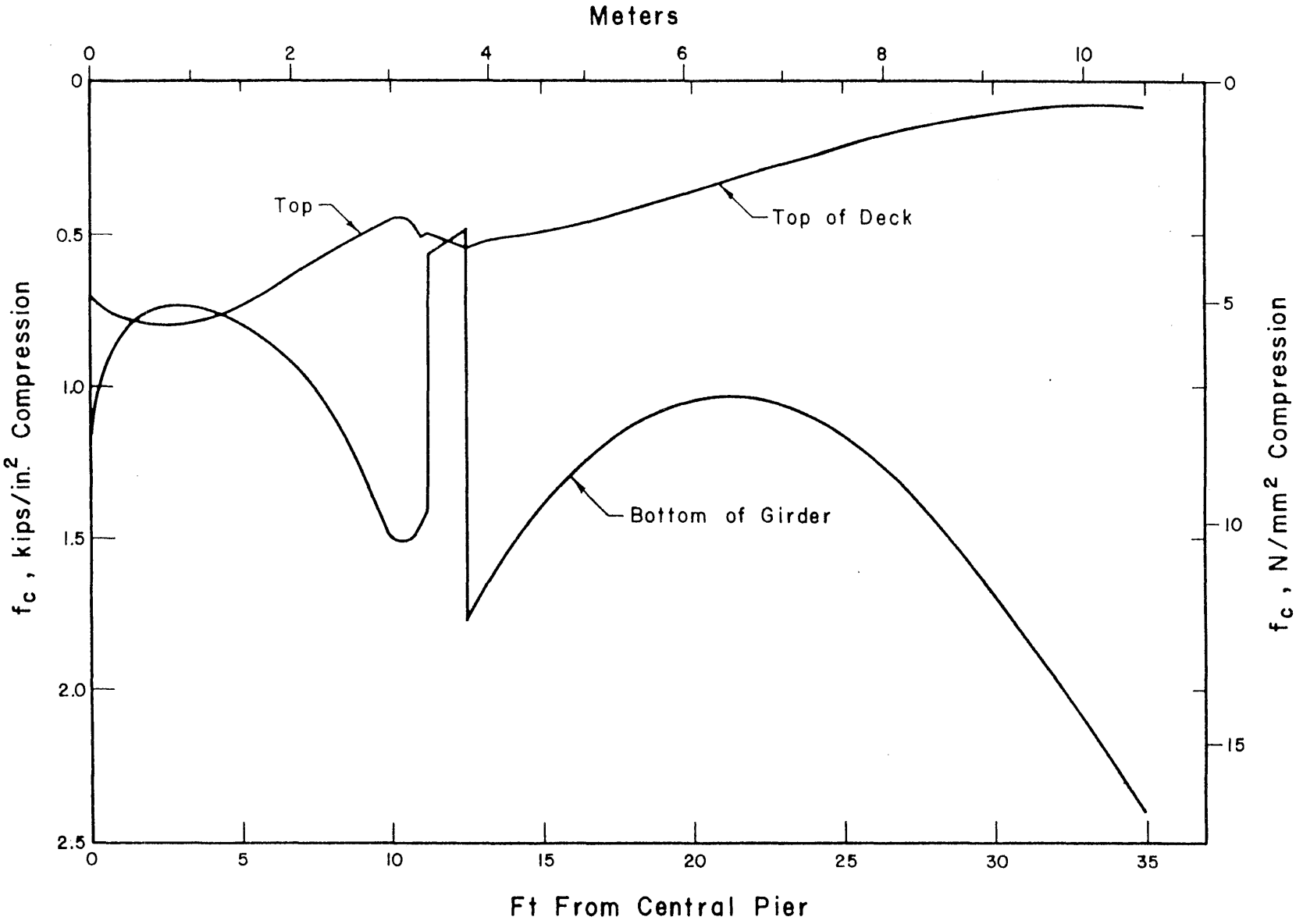


FIG. 6.4 DISTRIBUTION OF CONCRETE STRESSES ALONG TOP OF DECK AND BOTTOM OF GIRDER, MODEL 1

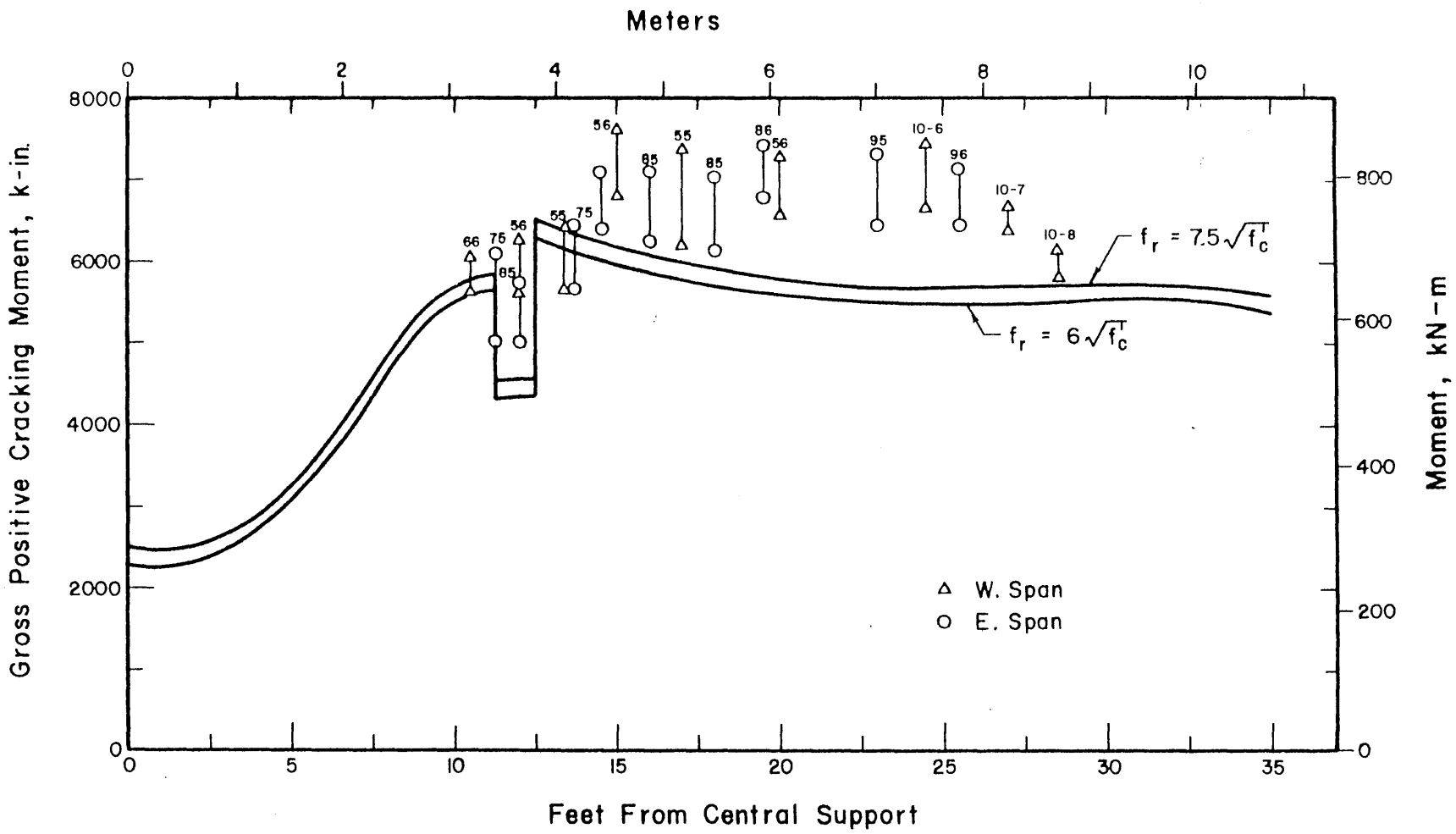


FIG. 6.5 COMPUTED AND OBSERVED POSITIVE CRACKING MOMENTS, MODEL 1

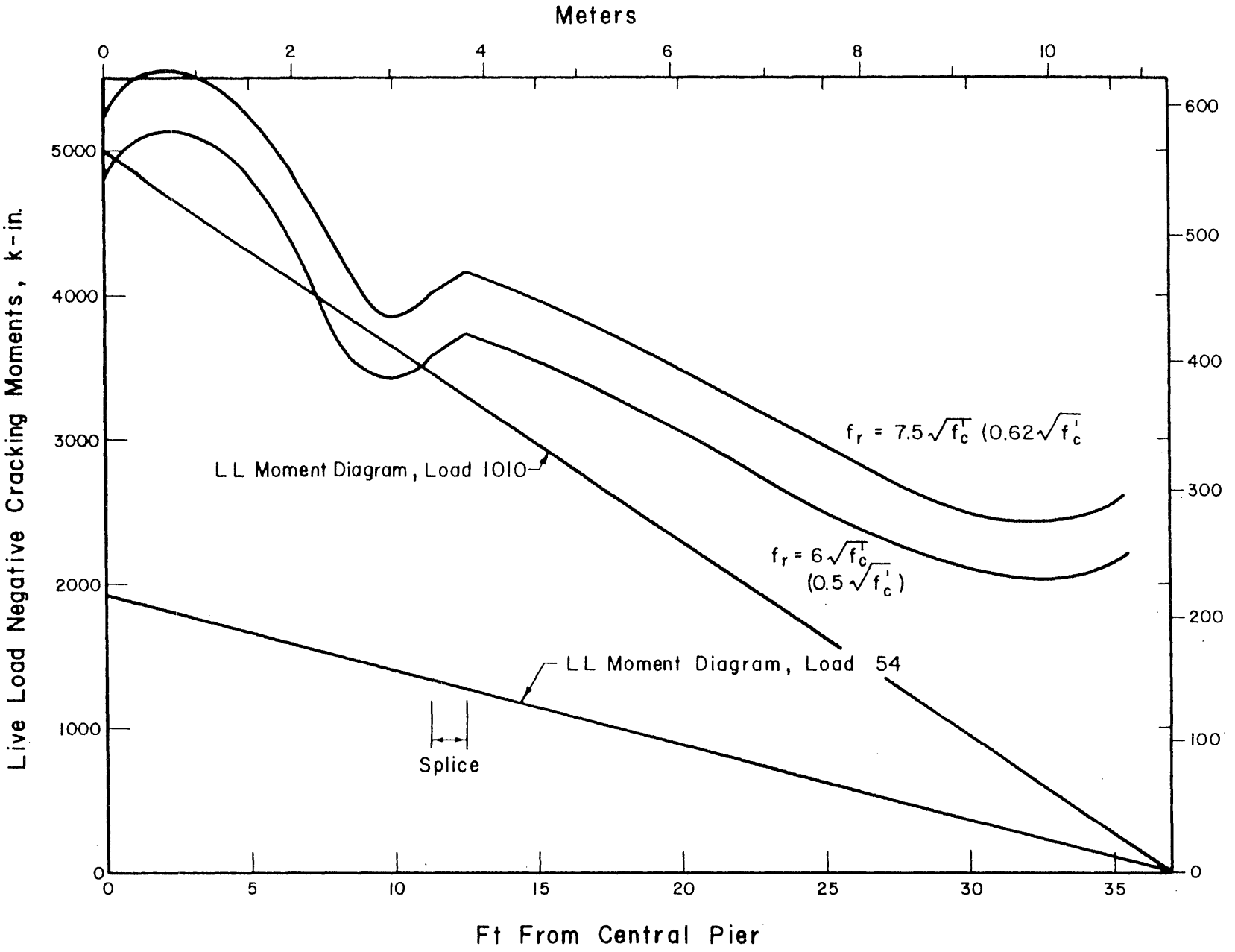


FIG. 6.6 COMPUTED AND OBSERVED NEGATIVE CRACKING MOMENTS, MODEL 1

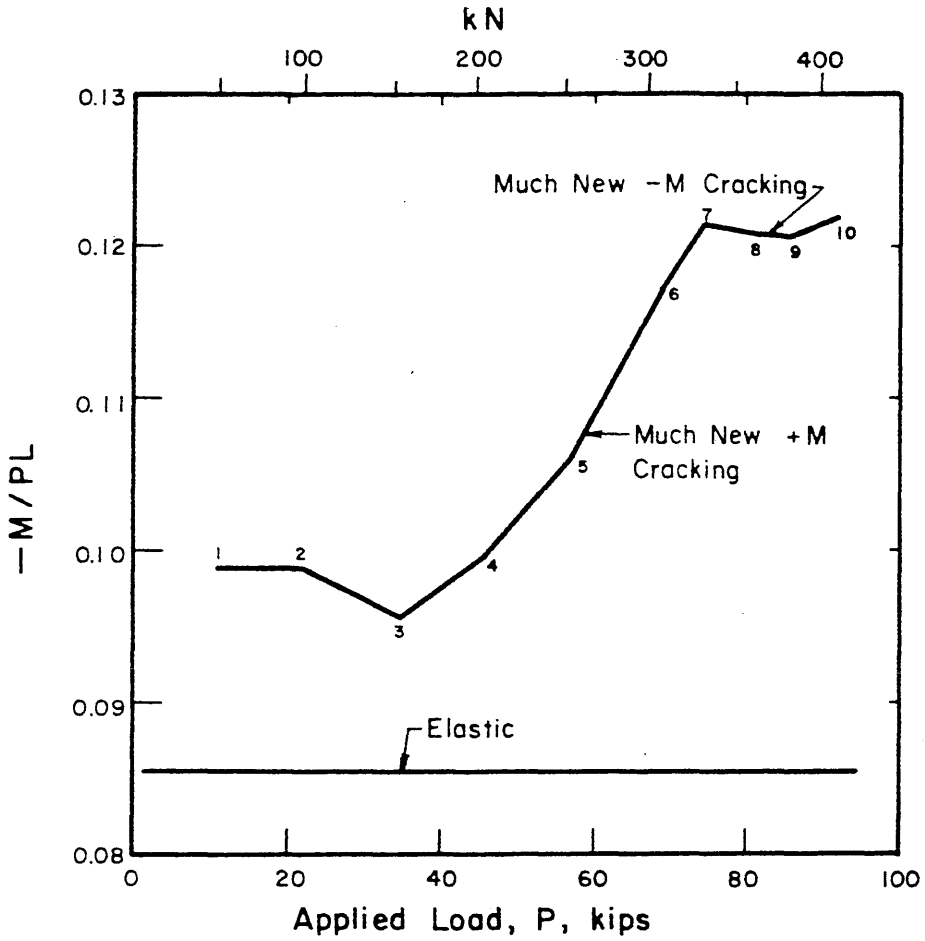


FIG. 6.7 LOAD-NEGATIVE MOMENT COEFFICIENT FOR TEST 10, MODEL 1

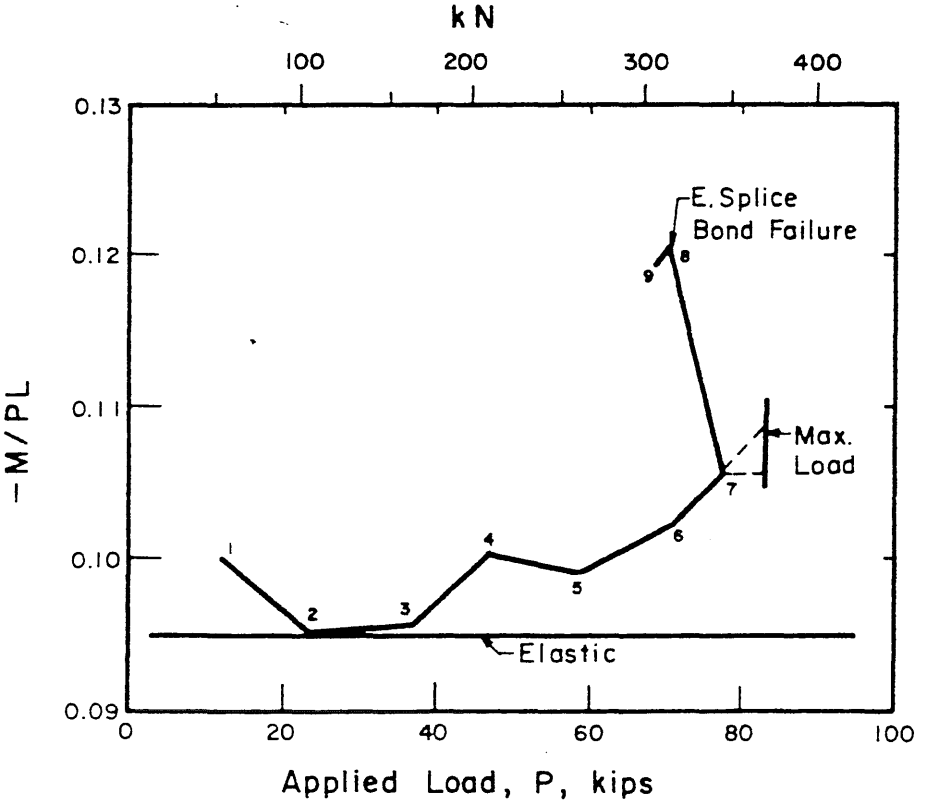


FIG. 6.8 LOAD-NEGATIVE MOMENT COEFFICIENT FOR TEST 11, MODEL 1

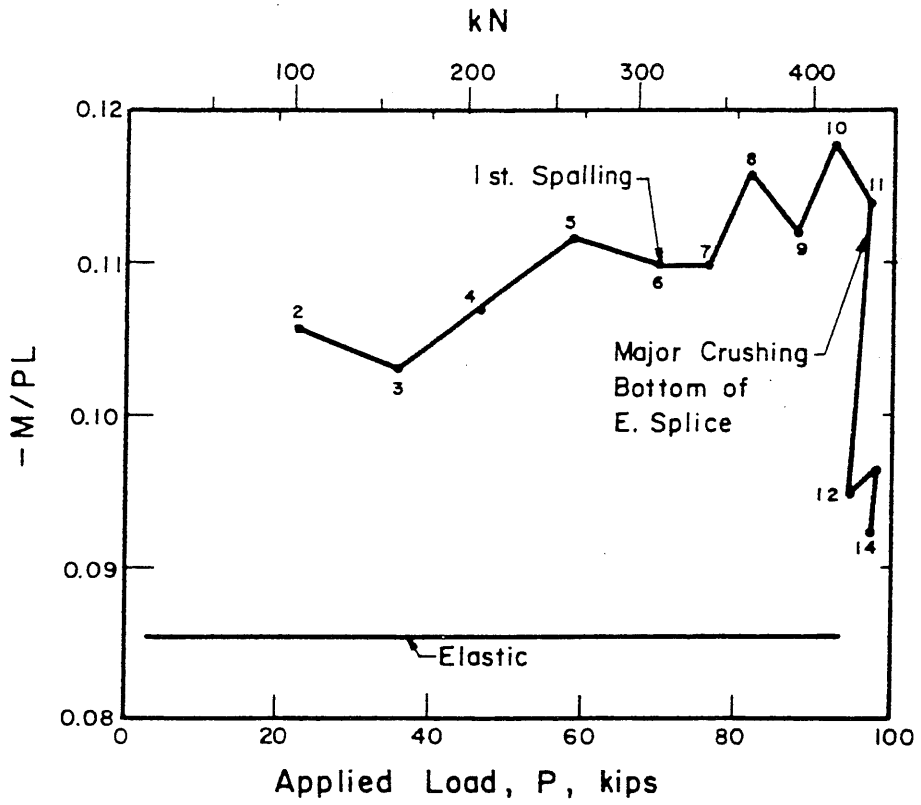


FIG. 6.9 LOAD-NEGATIVE MOMENT COEFFICIENT FOR TEST 12, MODEL 1

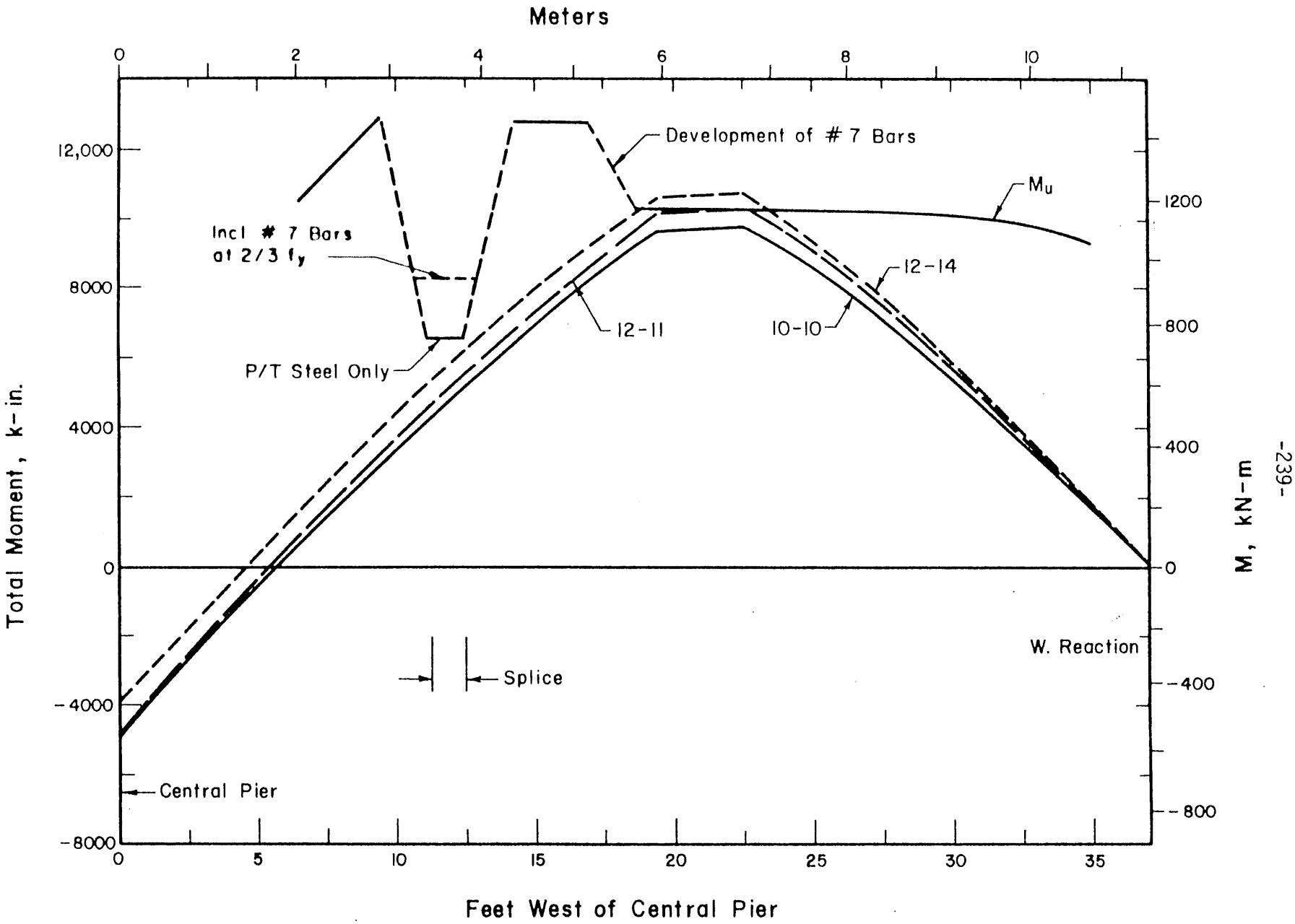


FIG. 6.10 COMPARISONS OF MOMENT DIAGRAMS AND RESISTING MOMENTS IN WEST SPAN, MODEL 1

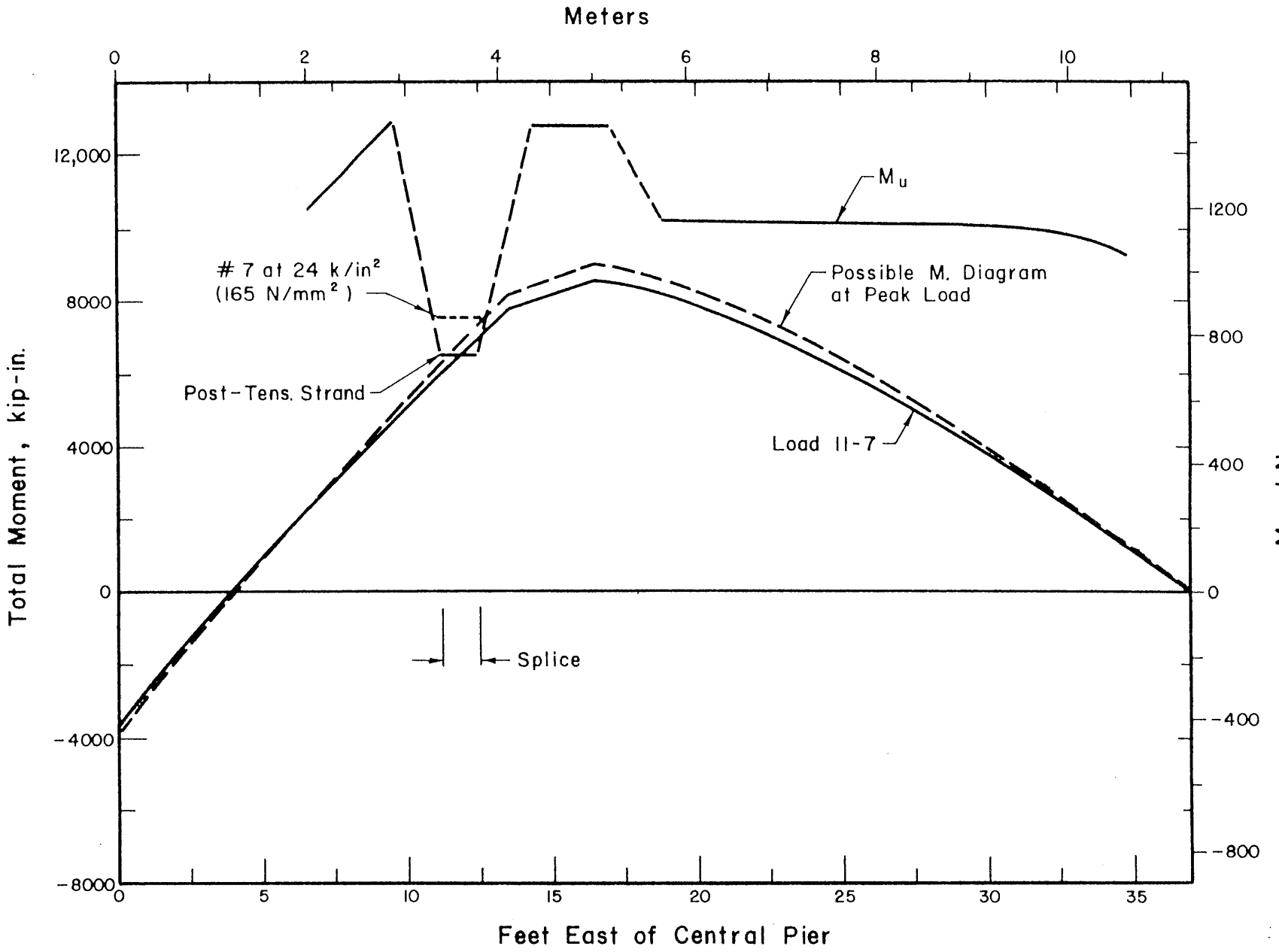


FIG. 6.11 COMPARISONS OF MOMENT DIAGRAMS AND RESISTING MOMENTS IN EAST SPAN, MODEL 1

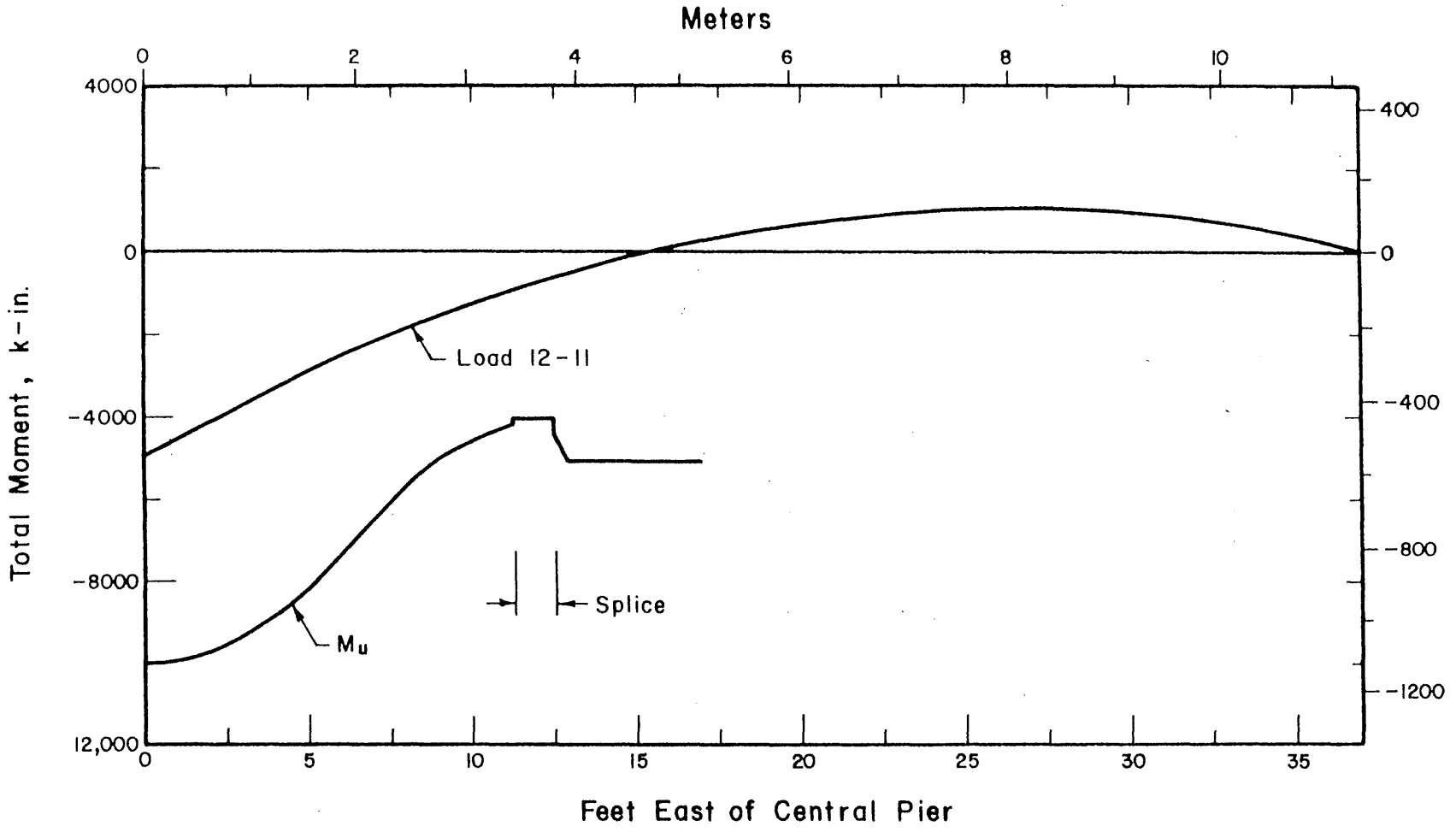


FIG. 6.12 COMPARISON OF NEGATIVE MOMENT CAPACITY AND MAXIMUM NEGATIVE MOMENTS, MODEL 1

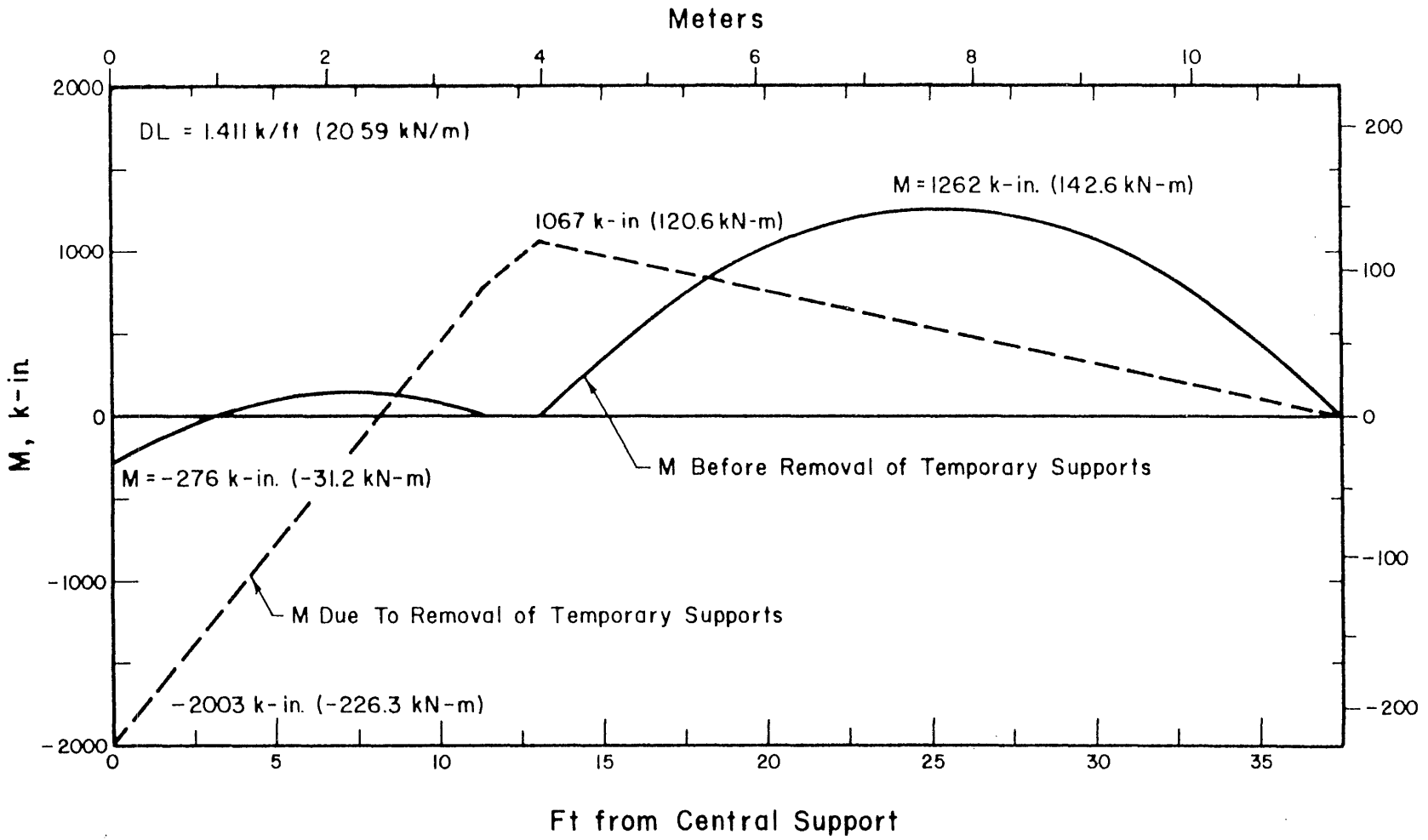


FIG. 6.13 MOMENT DIAGRAMS BEFORE SUPPORT REMOVAL AND DUE TO SUPPORT REMOVAL, MODEL 2

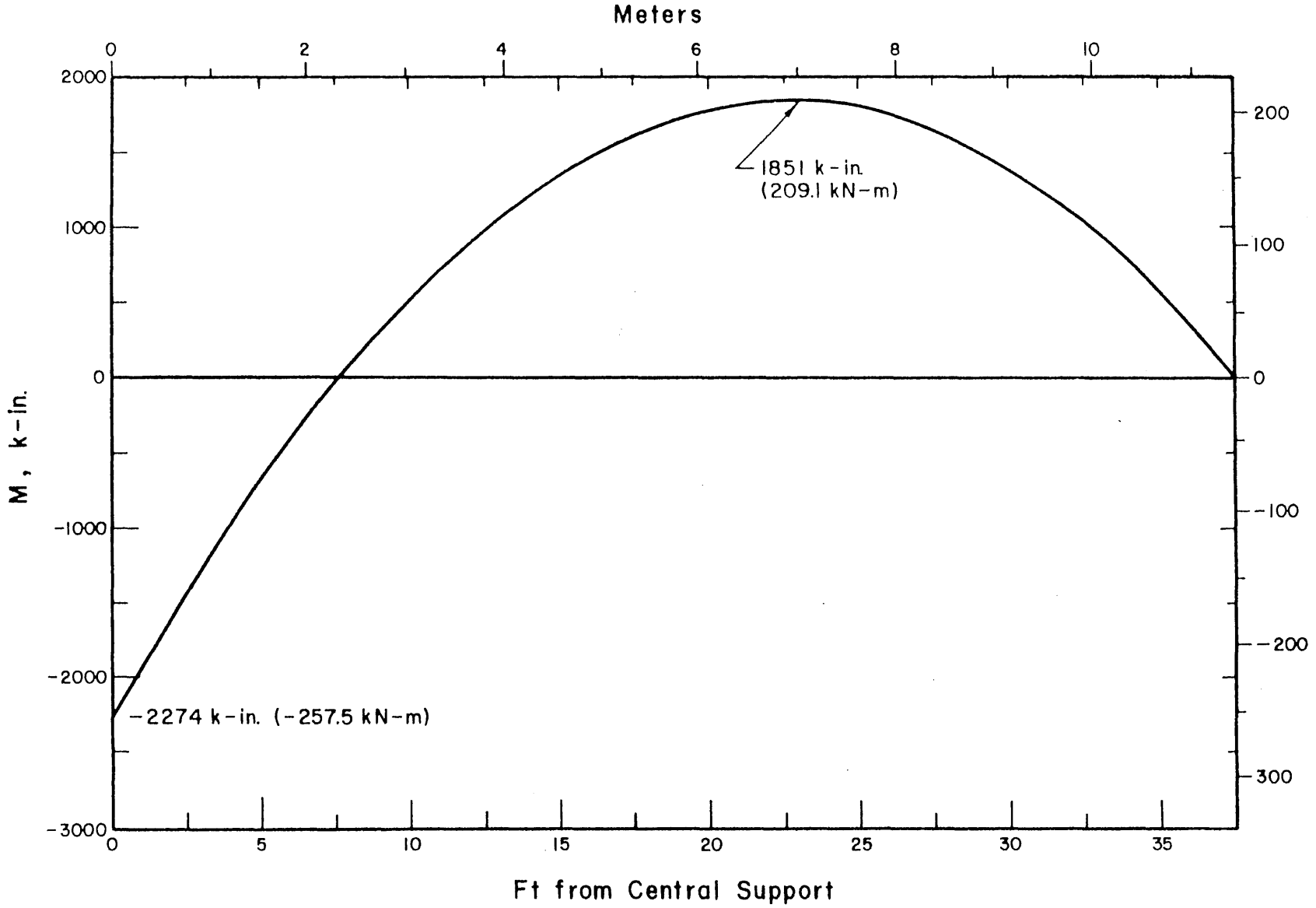


FIG. 6.14 DEAD LOAD MOMENT DIAGRAM FOR COMPLETED MODEL 2

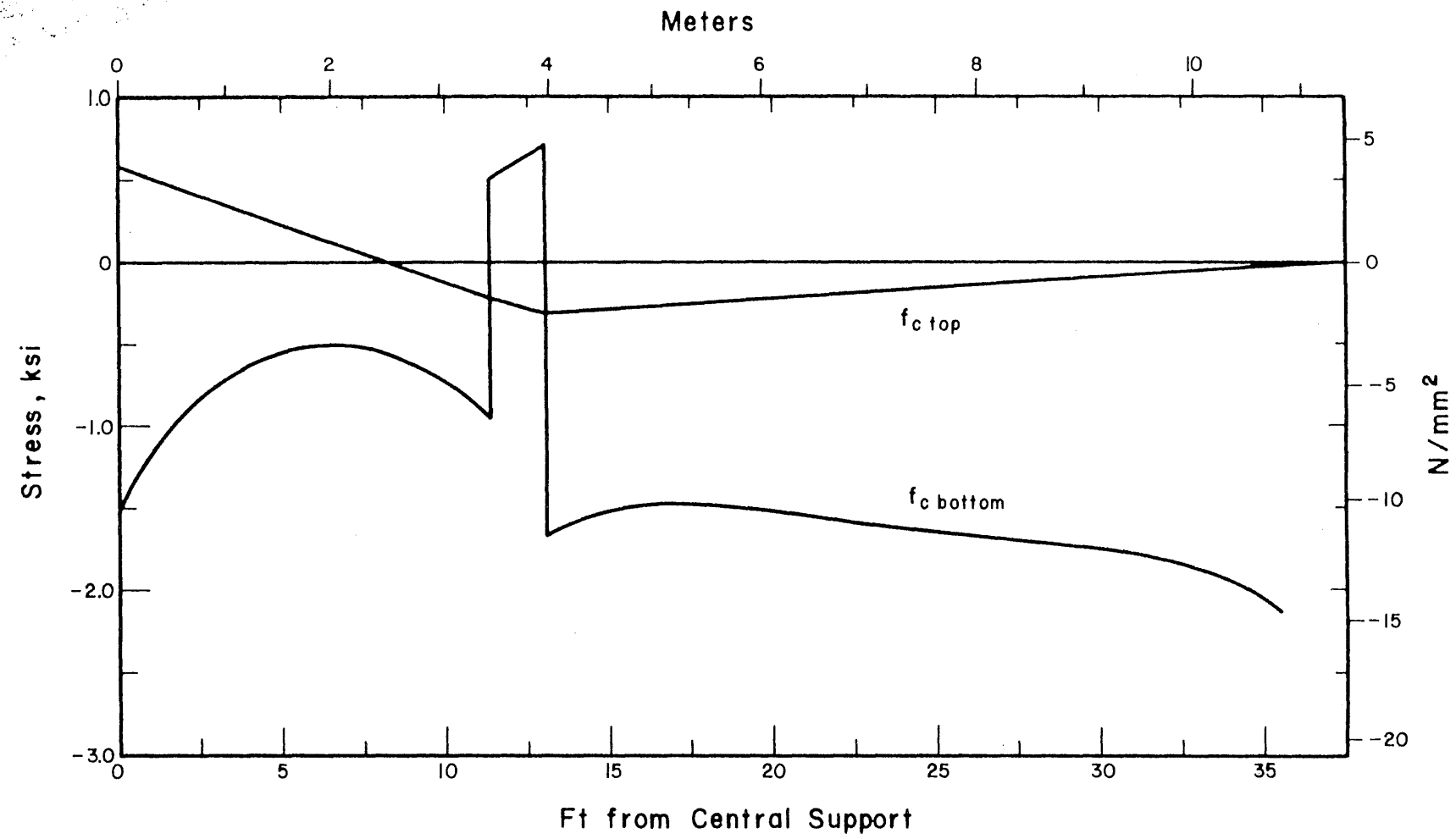


FIG. 6.15 DISTRIBUTION OF DEAD LOAD STRESSES ALONG TOP OF DECK AND BOTTOM OF GIRDER, MODEL 2

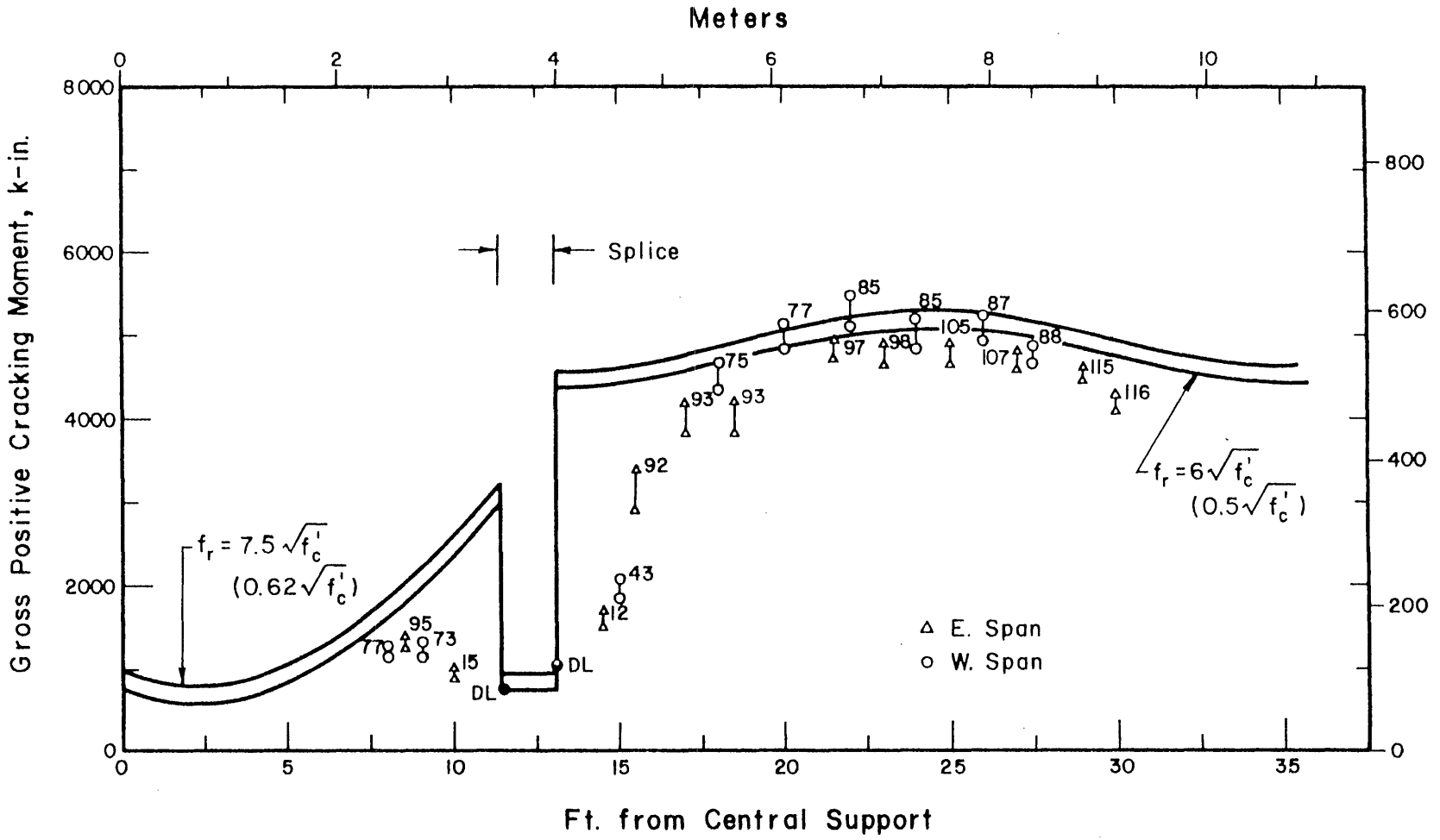


FIG. 6.16 COMPARISONS OF COMPUTED AND OBSERVED POSITIVE CRACKING MOMENTS, MODEL 2

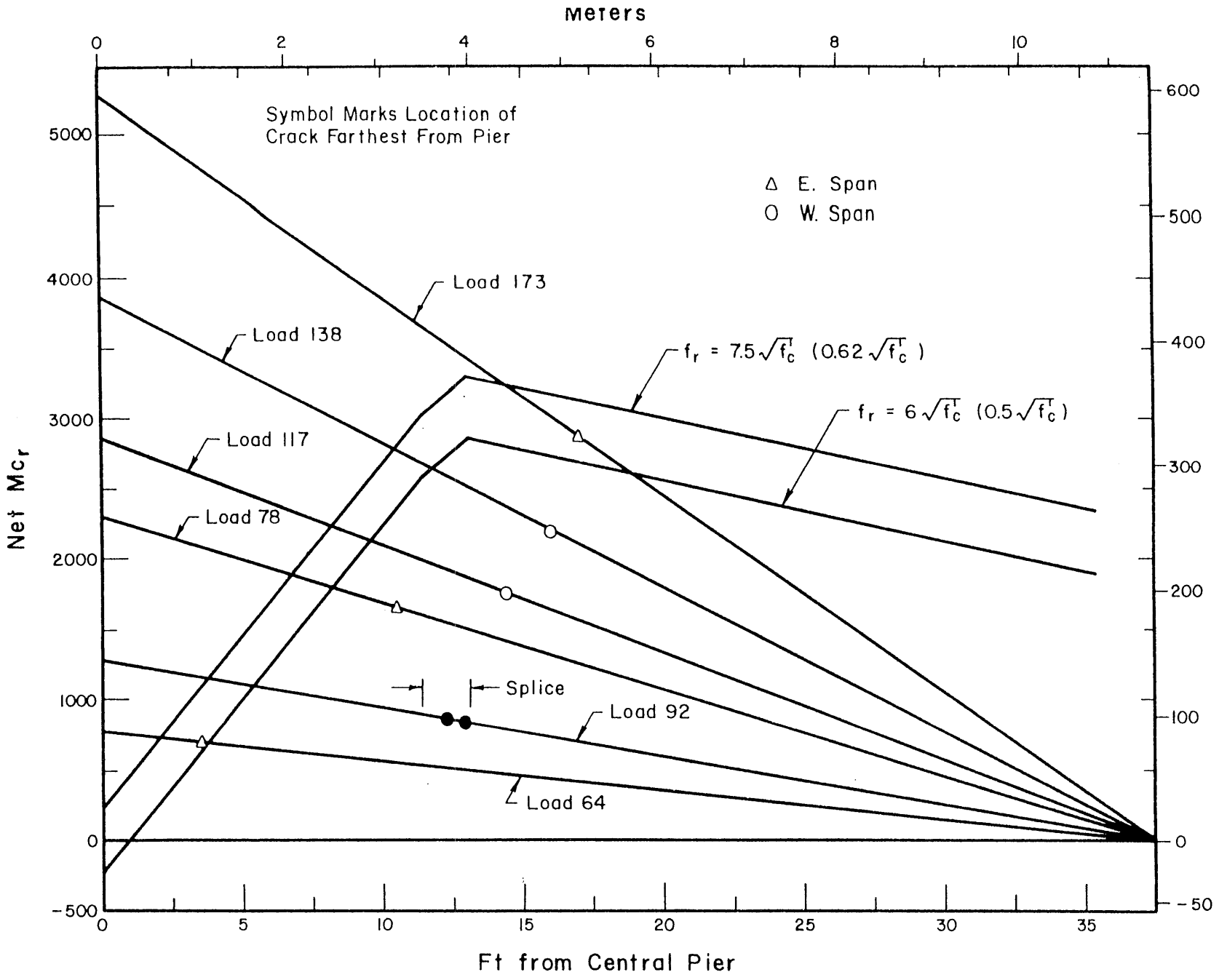


FIG. 6.17 COMPARISONS OF COMPUTED AND OBSERVED NEGATIVE CRACKING MOMENTS, MODEL 2

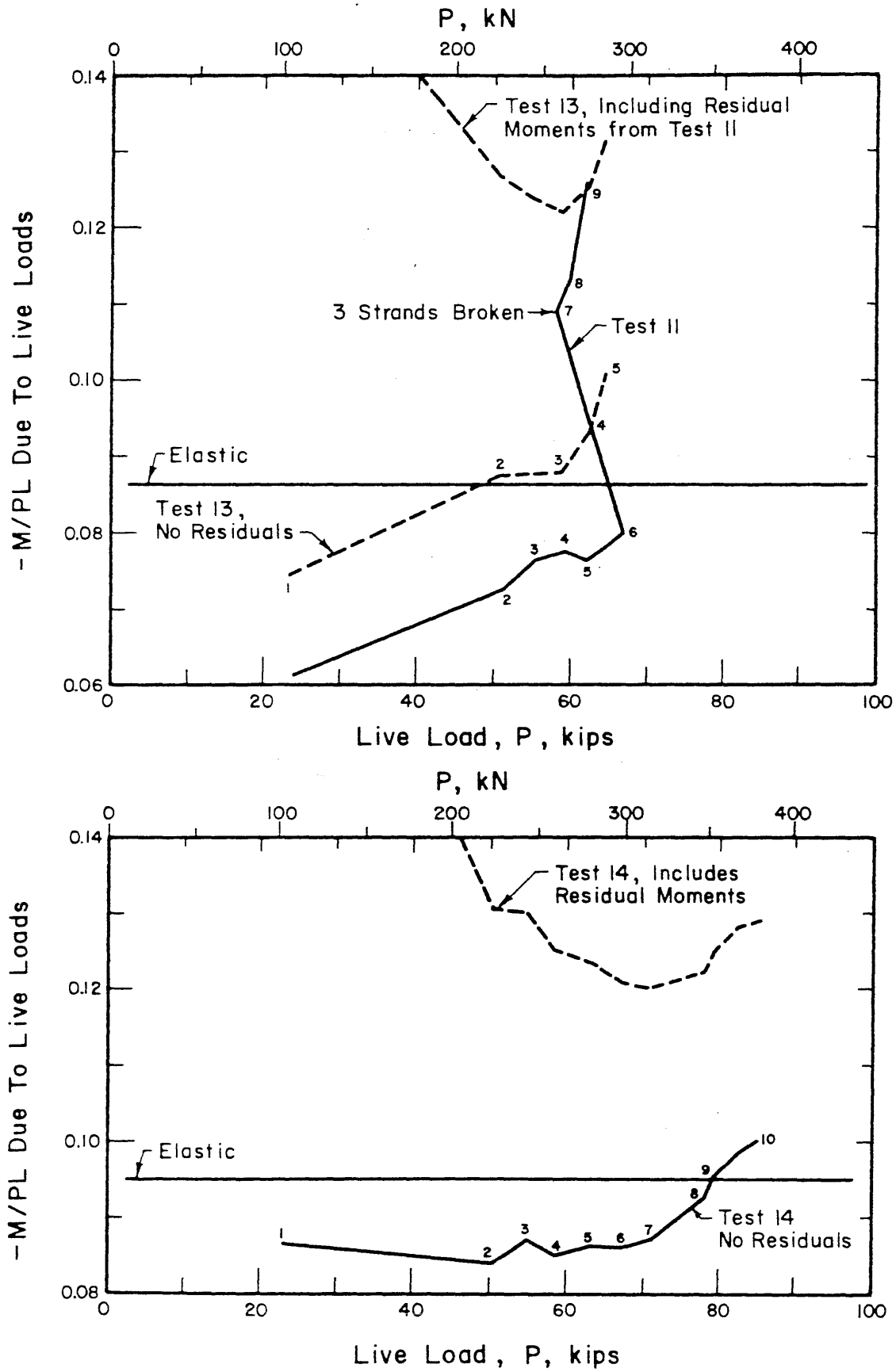


FIG. 6.18 LOAD-NEGATIVE MOMENT COEFFICIENTS FOR TESTS 11, 13, AND 14, MODEL 2

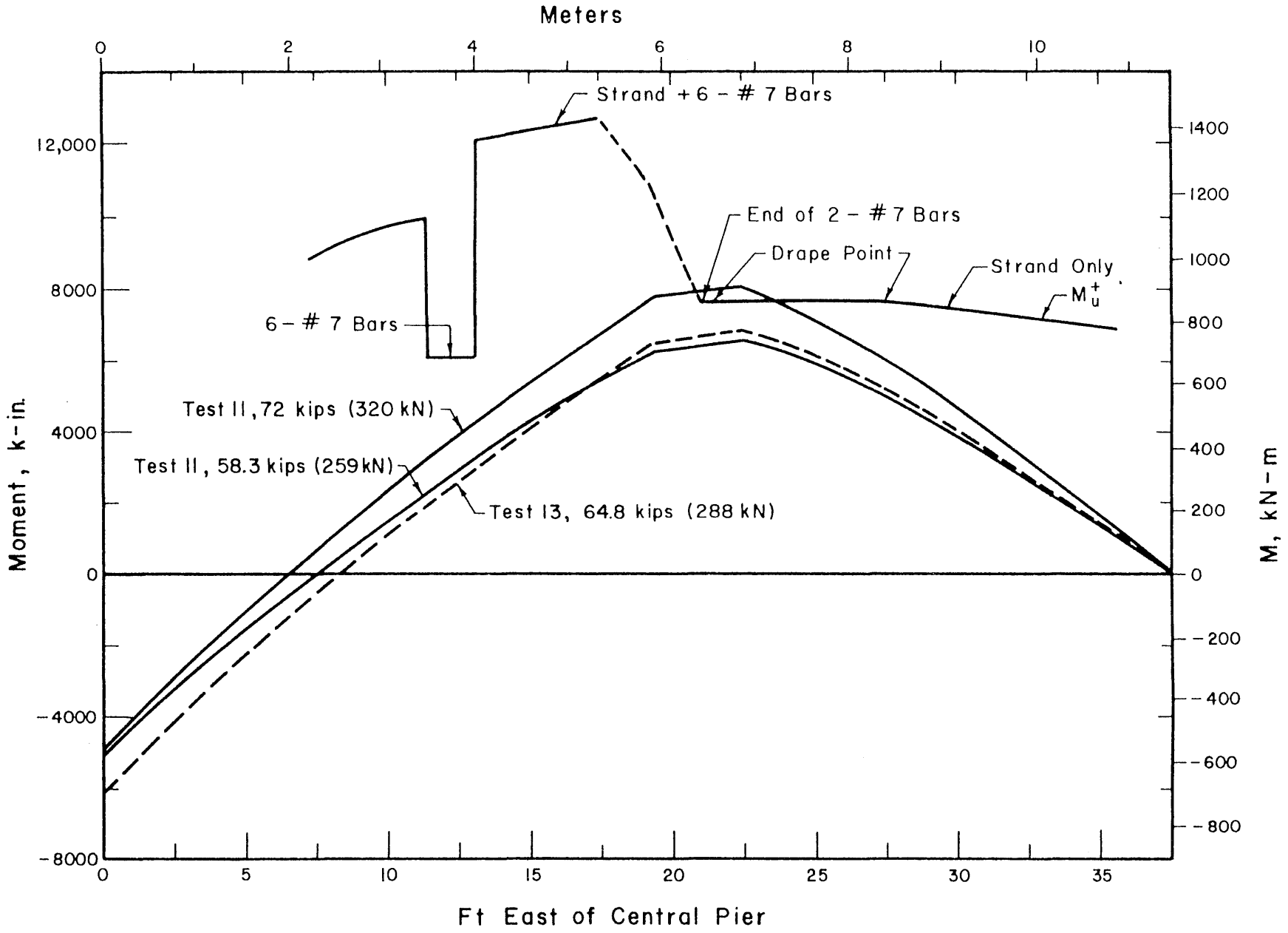


FIG. 6.19 COMPARISONS OF MOMENT DIAGRAMS AND RESISTING MOMENTS IN EAST SPAN, MODEL 2

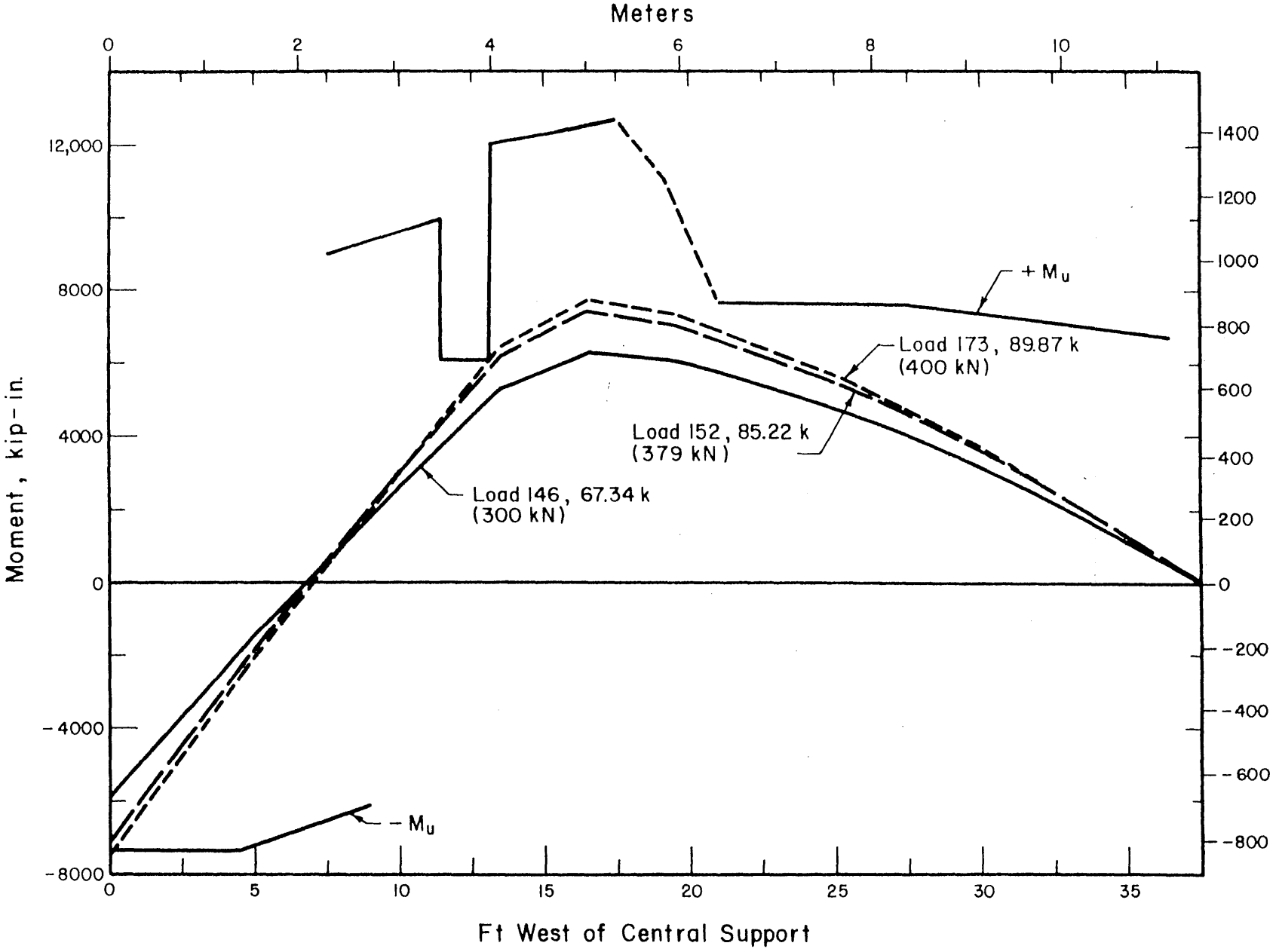


FIG. 6.20 COMPARISONS OF MOMENT DIAGRAMS AND RESISTING MOMENTS IN WEST SPAN, MODEL 2

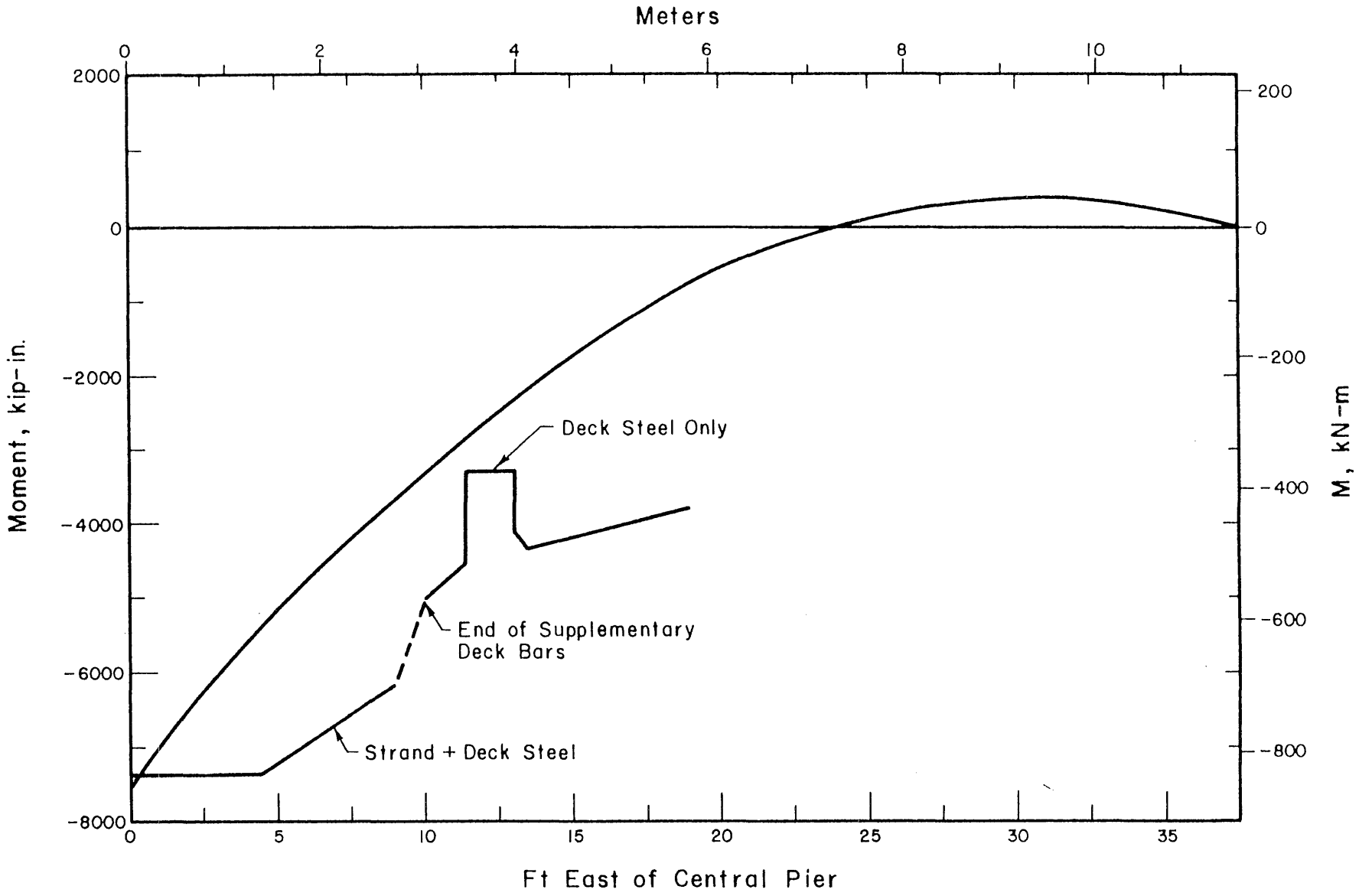


FIG. 6.21 COMPARISON OF MAXIMUM NEGATIVE MOMENT DIAGRAM AND NEGATIVE MOMENT CAPACITY, MODEL 2

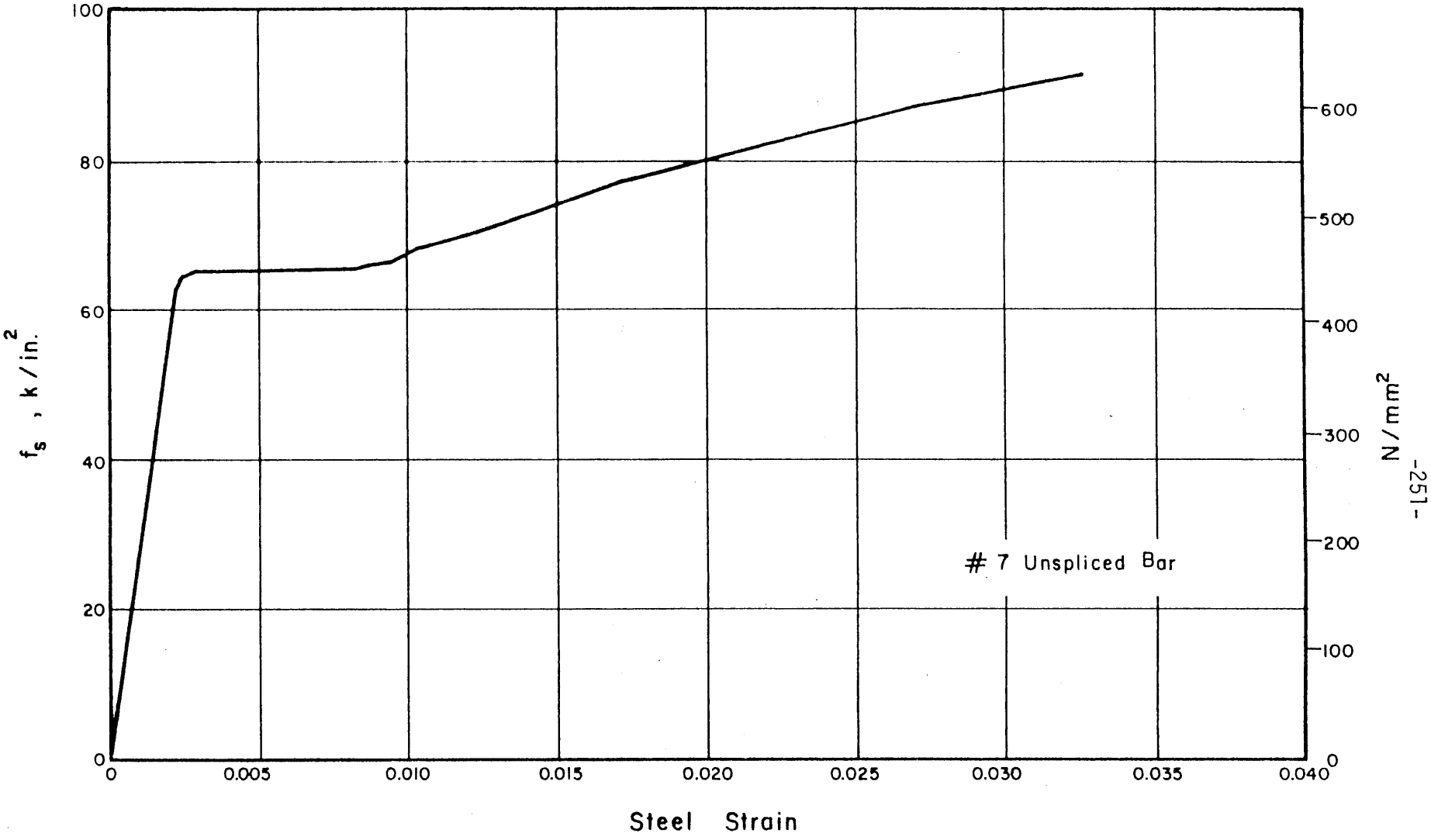


FIG. 6.22 STRESS-STRAIN CURVE FOR #7 (22.2 mm) REINFORCING BAR

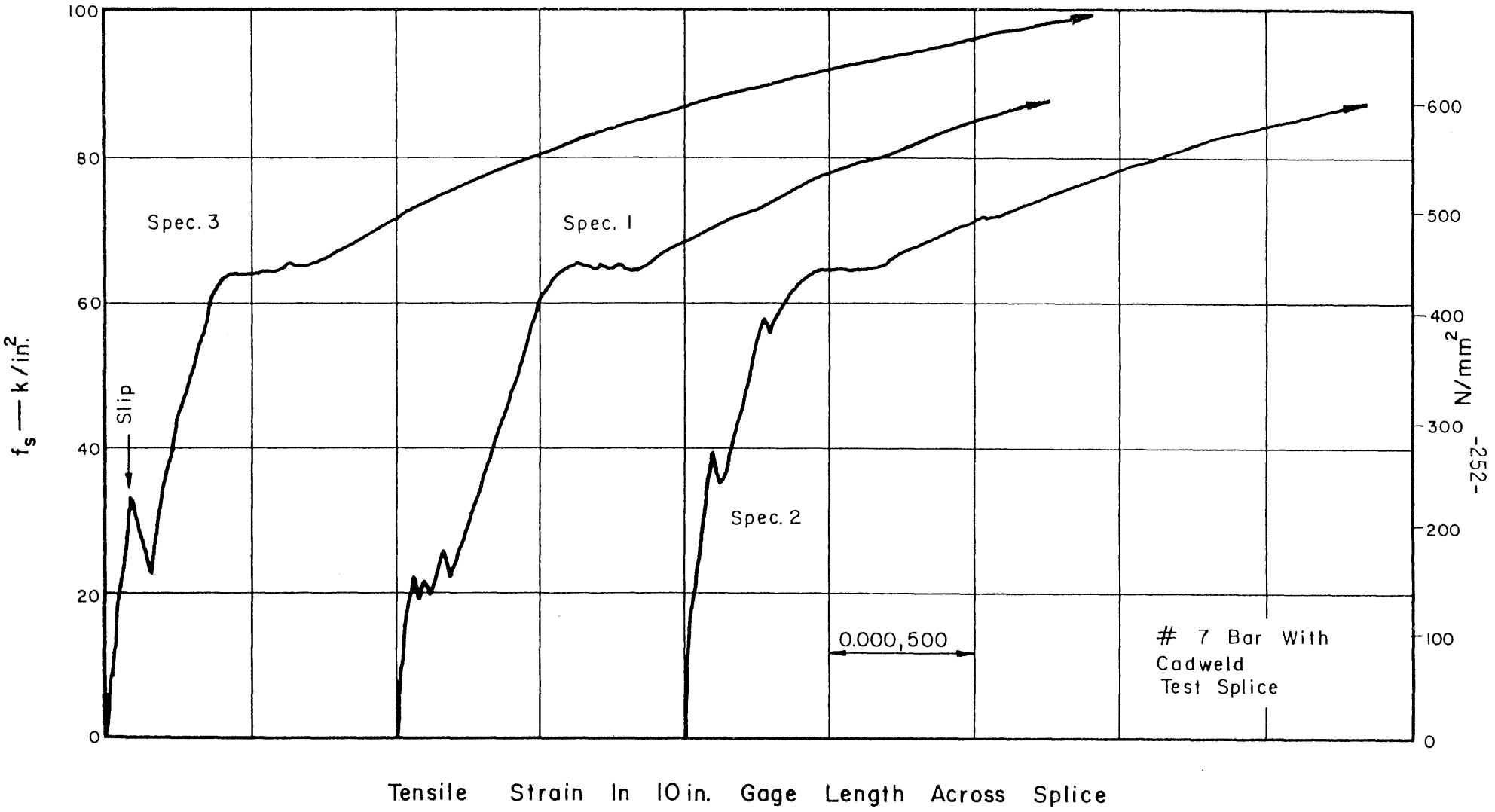


FIG. 6.23 STRESS-STRAIN CURVES FOR CADWELD SPLICES ON INITIAL LOADING

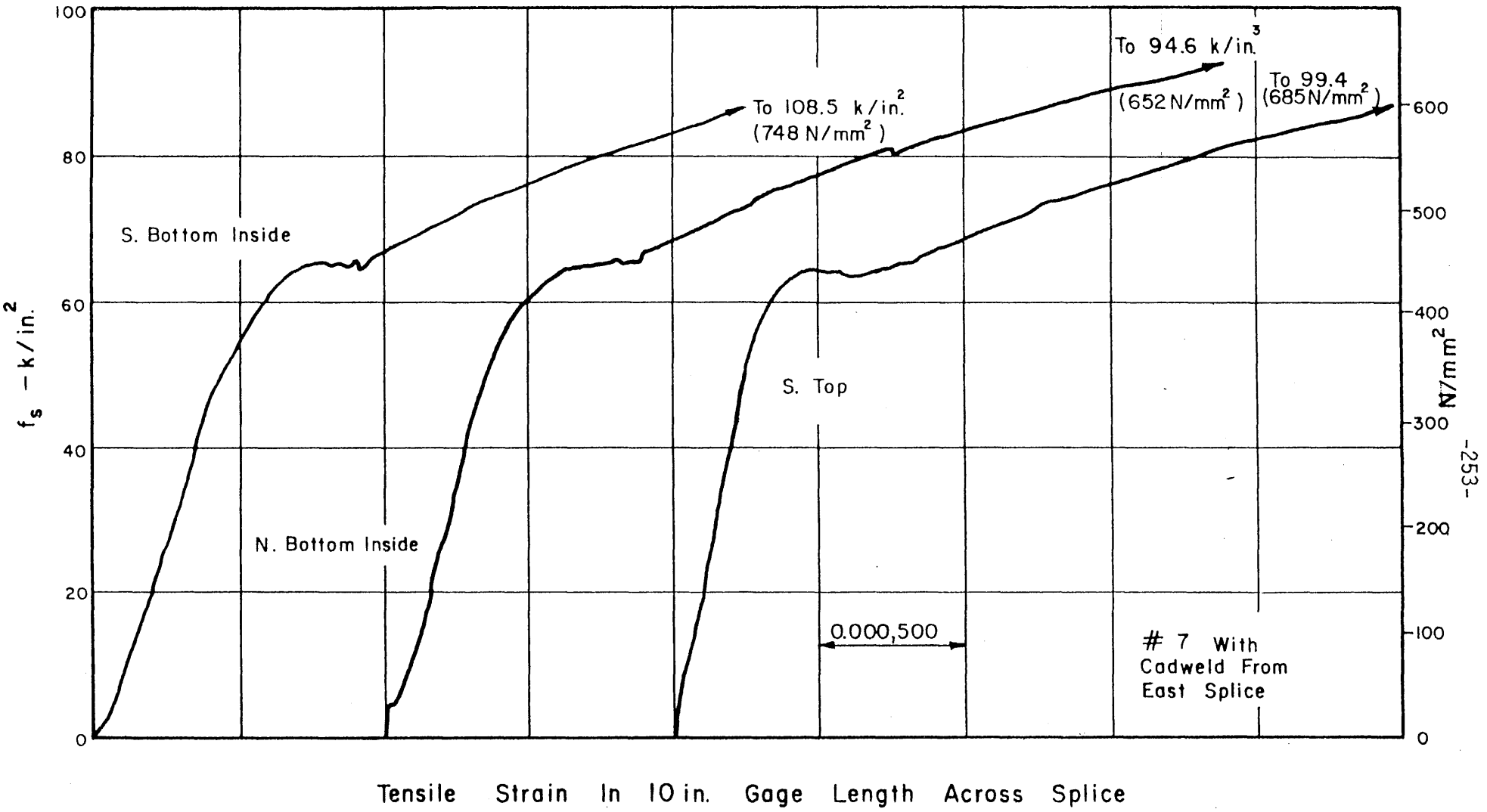


FIG. 6.24 STRESS-STRAIN CURVES FOR CADWELD SPLICES CUT FROM EAST SPLICE, MODEL 2

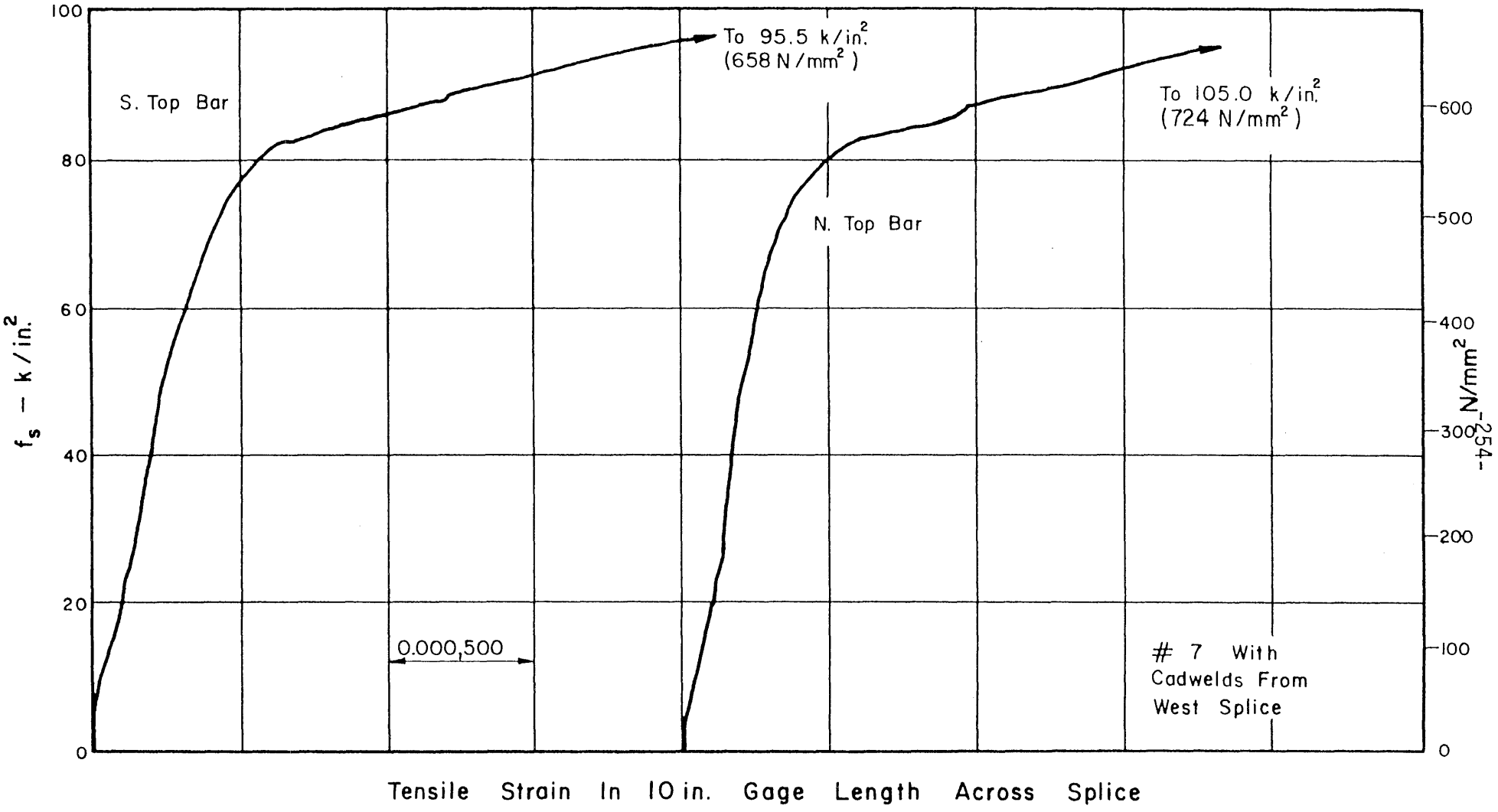


FIG. 6.25 STRESS-STRAIN CURVES FOR CADWELD SPLICES CUT FROM WEST SPLICE, MODEL 2

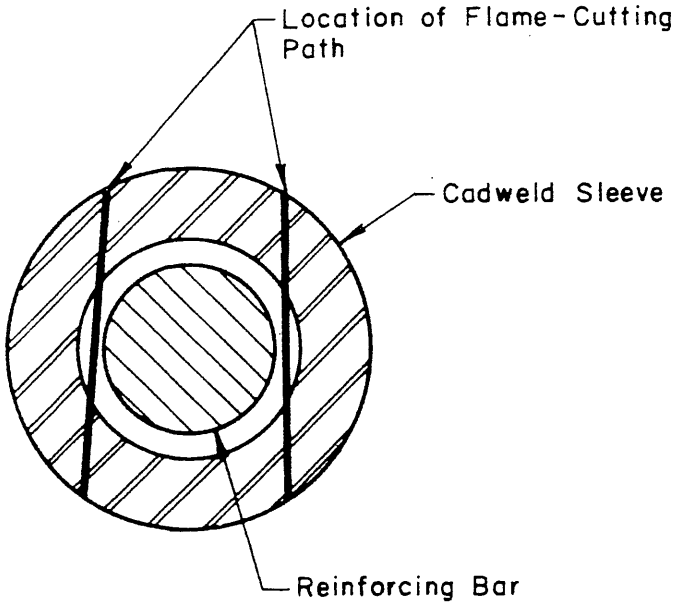


FIG. 6.26 LOCATIONS OF FLAME-CUTS MADE TO REMOVE CADWELD SPLICE SLEEVE

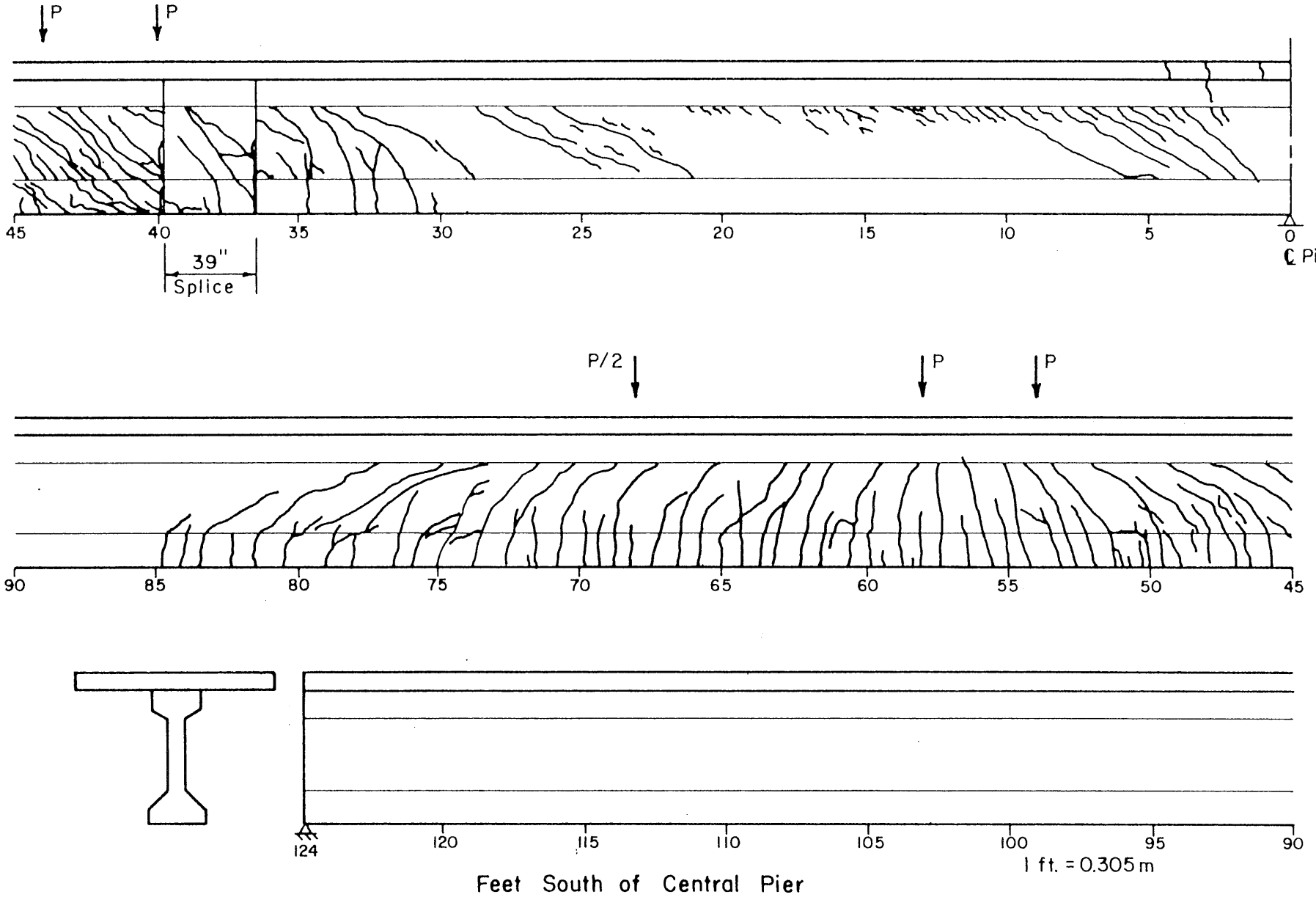


FIG. 6.27 CRACK PATTERN IN SOUTH SPAN OF PROTOTYPE STRUCTURE

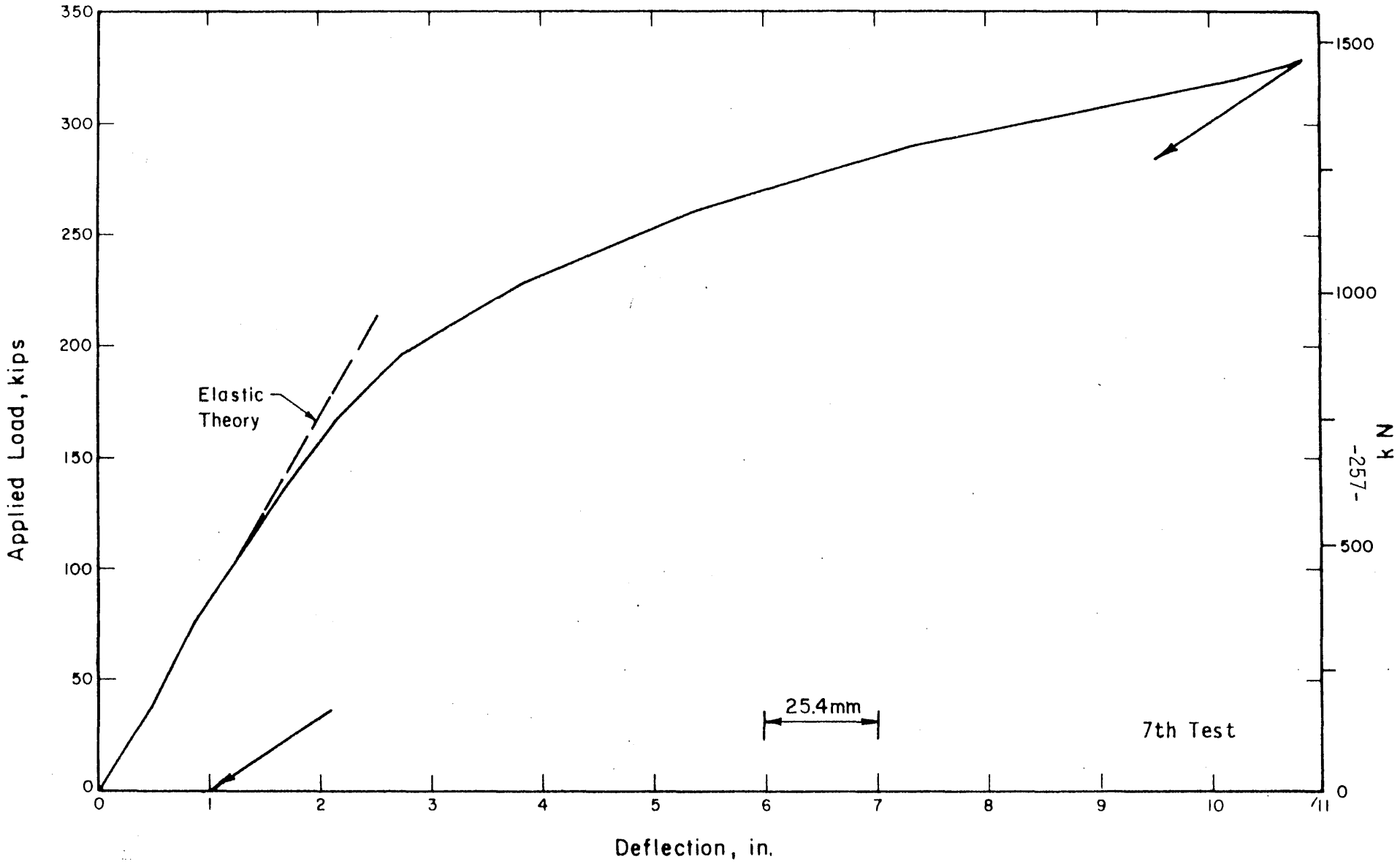


FIG. 6.28 LOAD-DEFLECTION CURVE FOR POINT AT 70 FT SOUTH, SOUTH SPAN OVERLOAD TEST, PROTOTYPE STRUCTURE

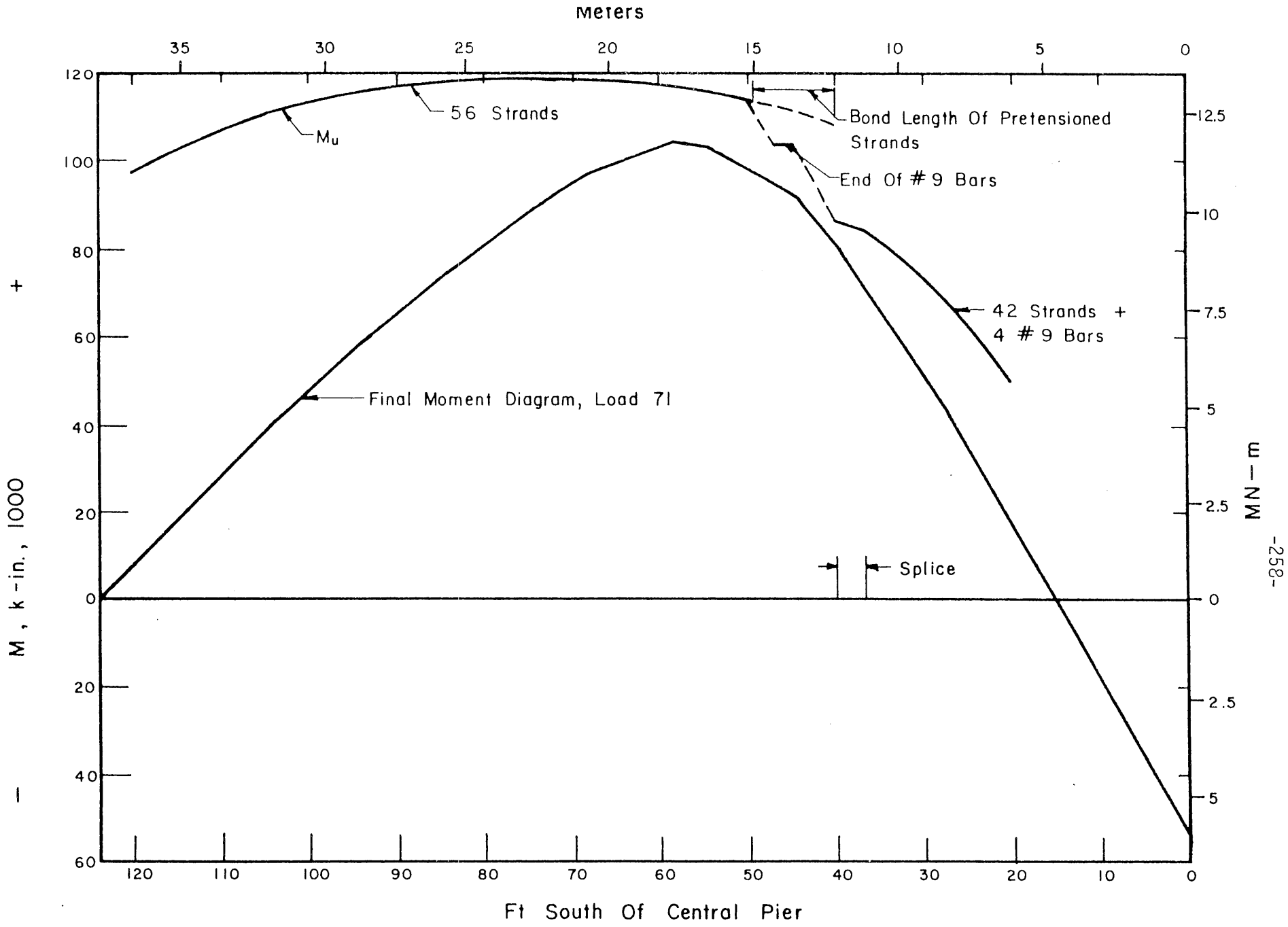


FIG. 6.29 APPLIED MOMENT AND MOMENT CAPACITY DIAGRAMS FOR SOUTH SPAN OF PROTOTYPE STRUCTURE

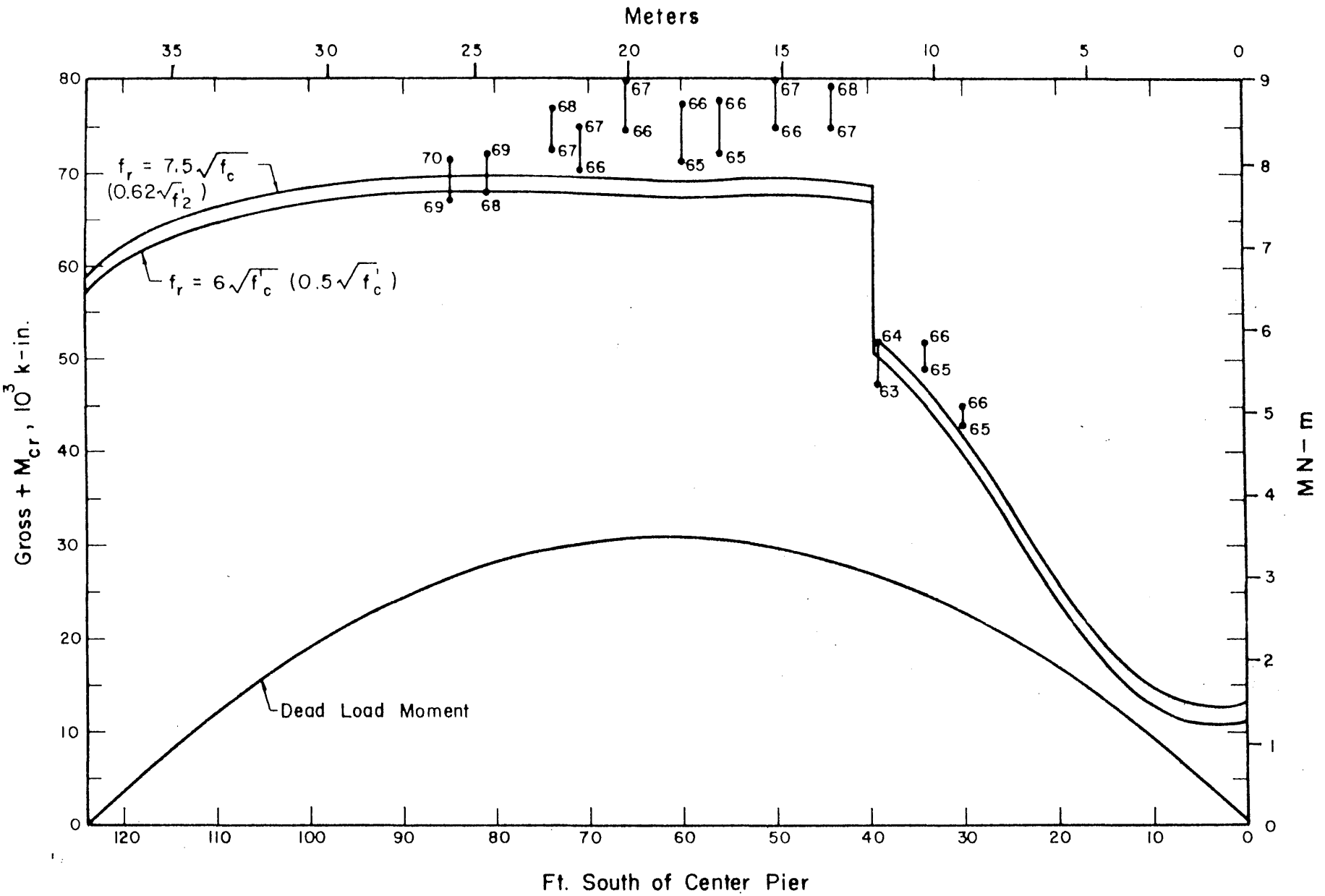


FIG. 6.30 MEASURED AND COMPUTED POSITIVE CRACKING MOMENTS, SOUTH SPAN OF PROTOTYPE STRUCTURE

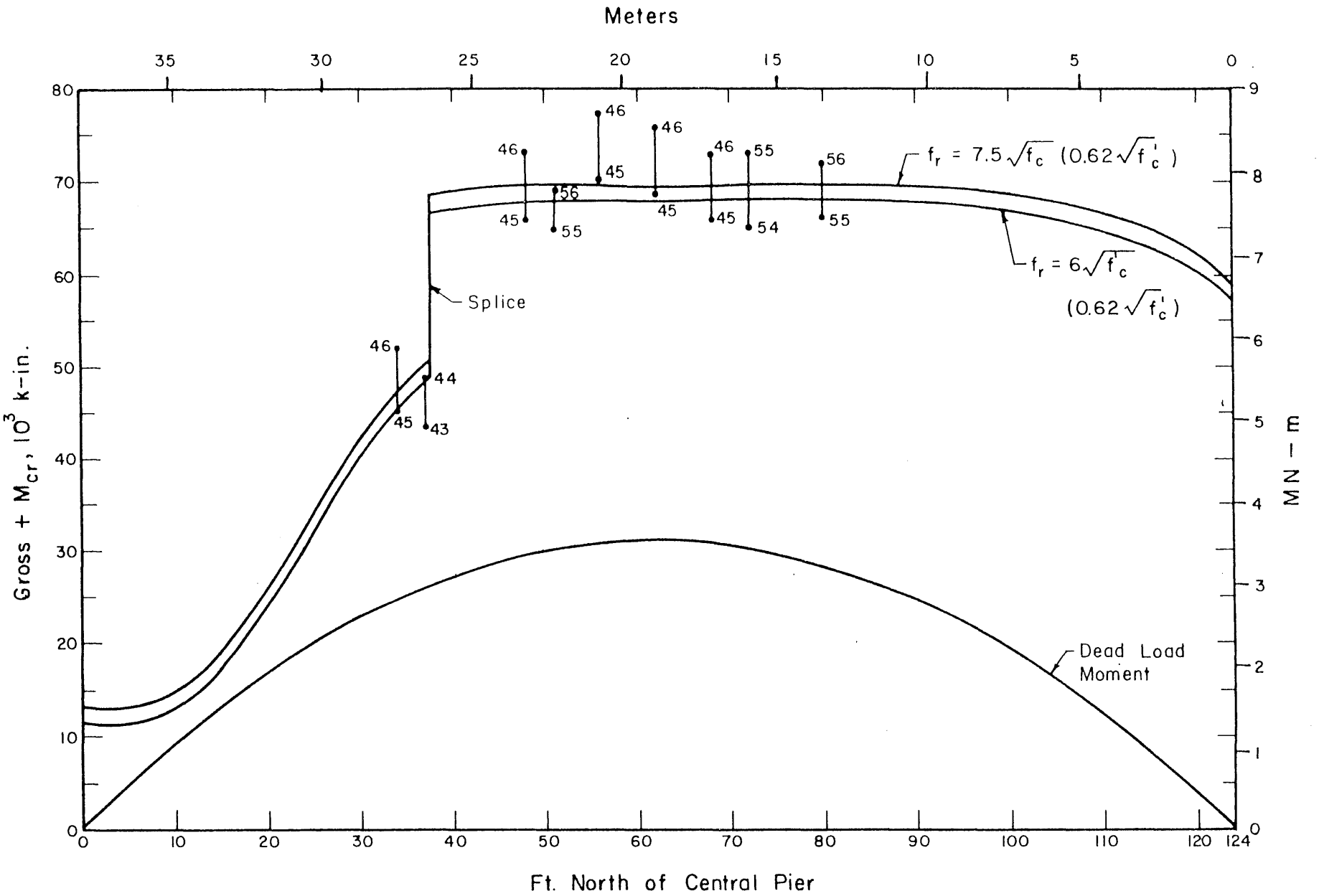


FIG. 6.31 MEASURED AND COMPUTED POSITIVE CRACKING MOMENTS, NORTH SPAN OF PROTOTYPE STRUCTURE

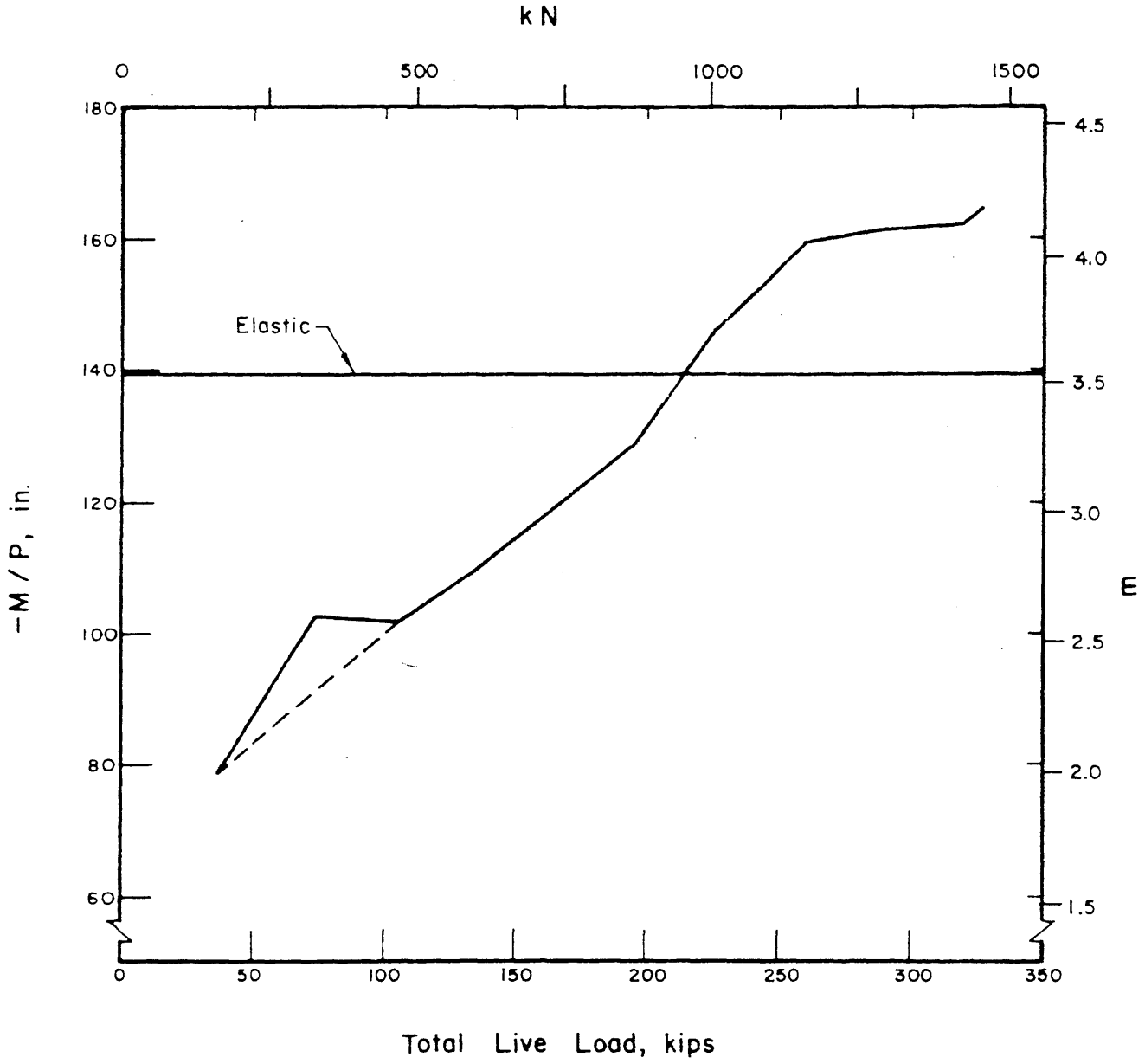


FIG. 6.32 LOAD-NEGATIVE MOMENT COEFFICIENT FROM IDEALIZED REACTIONS, SOUTH SPAN OVERLOAD TEST, PROTOTYPE STRUCTURE

APPENDIX A

SUMMARY OF INSTRUCTIONS FOR CADWELD SPLICING

1. Clean ends of reinforcing bars with wire brush to remove loose rust and mill scale.

2. Heat slightly to make sure that bars are absolutely dry. Also heat splice sleeve slightly.

3. Mark reinforcing bars to be spliced by placing paint or keel mark on bars 12 in. (300 mm) from bar ends. These marks will be used later to determine whether splice sleeve is properly centered. Do not mark with a punch, chisel, or file as the notch may initiate a brittle fracture.

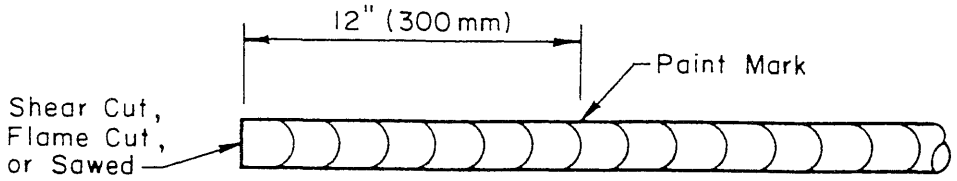


4. Slip splice sleeve onto one bar, and bring ends of bars to be spliced together. If bars are saw-cut, place 3/16 in. (4.8 mm) spacer between ends of bars. If bars are shear or flame-cut, a natural gap will be left when the bars are butted, but this gap must not exceed 3/8 in. (9.5 mm) at the widest point. If gap is too wide, reduce by trimming or rotating bars.

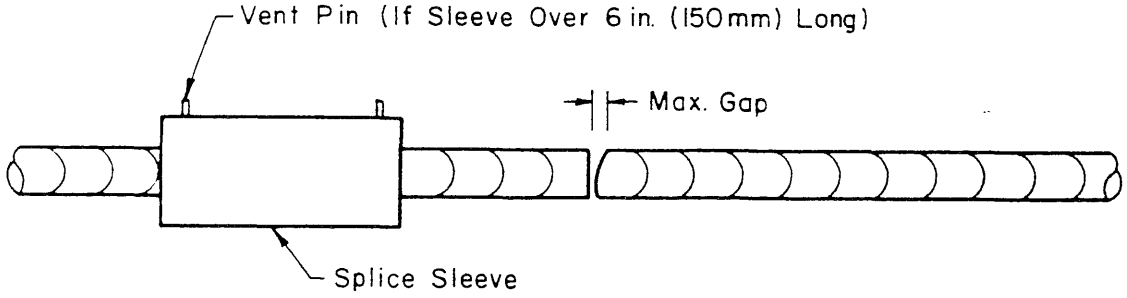


5. Center splice sleeve over gap between ends of bars. Tap hole in sleeve should be directly lined up with gap. (Filler metal may be introduced from either the top or the side of the sleeve, depending on the accessability of the splice. The tap hole may be either vertical or horizontal. The top-filled position is preferable, if possible. The following illustrations assume top filling, and side filling varies largely in the details of the equipment). The sleeve is lifted so that the bars are near the bottom of the hole through the sleeve, to facilitate flow of the filler metal into the space between the bar and the sleeve. The vent pins are driven in to hold the splice up.

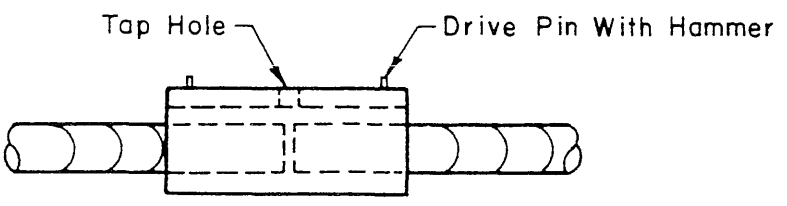


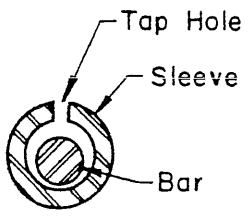

6. Wrap 2 turns of asbestos rope around bar at each end of sleeve. If sleeve does not have vent holes, use end of rope to hold sleeve up from bar. The rope is not forced into the gap between the sleeve and bar. Then place end alignment fittings, which are hinged clamping devices.

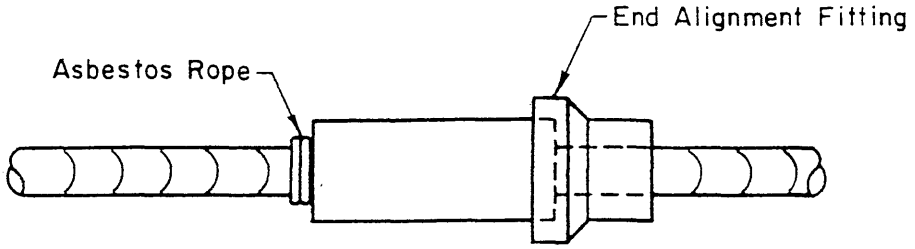


7. Place horizontal packing clamp to squeeze end alignment fittings over ends of splice sleeve, confining asbestos. Place metal guide tube into tap hole, and place ceramic insert over guide tube.

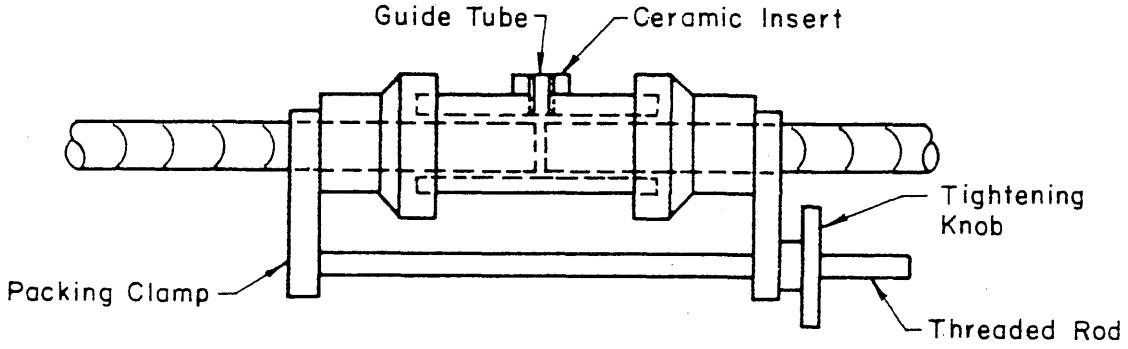


8. Place graphite pouring basin on top of sleeve, over ceramic insert. The pouring basin must be warmed to insure that it is completely dry. Clamp pouring basin to splice sleeve with roller chain clamp.

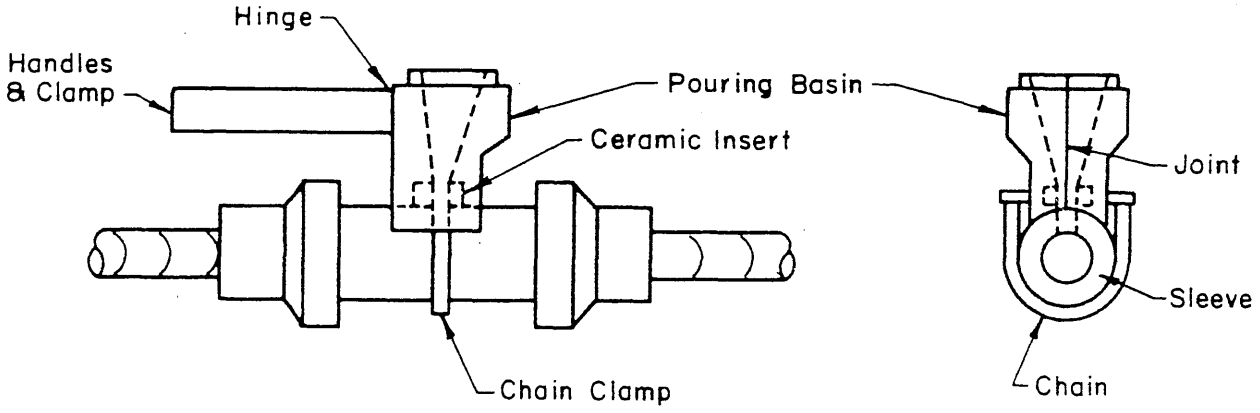

9. Place graphite crucible on top of pouring basin. Place crucible ceramic insert in hole in bottom of crucible, and place steel disk over ceramic piece and check that it is seated. Pour Cadweld Filler Metal Cartridge into crucible, being careful to not displace the steel disk, and level filler material. (Filler material contains iron oxide, finely powdered aluminum, and fluxing agents). Sprinkle starting powder (finely powdered aluminum) over top of filler material, saving a small portion for later. Place crucible extension and place remaining starting powder on inside lip of crucible extension. Place crucible cover. Ignite starting powder with flint gun, and move up-wind to avoid smoke. A strongly exothermic reaction follows, which produces molten iron which runs from the crucible through the pouring basin and into the space between the splice sleeve and the reinforcing bars.

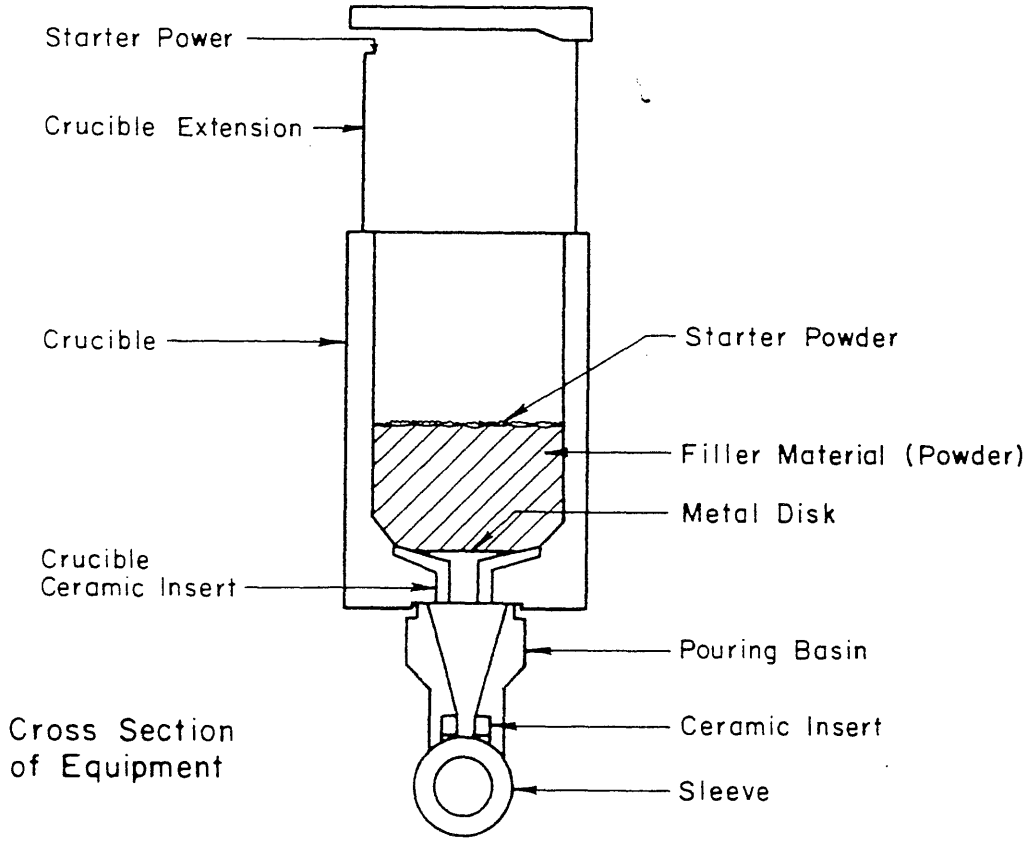


10. 15-20 seconds after completion of reaction, tilt crucible slightly to break slag at bottom of crucible. After slag has completely hardened, remove crucible. Remove pouring basin and all other hardware. Break off riser with hammer, inspect splice to insure that it is filled completely, and contains metal and not slag.